

✓

FOR REFERENCE ONLY

SWITCH MODE EMULATION OF LARGE VALUE
CAPACITORS IN THE ROTOR CIRCUIT TO
IMPROVE THE INDUCTION MOTOR
PERFORMANCE

CONSTANTIN SUCIU

2 - NOV 2000

A thesis submitted in partial fulfilment of the
requirements of The Nottingham Trent University
for the degree of Doctor of Philosophy

The research programme was carried out in collaboration
with Transilvania University of Brasov, Romania

JUNE 2000

40 0706372 0



ProQuest Number: 10183019

All rights reserved

INFORMATION TO ALL USERS

The quality of this reproduction is dependent upon the quality of the copy submitted.

In the unlikely event that the author did not send a complete manuscript and there are missing pages, these will be noted. Also, if material had to be removed, a note will indicate the deletion.



ProQuest 10183019

Published by ProQuest LLC (2017). Copyright of the Dissertation is held by the Author.

All rights reserved.

This work is protected against unauthorized copying under Title 17, United States Code
Microform Edition © ProQuest LLC.

ProQuest LLC.
789 East Eisenhower Parkway
P.O. Box 1346
Ann Arbor, MI 48106 – 1346

Abstract

This thesis describes an investigation into enhancing the performance of induction motors by secondary reactance control without injecting to or extracting energy from the rotor as in the case of double fed machines.

Firstly, a space-vector model of the motor is used to investigate the changes in performance induced by the insertion of equal capacitance in each secondary phase. The effect of the secondary capacitance is to introduce leading vars into the rotor. A set of equations that simplifies simulation of an induction motor performance, in both the short circuited rotor mode and with externally modified rotor impedance, are developed. The simulations showed that impractical high values for capacitors are required to phase advance the rotor current to achieve performance enhancement.

Electronic methods of achieving phase advance have been researched from literature and appraised. These methods were found not suitable for this application. A novel method using Pulse Width Modulated (PWM) controlled H-bridge with bi-directional switches and a capacitor as central component is presented in this thesis for controlling the phase angle in high power, low frequency RL circuits. The system increases the capacitive effect by several orders and thus reduces the physical size of the capacitor required.

The technique was applied to a low power induction motor. The results showed an enhancement of the motor performance.

The duty ratio and its resolution are dependent on the rotor circuit parameters that vary with the motor load. Fuzzy control for the duty ratio to achieve the required phase angle is investigated. Verification is presented by experimentation in a single-phase circuit.

Acknowledgements

I would like to thank my supervisors, Mr. M Kansara, Professor P. G. Holmes and Professor W. Szabo, for their time and effort in guiding me through this thesis.

I want to acknowledge my colleagues from Transilvania University, Dr. R. Campeanu, Dr. L. Dafinca and Professor I. Margineanu for the meaningful discussions we had and the disinterested help they gave.

I express my gratitude to my friend Dr. Adrian Szabo for the moral and informational support offered all these years.

I dedicate this thesis to my parents, Ana and Ioan Suci.

Table of Contents

1. Introduction	1
2. The analysis of the induction motor with externally varied rotor impedance	9
2.1 Brief presentation of the space phasors	9
2.2 Dynamic model of the induction motor	11
2.3 Steady state performances of the induction motor	14
2.3.1 Mechanical power and efficiency	16
2.4 Dynamic model of the induction motor with variable rotor impedance	17
2.5 Steady state performances of the induction motor with variable rotor impedance	20
2.6 Simulation results	25
2.7 Conclusions	43
3. Review of the electronic phase control methods	45
3.1 Gyrator concept	47
3.2 Gyrator implementation	50
3.3 Some considerations about gyrator in power circuits	57
3.4 Switched capacitors	61
3.5 Conclusions	65
4. Novel application of switched capacitors in RL circuits	67
4.1 Switched capacitors in active filters	67
4.2 Current phase control in RL circuits using a dc source	68
4.3 Simulation of RL circuit with switched dc source	73
4.4 Switched capacitor in RL circuits	76
4.5 Some physical considerations	81
4.6 Simulation results	82
4.7 Conclusions	90
5. Experimental results	91
5.1 Power Circuit	92
5.1.1 Bi-directional switches	92
5.2 Command system	93
5.2.1 Pulse generator & Reference circuit	93
5.2.2 Delay circuit	95
5.2.3 Driver system nodules	97
5.3 Data acquisition system	97
5.4 The experimental verification of switched capacitor principle	98
5.5 Induction machine experiment	106
5.6 Conclusions	113
6. A fuzzy control strategy for the switched capacitor principle	114
6.1 Fuzzy control	115
6.1.1 Fuzzy sets	116
6.1.2 Linguistic variables	118

6.1.3 Fuzzy controller	121
6.2 Application controller	123
6.3 Conclusions	130
7. Conclusions and further work	132
References	136
Publications	138
Appendix 2.1	A 2.1-1
Appendix 2.2	A 2.2-1
Appendix 2.3	A 2.3-1
Appendix 3.1	A 3.1-1
Appendix 3.2	A 3.2-1
Appendix 4.1	A 4.1-1
Appendix 4.2	A 4.2-1
Appendix 4.3	A 4.3-1
Appendix 5.1	A 5.1-1
Appendix 5.2	A 5.2-1
Appendix 5.3	A 5.3-1
Appendix 6.1	A 6.1-1

List of symbols and abbreviations

- $A_0, A_n, C_0, C_n, S_0, S_n$ - Fourier coefficients;
 C_e - emulated capacitor;
 C_{eff} - effective capacitor;
 C_r - inserted capacitor;
 $\cos \varphi_1$ - power factor;
 d - duty ratio;
 d and q – direct and quadrature axis of the two-axis model(chapter 2);
 D_w - damping constant;
DFM - doubly fed induction machine;
 e - error;
 E - DC power supply;
 E_r - air gap voltage;
 EV - equivalent DC power supply;
 Δe - change of error;
 f_s - switching frequency;
 f_{sam} - sampling frequency;
 g - gyration resistance;
 \tilde{i} - averaged value of the current over a switching period;
 I_{aux} - auxiliary current;
 i_d - desired current;
 i_i - input current;
 I_m - current amplitude;
 \bar{i}_r - space phasor of the rotor current in a reference frame fixed to the rotor circuit;
 \bar{i}'_r - space phasor of the rotor current in a reference frame fixed to the stator;
 i_{ra}, i_{rb}, i_{rc} - rotor currents;
 i_{rx}, i_{ry} - direct and quadrature components of \bar{i}_{rg} ;
 \bar{i}_s - space phasor of the stator current in a reference frame fixed to the stator circuit;
 \bar{i}'_s - space phasor of the stator current in a general reference frame;
 $|\bar{i}_s|, |\bar{i}_r|, |\bar{u}_s|, |\bar{u}_r|$ - modulus of the stator current, rotor current, stator voltage and rotor voltage space phasors;
 i_{sa}, i_{sb}, i_{sc} - stator currents;
 $\bar{i}_{sg}, \bar{i}'_{rg}$ - space phasors of the stator and rotor currents in a reference frame fixed to the stator circuit;
 i_{sx}, i_{sy} - direct and quadrature components of \bar{i}_{sg} ;
 i_o - output current;
 J - inertia of the rotor;

- L - inductance;
 L_m - three phase magnetising inductance;
 L_s - stator self inductance per phase;
 L_{sl} - leakage inductance of the stator;
 L_r - rotor self inductance per phase;
 L_{rl} - leakage inductance of the rotor;
 LFR - loss free resistor;
 LX - set of linguistic values;
 M_x - semantic function;
 N - rotor speed;
 N_s - synchronous speed of the induction machine;
 N_{se} - number of effective stator turns of an induction machine;
 N_{re} - number of effective rotor turns of an induction machine;
 NB, NM, NS - negative big, negative medium and negative small linguistic values;
 p - number of pole pairs;

 P - active power;
 P_{cu} - total copper losses in the induction machine;
 P_{cur} - copper losses in the rotor circuit;
 P_i - input power;
 P_M - mechanical power;

 P_o - output power;
 PB, PM, PS - positive big, positive medium and positive small linguistic values;
 PWM - pulse width modulation;
 Q - reactive power;
 Δq - charge variation;
 R - resistance;
 R_r - rotor resistance per phase;
 R_s - stator resistance per phase;
 s - slip;
 S - apparent complex power;
 S_1, S_2, S_3, S_4 - bi-directional switches;
 T - supply period;
 t_1 - time interval when a switch is ON;
 t_2 - time interval when a switch is OFF;
 t_e - electromagnetic torque;
 t_l - load torque;
 T_s - switching period;
 TVG - time variant gyrator;
 TVT - time variant transformer;

- \bar{u} - averaged value of the voltage over a switching period;
- \bar{u}_c - space phasor of capacitor voltage in a reference frame fixed to the rotor;
- u_{ca}, u_{cb}, u_{cc} - voltages across the capacitors inserted in the rotor circuit;
- \bar{u}_{cg} - space phasor of capacitor voltage in a general reference frame;
- u_{cx}, u_{cy} - direct and quadrature components of \bar{u}_{cg} ;
- U_m - voltage amplitude;
- \bar{u}_r - space phasor of the rotor voltage in a reference frame fixed to the rotor circuit;
- \bar{u}'_r - space phasor of the rotor voltage in a reference frame fixed to the stator circuit;
- u_{ra}, u_{rb}, u_{rc} - input rotor voltages;
- u_{rx}, u_{ry} - direct and quadrature components of \bar{u}_{rg} ;
- \bar{u}_s - space phasor of the stator voltage in a reference frame fixed to the stator circuit;
- \bar{u}'_s - space phasor of the stator voltage in a reference frame fixed to the rotor;
- u_{sa}, u_{sb}, u_{sc} - input stator voltages;
- $\bar{u}_{sg}, \bar{u}_{rg}$ - space phasors of the stator and rotor voltages in a general reference frame;
- u_{sx}, u_{sy} - direct and quadrature components of \bar{u}_{sg} ;
- \bar{v} - space phasor of v_a, v_b, v_c in a stationary reference frame;
- v_a, v_b, v_c - sinusoidal variables;
- V_{br} - output bridge voltage;
- V_{cap} - capacitor voltage;
- \bar{v}_g - space phasor of v_a, v_b, v_c in a general reference frame;
- v_i - input voltage;
- v_o - output voltage;
- V_{ref} - reference voltage;
- Z_{11} - input impedance;
- Z_{12} - reverse transfer impedance;
- Z_{21} - forward transfer impedance;
- Z_{22} - output impedance;
- Z_e - equivalent impedance;
- Z_i - input impedance;
- Z_l - load impedance;
- Z_o - output impedance;
- ZO - zero linguistic value of a fuzzy variable;
- X - symbolic name;

- α - phase angle produce by an RL circuit;
- α_s - phase angle of a space phasor \bar{v} ;
- β - phase angle produce by a RC circuit;
- η - efficiency;
- φ - the desired phase angle;

- μ - membership function;
- μ_C - clipped membership function;
- θ_g - space phasor angle of the general reference frame;
- ω - angular velocity of an AC circuit;
- ω_1 - angular velocity from the stator circuit;
- ω_2 - angular velocity from the rotor circuit;
- ω_g - angular speed of a general reference frame;
- ω_r - angular speed of the rotor circuit;
- Ω_r - rotor angular speed;
- $\bar{\psi}_s$ - space phasor of the stator flux in a reference frame fixed to the stator circuit;
- $\psi_{sa}, \psi_{sb}, \psi_{sc}$ - instantaneous values of the stator linkage flux;
- $\bar{\psi}_{sg}, \bar{\psi}_{rg}$ - space phasors of the stator and rotor fluxes in a general reference frame;
- $\bar{\psi}_r$ - space phasor of the rotor flux in a reference frame fixed to the rotor circuit;
- ζ - phase angle between the space phasors or the stator and rotor currents;
- \aleph - physical domain of a fuzzy variable;

Chapter 1

INTRODUCTION

The induction machine is widely used in industrial and domestic applications. The range of power varies between hundreds of watts to megawatts, depending upon the application. For domestic applications, the single phase induction motor is a common choice. The single phase induction motor is essentially a two phase machine with one winding in series with a capacitor to give the required phase shift. For industrial medium power applications a three phase squirrel-cage motor is preferred. These motors are relatively low cost and robust. In higher power applications, eg pumps and cranes, the wound rotor type of the induction machine is often used. Compared to the squirrel-cage machine the wound rotor motor is more expensive and with slip rings and carbon brushes on the shaft, is not as maintenance free as the squirrel cage machine.

Before the advent of power electronic control and variable frequency output inverters, the squirrel-cage induction motor was considered to be a near-constant speed machine. For modifying the synchronous speed and hence the operational speed, pole changing was the common technique used. The wound rotor motor permits the connection of external impedance which modifies the torque-speed characteristics and offers a degree of speed control. Other possibilities are the doubly-fed machine in which the rotor slip rings are connected to a second supply and the cascading of two machines by connecting the slip-rings of one machine to the stator of the second machine. Slip energy recovery schemes such as the Kramer, Scherbius or LeBlanc systems give efficient speed control. These complex schemes are expensive. The modification of the rotor impedance, due to the low rotor frequency, is mainly achieved with additional resistance and is inefficient due to losses in the added and rotor resistance. Speed variation in this case is dependent on the load torque. Constant torque drives are good examples of such applications.

The development of the static converters made possible the implementation of variable frequency and voltage power supplies. Considerable work has been done in developing new stator control strategies that offer better control properties and high efficiency. The

complexity of such drives increases with tighter performance specifications on accuracy, response time, speed range, etc. Apart from the complexity, the major disadvantage of these solid state drives are their relatively higher cost, especially at high power levels, as well as the harmonic distortion induced in the supply and the motor currents.

At present wound rotor motors still find applications in drives with high inertia loads like the pumping of water, oil and petroleum . In these applications, due to the high power levels, consideration of losses is of paramount importance. Of the two main methods, slip energy recovery offers the highest efficiencies. Rotor impedance modification is used mainly to increase starting torque. The slip power recovery method has its own inherent drawbacks like the necessity of auxiliary machines or frequency converters, rotor position sensing and instability problems at certain frequencies. These drawbacks have attracted the attention of many investigators.

For example, in [1], W. Cheng starts from the idea that vector or field control of a doubly fed induction machine without a shaft position sensor is more complicated than that of a singly-excited cage rotor machine. He tries to eliminate this drawback by the use of a control strategy to realise torque and reactive power control using a position sensorless scheme in which the torque angle is estimated from the rotor voltages and currents, plus the rotor reactance. He claims that in this way the cost is reduced and reliability is enhanced by the calculation of torque angle by a microprocessor or a PC.. He concludes that the torque angle can be estimated satisfactorily and that it contains information of the rotor mechanical speed and angle but there are problems at very low rotor frequencies or whenever the load torque is very light.

M. Ioannides approaches in [2] the problem of a generalised method for predicting the optimised performance of the doubly fed induction machine (DFM) at any load condition – in which torque depends on speed. The model of an optimally controlled DFM is deduced in the paper. The equations describing this model are expressed as functions of the voltage applied to the rotor. This voltage is analysed in direct and quadrature axis components giving a considerable simplification of the analysis. Each one of the electromagnetic characteristics of the optimally controlled DFM , such as

current, torque, power factor, losses, efficiency etc., are deduced as combination of one of the following pairs: magnitude of the rotor voltage and slip; magnitude of the direct component of the rotor voltage and slip; magnitude of the quadrature component of the rotor voltage and slip. M Ioannides concludes, as a result of the simulation and experimental results, that the model is ideal for the prediction of the performance of the machine in the steady state when it is used in a closed loop control system.

In the last decade, there have been some attempts to analyse and produce a rotor control technique that avoids double feeding and the associated disadvantages. The present work is based on modifying the rotor impedance, but instead of adding resistance, a capacitance is used to change the rotor circuit.

In [3] Y. Baghouz and O.T. Tan propose a method to improve the efficiency of a variable –speed induction motor drive with rotor resistance control by inserting external variable capacitors and inductive reactance in series with the external rotor resistance.

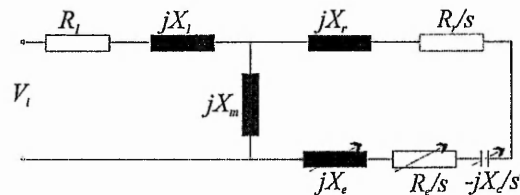
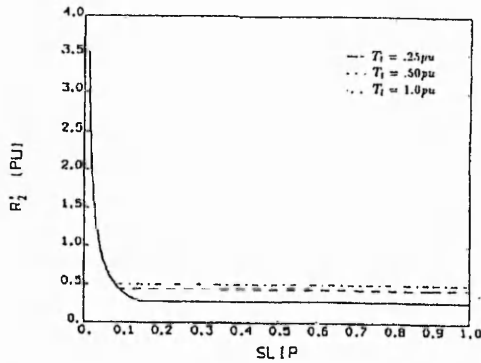
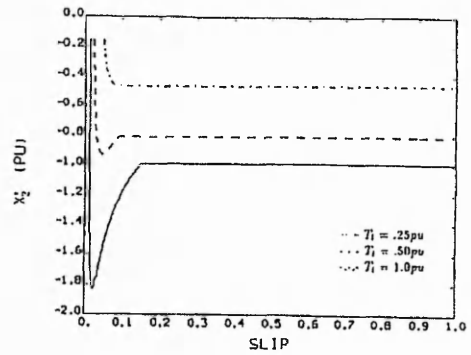
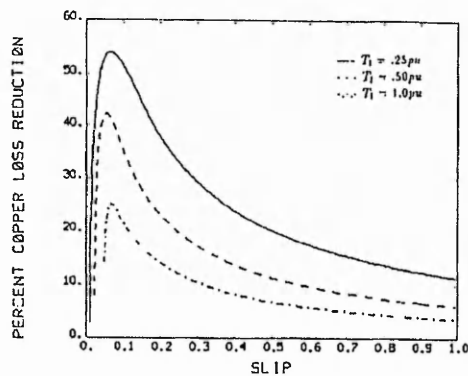


Fig. 1.3 – Lumped parameter equivalent circuit of the induction machine with external modified rotor impedance

The authors claim a reduction of the copper losses due to the improvement in the power factor of the rotor circuit. They present an algorithm to minimize the total copper losses using the conventional wound-rotor induction motor model. Their simulation results (fig 1.4) show a reduction of copper loss as a function of slip. For constant-torque loads, the percentage reduction in copper losses peaks at the lower values of slip, whereas for fan-type loads the most significant percentage copper loss reduction occurs at both the higher and the lower slip values. Also, it is proved that the acceleration of the rotor in start-up or a sudden change in the speed setting is considerably greater than the acceleration when a pure rotor resistance is added.

Fig.1.4 a PU rotor resistance /slipFig.1.4 b PU rotor reactance /slipFig 1.4 c PU copper losses/slip

Although authors do not specify clearly the capacitor values used in simulation, it can be deduced that there are situations (especially, for light loads) when the capacitance required exceeds 1 Farad (Fig. 1.4). Also, Baghouz and Tan mention that their capacitance is a bank that can only be switched in 9 discrete steps. They underline the necessity of developing a system of solid state devices to smoothly control the external rotor impedance.

In [4] Reinert shows the possibility of obtaining various torque-speed characteristics for a wound-induction motor by operating the motor with its rotor at resonance with resultant high starting and braking torques. The paper proposes an approach in which the induction motor can keep its natural shunt-characteristic over the whole speed range, which means that by considerable load changes give minimal slip changes, Reinert claims that the speed-torque characteristic obtained by varying the rotor impedance

suggests that the machine would act as a filter to the power supply and, therefore, the machine can be used with non-sinusoidal supply voltages.

Reinert starts from the idea that the maximum torque is obtained when the rotor resistance is approximately equal to the slip times the rotor reactance, i.e.: $R_r = sX_r$. This condition can be achieved either by increasing the rotor resistance (this imposes a limit to the rotor current) or by reducing the inductive reactance by the addition capacitive reactance. The experimental results were obtained by gradually reducing the supply voltage until the minimum voltage needed to hold the torque at the desired value (in the new configuration with capacitance) was achieved. The strategy was based on the fact that the maximum torque at any speed is proportional to the square root of the input voltage to the machine. This can be achieved by lowering the input voltage while holding the output torque at a specific value.

The simulation and experimental results show that large values of capacitance are required and, therefore, it is necessary to introduce a variable inductor to reduce the size of the capacitor required and, also, to implement a great flexibility of the system.

Salama extends in [5] the work of [3] by optimizing external rotor circuit parameters. Variable voltage and frequency stator supplies are introduced. The motor under test is considered to be operating on a variable frequency supply while delivering a torque near to the value obtained at full-load-slip at rated frequency. The variable-frequency source maintains constant air-gap flux at all frequencies. The author uses the results to conceive a design criteria to achieve the control strategy by a power electronic system.

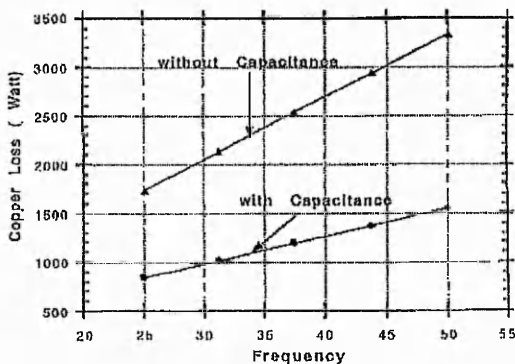


Fig. 1.5(a) Copper loss / frequency

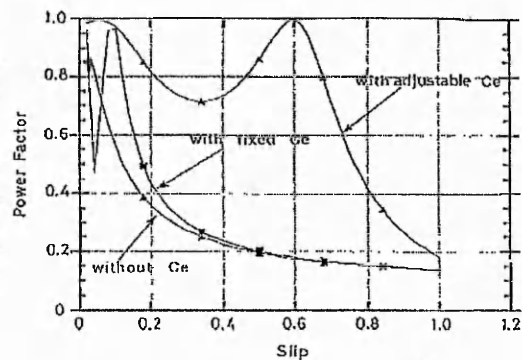


Fig. 1.5(b) Power factor / slip

A continuous current tuned-circuit analysis is used to provide the optimization data and, in this way, to deduce the values of capacitance for optimal performance. The

capacitance values are translated into a relationship between the induced emf and the rotor current. The paper mentions that the required capacitance values are often impractically large and no viable method is specified to implement such big values. The authors calculate some steady-performances of the machine for capacitor of either a fixed or a continually adjustable value with respect to the rotor (Fig. 1.5).

The main drawbacks of the proposed methods in references [3], [4], [5] are:

1. To determine the required value of capacitance, the rotor speed or the e.m.f. induced in the rotor circuit is required.
2. The capacitor values required are very high, in Farads, and are not practical. This be to achieved by the parallel connection of several capacitors, leading to a bulky and costly solution, or by using a step-up transformer. Also, to optimise the machine performance as a function of the load it is necessary to modify the capacitor value dynamically.

A capacitor is also used to enhance the performance of a single phase induction motor which has two phases designed to operate in quadrature. Quadrature fluxes are produced by connecting a capacitor in series with one of the windings. Appropriate choice of capacitance can optimise performance. The capacitor is important both at starting and in steady-state. The main problem is in the choice of the capacitor. The capacitor size must carefully determined according to the terminal impedance and from the fact that two different values of the capacitor are required for starting and steady state running. The capacitor used in the steady state is between five and ten times as small as the capacitor used for starting. The difference between these two values results in the use of two different capacitors, the large value is placed in series with the auxiliary winding during starting and the small one is switched in the circuit when the machine reaches full speed. At the instant of switching in the small capacitor, the large capacitor is switched out of circuit.

The authors of [6], [7], [8] proposed methods of avoiding the use of two capacitors in the auxiliary winding and they have generally succeeded. The approaches used in these papers are similar but there is a significant difference. T.A.Lettenmaier emulates the starting and running capacitor using a DC capacitor placed in a H bridge with uni-directional switches, while T.H.Liu and E.Muljadi use an AC capacitor equal, in value,

with the capacitor required for steady-state operation periodically short-circuited during starting by a switch placed in parallel with it. Both principles will be analysed in chapter 3.

T.A.Lettenmaier claims that the single phase machine develops better performance in his configuration than in the standard configuration with AC capacitors. Both, T.H.Liu and E.Muljadi, state that starting performances obtained using their method are very close to the performance of the single phase machine with a starting-capacitor. Liu presents optimisation algorithms, which obtain a maximum starting torque by electronically adjusting the value of the appropriate capacitor. Also, they expect the reliability of their method to be higher than the traditional one in which the centrifugal switch is the component most prone to failure due to arcing.

The main disadvantage is the current deformation in the auxiliary winding.

The objective of the thesis

Based on background reading [3-5], the following objectives were set:

- to extend the theoretical investigation into the influence on the induction machine performance due to the insertion of capacitor in the rotor circuit.
- to develop a method of producing effects of high valued capacitor in a low frequency, high powered RL circuit.
- to verify this method experimentally.
- to test it in the rotor circuit of an induction machine.

Outline of the thesis

The objective was fulfilled as follows:

Chapter 2 presents the mathematical model of the induction machine with externally modified rotor impedance by inserting capacitors. A novel algorithm to estimate the required capacitance for performance improvement and an algorithm to evaluate the performance as a function of the inserted capacitance are presented.

Chapter 3 reviews the potential methods of emulating the high values of capacitance and their practical viability.

Chapter 4 introduces a method of capacitor switching which is widely used in microelectronics to emulate resistors. Further, in the chapter, the method is extended to a novel application of controlling the phase angle of the current in a low frequency, high powered inductive circuit. The resulting system is simulated.

Chapter 5 presents practical implementation of the system and the experimental verification of the novel application. The new system is placed in the rotor circuit of a small induction motor and the effect on the performance is analysed.

Chapter 6 describes a control strategy, based on fuzzy theory, of the phase angle of a power RL circuit. Experimental tests are performed.

Chapter 7 concludes the achievements of this work and makes suggestions for further work.

Chapter 2

THE ANALYSIS OF THE INDUCTION MOTOR WITH EXTERNALLY VARIED ROTOR IMPEDANCE

Abstract: The mathematical analysis of the both motors: short-circuited rotor and with externally modified rotor impedance is introduced. A set of equations that predicts the dynamic behavior and the performances is deduced. Simulation results for 3 different induction motors are presented.

The referenced papers [3,4,5] do not tackle the complete mathematical modelling of the induction motor with variable rotor impedance for performance prediction. Baghouz[3] and Salama[5] used a relation that estimates the steady state evolution of the copper losses of an induction motor that has the rotor impedance externally modified by the insertion of a variable capacitor. The output of this relation is obviously the copper losses whilst the inputs are the motor parameters, the load torque and the rotor speed. Reinert[4] deduced a formula that evaluates the influence of the inserted capacitor over the speed-torque characteristic. The author considers in his analysis, that besides measurement of the motor parameters, the e.m.f. induced in the rotor as also measured.

In this chapter, a set of equations capable of evaluating the performance (efficiency, power factor, copper losses, starting and peak torque, etc.) of the induction motor in both configurations: short circuited rotor and with modified rotor impedance are presented. This analysis is based on space vector theory applied to the induction motor and a few drawbacks of the methods presented in [3,4,5] are overcome.

2.1 Brief presentation of the space phasors

Phasor theory and the space vector basics of the induction motor are given in reference [9]. A summary of space phasors is made in the following section.

Three variables v_a , v_b and v_c are defined in a stationary reference frame. If v_b is multiplied by a and v_c by a^2 , where $a=e^{j*2*\pi/3}$ and the products are added :

$$\bar{v} = \frac{2}{3}(v_a(t) + v_b(t)^* a + v_c(t)^* a^2) = |\bar{v}|e^{j\alpha_s} = v_d + jv_q \quad (2.1)$$

Where \bar{v} is called the space phasor of v_a, v_b and v_c and $|\bar{v}|, \alpha_s$ are the modulus and the phase angle respectively related to the real axis of the stationary reference frame. The space phasor \bar{v} has real and imaginary components which are given by the formulae:

$$\begin{aligned} v_d &= \frac{2}{3}\left(v_a - \frac{1}{2}v_b - \frac{1}{2}v_c\right) \\ v_q &= \frac{2}{3}(v_b - v_c) \end{aligned} \quad (2.2)$$

where d and q are the conventional direct and quadrature axes of a two-axis model.

If v_a, v_b and v_c are symmetrical and balanced, the tip of \bar{v} will describe a circle, if otherwise, an ellipse will be described.

If v_a, v_b and v_c have the expressions:

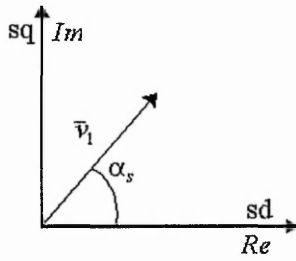
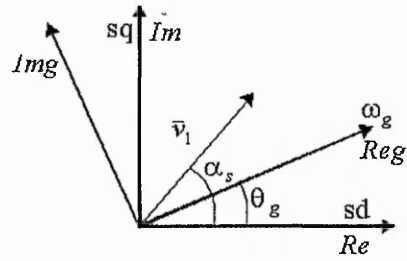
$$\begin{aligned} v_a &= V \cos(\omega t + \delta) \\ v_b &= V \cos(\omega t + \delta - 2\pi/3) \\ v_c &= V \cos(\omega t + \delta + 2\pi/3) \end{aligned} \quad (2.3)$$

where ω is constant, then the space phasor of v_a, v_b and v_c will be of the form:

$$\bar{v} = V e^{j(\omega t + \delta)} \quad (2.4)$$

In figure 2.1a the space phasor \bar{v} is represented in a fixed reference frame and $\alpha_s = \omega t + \delta$. Then, in fig. 2.1b, a frame is considered as a general reference frame that is spinning with the angular speed ω_g ($\theta_g = \omega_g t$) with respect to stationary reference frame. The space phasor of v_a, v_b and v_c expressed in the new reference frame is \bar{v}_g :

$$\bar{v}_g = |\bar{v}| e^{j(\alpha_s - \theta_g)} = \bar{v} e^{-j\omega_g t} \quad (2.5)$$

Fig. 2.1a – Fixed reference frameFig. 2.1b – General reference frame

Equation (2.5) defines the connection between the space phasors of the same components expressed in a different reference frame.

2.2 Dynamic model of the induction motor

In [9] the mathematical model of the induction motor is presented with the following assumptions : that the stator and rotor are cylindrical with a smooth air gap with symmetrical three-phase windings displaced by 120° electrical degrees. In this analysis the magnetic circuit is assumed to be infinitely permeable, the flux density is assumed to be radial in the air gap and the effect of iron losses and end-effects are neglected. The number of effective stator turns, N_{se} , and effective rotor turns N_{re} are equal. The stator winding voltages are:

$$\begin{aligned} u_{sa} &= R_s i_{sa} + \frac{d\psi_{sa}}{dt} \\ u_{sb} &= R_s i_{sb} + \frac{d\psi_{sb}}{dt} \\ u_{sc} &= R_s i_{sc} + \frac{d\psi_{sc}}{dt} \end{aligned}$$

where u_{sa}, u_{sb}, u_{sc} are the input stator voltages, i_{sa}, i_{sb}, i_{sc} are the stator currents, R_s is the stator resistance per phase, $\psi_{sa}, \psi_{sb}, \psi_{sc}$ are the instantaneous values of the stator flux linkages of each of the three phases.

Starting from this system, it is possible to write the space phasor equation that characterises the stator circuit in a reference frame fixed to the stator (stator reference frame):

$$\bar{u}_s = R_s \bar{i}_s + \frac{d\bar{\psi}_s}{dt} = R_s \bar{i}_s + L_s \frac{d\bar{i}_s}{dt} + L_m \frac{d\bar{i}_r}{dt} \quad (2.6)$$

where $\bar{u}_s, \bar{i}_s, \bar{\psi}_s, \bar{i}_r$ are the space phasors in the given reference frame of stator voltage, stator current, stator flux and rotor current ; L_s and L_m are the stator self inductance per phase and three phase magnetising inductance respectively.

Similarly for the rotor circuit in a reference frame fixed to the rotor (rotor reference frame):

$$\bar{u}_r = R_r \bar{i}_r + \frac{d\bar{\psi}_r}{dt} = R_r \bar{i}_r + L_r \frac{d\bar{i}_r}{dt} + L_m \frac{d\bar{i}_s}{dt} \quad (2.7)$$

where R_r is the rotor resistance per phase, L_r is the rotor self inductance per phase $\bar{u}_r, \bar{i}_r, \bar{\psi}_r, \bar{i}_s$ are the space phasors in the given reference frame of rotor voltage, rotor current, rotor flux and stator current.

Equations (2.6) and (2.7) are written in the stator reference frame and in the rotor reference frame respectively. These equations are rewritten in a common reference frame and, in this way, it will be possible to describe the behavior of the motor. To transform from one reference frame to another, equation (2.5) is used to give :

$$\begin{aligned} \bar{u}_{sg} &= R_s \bar{i}_{sg} + L_s \frac{d\bar{i}_{sg}}{dt} + L_m \frac{d\bar{i}_{rg}}{dt} + j\omega_g (L_s \bar{i}_{sg} + L_m \bar{i}_{rg}) \\ \bar{u}_{rg} &= R_r \bar{i}_{rg} + L_r \frac{d\bar{i}_{rg}}{dt} + L_m \frac{d\bar{i}_{sg}}{dt} + j(\omega_g - \omega_r)(L_m \bar{i}_{sg} + L_r \bar{i}_{rg}) \end{aligned} \quad (2.8)$$

where ω_g is the angular velocity of the spinning general reference frame, ω_r is the angular speed of the rotor; all the space phasors are represented with respect to the general reference frame.

Also from [9], the system defined in equation (2.8) is completed with the mechanical equation of motion :

$$t_e - t_l = J \frac{d\omega_r}{dt} + D_w \omega_r \quad (2.9)$$

where t_e is the electromagnetic torque produced by motor(Nm), t_l is the load torque (Nm), J is the inertia of the motor (kgm^2) and D_w is damping constant -representing the dissipation of energy due to windage and friction.

Equations (2.8) and (2.9) along with torque expression:

$$t_e = \frac{3}{2} p \bar{\psi}_{sg} \times \bar{i}_{sg} = -\frac{3}{2} p \bar{\psi}_{rg} \times \bar{i}_{rg} \quad (2.10)$$

describes the behaviour of the induction motor (where p is the number of pole pairs).

The following system is obtained if we split the equations from system (2.8) into the direct and quadrature components and if we operate a few mathematical operations (see Appendix 2.1):

$$\begin{aligned} \frac{di_{sx}}{dt} &= \frac{-R_s L_r i_{sx} + \omega_r L_m^2 i_{sy} + R_r L_m i_{rx} + \omega_r L_m L_r i_{ry} + L_r u_{sx} - L_m u_{rx}}{LD} + \omega_g i_{sy} \\ \frac{di_{yx}}{dt} &= \frac{R_s L_m i_{sx} - \omega_r L_m L_s i_{sy} - R_r L_s i_{rx} - \omega_r L_s L_r i_{ry} - L_m u_{sx} + L_s u_{rx}}{LD} + \omega_g i_{ry} \\ \frac{di_{sy}}{dt} &= \frac{-\omega_r L_m^2 i_{sx} - L_r R_s i_{sy} - \omega_r L_r L_m i_{rx} + L_m R_r i_{ry} + L_r u_{sy} - L_m u_{ry}}{LD} - \omega_g i_{sx} \\ \frac{di_{ry}}{dt} &= \frac{\omega_r L_m L_s i_{sx} + L_m R_s i_{sy} + \omega_r L_r L_s i_{rx} - L_s R_r i_{ry} - L_m u_{sy} + L_s u_{ry}}{LD} - \omega_g i_{sx} \end{aligned} \quad (2.11)$$

where $LD = L_s L_r - L_m^2$.

Equation (2.10) can be rewritten as:

$$t_e = \frac{3}{2} p (L_m \bar{i}_{rg} + L_s \bar{i}_{sg}) \times \bar{i}_{sg} = \frac{3}{2} p L_m \bar{i}_{rg} \times \bar{i}_{sg} = \frac{3}{2} p L_m (i_{rx} i_{sy} - i_{sx} i_{ry}) \quad (2.12a)$$

Equation (2.12a) can be, also, expressed as function of the modulus of both rotor current and stator current space vectors, and the displacement angle ζ between these two vectors:

$$t_e = \frac{3}{2} p L_m |\bar{i}_{rg}| |\bar{i}_{sg}| \sin \zeta \quad (2.12b)$$

Equation (2.9) is brought to the following form:

$$\frac{d\omega_r}{dt} = \frac{t_l - t_e - D_w \omega_r}{J} \quad (2.13)$$

Equations (2.11), (2.12a) and (2.13) form a differential equation system that facilitates the simulation of the dynamic behavior of an induction motor using Runge-Kutta algorithm for solving differential equations.

2.3 Steady state performances of the induction motor

Starting from equation (2.8), stator equation is rewritten in the stator reference frame and the rotor equation written in the rotor reference frame.

$$\bar{u}_s = R_s \bar{i}_s + L_s \frac{d\bar{i}_s}{dt} + L_m \frac{d\bar{i}_r'}{dt} \quad (2.14)$$

$$\bar{u}_r = R_r \bar{i}_r + L_r \frac{d\bar{i}_r}{dt} + L_m \frac{d\bar{i}_s'}{dt} \quad (2.15)$$

The induction motor (without added capacitance) is analyzed in steady state and the rotor supply voltage is zero. This means $|\bar{i}_s|, |\bar{i}_r|$ and ω_r are constant and $|\bar{u}_r| = 0$. D_w is neglected. From (2.14) will result:

$$\begin{aligned} \bar{u}_s &= R_s \bar{i}_s + j\omega_1 L_s \bar{i}_s + j\omega_1 L_m \bar{i}_r' \\ \bar{i}_s &= \frac{\bar{u}_s - j\omega_1 L_m \bar{i}_r'}{R_s + j\omega_1 L_s} \end{aligned} \quad (2.16)$$

From equation (2.15) results :

$$0 = R_r \bar{i}_r + j\omega_2 L_m \bar{i}_s' + j\omega_2 L_r \bar{i}_r \quad (2.17)$$

where ω_1 is the angular velocity from the stator circuit and ω_2 is the angular velocity from the rotor circuit.

Substituting equation (2.16) into (2.17) and introducing space vector transformation from the stator reference frame to the rotor reference gives :

$$\bar{i}_r = \frac{-j\omega_2 L_m \bar{u}_s'}{(R_r R_s + \omega_1 \omega_2 L_m^2 - \omega_1 \omega_2 L_r L_s) + j(\omega_1 L_s R_r + \omega_2 L_r R_s)} \quad (2.18)$$

$$|\bar{i}_r| = \frac{\omega_2 L_m |\bar{u}_s'|}{\sqrt{A\omega_2^2 + B\omega_2 + C}} \quad (2.19)$$

where

$$A = \omega_2^2 L_m^4 + \omega_1^2 L_r^2 L_s^2 - 2\omega_1^2 L_m^2 L_r L_s + L_r^2 R_s^2 = (\omega_1 L_m^2 - \omega_1 L_r L_s)^2 + L_r^2 R_s^2$$

$$B = 2\omega_1 R_r R_s L_m^2$$

$$C = R_r^2 R_s^2 + \omega_1^2 L_s^2 R_r^2$$

The relationship between the copper rotor losses (P_{cur}) and the electromagnetic torque is then used:

$$t_e = \frac{P_{cur}}{\omega_2} = \frac{3}{2} \frac{pR_r |\bar{i}_r|^2}{\omega_2} \rightarrow |\bar{i}_r|^2 = \frac{2}{3} \frac{t_e \omega_2}{pR_r} \quad (2.20)$$

Combining equations (2.19) and (2.20) results in the following second order equation for rotor angular frequency:

$$A\omega_2^2 + (B - D)\omega_2 + C = 0 \quad (2.21)$$

where

$$D = \frac{3}{2} pR_r \frac{\omega_2 L_m^2}{t_e} |\bar{u}_s|$$

If the equation (2.21) has two real positive solutions, the smallest represents the rotor angular velocity, the other one is the equivalent point on the unstable branch of the speed-torque characteristic for the given torque. If there are no positive solutions the load torque is bigger than the peak torque developed by the motor.

Then, using (2.20), it is possible to calculate $|\bar{i}_r|$ and $|\bar{i}_s|$ from equation (2.22):

$$|\bar{i}_s| = \frac{\sqrt{R_r^2 + \omega_2^2 L_r^2}}{\omega_2 L_m} |\bar{i}_r| \quad (2.22)$$

The copper losses are calculated using the expression given in reference [9]:

$$P_{cu} = \frac{3}{2} (R_r |\bar{i}_r|^2 + R_s |\bar{i}_s|^2) \quad (2.23)$$

Considering the expressions of torque:

$$t_e = \frac{3}{2} \frac{pR_r |\bar{i}_r|^2}{\omega_2} \quad (2.24a)$$

or

$$t_e = \frac{3}{2} \frac{p\omega_2 L_m^2 R_r |\bar{i}_s|^2}{R_r^2 + \omega_2^2 L_r^2} \quad (2.24b)$$

and combining (2.23) with (2.24a) or (2.24b), an expression for copper losses as function of angular velocity of the rotor circuit and induction motor parameters results:

$$P_{cu} = \frac{t_e}{p} \left(\omega_2 + \frac{R_s}{R_r} \frac{R_r^2 + \omega_2^2 L_r^2}{\omega_2 L_m^2} \right) \quad (2.25)$$

One of the most important characteristics of the induction motor is the torque-speed characteristic. This characteristic can be drawn from equations (2.19) and (2.20) if the motor parameters are known, giving the expression :

$$t_e = \frac{3}{2} \frac{p R_r \omega_2 L_m^2 |\bar{u}_s'|^2}{A \omega_2^2 + B \omega_2 + C} \quad (2.26)$$

2.3.1. Mechanical power and efficiency

Another two performances of the induction motor can be analysed using the space vector equations of the motor: the efficiency and the power factor.

The expression of the rotor current space vector from equation (2.17) gives:

$$\bar{i}_r = \frac{-j \omega_2 L_m \bar{i}_s'}{R_r + j \omega_2 L_r} \quad (2.27)$$

Similarly using equation (2.16) and making the appropriate space transformations from the rotor reference frame to the stator reference frame gives the space vector of the stator current:

$$\bar{i}_s = \frac{\bar{u}_s (R_r + j \omega_2 L_r)}{V + jW}$$

where:

$$V = R_r R_s + \omega_1 \omega_2 (L_m^2 - L_r L_s)$$

$$W = \omega_1 L_s R_r + \omega_2 L_r R_s$$

The apparent complex power \bar{S} can be expressed in space-vector terms of the stator voltage and of the complex conjugate of the stator current as given in reference[9]:

$$\bar{S} = \frac{3}{2} \bar{u}_s \bar{i}_s^* \quad (2.28)$$

$$\bar{S} = \frac{3}{2} \bar{u}_s \bar{i}_s^* = \frac{3}{2} \frac{|\bar{u}_s|^2 (R_r - j \omega_2 L_r) (V + jW)}{V^2 + W^2}$$

The real component of \bar{S} gives the input active power (P):

$$P = \text{Re}(\bar{S}) = \frac{3}{2} \frac{|\bar{u}_s|^2 (R_r V + \omega_2 L_r W)}{V^2 + W^2} \quad (2.29)$$

The imaginary component of \bar{S} gives the input reactive power (Q):

$$Q = \text{Im}(\bar{S}) = \frac{3}{2} \frac{|\bar{u}_s|^2 (R_r W - \omega_2 L_r V)}{V^2 + W^2} \quad (2.30)$$

The power factor $\cos \phi_1$, is then calculated from the input active and reactive powers using the expression of (2.31):

$$\cos \phi_1 = \frac{P}{\sqrt{P^2 + Q^2}} \quad (2.31)$$

The mechanical power developed by the motor is expressed by:

$$P_M = t_e \Omega_r \quad (2.32)$$

where Ω_r , the rotor angular speed and can be calculated:

$$\Omega_r = \frac{\omega_1 - \omega_2}{p} \quad (2.33)$$

The motor efficiency may be expressed by the ratio between the mechanical power developed by the motor and the active input power (D_w being neglected, P_M is equal with power transmitted to the motor shaft):

$$\eta = \frac{P_M}{P} \quad (2.34)$$

2.4 Dynamic model of the induction motor with variable rotor impedance

In the present section, a set of differential equations that predicts the dynamic behavior of a motor with externally controlled rotor impedance is developed using the space vector model of the induction motor. Starting from this system, the steady state performances of the induction motor with variable rotor impedance will be achieved.

If a capacitor is introduced on each phase of the rotor circuit, each phase of the rotor circuit will have the following configuration:

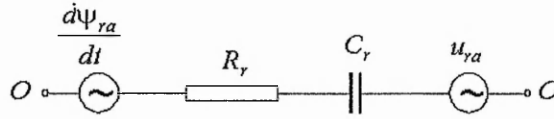


Fig. 2.2 – General configuration of the rotor circuit with modified impedance

The behavior of phase A is described by the following equations:

$$u_{ra} = R_r i_{ra} + \frac{d\psi_{ra}}{dt} + u_{ca}$$

$$\frac{du_{ca}}{dt} = \frac{i_{ra}}{C_r}$$

where u_{ca} is voltage across the capacitor.

Similar equations can be written for each phase of the rotor:

$$u_{rb} = R_r i_{rb} + \frac{d\psi_{rb}}{dt} + u_{cb}$$

$$\frac{du_{cb}}{dt} = \frac{i_{rb}}{C_r}$$

$$u_{rc} = R_r i_{rc} + \frac{d\psi_{rc}}{dt} + u_{cc}$$

$$\frac{du_{cc}}{dt} = \frac{i_{rc}}{C_r}$$

The space vector equations can now be written in a reference frame fixed to the rotor, starting from the above equations :

$$\bar{u}_r = R_r \bar{i}_r + \frac{d\bar{\psi}_r}{dt} + \bar{u}_c$$

$$\frac{d\bar{u}_c}{dt} = \frac{\bar{i}_r}{C_r}$$

Combining with (2.7) results in:

$$\bar{u}_r = R_r \bar{i}_r + L_r \frac{d\bar{i}_r}{dt} + L_m \frac{d\bar{i}_s'}{dt} + \bar{u}_c \quad (2.35)$$

$$\frac{d\bar{u}_c}{dt} = \frac{\bar{i}_r}{C_r} \quad (2.36)$$

The stator circuit equation is not affected by the insertion of capacitors. Considering a general reference frame for equations (2.6), (2.35), (2.36) and using the transformation rules from one reference system to another, results in :

$$\begin{aligned}\bar{u}_{sg} &= R_s \bar{i}_{sg} + L_s \frac{d\bar{i}_{sg}}{dt} + L_m \frac{d\bar{i}_{rg}}{dt} + j\omega_g (L_s \bar{i}_{sg} + L_m \bar{i}_{rg}) \\ \bar{u}_{rg} &= R_r \bar{i}_{rg} + L_r \frac{d\bar{i}_{rg}}{dt} + L_m \frac{d\bar{i}_{sg}}{dt} + j(\omega_g - \omega_r)(L_m \bar{i}_{sg} + L_r \bar{i}_{rg}) + \bar{u}_{cg} \\ \frac{d\bar{u}_{cg}}{dt} &= \frac{\bar{i}_{rg}}{C_r} - j(\omega_g - \omega_r)\bar{u}_{cg}\end{aligned}\quad (2.37)$$

This system in combination with equations (2.12a) and (2.13) describes the behaviour of an induction motor with variable rotor impedance in a general reference frame.

The induction motor will be considered in the stator reference frame (this implies $\omega_g = 0$), with no voltage supplied into motor from the rotor side ($|\bar{u}_r| = 0$), with D_w neglected and a system similar to (2.11) is obtained by splitting the equations (2.37) into the direct and quadrature components

$$\begin{aligned}\frac{di_{sx}}{dt} &= \frac{-R_s L_r i_{sx} + \omega_r L_m^2 i_{sy} + R_r L_m i_{rx} + \omega_r L_m L_r i_{ry} + L_r u_{sx} + L_m u_{cx}}{LD} \\ \frac{di_{rx}}{dt} &= \frac{R_s L_m i_{sx} - \omega_r L_m L_s i_{sy} - R_r L_s i_{rx} - \omega_r L_s L_r i_{ry} - L_m u_{sx} - L_s u_{cx}}{LD} \\ \frac{di_{sy}}{dt} &= \frac{-\omega_r L_m^2 i_{sx} - L_r R_s i_{sy} - \omega_r L_r L_m i_{rx} + L_m R_r i_{ry} + L_r u_{sy} + L_m u_{cy}}{LD} \\ \frac{di_{ry}}{dt} &= \frac{\omega_r L_m L_s i_{sx} + L_m R_s i_{sy} + \omega_r L_r L_s i_{rx} - L_s R_r i_{ry} - L_m u_{sy} - L_s u_{cy}}{LD} \\ \frac{du_{cx}}{dt} &= \frac{i_{rx}}{C_r} - \omega_r u_{cy} \\ \frac{du_{cy}}{dt} &= \frac{i_{ry}}{C_r} + \omega_r u_{cx}\end{aligned}\quad (2.38)$$

where $LD = L_s L_r - L_m^2$.

The expression of the torque equation remains the same and, thus, system (2.38) along with equations (2.12a) and (2.13), offers the possibility to analyze the induction motor with modified rotor impedance in dynamic regime.

2.5 Steady state performances of the induction motor with variable rotor impedance

The equations (2.6) and (2.35) form the basis for the motor model in steady state operation. This means $|\bar{i}_s|$, $|\bar{i}_r|$ and ω_r are constant. Equation (2.6) is then modified to the form:

$$\bar{i}_s = \frac{\bar{u}_s - j\omega_1 L_m \bar{i}_r}{R_s + j\omega_1 L_s} \quad (2.39)$$

The expression is identical with the equation of the induction motor without capacitance.

Equation (2.35) is different from the equivalent equation of the induction motor in standard configuration given in (2.7), resulting in:

$$0 = R_r \bar{i}_r + j\omega_2 L_m \bar{i}_s + j\omega_2 L_r \bar{i}_r + \frac{\bar{i}_r}{j\omega_2 C_r} \quad (2.40)$$

where ω_1 is the stator angular velocity and ω_2 is the rotor angular velocity.

The mathematical combination of (2.39) and (2.40) gives :

$$0 = \left((R_r R_s + \omega_1 \omega_2 L_m^2 - \omega_1 \omega_2 L_s L_r + \frac{\omega_1 L_s}{\omega_2 C_r}) + j(\omega_2 L_s R_r + \omega_2 L_r R_s - \frac{R_s}{\omega_2 C_r}) \right) \bar{i}_r + j\omega_2 L_m \bar{u}_s$$

The modulus of the rotor vector current is obtained from:

$$\bar{i}_r = - \frac{j\omega_2 L_m \bar{u}_s}{(R_r R_s + \omega_1 \omega_2 L_m^2 - \omega_1 \omega_2 L_s L_r + \frac{\omega_1 L_s}{\omega_2 C_r}) + j(\omega_2 L_s R_r + \omega_2 L_r R_s - \frac{R_s}{\omega_2 C_r})}$$

and results in:

$$|\bar{i}_r| = \frac{\omega_2 L_m |\bar{u}_s|}{\sqrt{A_m \omega_2^2 + B_m \omega_2 + C_m + \frac{D_m}{\omega_2^2}}} \quad (2.41)$$

where:

$$A_m = (\omega_1 L_m^2 - \omega_1 L_s L_r)^2 + L_r^2 R_s^2$$

$$B_m = 2\omega_1 R_r R_s L_m^2$$

$$C_m = (R_r R_s)^2 + (\omega_1 L_s R_r)^2 - 2 \frac{\omega_1^2 L_s^2 L_r}{C_r} + 2 \frac{\omega_1^2 L_m^2 L_s}{C_r} - \frac{2L_r R_s^2}{C_r}$$

$$D_m = \left(\frac{\omega_1 L_s}{C_r} \right)^2 + \left(\frac{R_s}{C_r} \right)^2$$

In (2.41) all variables except ω_2 are known, the rotor angular velocity will be determined from the relation between the electromagnetic torque and the rotor current as follows:

$$t_e = \frac{3 p R_r |\bar{i}_r|^2}{2 \omega_2} \quad (2.42)$$

Which results in a the fourth order polynomial in ω_2 :

$$A_m \omega_2^4 + (B_m - E_m) \omega_2^3 + C_m \omega_2^2 + D_m = 0 \quad (2.43)$$

where:

$$E_m = \frac{3 L_m^2 |\bar{u}_s|^2 p R_r}{2 t_e}$$

Equation (2.43) will give the solution of the rotor angular velocity. This equation has maximum 2 real positive solutions as discussed in the following paragraph.

First, equation (2.43) is split in two separate functions:

$$f_1 = A_m \omega_2^4 + (B_m - E_m) \omega_2^3 + C_m \omega_2^2$$

$$f_2 = -D_m$$

It can be seen that, for a given capacitance, f_2 is negative and constant. Function f_1 is variable in ω_2 and its parameters depending on C_r . The intersection points between the graphic representations of f_1 and f_2 represent the solutions of equation (2.43). Also, f_1 could be considered as a combination of the two following second order functions:

$$g_1 = A_m \omega_2^2 + (B_m - E_m) \omega_2 + C_m$$

$$g_2 = \omega_2^2$$

If g_1 and g_2 are regarded just as second order functions (without any implications about the induction motor), it can be noticed that g_2 is a positive parabola depending only on ω_2^2 .

The case when g_1 is positive for the whole range of the rotor angular velocities, is not relevant because the resulting f_1 is positive too. If g_1 has negative values, this implies that equation $g_1 = 0$ has 2 real solutions and there are 3 distinctive cases to be considered:

- Equation $g_1 = 0$ has 2 negative solutions (fig. 3a). This implies that f_1 gets negative values just for negative rotor angular velocities and the intersection points between f_1 and f_2 correspond to negative ω_2 .
- Equation $g_1 = 0$ has one negative and one positive solution (fig. 3b). This means that f_1 is negative for negative and positive values of ω_2 . It is possible that f_1 to intersect f_2 in 4 points corresponding to 2 negative and 2 positive values of ω_2 .
- Equation $g_1 = 0$ has 2 positive solutions (fig. 3c). Function f_1 reaches negative range just for positive values of ω_2 , implying that the intersection of f_1 with f_2 might occur in maximum 2 points.

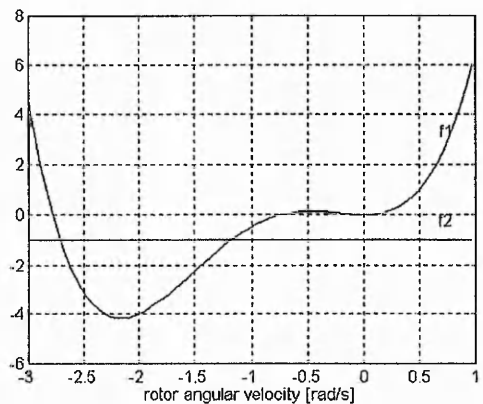
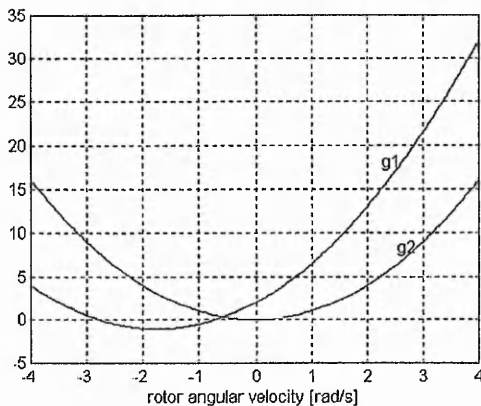


Fig. 3a - Quadratic and Fourth order functions against rotor frequency

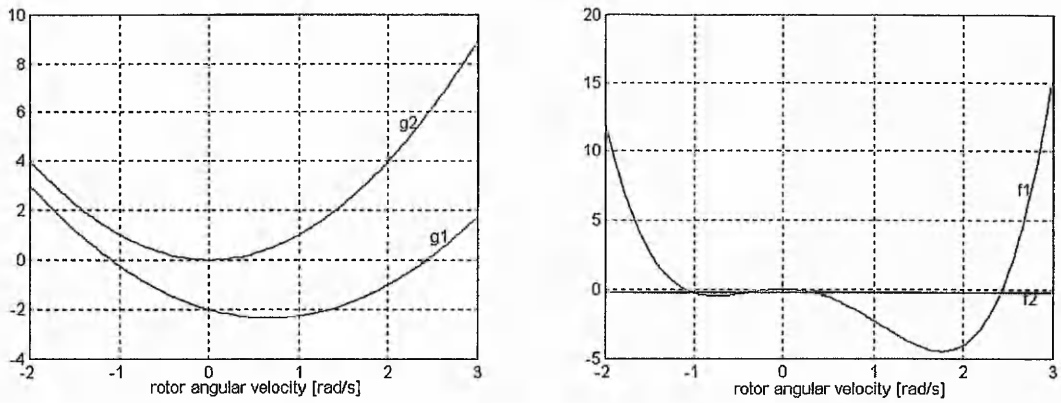


Fig. 3b - Quadratic and Fourth order functions against rotor frequency

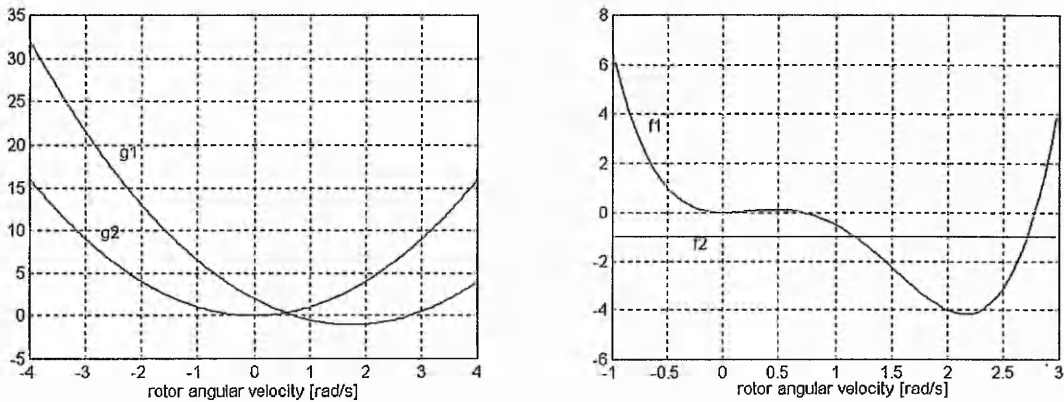


Fig. 3c - Quadratic and Fourth order functions against rotor frequency

The cases 3b and 3c are interesting as potentially real operating conditions of the motor. In these cases (3b, 3c), if two real positive solutions exist, the smallest one is the sought value. The other one is probably the rotor frequency from the unstable branch of the speed-torque diagram. Of course, the real negative solutions (3b) are not taken into account because they might correspond braking operating mode of the induction motor. The case when there is just one positive solution, represents the maximum torque condition.

This is a theoretical analysis. In practice a numerical method or a matrix solution can be used to solve equation (2.43). The matrix method is implemented in MATLAB and is used in future simulations(see appendix 2.2).

Similarly to the solution when the induction motor is in the normal configuration, it is possible to calculate the modulus of the stator vector current:

$$|\bar{i}_s| = \frac{\sqrt{R_r^2 + \omega_2^2 \left(L_r - \frac{1}{\omega_2^2 C_r} \right)^2}}{\omega_2 L_m} |\bar{i}_r| \quad (2.44)$$

Then using the expressions of the electromagnetic torque will be determined the copper losses:

$$P_{cu} = \frac{t_e}{p} \left(\omega_2 + \frac{R_s}{R_r} \frac{R_r^2 + \omega_2^2 \left(L_r - \frac{1}{\omega_2^2 C_r} \right)^2}{\omega_2 L_m^2} \right) \quad (2.45)$$

It is possible to draw the torque-speed diagram using space vector approach, from a knowledge of just the motor parameters. Equation (2.41) will be used for this purpose.

The modulus of rotor current vector is introduced in (2.42):

$$t_e = \frac{3}{2} \frac{p R_r \omega_2^3 L_m^2 |\bar{u}_s|^2}{A_m \omega_2^4 + B_m \omega_2^3 + C_m \omega_2^2 + D_m} \quad (2.46)$$

Similarly to the induction motor in normal configuration, the expression of rotor current space vector is deduced from (2.40):

$$\bar{i}_r = \frac{-j \omega_2 L_m \bar{i}_s}{R_r + j \omega_2 \left(L_r - \frac{1}{\omega_2^2 C_r} \right)}$$

The last expression substituted in (2.39) gives:

$$\bar{i}_s = \frac{\bar{u}_s \left(R_r + j \omega_2 \left(L_r - \frac{1}{\omega_2^2 C_r} \right) \right)}{V_m + j W_m} \quad (2.47)$$

where:

$$V_m = R_s R_r + \omega_1 \omega_2 L_m^2 - \omega_1 \omega_2 L_s \left(L_r - \frac{1}{\omega_2^2 C_r} \right)$$

$$W_m = \omega_1 L_s R_r + \omega_2 R_s \left(L_r - \frac{1}{\omega_2^2 C_r} \right)$$

The input active power is given by:

$$P = \frac{3}{2} \frac{|\bar{u}_s|^2 \left(R_r V_m + \omega_2 W_m \left(L_r - \frac{1}{\omega_2^2 C_r} \right) \right)}{V_m^2 + W_m^2} \quad (2.48)$$

and the input reactive power is given by:

$$Q = \frac{3}{2} \frac{|\bar{u}_s|^2 \left(R_r W_m - V_m \omega_2 \left(L_r - \frac{1}{\omega_2^2 C_r} \right) \right)}{V_m^2 + W_m^2} \quad (2.49)$$

are deduced, starting from the expression of the apparent complex power \bar{S} .

Thus, it is possible to calculate power factor and the motor efficiency using (2.31), respective (2.34).

2.6 Simulation results

Starting from the space vector model of the induction motor, given in the previous sections, expressions that permit the calculation of the speed-torque characteristic, the total copper losses, the efficiency, the power factor of the induction motor in normal (short-circuited rotor) operation and when operating with variable rotor impedance were derived.

The speed-torque characteristic can be analysed using equations (2.26) and (2.46) respectively, where slip s ($\omega_2 = s\omega_1$) is varied between 0 and 1. Reinert[4] makes a similar theoretical analysis using formula:

$$t_e = \frac{E_r^2 R_r (N_s - N)}{k N_s^2 \left[R_r^2 + \left[k(N_s - N) L_r - \frac{1}{k(N_s - N) C_r} \right]^2 \right]} \quad (2.50)$$

where:

N_s - synchronous speed

N - rotor speed

k - constant : $2\pi / 60$

E_r - e.m.f. induced in the rotor circuit

This paper relies on a measured e.m.f. in addition to the motor parameters. In this thesis, this drawback is overcome by the use of equations (2.26) and (2.46) respectively and using the the supply voltage (which can be considered a motor parameter) , instead of the measured e.m.f.

Salama [5] uses the following formula to calculate the losses:

$$P_{cu} = t_e \omega \left(s + \frac{R_s}{X_m} \left(\left(\frac{R_r + R_e}{s} \right) + s \frac{\left(X_m + \omega(L_r + L_e) - \frac{1}{s^2 \omega C_e} \right)^2}{R_r + R_e} \right) \right) \quad (2.51)$$

where

L_r - leakage inductance of rotor referred to the stator;

L_e - external inductance of rotor referred to the stator;

R_e - external rotor resistance referred to the stator;

Equation (2.45) is similar to (2.51). The difference is in the consideration of the slip value: Salama considers slip as measured and, here, the slip is calculated using (2.43) for a given load..

The efficiency and power factor are determined using (2.34) and (2.31) in combination with (2.29) and (2.30) respective (2.48) and (2.49).

Theoretical investigations by simulations were carried out to explore the effect of introducing capacitance in the rotor circuit over motor performances of three motors for which the parameters were known. The details of these motors are given below:

Motor 1:

380V, 50Hz, 4 pole, wound motor 20KW

$$R_s = 1.64\Omega, R_r = 1.45\Omega$$

$$L_{sl} = 3mH, L_{rl} = 3mH, L_m = 163.6mH, J = 0.203kgm^2$$

Motor 2:

220V, 50Hz, 4 pole, wound motor 1KW

$$R_s = 10\Omega, R_r = 6.5\Omega$$

$$L_{sl} = 43.067mH, L_{rl} = 40.107mH, L_m = 421.19mH, J = 0.01kgm^2$$

Motor 3:

460V, 50Hz, 4 pole, wound motor 1MW

$$R_s = 0.04\Omega, R_r = 0.04\Omega$$

$$L_{sl} = 0.1687mH, L_{rl} = 0.1687mH, L_m = 7.3mH, J = 22kgm^2$$

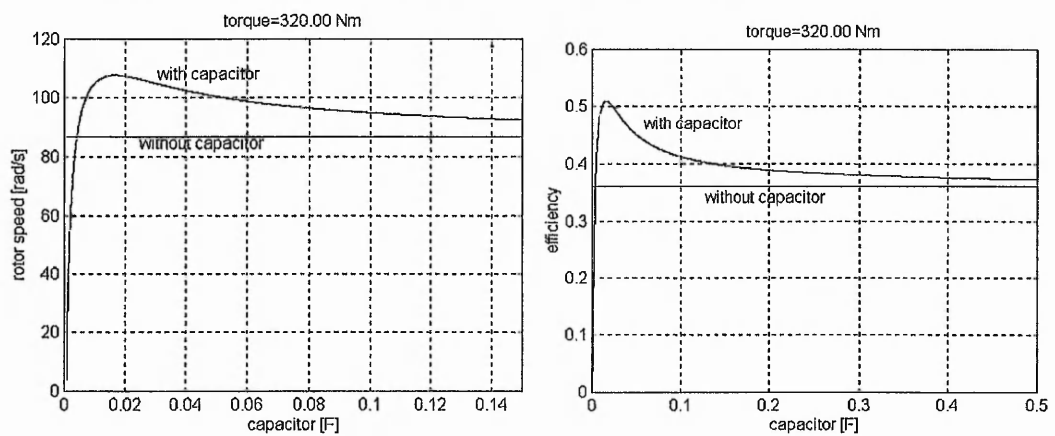
To study the effect of the capacitor insertion in the rotor circuit over the motor performances the following simulation strategy is considered:

- to survey the effect of a variable capacitor over the speed, efficiency, power factor and copper losses at a given torque; for each motor, there are considered 3 different loads from the areas of peak torque, operating torque and small torque.
- to study the steady state response of the motors for a constant capacitor for whole slip range; there are to be considered 3 different capacitors and targeted torque/slip, efficiency/slip, power factor/slip, efficiency/torque and power factor/torque characteristics.
- the possibility to achieve certain slips for different load torques varying the inserted capacitor is undertaken, including the unity slip case that

corresponds to the starting torque.

- the dynamic response of the induction motor with modified rotor impedance to the load torque variation or to the inserted capacitor variation is to be studied.

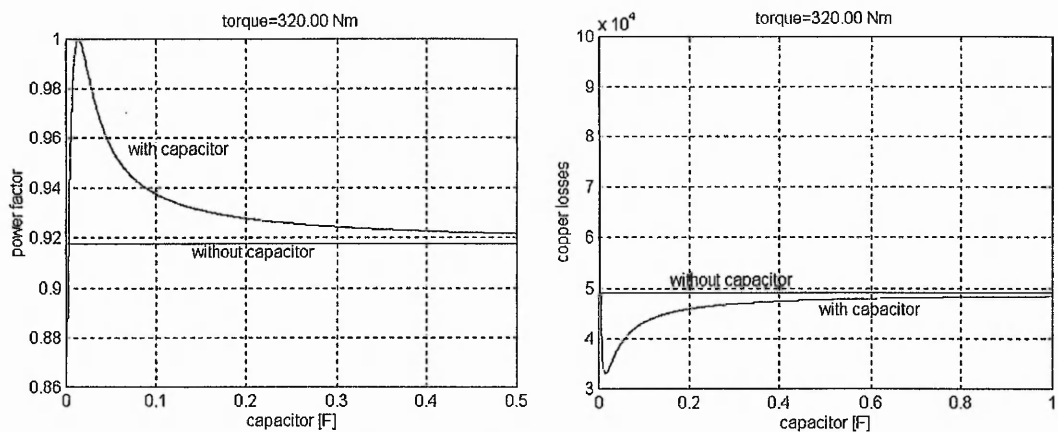
The first set of simulations considers the behavior of the speed, efficiency, power factor and copper losses as a function of added rotor capacitance with load torque remaining constant; the values were chosen from peak, rated and low torque regions. The characteristics were generated using the program pfef.m given in Appendix 2.2 and the results are given in figures 2.4-2.12. The speed, efficiency, power factor and copper losses deduced for short circuited rotor are also shown in the figures.



Constant torque characteristics $T=320\text{Nm}$

a) Rotor speed/Capacitance

b) Efficiency/Capacitance

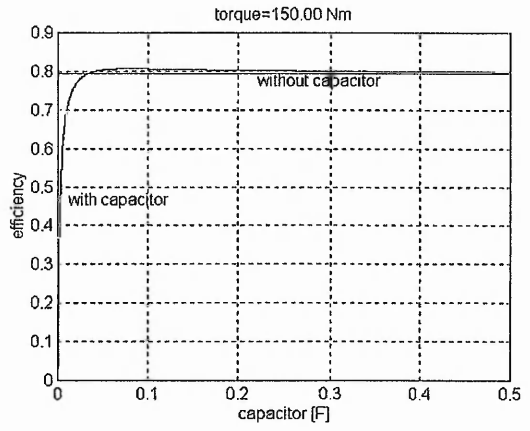
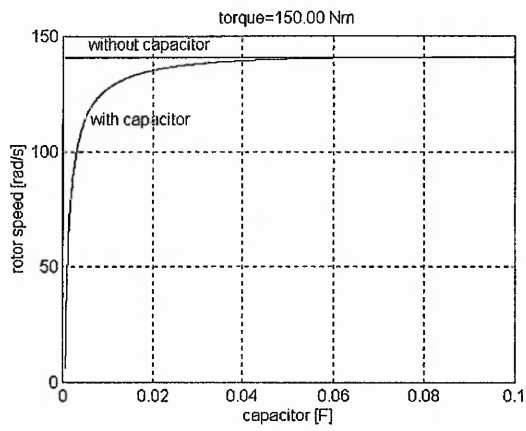


Constant torque characteristic $T=320\text{Nm}$

c) Power factor/Capacitance

d) Copper Losses/Capacitance

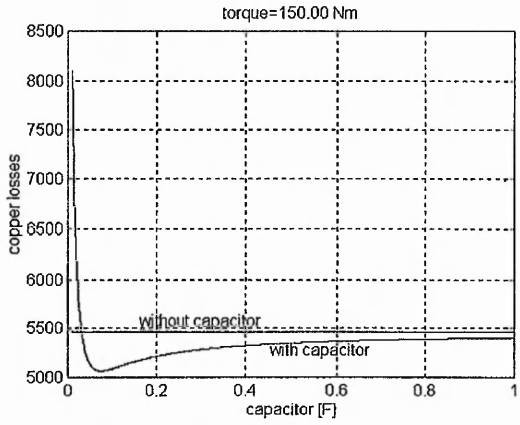
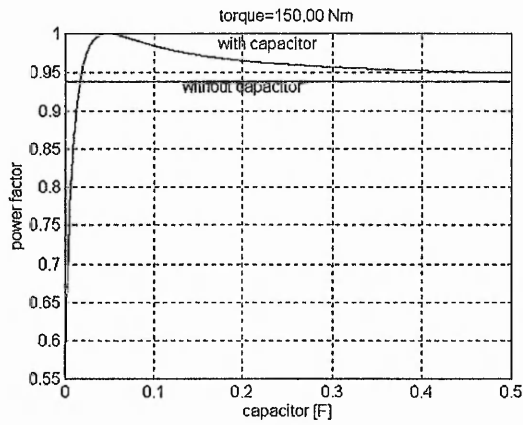
Fig. 2.4 – Motor1 (20KW)



Constant torque characteristics $T=150\text{Nm}$

a) Rotor speed/Capacitance

b) Efficiency/Capacitance

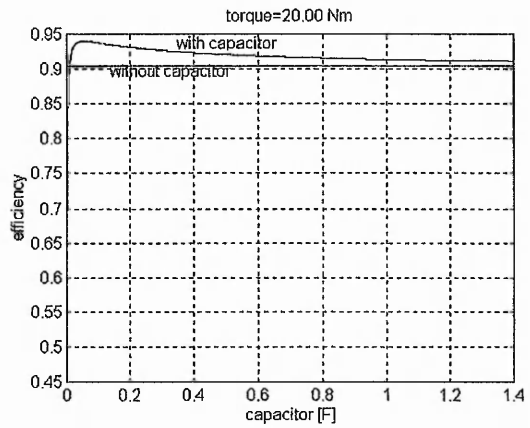
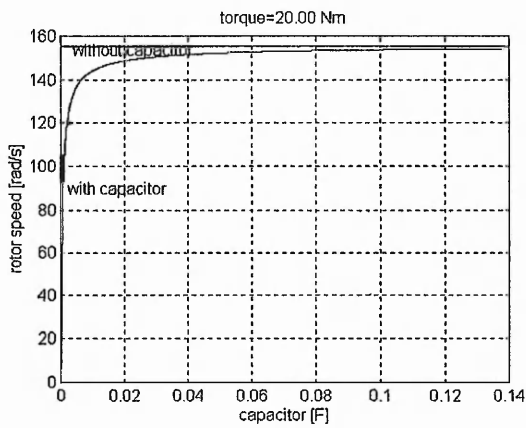


Constant torque characteristic $T=150\text{Nm}$

c) Power factor/Capacitance

d) Copper Losses/Capacitance

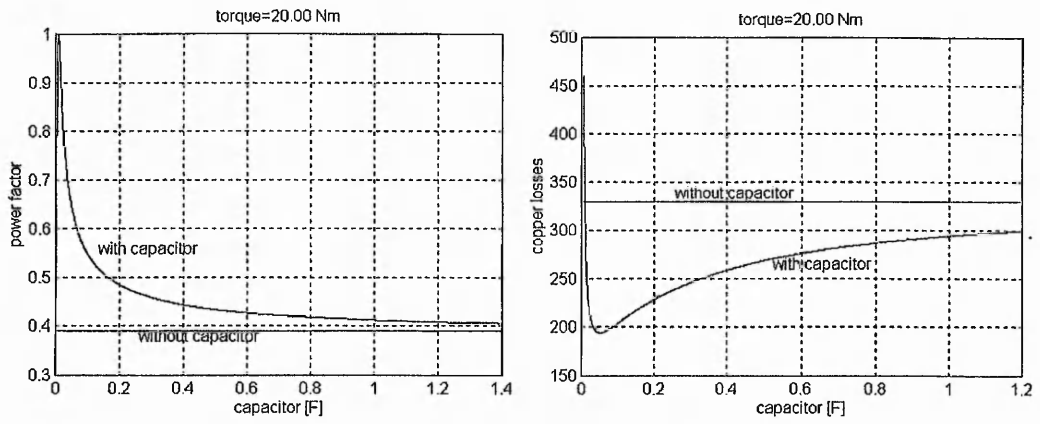
Fig. 2.5 – Motor1 (20KW)



Constant torque characteristics $T=20\text{Nm}$

a) Rotor speed/Capacitance

b) Efficiency/Capacitance

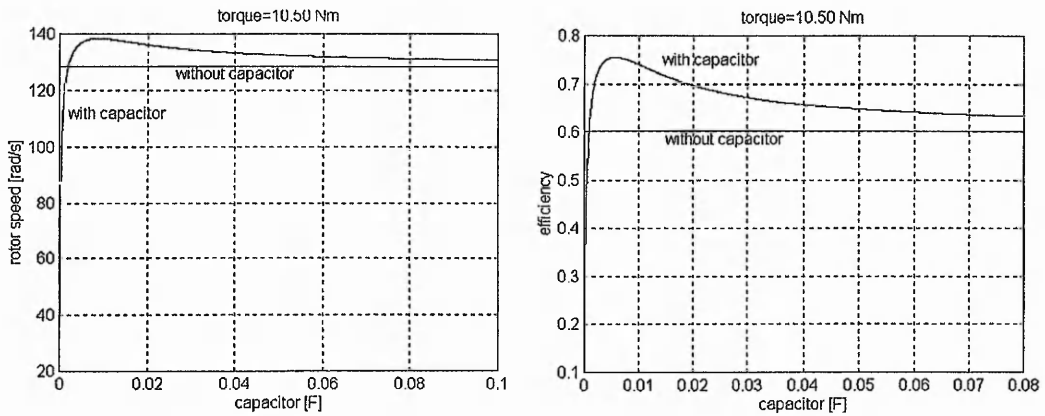


Constant torque characteristic $T=20Nm$

c) Power factor/Capacitance

d) Copper Losses/Capacitance

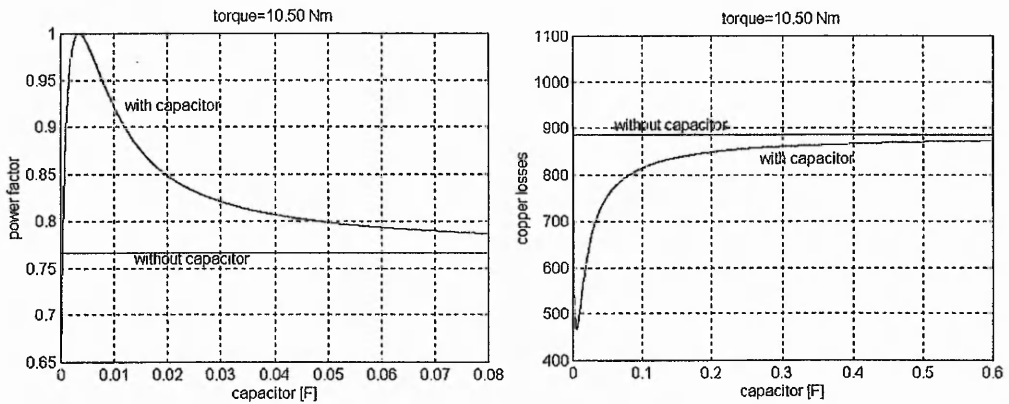
Fig. 2.6 – Motor1 (20KW)



Constant torque characteristics $T=10.5Nm$

a) Rotor speed/Capacitance

b) Efficiency/Capacitance

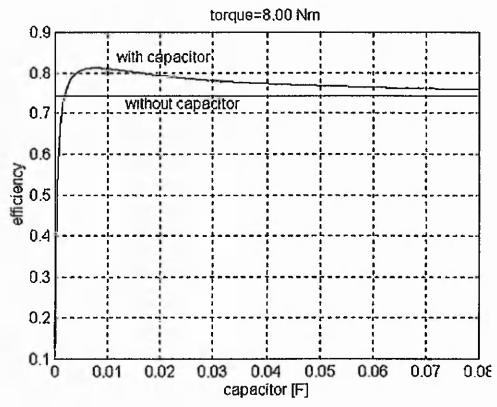
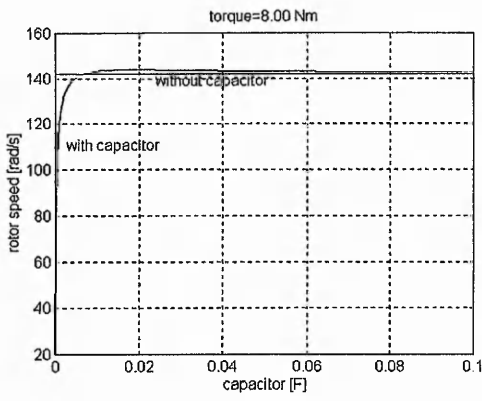


Constant torque characteristic $T=10.5Nm$

c) Power factor/Capacitance

d) Copper Losses/Capacitance

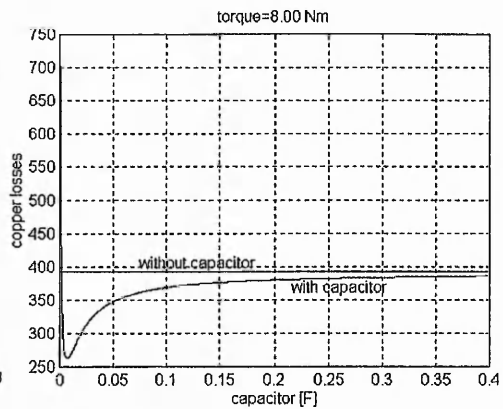
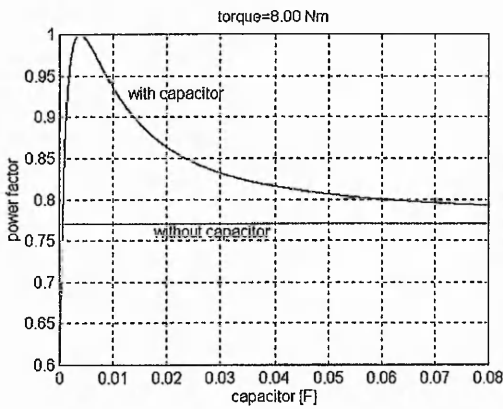
Fig.2.7 – Motor2 (1KW)



Constant torque characteristics $T=8Nm$

a) Rotor speed/Capacitance

b) Efficiency/Capacitance

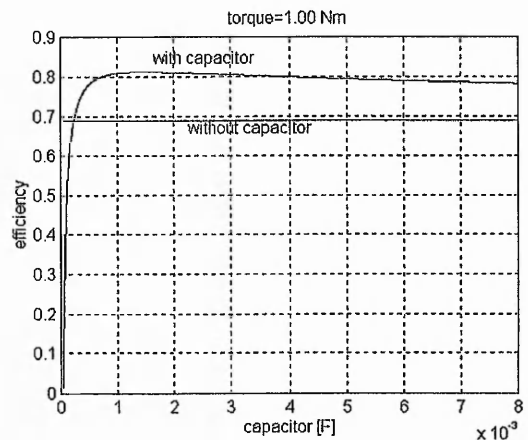
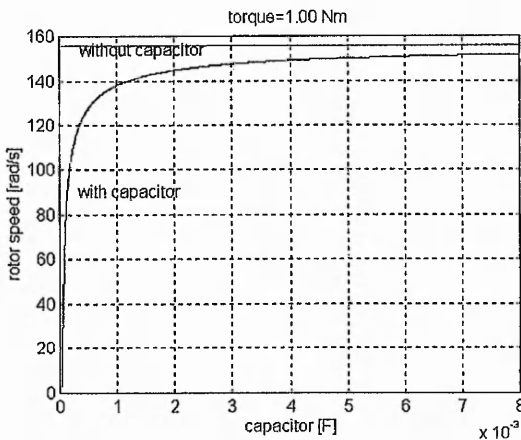


Constant torque characteristic $T=8Nm$

c) Power factor/Capacitance

d) Copper Losses/Capacitance

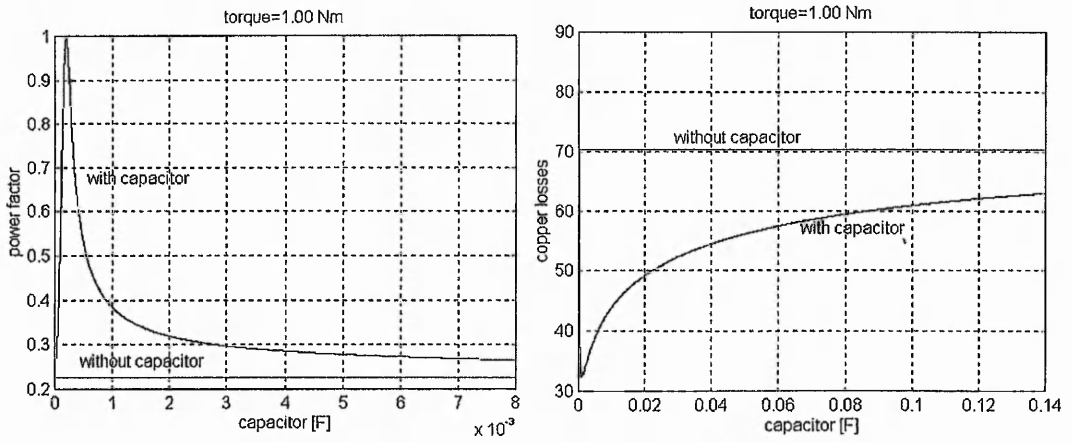
Fig. 2.8 – Motor2 (1KW)



Constant torque characteristics $T=1 Nm$

a) Rotor speed/Capacitance

b) Efficiency/Capacitance

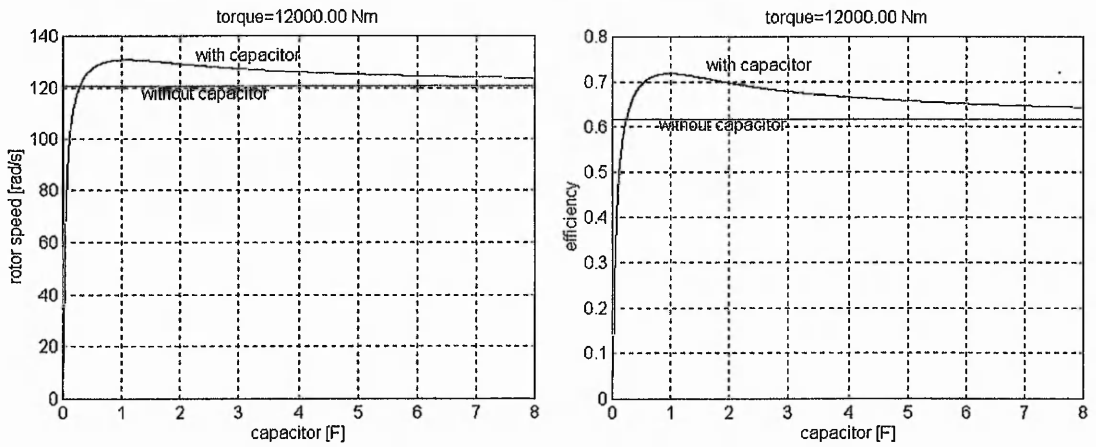


Constant torque characteristic $T=1 \text{ Nm}$

c) Power factor/Capacitance

d) Copper Losses/Capacitance

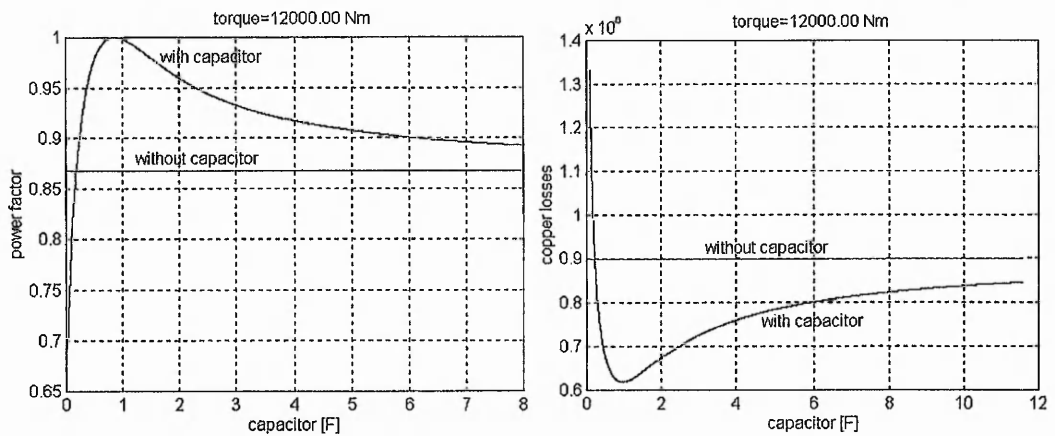
Fig. 2.9 – Motor2 (1KW)



Constant torque characteristics $T=12 \text{ kNm}$

a) Rotor speed/Capacitance

b) Efficiency/Capacitance

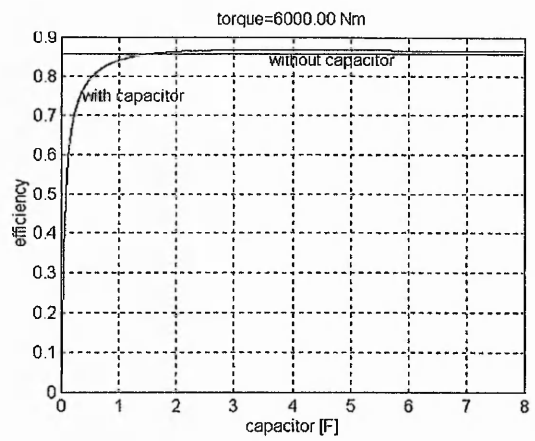
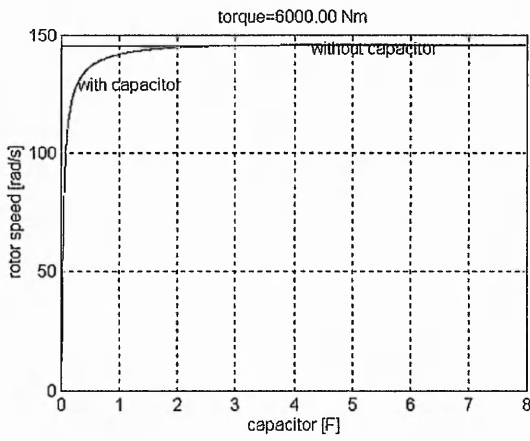


Constant torque characteristic $T=12 \text{ kNm}$

c) Power factor/Capacitance

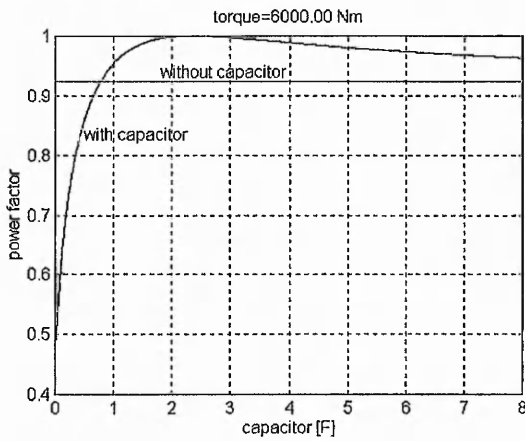
d) Copper Losses/Capacitance

Fig. 2.10 – Motor3 (1MW)

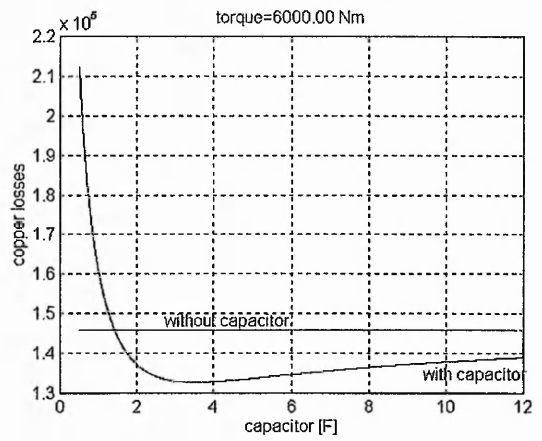


Constant torque characteristics $T=6kNm$

a) Rotor speed/Capacitance



b) Efficiency/Capacitance

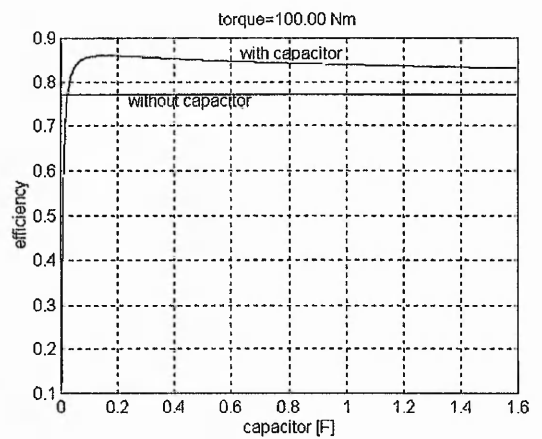
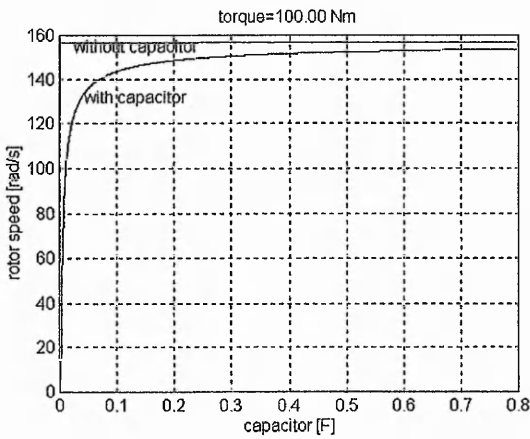


Constant torque characteristic $T=6kNm$

c) Power factor/Capacitance

d) Copper Losses/Capacitance

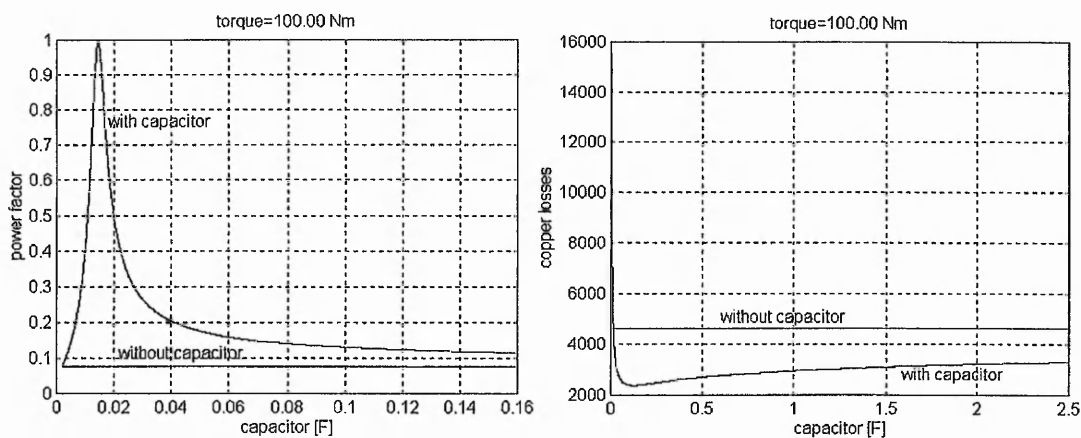
Fig. 2.11 – Motor3 (1MW)



Constant torque characteristics $T=100Nm$

a) Rotor speed/Capacitance

b) Efficiency/Capacitance



Constant torque characteristic $T=100\text{Nm}$

c) Power factor/Capacitance

d) Copper Losses/Capacitance

Fig. 2.12 – Motor3 (1MW)

By varying the capacitor value, the rotor speed may be controlled between 0 and the value of the speed that will be reached if the rotor circuit was short-circuited (graphs *a*). When the load torque is in the peak area (the peak torque of the short-circuited rotor configuration), higher rotor speeds may be achieved (figures 2.4*a*, 2.7*a*, 2.10*a*). If the inserted capacitor is too small, the motor may become unstable.

The efficiency and power factor may be improved (graphs *b* and *c*) if the capacitor is varied. The efficiency has significant improvements in the low and high torque areas (figures 2.4, 2.7, 2.9, 2.10, 2.12). Around the normal operating point the improvement is not that significant. The power factor may be “pushed” towards almost unity in any load condition.

The copper losses for a given load can be controlled if a capacitor is inserted in the rotor circuit (graphs *d*). A low capacitance value produces an increase of losses (this confirms the low efficiency for small capacitor values in graphs *b*). Increasing the capacitor decreases the losses and it is possible to reduce these to half of the losses of the short-circuited rotor configuration. A high value of capacitance has the same effects as in normal configuration. The percentage of copper losses reduction is significant for high and low loads. This gives appreciable energy saving in high power motors.

The former set of simulations was generated for a variable capacitor. The next set (figures 2.13-2.15) has been achieved with constant values of capacitance inserted in the rotor circuit. The speed-torque characteristics are given for the three motors with different capacitor values (graphs *a*). On the same graph, the speed-torque curve of the

motor in standard configuration is presented. Equations (2.26) and (2.46) have been used for simulation. The evolution of the efficiency is displayed on graphs *b* and equation (2.31) in corroboration with (2.29),(2.30) and (2.48),(2.49) respectively have been used. Equations (2.32),(2.34),(2.29),(2.48) have been used to represent the power factor as a function of slip (graphs *c*) (see program *tst.m* from Appendix 2.2).

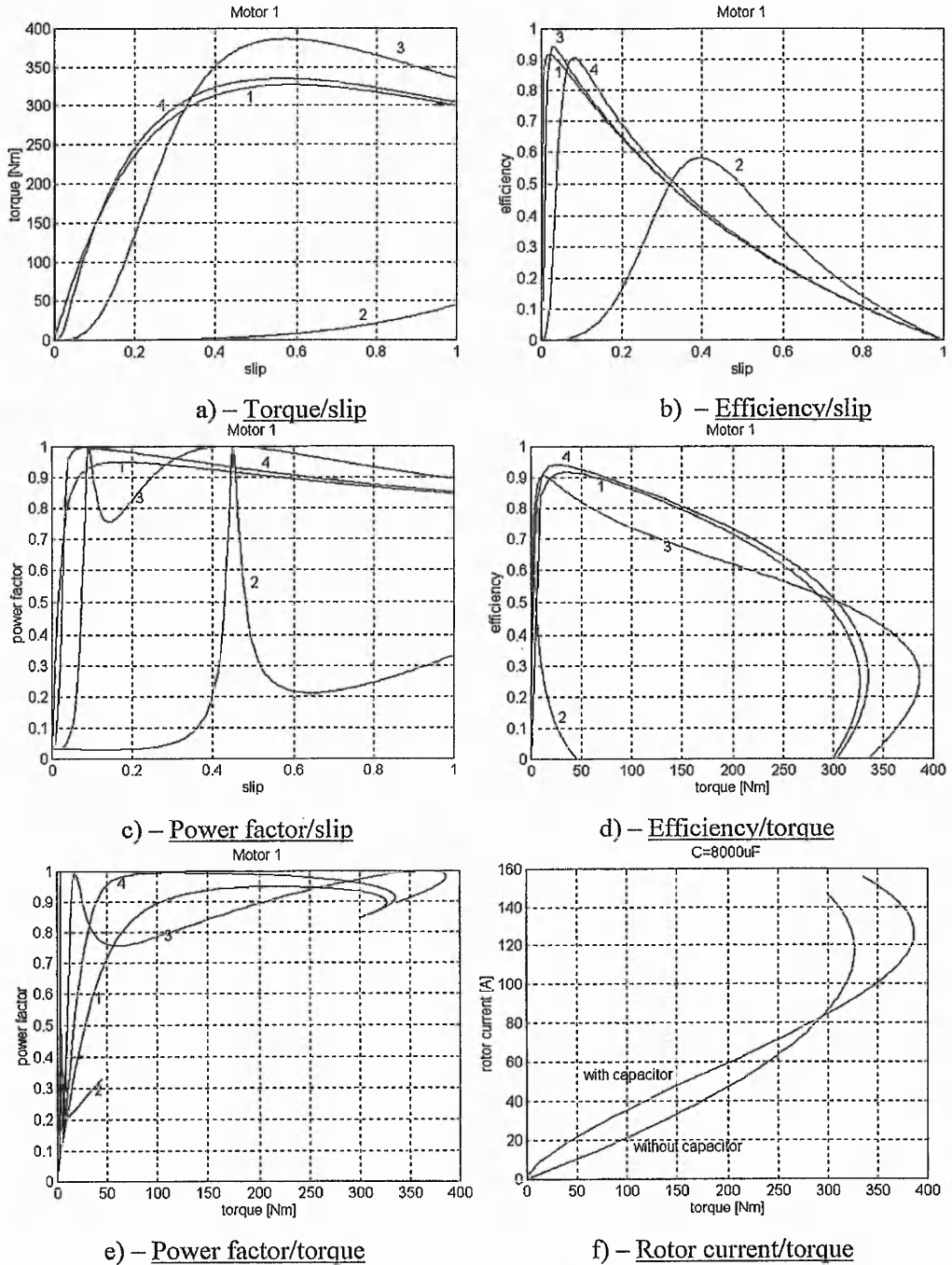
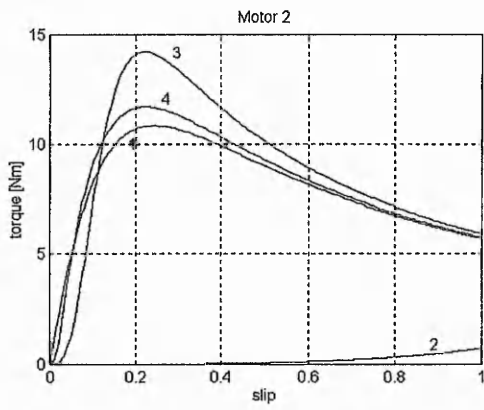


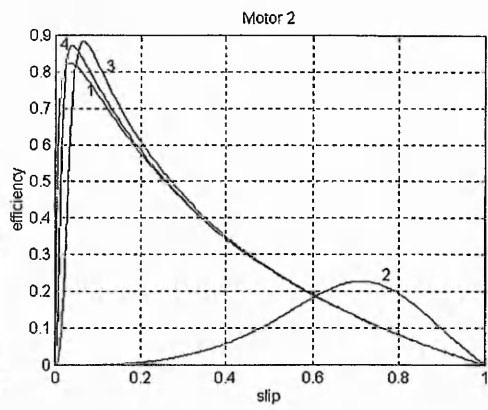
Fig. 2.13 - Motor1 (20KW)

Curve 1: without capacitor; Curve 2: with a capacitor of 300 μ F;

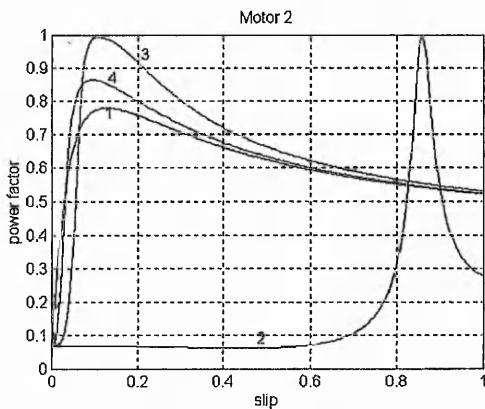
Curve 3: with a capacitor of 8000 μ F; Curve 4: with a capacitor of 70*10³ μ F;



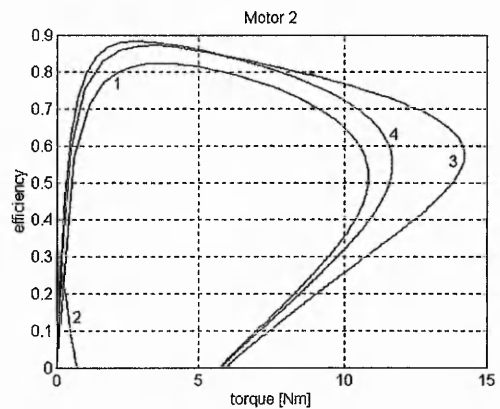
a) - Torque/slip



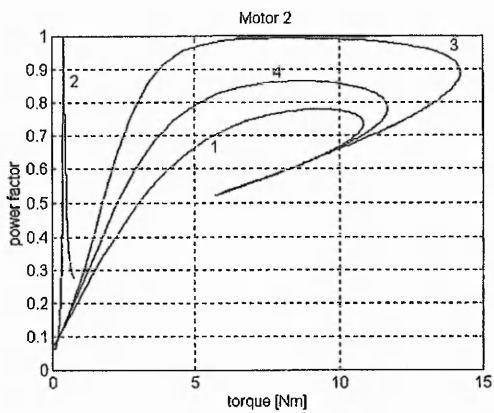
b) - Efficiency/slip



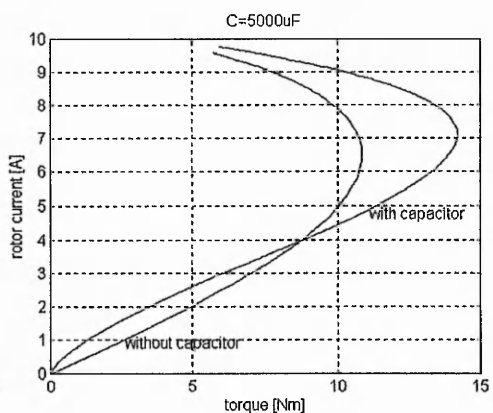
c) - Power factor/slip



d) - Efficiency/torque



e) - Power factor/torque



f) - Rotor current/torque

Fig. 2.14 - Motor2 (1KW)

Curve 1: without capacitor; Curve 2: with a capacitor of $30\mu\text{F}$;

Curve 3: with a capacitor of $5000\mu\text{F}$; Curve 4: with a capacitor of $20 \cdot 10^3\mu\text{F}$;

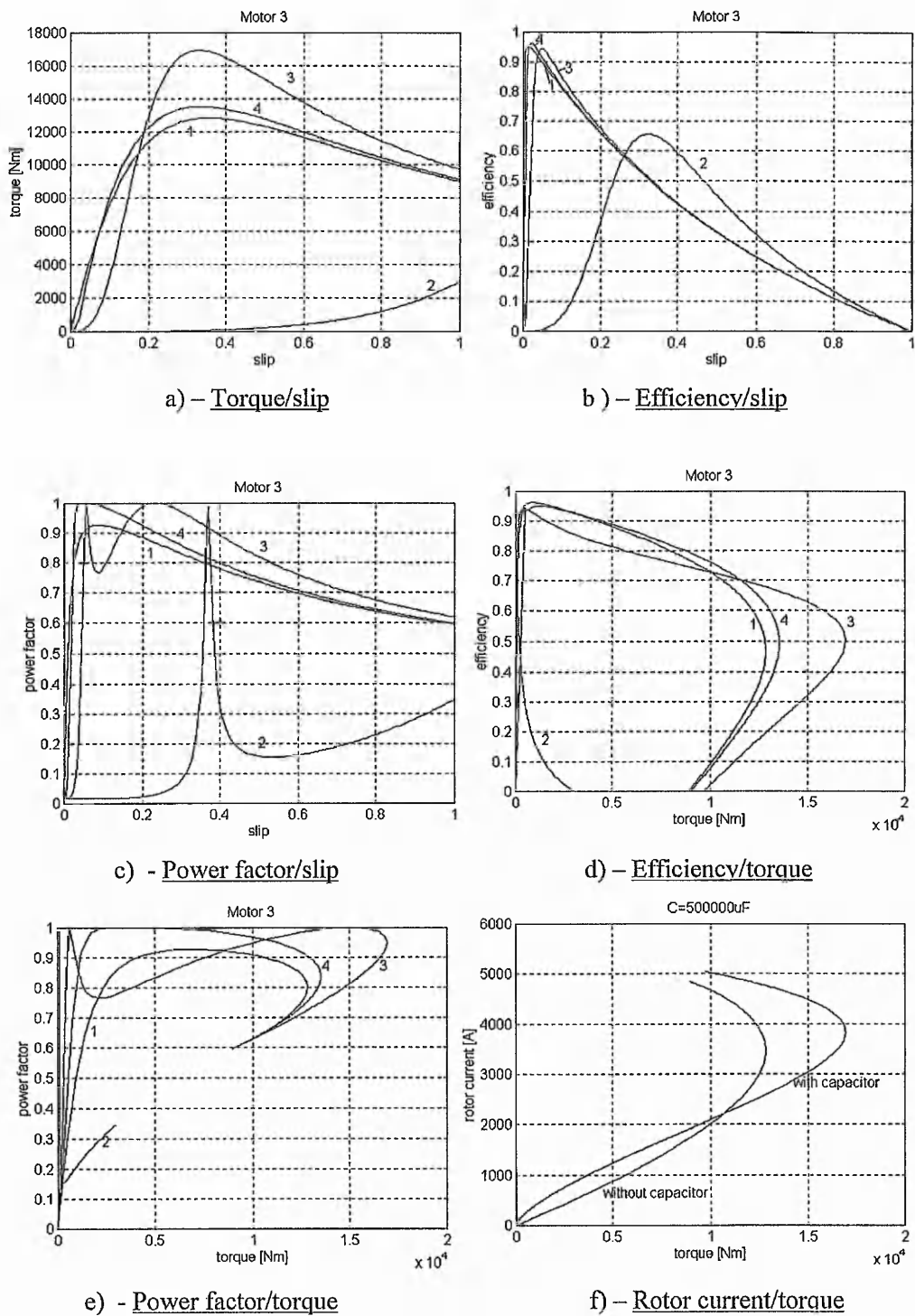


Fig. 2.15 - Motor3 (1MW)

Curve 1: without capacitor; Curve 2: with a capacitor of 10mF;

Curve 3: with a capacitor of $500 \cdot 10^3 \mu\text{F}$; Curve 4: with a capacitor of $3 \cdot 10^6 \mu\text{F}$;

The simulation results can be grouped in 3 categories determined by the value of used capacitor.

First category consists of curves 2 from figures 2.13, 2.14, 2.15. It can be seen that the value of the capacitance used is very small and that the motors are not operable, the starting torque being very small and, in general, the overall efficiency and power factor are smaller than in the case of the short-circuited rotor.

A second category consists of curves 4 from figures 2.13, 2.14, 2.15. The performance of the induction motors with externally modified rotor impedance do not differ significantly from the performances of the induction motors in a standard configuration.

The third group is formed of curves 3 from figures 2.13, 2.14, 2.15. It is noticeable the peak and starting torque are improved. The graphs *b* and *c* of each figure show that the power factor and efficiency as a function of slip do not have significant improvements – there are situations when they are even worse than those of the short-circuited rotor configuration. This suggests that the modification of rotor impedance is recommended in applications where the speed is not regulated within a narrow band.

The power factor and efficiency representations from graphs *d, e* show that a constant improvement of these performance for the whole range of torque could be achieved by just varying the capacitor value in accordance to the load. The improvement of the performances, keeping the capacitor constant, are achieved for limited torque regions, for the rest of the loads the performances are worse than in short-circuited rotor configuration.

The evolution of curves 3 that represents the power factor on graphs *c* of each figure might raise doubts about its validity as function of slip. In such representations, the unity power factor is reached twice for different slip value (load torques) or the same power factor is achieved more than twice. As it can be seen, in short-circuited rotor configuration such situations do not occur.

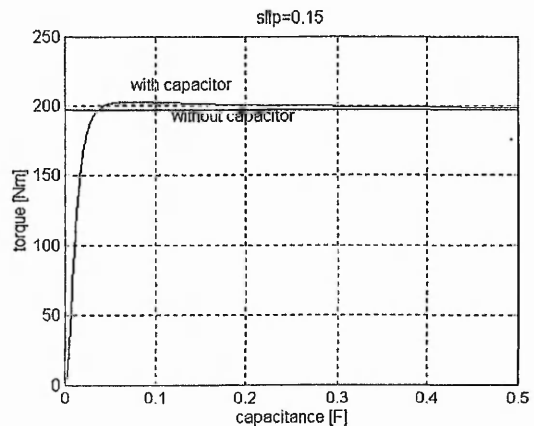
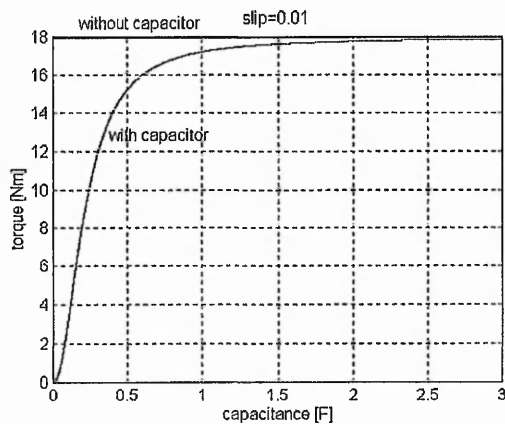
The short-circuited rotor induction motor is seen from the supply side as a combination of resistors and inductances that form a second order circuit. The addition of capacitors in the rotor circuit modifies the order of the circuit and the equation for power factor

rises from second order to fourth order (see appendix 2.3). This implies that the same power factor may be achieved for different load torques.

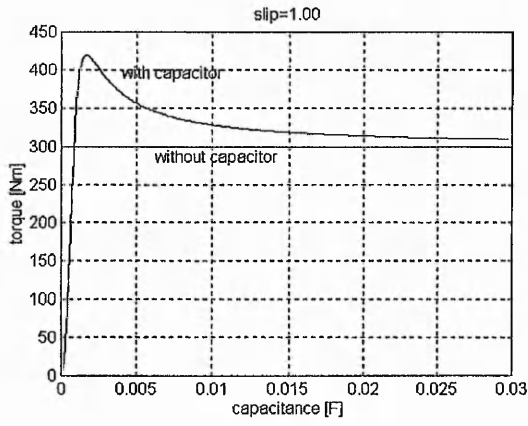
The rotor current/torque evolution for each motor with capacitor values used to draw curves 3 of each figure, is represented to explain the decrease of the rotor speed in the first section of the torque/slip characteristic when a capacitor is inserted. It is noted that the rotor current increases its value on the respective section in the configuration with capacitor. The decrease in the rotor speed is in accordance with equation (2.42).

If the capacitor is kept constant while the motor is running, an improvement of the peak and starting torque can be achieved. Other performances are not significantly improved. If the capacitor is too small the motor is not operable and the use of a too large a capacitor does not improve the motor performance greatly. The capacitor values are influenced by the motor power. The higher power of the motor, the higher the capacitor value required.

The capacitor values required to maintain the desired slip for different loads are presented in the third set of simulated results. The torque value that produces the same slip in the case of a short-circuited rotor motor is displayed. Equations (2.26) and (2.46) are the basis of the calculation used. The capacitor is varied for the given slip and the resulting torque is recorded (program testb.m from Appendix 2.2).

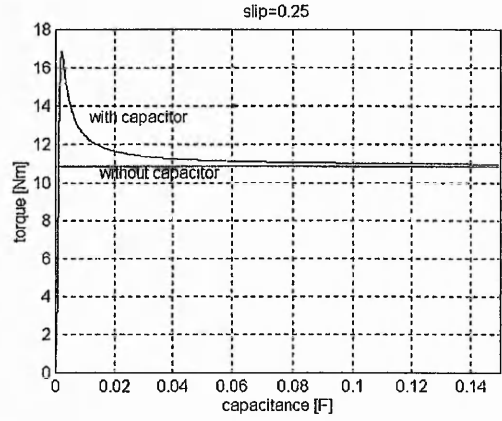
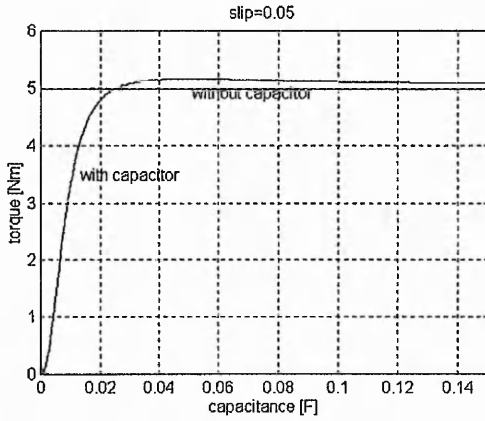


a) $s=0.01$ Torque/Capacitance at constant slip and Torque without capacitance b) $s=0.15$

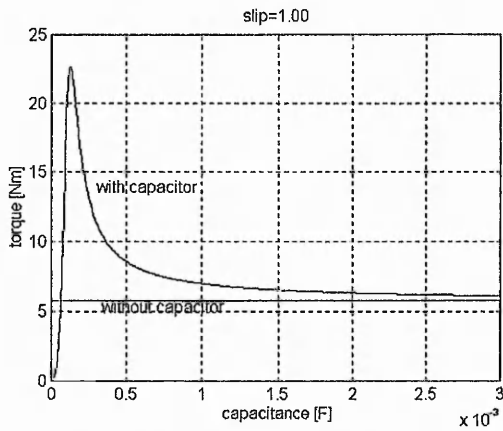


c) $s=1$ Torque/capacitance at constant slip and Torque without capacitance

Fig. 2.16 - Motor1 (20KW)

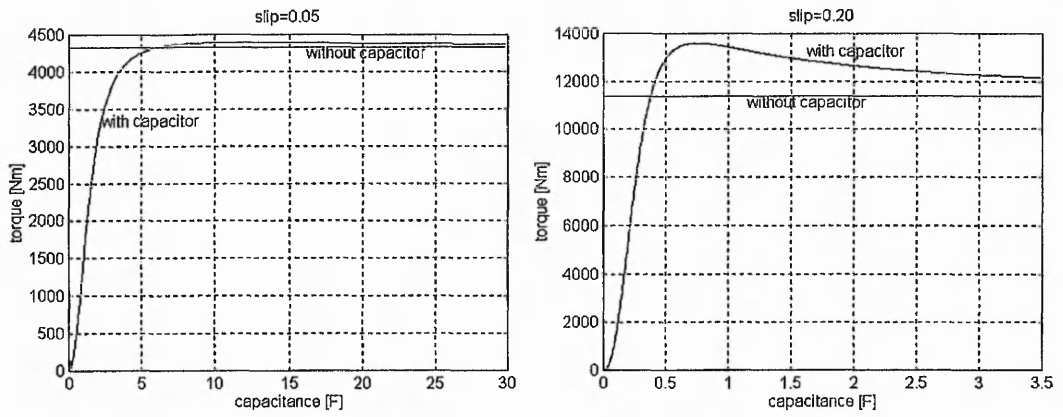


a) $s=0.05$ Torque/Capacitance at constant slip and Torque without capacitance b) $s=0.25$

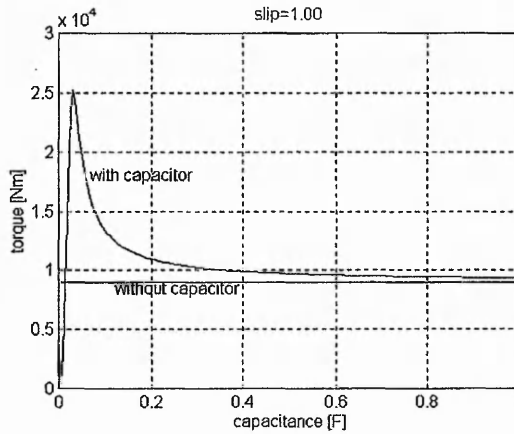


c) $s=1$ Torque/capacitance at constant slip and Torque without capacitance

Fig. 2.17 - Motor2 (1KW)



a) $s=0.05$ Torque/Capacitance at constant slip and Torque without capacitance b) $s=0.2$



c) $s=1$ Torque/capacitance at constant slip and Torque without capacitance

Fig. 2.18 - Motor3 (1MW)

The simulations show that by varying the capacitor, the desired slip may be achieved for a torque smaller than the torque that produces the same slip in the short-circuited rotor configuration. The slip may be kept constant even for a torque bigger than the normal one, but this case is not valid for small slips.

An interesting case is the case of unity slip that corresponds to the starting moment. The graphs *c* show that varying the capacitor it is possible to achieve superior starting torque. The results confirm the improvement of the speed-torque characteristics that were achieved in some situations of the figures 2.13-2.15.

The last set of simulations concerns the dynamic response of the motor to the change of the capacitor value at constant load torque and the modification of the load torque, when the capacitor is kept constant. The simulations (figures 2.19, 2.20) have been made

using the differential equation system (2.38), (2.12a) and (2.13) (program dinc.m from Appendix 2.1).

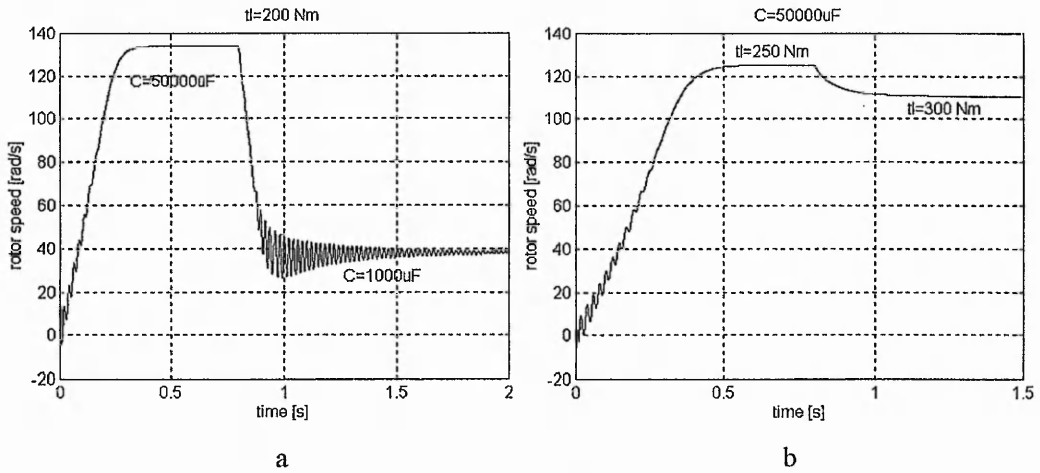


Fig. 2.19 – Motor1 (20KW):

- a) constant load torque (200Nm), variable capacitor ($50 \cdot 10^3 \mu\text{F}$ respective $1000 \mu\text{F}$)
 b) constant capacitor ($50 \cdot 10^3 \mu\text{F}$), variable load torque (250 Nm respective 300Nm)

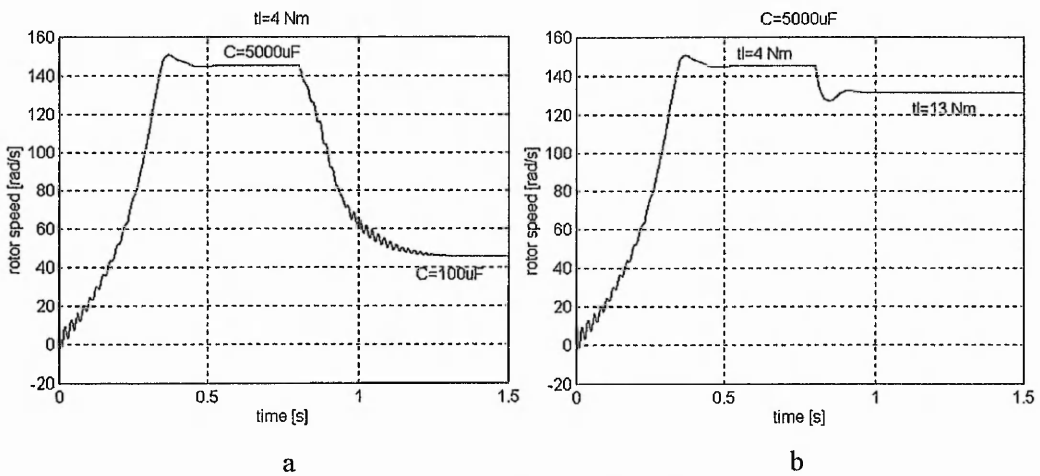


Fig. 2.20 – Motor2 (1KW):

- a) constant load torque (4Nm), variable capacitor ($5 \cdot 10^3 \mu\text{F}$ respective $100 \mu\text{F}$)
 b) constant capacitor ($5 \cdot 10^3 \mu\text{F}$), variable load torque (4Nm respective 13 Nm)

The simulation results show that the modification of one of the parameters - capacitor (graphs *a*) or torque (graphs *b*)- produces a transient regime (exemplified on the graphs with the speed modification) that is proportional to the parameters of the motor parameters (rotor resistance and inductance, inserted capacitor), and the time constant of the rotor circuit. These simulations open the possibility of a dynamic control of the

speed by varying the value of the inserted capacitor.

2.7 Conclusions

Theoretical analysis and simulation results confirm the conclusions stated in the [3,4,5]: that the performance of an induction motor may be improved from the rotor side, without the need for a second supply, by inserting a capacitor on each phase of the rotor circuit and that the required value of such a capacitor is very large.

This chapter introduced a set of differential equations based on space vector theory. These equations have estimated the dynamic behavior of the induction motor.

A set of equations that evaluates the impact of the inserted capacitor over the motor performances has been derived. This algorithm in comparison with similar methods does not need supplementary information relating to motor such as: induced e.m.f. or slip that are considered measured in [3,4,5].

The simulations show that improvements of the speed torque characteristic may be achieved, principally an increase of the peak and starting torque.

An optimization of the efficiency and of the power factor can be realized if the capacitor is varied as a function of the load torque, achieving significant improvements of the efficiency in the low and high torque areas and a power factor close to unity.

The steady state analysis and the simulations in the dynamic case show the possibility of speed control of the motor by varying the value of the inserted capacitor. This method may be a practical product but limitations when the capacitor becomes too small, have to be considered.

If the inserted capacitors are too small the motor becomes unstable (low efficiency, huge copper losses, etc.) and if the capacitor is too big, the performance of the motor tends to overlap the performances of the short-circuited rotor motor. The value of capacitance required is proportional to the motor power.

The theoretical analysis of the induction motor with modified rotor impedance shows that such a control method is appropriate in applications in which better efficiency, power factor or torque are sought rather than speed.

Simulation results confirm what was stated in [3] about the significant values of the capacitor that are required. In fact, this was the main impediment in experimental checking of the theoretical analysis presented in these papers. Just, Reinert makes exception with some experimental attempts but he remarks the necessity of a dynamic variation of the capacitor value.

These appreciable capacitor values and the necessity for their dynamic and fine control require electronic methods to emulate the effects of these capacitances.

Chapter 3

REVIEW OF THE ELECTRONIC PHASE CONTROL METHODS

Abstract: Modification possibilities of the current phase angle are reviewed. A few methods for power factor control are reviewed. Also, this chapter presents some concepts such as: gyrator, switched capacitor that could be used in generating high capacitive effects. Implementation methods and their viability for this project are discussed.

In the previous chapter, it was shown by simulations that large capacitor values are required for the improvement of induction motor performances by secondary control, varying from several hundred micro-Farads (small motors) to Farads (high power motors). This large capacitance can be implemented using capacitor banks but the physical size will be too large to be practical. It is possible to reduce the capacitor value by transformer coupling to the rotor slip-rings but the low values of rotor frequency will make the transformer size very large. Dynamic load changes will necessitate variation of rotor capacitor values with the load. All these elements make passive component solutions impractical.

The insertion of a capacitor in a RL circuit modifies the circuit impedance and changes the circuit power factor. The reference list shows how the dynamic power factor control has been achieved using different types of electronic converter. Fig. 3.1 show common ac to dc converter:

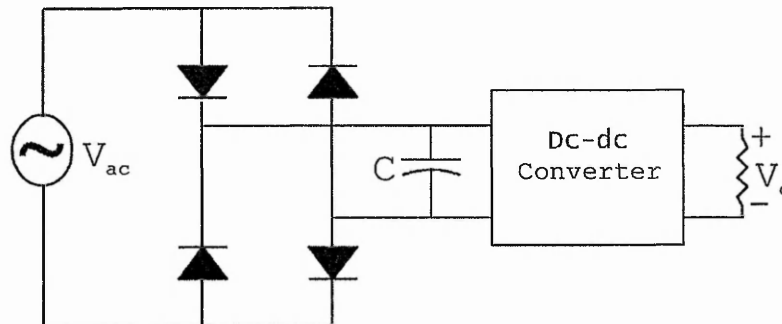


Fig. 3.1 – Standard structure in AC/DC conversion applications

M.J. Schutten et al [12] consider that when the DC voltage obtained from a single phase rectifier with a small DC link capacitor is applied to the input of a parallel resonant converter, a relatively high power factor inherently results, even with no active control of the input line current but, high total harmonic current distortion occurs. He showed that dual closed-loop control consisting of an inner current loop and an outer voltage loop, produces a near unity power factor and low input harmonic currents.

D.R. Vaes et al. [13] present a novel PWM voltage source rectifier controlled by the load DC current. This method has the advantages over the direct current control method in the elimination of the need for input current sensors and an unchangeable and unique PWM pattern. This system may give leading power factor operation for all load conditions but with the drawback that the power factor is load dependent and, hence, it requires adjustment for each load condition.

B.M.M. Mwinyiwiwa et al [14] describe a delta modulated, current source, three phase rectifier designed to work in conjunction with controlled current inverters. The control system consists of an outer feedback loop regulating the unidirectional output current flowing through the DC link and of an inner feedback loop that maintains near sinusoidal waveform input currents at unity or leading power factor. The inner loop controls the current indirectly by delta modulation of the voltage across the AC terminals of the converter.

R. Liu [15] gives an analytical design procedure for the optimization of power factor correction in driven series resonant converters. This method eliminates much of switching losses occurring in converters like boost or flyback when employed in similar tasks.

A.F. de Sousa [16] introduces a new single phase power rectifier that features regulation by conventional PWM, soft commutation and instantaneous average line current control. He claims that the new topology provides a significant reduction in conduction losses in comparison with the conventional configuration composed by four diodes front end rectifier followed by a boost converter.

There is a consistent sequence of system elements in most applications dealing with the problem of power factor control. This sequence shown in Fig. 3.2 consists of supply, converter and load.

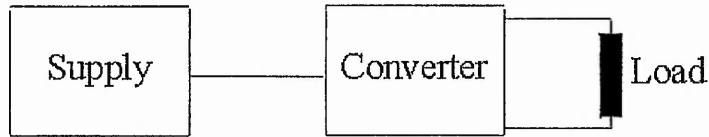


Fig. 3.2 – Regulator component sequence

In the rotor circuit, the induced voltage is the supply and the rotor winding is the element producing the current phase angle between voltage and current (the load). This situation modifies the sequence to supply, load, converter as shown in fig. 3.3.

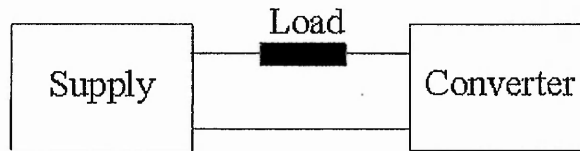


Fig. 3.3 – Rotor circuit schematic

The sequence of fig. 3.3 requires different solutions to produce the required capacitor values using novel converter structures. This chapter presents several methods that could be candidates in implementing high capacitive effects, starting with the gyrator concept.

3.1 Gyrator concept

B.D.H. Tellegen [17] introduced the idea that, in addition to the elements capacitor, resistor, inductor or ideal transformer, a new linear, constant, passive network element is conceivable. First, he analyzed the four main properties that characterizes the passive networks known at that time of writing 1948. There were:

1. That the relation between the terminal voltages and currents is formed by a system of ordinary linear differential equations.
2. That these differential equations have constant coefficients.
3. That the $2n$ -pole is passive, i.e. it can deliver no energy, because includes just passive elements.

4. That the reciprocity relationship between input and output current and voltages must be satisfied.

Tellegen considered that, in conceiving a new network element, one or more from these properties has to be dropped. Dropping any of the first three properties is not recommended because the implementation of the resulting system would be complicated. For example: if the third property is dropped the system requires an energy source. Amplifier valves and operational amplifiers, for instance, require DC energy sources and thus constitute elements are more complicated than the passive elements.

Tellegen believed that the fourth property was less important than the other three properties and he considered dropping the reciprocity requirement.

A 4 pole network ($n=2$) shown in fig. 3.4, is considered in the investigation of dropping the fourth rule. This can be mathematical described by the equations:

$$\begin{aligned} v_1 &= Z_{11}i_1 + Z_{12}i_2 \\ v_2 &= Z_{21}i_1 + Z_{22}i_2 \end{aligned} \quad (3.1)$$

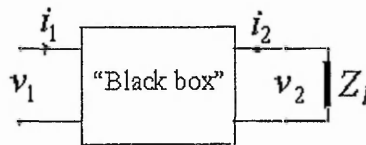


Fig. 3.4 - Four-terminal network

The black box may represent a converter.

For four-terminal networks of this type, the reciprocity law is shown by the equality:

$$Z_{12} = Z_{21} \quad (3.2)$$

and (3.1) could be written as:

$$\begin{aligned} v_1 &= \frac{Z_{11}}{Z_{21}}v_2 + \left(\frac{Z_{22}Z_{21} - Z_{21}Z_{12}}{Z_{21}} \right) i_2 \\ i_1 &= \frac{1}{Z_{21}}v_2 - \frac{Z_{22}}{Z_{21}}i_2 \end{aligned} \quad (3.3)$$

The expression relating the input impedance to the output impedance (see Appendix 3.1) is given by:

$$Z_i = \frac{Z_{11}Z_l - (Z_{12}Z_{21} - Z_{22}Z_{11})}{Z_l - Z_{22}} \quad (3.4)$$

where Z_l is the load impedance and Z_i is the input impedance.

The ideal transformer is an example of a four-pole network satisfying the reciprocity relation:

$$\begin{aligned} i_1 &= -ui_2 \\ v_1 &= uv_2 \end{aligned} \quad (3.5)$$

Tellegen, starting from these considerations, introduced a new network element that does not obey the reciprocity rule. He called this element ideal gyrator and it is described by the equations:

$$\begin{aligned} v_1 &= -gi_2 \\ v_2 &= gi_1 \end{aligned} \quad (3.6)$$

The coefficient g is the gyration resistance and has the dimension of a resistance.

The ideal gyrator has the property, resulting from (3.6), that it “gyrates” a current into voltage, and vice versa. Thus, if we connect an impedance Z between the secondary terminals, the impedance between the input terminals is g^2/Z . An example of this is an inductance L connected to the output of the gyrator. This causes an emulated capacitance $C = L/g^2$ between the input terminals of the element. Similarly, if a capacitance C is connected to the output terminals, an inductance $L = g^2C$ will appear across the input terminals.

A gyrator structure implies

$$Z_i = -\frac{Z_{12}Z_{21}}{Z_l} \quad (3.7)$$

Considering (3.4) and (3.7), results that:

$$Z_{11} = 0, Z_{22} = 0 \quad (3.8)$$

Two ideal gyrators in cascade compose an ideal transformer, an ideal gyrator and an ideal transformer in cascade constitute another gyrator, but two ideal transformers in cascade do not create an ideal gyrator[15].

3.2 Gyrator implementation

As shown in chapter 2, high capacitor values are required in the rotor circuit of an induction motor to improve efficiency and power factor. The gyrator concept is one of the paths that can be followed in the investigation of emulating high capacitive effects. The main problem is how to implement a gyrator structure at power electronic levels.

The gyrator concept has a wide application in microelectronics and in integrated circuits where the technology does not permit the inductor implementation. A gyrator structure with a capacitor connected at the output terminals emulates the inductive effects that are required in integrated circuits, especially for filters. A common gyrator structure is built using a network of operational amplifiers [18] as shown in Fig.3.5 (see appendix 3.2 for the analysis).

The high input impedance and the “infinite” amplification of the operational amplifiers, allow the breaking of the reciprocity relation and make possible the generation of the gyration effect.

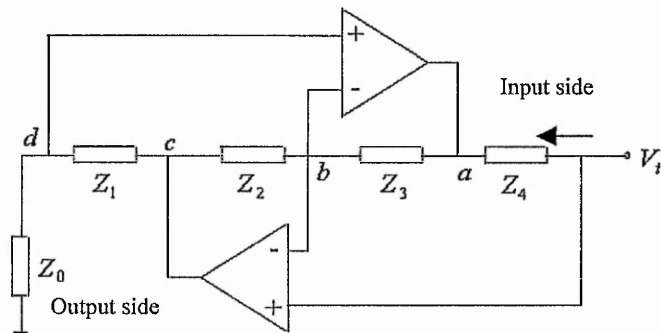


Fig. 3.5 – Gyrator implementation using operational amplifiers

Unfortunately, at power electronic energy levels a single device with the performance of an operational amplifier has not yet been implemented and thus it has to be implemented in other ways if gyrator effect is to be achieved.

S. Singer is one of the first researchers to try to apply the gyrator in power electronics. In [19] he considered that theoretically gyrator may be implemented in following fields:

- The transformation of voltage sources into current sources: The author took into account the current flow stability problem that occurs at points of direct connection between loads, like storage batteries or motors, and sources, or at the coupling by means of a transformer, due to the high sensitivity of the operating point. Singer states that a gyrator principle may be used to achieve a stable intersection between source and load characteristics at correct angle and in this way to have a lower sensitivity of the operating point to voltage variation.
- dc/dc conversion: Singer projected the insertion of the gyrator as a current regulator between the load and source, ensuring in this way a lower variation of the current;
- ac/dc conversion: Singer considered that the power flow control between an AC source and a DC source can be achieved by means of a time variable gyrator , obtaining in this way a harmonic-free conversion by the regulation of the gyrator resistance $g(t)$;
- capacitor var generation: The author assumes that capacitive var generation can be achieved by coupling an inductance to an AC source through a gyrator with constant gyration resistance. Conforming to gyrator principle, the inductance and its series resistor are transformed into their dual: a capacitor in parallel with an admittance;

Singer states that gyrator structures can be implemented by the means of converters whose input power $P_i(t)$ equals the output power $P_o(t)$ (PIPO converters):

$$P_i(t) = P_o(t) \quad (3.9)$$

and offers the possibility to control the input or output current value in such a way that it achieves the required values. If the imposed output current is $i_o^*(t)$ from (3.9) results:

$$i_i(t) = \left(\frac{i_o^*(t)}{v_i(t)} \right) v_o(t) \quad (3.10)$$

If the desired gyrator structure is characterized by the gyrator resistance $g(t)$, the required output current is:

$$i_o^*(t) = g(t)v_i(t) \quad (3.11)$$

and the control circuit would have the following structure:

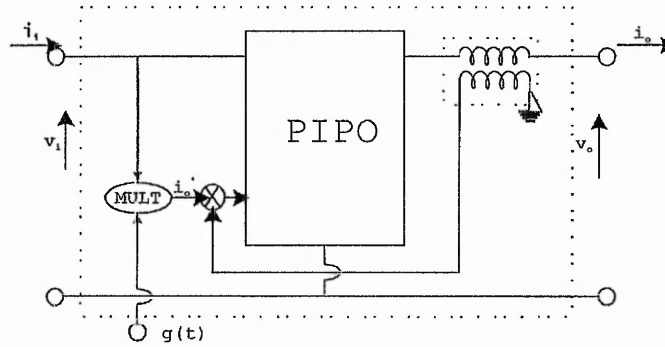


Fig. 3.6 – Gyration with output current controlled by a drive i_o^*

Singer considered that POPI equation is completely obeyed just by circuits based on transformer or gyration and can be satisfied by some other circuits that include source elements. He estimated that a reasonable reduction in gyration implementation is the equality of average powers:

$$\frac{1}{T} \int_0^T P_i(t) - P_o(t) dt = 0 \quad (3.12)$$

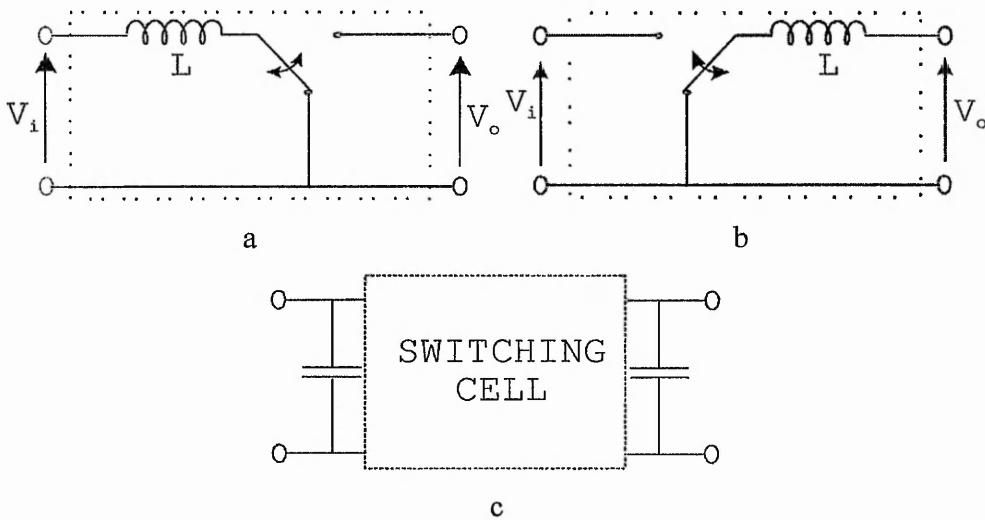


Fig. 3.7 – A basic family of switching converters suitable for gyration realization

- a) Boost; b) Buck; c) Basic switching cell with input and output capacitors applied for continuous conduction and ripple reduction

Singer considered that a classical family of circuits satisfying (3.12) is one that includes the buck, boost, buck-boost converters (fig. 3.7). The basic switching cell (from which all three converters are derived) includes inductance switched at high frequency

between the input and output terminals. Input or output current regulation is achieved by the inductance charging process. During each switching cycle the charging current increases as a ramp function until it equals the reference current signal. Then the inductance is switched to the output and discharged until the end of the switching period. The voltage transfer function v_o/v_i is determined by the duty cycle d , where d is proportion of the period during which the inductance is switched to the input terminal. The average value of d must be determined by the feedback and control circuit so that the relations mentioned above ((3.11) and (3.12)) are obeyed, when voltage sources are connected to the input and output terminals of the switching cell.

Singer and Erikson [20] show that some converters under certain conditions operate naturally like gyrators: Cuk or resonant converters as shown in fig. 3.8 are in this category. They proved their statement analyzing the resonant converter behavior, starting from the fact that this type of circuit exhibits current-source output characteristics. The converter is modeled by the equations:

$$\begin{aligned} i_i &= gv_o \\ i_o &= -gv_i \end{aligned} \tag{3.13}$$

where

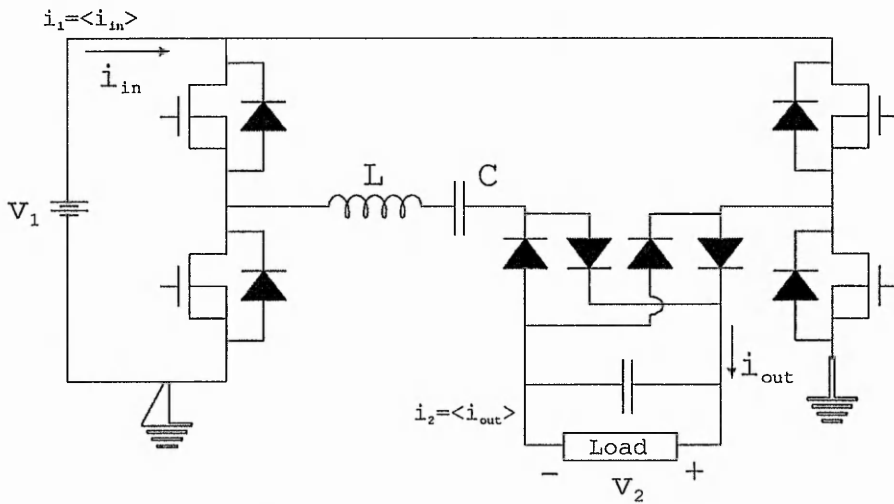
$$g = \frac{1}{R_0} \frac{4}{\pi} \frac{f_s}{f_0}$$

$$R_0 = \sqrt{\frac{L}{C}}$$

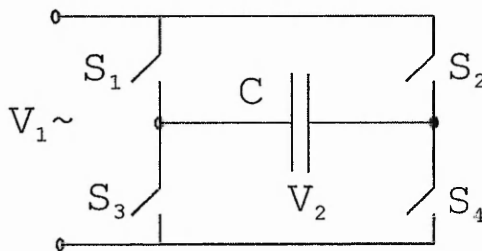
$$f_0 = \frac{1}{2\pi\sqrt{LC}}$$

f_s is the switching frequency

Singer and Erikson emphasized that all of these considerations are valid when the enumerated converters work in discontinuous conduction mode.

Fig. 3.8 – Series resonant converter

D.M Divan[21] tackled the gyrator realization using non-dissipative switched networks. He attempts to prove that an AC/AC full or half bridge converter can be emulated as a gyrator. In his strategy the capacitive load is to be transformed into its dual as an inductor and the switches $S_1 - S_4$ are modulated at a high frequency using a PWM strategy. The bridge shown in fig. 3.9 is supplied with a sinusoidal supply.

Fig. 3.9 – Full wave a.c. bridge with capacitive load

A control loop determines the modulation to maintain the capacitor voltage proportional to the input current, at the supply frequency ω . The input and output voltages are determined in Divan's vision by the relations:

$$v_2(t) = \frac{i_1(t)}{g} = \frac{I}{g} \cos \omega t \quad (3.14)$$

$$v_1(t) = -\frac{i_2(t)}{g} = -\frac{C}{g} \frac{dv_2}{dt} = \frac{\omega C I}{g^2} \sin \omega t \quad (3.15)$$

The terminal equations represent a gyrator with resistance g . The driving point impedance is jC/g^2 .

Divan stated that the duty ratio d is not constant and that for a sufficiently high switching frequency, the duty ratio expression derived from (3.14) and (3.15) is:

$$d = \frac{1}{2} \left(\frac{g}{\omega C} \tan \omega t + 1 \right) \quad (3.16)$$

According to (3.16), the duty ratio is time dependent and gets values higher than 1 that are not possible in a PWM switching strategy.

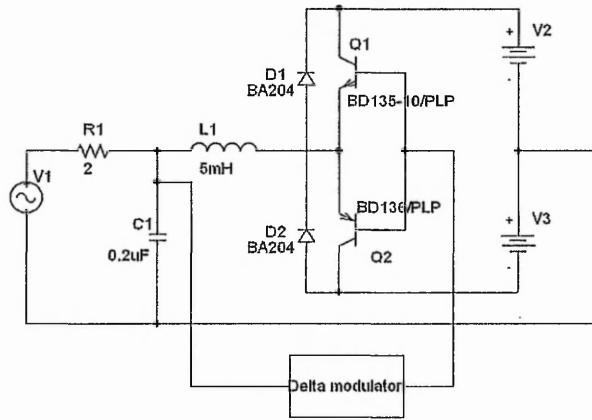


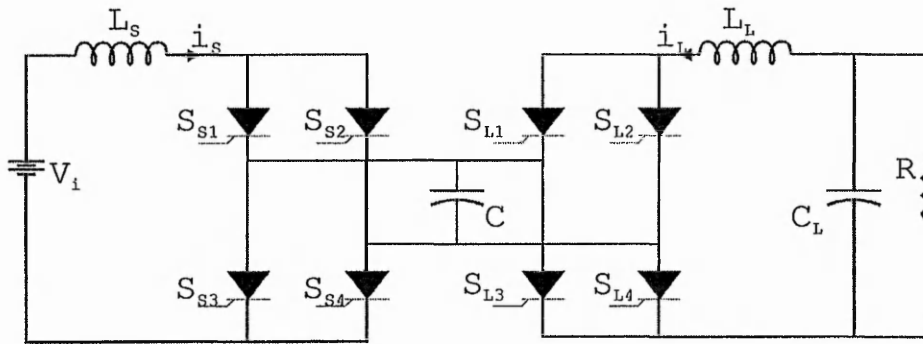
Fig. 3.10 – Delta modulated half bridge converter

In the same paper, D.M. Divan presented the implementation of a “negative” inductor using a half bridge converter shown in fig. 3.10 driven by a delta modulator controller. The value of the equivalent “negative” inductor is found to be:

$$L_{eq} = -qL_1 \quad (3.17)$$

where q is a correction factor, set in the delta controller. The author considered the circuit adequate for VAR compensation applications.

M. Eshani et al [22] introduced a new topological concept of a converter for DC-DC power conversion claimed by the authors to give advantages of smaller size and lower weight than similar converters at the same power rating. The new converter is called the inverse dual converter (IDC) and is basically a modification of the inductor converter bridge (ICB). In this paper and in [23], the authors modelled the new structure based on gyrator theory, stating that this converter shown in fig. 3.11 naturally behaves as a gyrator with no need for an extra control circuit.

Fig. 3.11 – Inverse dual converter

The converter is driven by a clock sequence of pulses with constant switching intervals $S_{S1}S_{S4}, S_{S2}S_{S3}, S_{S1}S_{S4}$ etc. in the source converter. The same switching sequence and frequency is used on the load side. The source and load side converter switching events need not be synchronized but must be of the same frequency. The capacitor C in the AC link serves two purposes, it temporally stores the energy that is transferred from one side to the other and supplies the reverse voltage required for the commutation of the switches. Output voltage control and input current continuity is accomplished by two control variables, the common converter frequency and the phase-difference between the two converters.

M. Eshani deduced the following equations that define the converter:

$$v_s = -L_s \frac{di_s}{dt} = ki_L \quad (3.18)$$

$$v_L = -L_L \frac{di_L}{dt} = -ki_s \quad (3.19)$$

with

$$k = \frac{\phi - (\phi^2/\pi)}{\omega C}, \quad 0 < \phi < \pi \quad (3.20)$$

where ω is operating angular velocity and ϕ is the load converter advance angle.

From equations (3.18) and (3.19),

$$\frac{\langle v_L \rangle}{\langle i_S \rangle} = -\frac{\langle v_S \rangle}{\langle i_L \rangle} = k \quad (3.21)$$

Comparing (3.21) with the gyrator equation (3.6), shows that the IDC is characterized by a gyration conductance:

$$g = \frac{1}{k} = \frac{\omega C}{\phi - (\phi^2/\pi)} \quad (3.22)$$

M. Eshani concluded that the inverse dual converter is capable of continuous voltage step up/down control over a wide range and that the input voltage is viewed from the load side as a constant current source (a gyration process).

The only practical realization of the gyrator in power applications is mentioned in [24]. There, S. Singer started from the idea that resistors inserted in power circuits, damp oscillations and balance the power flow in AC/DC conversion systems. The energy dissipated by such resistors is the main drawback of the method. To overcome this, S. Singer conceived a system that emulates a loss free resistor (LFR), using concepts like the time variant transformer (TVT) or the time variant gyrator (TVG) (transformers or gyrators with time variable transformation ratios and time variable gyrator resistance respectively). These structures were implemented with switched-mode converters, combining a buck converter and an inverter, composed of loss free elements (excluding the switching losses). The author designed a practical circuit based on a LFR synthesis for a CO₂ LASER system.

3.3 Some considerations about gyrator in power circuits

The gyrator is an attractive concept for the regulation process in high power circuits. The possible applications of this 4 pole network element listed by Singer in [19], provided the stimulus for implementation.

This chapter has reviewed the relevant papers presenting gyrators in power electronic systems. The interest in this concept is relatively new and this explains the relatively small number of significant papers and the fact that most of them are published after 1987.

Most of the theoretical and practical attempts to implement gyrators in power circuits were made using DC structures, but there is a significant exception where D.M. Divan [21] developed a negative inductor in an RL circuit using 2 supplementary DC sources that is in contradiction with the 3rd rule of the passive network elements. In the same paper, the structure proposed for emulating inductive effects is impossible to implement due to the duty ratios above unity that result from (3.16).

Singer and Erickson [20] proposed to implement the gyrator using buck, boost or Cuk DC converters.

These DC converters have corresponding AC converters, one example of these is shown in Fig.3.12. S.Sirivasan [25] analyses AC boost, buck, flyback and Cuk converters concluding that the AC voltage transfer ratios are the same as the ratios in the corresponding DC converters.

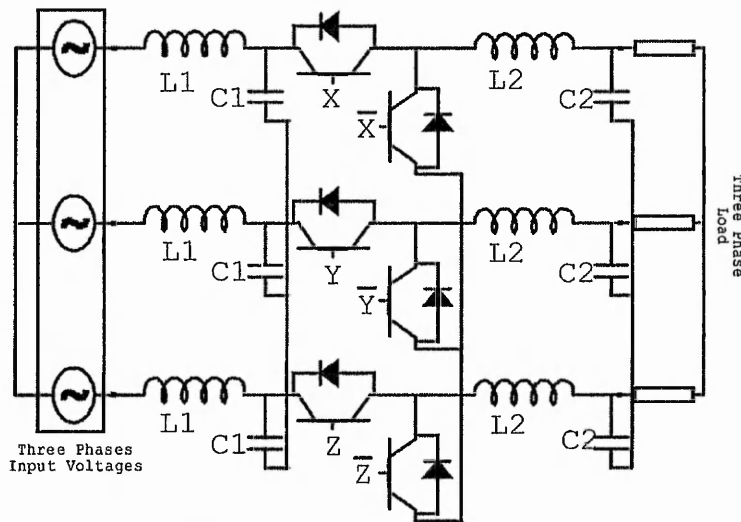


Fig. 3.12 - Three Phase Buck converter with input filters

Singer also stated in [19] that: “The gyrator can be realized by each circuit whose input power equals its output $P_i(t) = P_o(t)$ (denoted PIPO) in which the input (or output) current can be controlled. This can be *approximately* achieved by a family of switched-mode circuits including buck, boost, buck-boost and flyback”.

Alternatively consider a boost converter with an inductance for a load. The converter output has a capacitor connected in parallel with the load as Singer [19] recommended. This is shown in Fig.3.13.

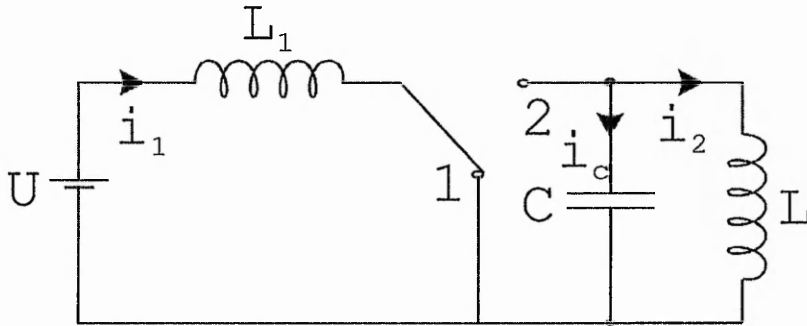


Fig. 3.13 - Boost converter with inductance for a load

When the switch is in position 1 (time interval $0 - t_1$), the following equations are valid :

$$\begin{aligned} \frac{di_1}{dt} &= \frac{u}{L_1} \\ \frac{du_c}{dt} &= -\frac{i_c}{C} \\ \frac{di_2}{dt} &= \frac{u_c}{L} \end{aligned} \quad (3.23)$$

where u_c is the voltage across the capacitor , i_1 is the current through L_1 , i_2 is the current through L .

During the time interval $(t_1 - T_s)$, the following equations apply:

$$\begin{aligned} \frac{di_1}{dt} &= \frac{u - u_c}{L_1} \\ \frac{du_c}{dt} &= \frac{i_1 - i_2}{C} \\ \frac{di_2}{dt} &= \frac{u_c}{L} \end{aligned} \quad (3.24)$$

where T_s is the switching frequency. The duty ratio d is defined as : $d = 1/T_s$, $d' = 1 - d$.

Using the averaging space method [27] for the analysis of systems (3.23) and (3.24), gives the following result :

$$\begin{aligned}\frac{di_1}{dt} &= \frac{u - d' u_c}{L_1} \\ \frac{du_c}{dt} &= \frac{d'i_1 - i_2}{C} \\ \frac{di_2}{dt} &= \frac{u_c}{L}\end{aligned}\tag{3.25}$$

Applying Laplace transforms to equation (3.25):

$$\begin{aligned}sI_1 &= \frac{U - d'U_c}{L_1} \\ sU_c &= \frac{d'I_1 - I_2}{C} \\ sI_2 &= \frac{U_c}{L}\end{aligned}\tag{3.26}$$

From (3.26), the input impedance is deduced to be:

$$Z_i = \frac{U}{I} = \frac{s^3 L L_1 C + s L_1 + s(d')^2 L}{s^2 L C + 1}$$

The load impedance is given by the expression: $Z_l = sL$ and gives :

$$Z_i = \frac{Z_l (s^2 L_1 C + (d')^2) + s L_1}{Z_l s C + 1}\tag{3.27}$$

If the boost converter had acted as the gyrator, then the input impedance would have had the following form :

$$Z_i = \frac{g^2}{Z_l}\tag{3.28}$$

There is a significant difference between the form of the expressions in equations (3.27) and (3.28).

The gyrator structure presented by Singer in [20], based on resonant converters, has the disadvantage of operating in the discontinuous conduction mode, which is a major drawback.

Bilgic's converter [23] has natural gyrator behavior, but has the same disadvantage as other implementations based on converters. All the foregoing methods involve the rectification of the ac source at some stage. Due to this rectification stage, in three phase circuits, the conduction period on each phase is less than 180 degrees. This introduces harmonics of lower order with relatively large magnitudes.

Gyrator theory states that an inductor placed at the output of a gyrator structure is "seen" as a capacitor at the input. The gyrator box (fig. 3.14) is constituted in a supply for the inductor. This then absorbs reactive energy from the box, while the source that supplies the gyrator sees the input of the box as a capacitor. This means that the supply system receives reactive energy from the gyrator. The gyrator therefore delivers reactive energy to both input and output ports. If the circuit uses no energy source, it is a perpetual VAR generator. Clearly this is nonsense in the case of boost, buck, cuk converters etc.

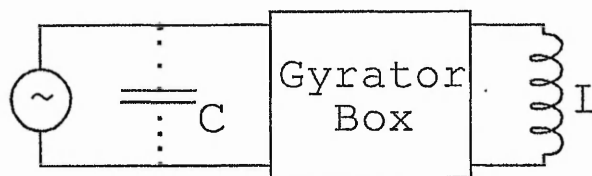


Fig. 3.14 - Inductor supply through gyrator box

3.4 Switched capacitors

The interest that exists in the field of single-phase induction motor operation for avoiding the need of two different capacitors for starting and running was mentioned in the introduction chapter. The research efforts were focused in finding solutions of emulating the starting capacitor and two methods were developed: one introduced by T.H. Liu[8] and E. Muljadi[7] and another one presented by T.A Lettenmaier [6].

Liu's and Muljadi's methods consist of placing in series with an ac RL circuit, an ac capacitor in parallel with a solid state switch that must allow bidirectional current flow

as with a mechanical switch (fig. 3.15). When the switch is open, current flows through the capacitor and a RLC circuit is formed. The current bypasses the capacitor when the switch is closed (RL circuit case). The switch is closed at the instant the voltage across the capacitor reaches zero. Thus, a zero voltage switching operation is performed and the switch is reopened after the shorting interval γ has passed. By shorting the switch periodically, the fundamental component of the voltage across the capacitor appears to be lower than the case without the periodic shorting interval so that the effective size of the capacitor appears to be larger than the actual size. As the shorting interval γ reaches π rad, the effective size of the capacitor approaches infinity.

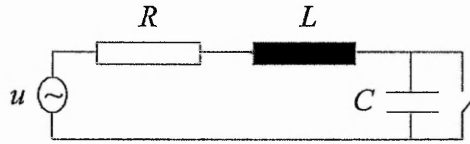


Fig. 3.15 – Switched capacitor in inductive circuits

In [8], it is stated that the emulated capacitance has the value:

$$C_{\text{effective}} = C_{\text{running}} \frac{1}{1-d} \quad (3.29)$$

where $d = \frac{\gamma}{T_s}$ and $T_s = \gamma + t_{\text{off}}$, t_{off} is the turn off interval of the electronic switch.

If we examine closely what is happening during the γ interval the following equations are valid:

$$\begin{aligned} \frac{di}{dt} &= \frac{u - Ri}{L} \\ \frac{du_c}{dt} &= 0 \end{aligned} \quad (3.30)$$

The capacitor is separated from the active circuit and no charge passes through it. The things change when the switch is turned off and the current flows through the capacitor. The t_{off} interval lasts until the capacitor voltage again reaches zero and the equations in the off interval are:

$$\begin{aligned} \frac{di}{dt} &= \frac{u - Ri - u_c}{L} \\ \frac{du_c}{dt} &= \frac{i}{C} \end{aligned} \quad (3.31)$$

Using equation sets (3.30) and (3.31), the system can be simulated. The resulting waveforms of the current and capacitor voltage are shown in figures 3.16 and 3.17, where $u = 20\sin(100\pi t)$, $L = 20mH$, $C = 50\mu F$, $R = 5\Omega$.

Legend: Input voltage divided by 4,

Current divided by 2,

Voltage across capacitor divided by 30

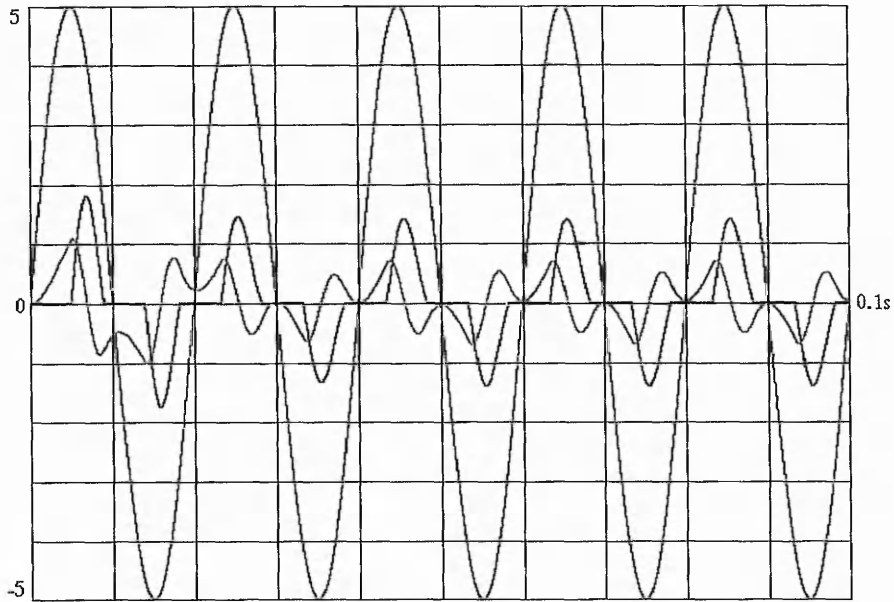


Fig. 3.16 – Current and capacitor voltage when $\gamma = 0.005s$

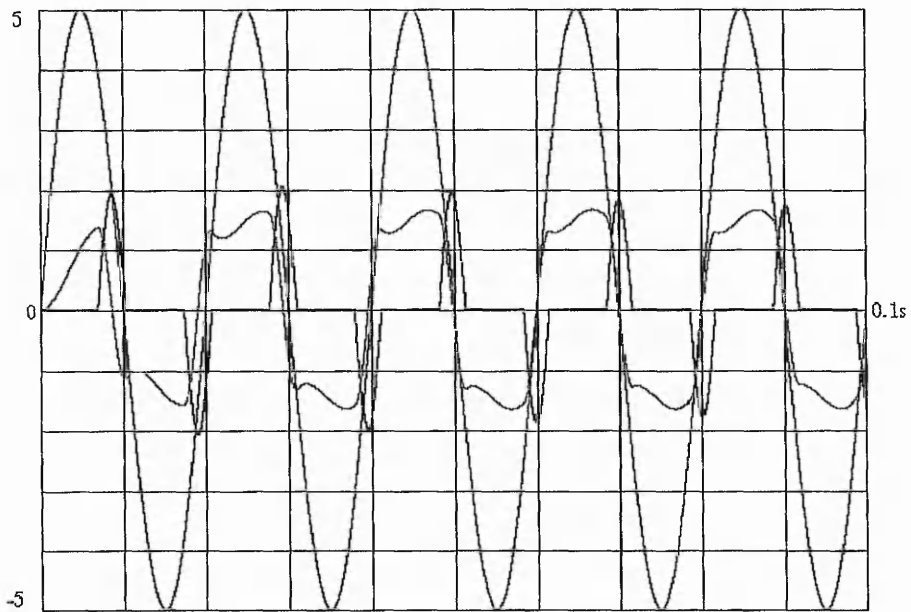


Fig. 3.17 – Current and capacitor voltage when $\gamma = 0.007s$

The simulation results are in agreement with the waveforms presented in [7], [8]. The graphs show that the control of phase difference between the supply voltage and the current is achieved by varying γ . However the graphs show that the resulting current is quite distorted.

Another drawback of this method is the dependence of the period T_s on the charge and discharge times of the capacitor. This defines the interval when the switch is off. In fact, this means that t_{off} is function of circuit parameters and supply frequency.

Lettenmaier [6] proposed a method of using electronic switching to replace centrifugal switch that introduces/removes the starting capacitor in the auxiliary winding of the single phase induction motor. The method used presents the motor with a continuously variable capacitance. It is achieved by using a transistor H bridge to switch a DC charged capacitor. The capacitor is charged from the motor AC supply and the bridge is pulse-width modulated using the sine-triangle modulation algorithm. The author uses a reference voltage V_{ref} synchronised with V_s . The capacitor is considered to be large enough for the capacitor voltage V_{cap} to be considered to be DC with negligible ripple. Therefore, the bridge output voltage V_{br} is a pulse width modulated approximation to the sine wave with a fundamental component phase angle adjustable in relation to the supply voltage V_s . The phase angle between the bridge voltage V_{br} and V_s is called bridge phase angle and is the primary adjustment factor used to control the transistor switching. The bridge output synthesizes a capacitance that can be varied if the switching is made in an appropriate manner. The author states that the size of the DC capacitor from the bridge needs only to be large enough to compensate the AC ripple at the capacitor terminals.

Controlling the peak of the triangle wave V_{tr} , it is possible to adjust the magnitude of the modulation. The effect of this adjustment is to change the capacitor DC voltage.

Lettenmaier states that the effective capacitance at the output of the bridge circuit can be calculated from:

$$C_{eff} = \frac{|I_{aux}|}{\omega|V_{br}|} \quad (3.28)$$

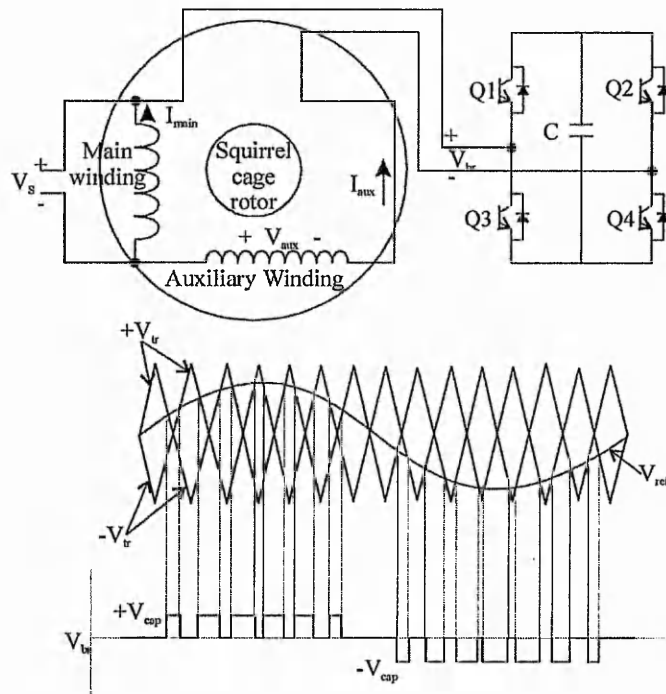


Fig. 3.18 – Switched DC capacitor

In this paper, Lettenmaier uses a $100\mu\text{F}$ dc capacitor to achieve performance of a single phase motor similar to of a $5\mu\text{F}$ ac capacitor. The DC capacitor is priory charged. The waveforms of the auxiliary current are similar to the currents presented in figures 3.16 and 3.17. In fact, the system developed in [7,8] was derived from Lettenmaier's bridge-capacitor.

3.5 Conclusions

This chapter reviews electronic power factor control methods as presented in recent literature. The research undertaken for electronic power factor control is critically appraised in the context of secondary control of three-phase induction motors. In this application, the system power level is high, while except in starting and acceleration to full speed, the rotor voltages and frequencies are small. The basic systems introduced in [10 to 14] are difficult to use in the motor application because the sequence of elements, supply – converter – load does not correspond to the induction motor sequence of

supply – load – converter. The present research aims to introduce controlled phase angle performance in a system in which the load precedes the converter.

The gyrator principle, even if it is extremely generous, does not have a viable implementation. The attempts that were made, produced either just approximate implementations or required the use of a supplementary supply, which is not convenient in current application. Despite this, the gyrator remains an interesting element for high power circuit, its implementation in alternative circuit could revolutionize these systems.

The impedance control applications in references [6-8] using an ac capacitor in parallel with a bi-directional switch or a dc capacitor in a bridge are close to the requirements of the present application. Simulation has shown that relatively good control of the current phase angle relative to the voltage is possible. The main disadvantage is the distortion of the current.

Chapter 3 has critically appraised the present state of the art in electronic control of phase angle. The limitations of the present systems have been determined.

Chapter 4NOVEL APPLICATION OF SWITCHED
CAPACITORS IN RL CIRCUITS

Abstract: The switched capacitor principle used in I.C. RC filters is reviewed at the beginning of the chapter. The development of the RL circuit in series with a H bridge with a DC supply in the middle, is analyzed. A novel application of switched capacitors in alternating RL circuits is presented and analyzed. The operation of the application is verified by simulation.

In chapter 3 a few concepts that could be used to implement high value capacitors were presented. Some of the methods (based on the gyrator concept) are not currently viable for emulating high capacitance at motor power levels due to hardware limitations or need of an additional power supply. Applications based on a capacitor in parallel with a bi-directional switch are closer to the requirements of this project, but have the disadvantage of generating harmonics in the rotor circuit and the supply current. The system will operate inefficiently and is unlikely to satisfy the electromagnetic compatibility (EMC) requirements.

Divan [21] used the principle of switched capacitor to implement inductive effects. His system used the RC filter concept from microelectronics.

4.1 Switched capacitors in active filters

In Integrated Circuit active filters, the resistor is emulated using switched capacitors with the advantage that this implementation occupies a silicon area that is a hundred times as small as the area required by a conventional resistor [26]. Fig.4.1 shows the technique for emulating resistive effect using switched capacitor.

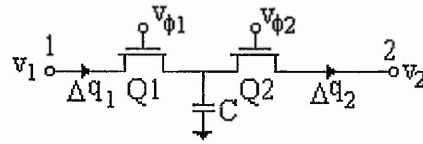


Fig. 4.1 – Two switch resistor simulation and voltage distribution

Let us consider the charge Δq_1 that enters the capacitor C from the input terminal 1 while $v_{\phi 1}$ is high and the device Q_1 conducts. The capacitor C charges to v_1 from its previous voltage level v_2 . Assuming $v_1 > v_2$,

$$\Delta q_1 = C(v_1 - v_2) \quad (4.1)$$

Then $v_{\phi 1}$ falls to zero, Q_1 cuts off and C holds its voltage at v_1 . Then $v_{\phi 2}$ goes high and while Q_2 conducts the voltage across C changes from v_1 to v_2 . The charge given by:

$$\Delta q_2 = -C(v_1 - v_2) \quad (4.2)$$

is released by capacitor C. Since the ON times of Q_1 and Q_2 are equal, $|\Delta q_1| = |\Delta q_2|$.

A mean current is established between terminals 1 and 2 and is given by :

$$i = \frac{\Delta q_1}{T_s} = \frac{C}{T_s}(v_1 - v_2) \quad (4.3)$$

where T_s is the switching frequency.

Comparing equation (4.3) with:

$$i = \frac{1}{R}(v_1 - v_2) \quad (4.4)$$

it can be deduced that the circuit emulates a resistor of value $\frac{T_s}{C}$ ohms.

4.2 Current phase control in RL circuits using a dc source

The insertion of a capacitor in a RL circuit (which can be a phase of an induction machine) modifies the current phase and amplitude. Varying the capacitor value will further change current phase and amplitude giving an element of control.

One of the aims of this work is to control the phase of the current. Fig. 4.2 shows RL components in series with a switched H bridge containing a dc source. The system is strictly doubly-fed, although one source is dc.

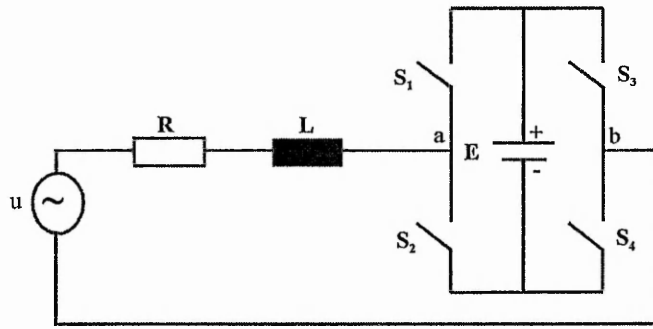


Fig. 4.2 - Switched capacitor H bridge in ac circuit

Switches S_1, S_4 are ON (S_2, S_3 OFF) during the time interval t_1 and S_2, S_3 are ON (S_1, S_4 OFF) in time interval t_2 . The switching period, $T_s = t_1 + t_2$ is maintained constant. Thus, it is possible to define the duty ratio :

$$d = \frac{t_1}{T_s} \tag{4.5}$$

Considered in diakoptics, for the interval, t_1 , the circuit has the configuration of figure 4.3. Equation (4.6) expresses this configuration:

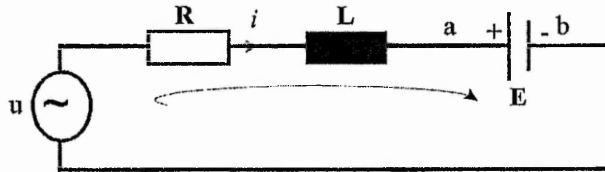


Fig. 4.3 - Circuit for time interval t_1

$$u = Ri + L \frac{di}{dt} + E \tag{4.6}$$

where

$$u = U_m \sin(\omega t)$$

$$\tan(\alpha) = \frac{\omega L}{R}$$

and ω is the angular velocity and α is the natural phase angle between the input voltage u and the current i .

For the interval t_2 , the circuit has the configuration of figure 4.4 and equation (4.7) expresses this configuration :

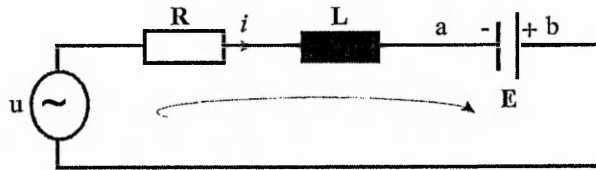


Fig. 4.4 - Circuit for time interval t_2

$$u = Ri + L \frac{di}{dt} - E \quad (4.7)$$

An equivalent circuit can be drawn from figures (4.3) and (4.4):

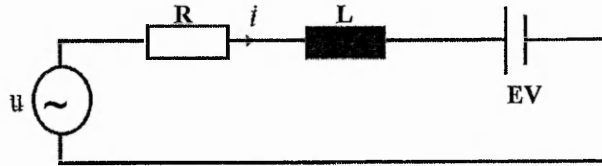


Fig. 4.5 - Equivalent circuit

$$\text{where } EV = \begin{cases} +E & \text{for } t \in (n^*T_s, n^*T_s + t_1) \\ -E & \text{for } t \in (n^*T_s + t_1, (n+1)^*T_s) \end{cases}$$

where n is a natural number between 0 and infinity.

And the network equation is :

$$u(t) = Ri(t) + L \frac{di(t)}{dt} + EV \quad (4.8a)$$

State space averaging technique[27] is applied to equation (4.8a) for one switching period T_s :

$$\begin{aligned} \frac{1}{T_s} \int_0^{T_s} u(t) dt &= \frac{R}{T_s} \int_0^{T_s} i(t) dt + \frac{L}{T_s} \frac{d}{dt} \left(\int_0^{T_s} i(t) dt \right) + \frac{1}{T_s} \int_0^{T_s} EV dt \\ &= \frac{R}{T_s} \int_0^{T_s} i(t) dt + \frac{L}{T_s} \frac{d}{dt} \left(\int_0^{T_s} i(t) dt \right) + \frac{E}{T_s} \left(\int_0^{t_1} 1 dt - \int_{t_1}^{T_s} 1 dt \right) \end{aligned} \quad (4.8b)$$

Equation (4.8b) is transformed to (4.9) by considering its each component value averaged over each switching period for a full supply cycle:

$$\tilde{u}(t) = R\tilde{i}(t) + L \frac{d\tilde{i}(t)}{dt} + (2d(t) - 1)E \quad (4.9)$$

where

$\tilde{u}(t) = u_{avn}$ for $t \in [nT_s, (n+1)T_s)$, $n \in N$ & $n = 0, \text{mod} \left(\frac{T}{T_s} - 1 \right)$, where u_{avn} is the average value

for the n^{th} interval

$\tilde{i}(t) = i_{avn}$ for $t \in [nT_s, (n+1)T_s)$, $n \in N$ & $n = 0, \text{mod} \left(\frac{T}{T_s} - 1 \right)$, where i_{avn} is the average value

for the n^{th} interval

and T is the supply period.

If the effective value of current $\tilde{i}(t)$ is calculated, the result is a constant value (current) I_{dc} , but this constant value can be considered to be the RMS value of a pure sinusoidal variable.

In this case, u is, of course, the equivalent variable of \tilde{u} and \tilde{i} will be considered as the equivalent of the desired current i_d , where :

$$i_d(t) = I_m \sin(\omega t - \varphi) = \frac{U_m}{Z_e} \sin(\omega t - \varphi)$$

φ is the desired phase angle between the current and the input voltage (the desired angle is referred to the current phasor- see appendix 4.2), Z_e is the resulting equivalent impedance of the circuit in the condition when the desired current i_d is reached and $I_m = I_{dc} \sqrt{2}$.

The resulting impedance can also be expressed in the form :

$$Z_e = \frac{R}{\cos(\varphi)}$$

Thus, the equation of the desired current can be rewritten as :

$$i_d(t) = \frac{U_m}{R} \cos(\varphi) \sin(\omega t - \varphi) \quad (4.10a)$$

The value of $d(t)$ for which the circuit accomplishes the phase difference φ has to be calculated. The equivalent variables u and i_d are substituted into equation (4.9), giving

$$U_m \sin(\omega t) = U_m \cos(\varphi) \sin(\omega t - \varphi) + \frac{\omega L U_m}{R} \cos(\varphi) \cos(\omega t - \varphi) + (2d(t) - 1)E$$

$$(2d(t) - 1)E = U_m (\sin(\omega t) - \cos(\varphi) (\sin(\omega t - \varphi) + \tan(\alpha) \cos(\omega t - \varphi)))$$

The following relationship is used :

$$\begin{aligned}
 X &= \sin(\omega t) - \cos(\varphi)(\sin(\omega t - \varphi) + \tan(\alpha)\cos(\omega t - \varphi)) \\
 X &= \sin(\omega t) - \frac{\sin(\omega t) + \sin(\omega t - 2\varphi)}{2} - \tan(\alpha)\frac{\cos(\omega t) + \cos(\omega t - 2\varphi)}{2} \\
 &= \frac{\sin(\omega t)\cos(\alpha) - \sin(\omega t - 2\varphi)\cos(\alpha) - \sin(\alpha)\cos(\omega t - 2\varphi) - \sin(\alpha)\cos(\omega t)}{2\cos(\alpha)} \\
 X &= \frac{\sin(\omega t - \alpha) - \sin(\omega t - 2\varphi + \alpha)}{2\cos(\alpha)} = -\frac{\sin(\alpha - \varphi)\cos(\omega t - \varphi)}{\cos(\alpha)} \quad (4.10b)
 \end{aligned}$$

And results in :

$$d(t) = \frac{1}{2} - \frac{U_m \sin(\alpha - \varphi)\cos(\omega t - \varphi)}{2E \cos(\alpha)} \quad (4.11)$$

It results from (4.11) that the duty ratio $d(t)$ has a sinusoidal variation during the process. The amplitude of the variation is influenced by the value of the DC source.

The practical limits of the duty ratio $d(t)$ are 0 and 1, for a proper operation of the H-bridge, i.e. $0 \leq d(t) \leq 1$

At the first limit :

$$\begin{aligned}
 d(t) \geq 0 &\rightarrow \frac{U_m \sin(\alpha - \varphi)\cos(\omega t - \varphi)}{2E \cos(\alpha)} \leq \frac{1}{2} \\
 U_m \sin(\alpha - \varphi)\cos(\omega t - \varphi) &\leq E \cos(\alpha) \quad (4.12)
 \end{aligned}$$

Taking the worst case value of unity for the time variant term $\cos(\omega t - \varphi)$, the relation to be satisfied by E is given in equation (4.13).

$$E \geq \frac{U_m \sin(\alpha - \varphi)}{\cos(\alpha)} \quad (4.13)$$

At the second limit :

$$\begin{aligned}
 d(t) \leq 1 &\rightarrow -\frac{U_m \sin(\alpha - \varphi)\cos(\omega t - \varphi)}{2E \cos(\alpha)} \leq \frac{1}{2} \\
 U_m \sin(\alpha - \varphi)\cos(\omega t - \varphi + \pi) &\leq E \cos(\alpha)
 \end{aligned}$$

A similar reasoning to that one used from equation (4.12) leads to the same relationship (4.13).

4.4 Simulation of RL circuit with switched dc source

Before any simulation is made, an analysis algorithm permitting the transient analysis of the input voltage and resulting current such that it is possible to calculate the phase difference between the input voltage and the current has to be established.

Fourier series can be used for this purpose because the signals in the analysis are periodical. Any periodical signal $x(t)$ can be expressed:

$$x(t) = \frac{A_0}{2} + \sum_{n=1}^{\infty} A_n \cos(n\omega t + \varphi_n)$$

where A_n and φ_n are the amplitude and phase of the n th harmonic, A_0 is the dc component of the wave, C_n and S_n are Fourier coefficients that are calculated with:

$$C_0 = \frac{1}{T} \int_0^T f(t) dt$$

$$C_n = \frac{2}{T} \int_0^T f(t) \cos(n\omega t) dt$$

$$S_n = \frac{2}{T} \int_0^T f(t) \sin(n\omega t) dt$$

where $T = \frac{\omega}{2\pi}$.

The amplitude of each harmonic is calculated using the relations :

$$A_0 = C_0$$

respective

$$A_n = \sqrt{C_n^2 + S_n^2}$$

Equations (4.6) and (4.7) are brought into the simulation in the forms :

$$\frac{di}{dt} = \frac{u - Ri - E}{L}$$

$$\frac{di}{dt} = \frac{u - Ri + E}{L}$$

It is possible to simulate the system by solving the differential equations using a Runge-Kutta algorithm. The duty ratio is recalculated at the beginning of each switching cycle. Periodical samples of the current and voltage are taken during the simulation and, thus,

the current amplitude and the phase difference are calculated. The simulations are performed using a C++ program that, along with the flow chart, is listed in Appendix 4.1.

The circuit is simulated with two sets of parameters at two different frequencies for each set. Two different DC sources are used for each set, imposing two phase differences between current and input voltage. Figs.4.6 to 4.11 show results for Circuits 1 and 2. It has to be noticed that for the equivalent time of two supply periods the switched DC source is not inserted in the circuit and the duty ratio d is zero.

Circuit 1

$R = 10\Omega$, $L = 500mH$, $U_m = 10V$, $f = 5Hz$, $f_s = 1kHz$, natural phase angle of 52° where f_s is the switching frequency.

Circuit 2

$R = 5\Omega$, $L = 20mH$, $U_m = 10V$, $f = 50Hz$, $f_s = 10kHz$, natural phase angle of 51°

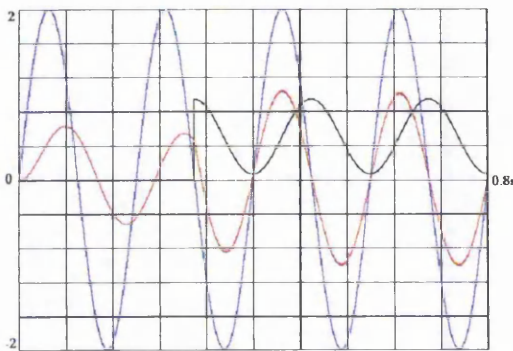


Fig. 4.6 - Circuit 1: $E = 18V$, $\varphi = 0$

$$i_m = 1, \varphi_m = -0.6$$

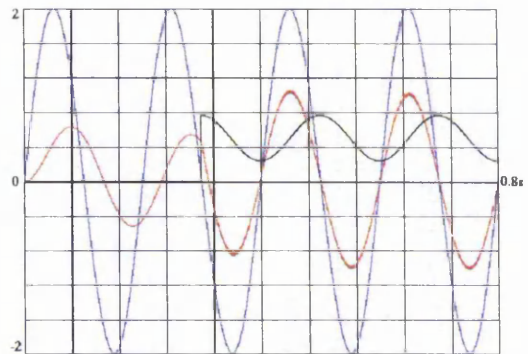


Fig. 4.7 - Circuit 1: $E = 30V$, $\varphi = 0$

$$i_m = 1, \varphi_m = -0.6$$

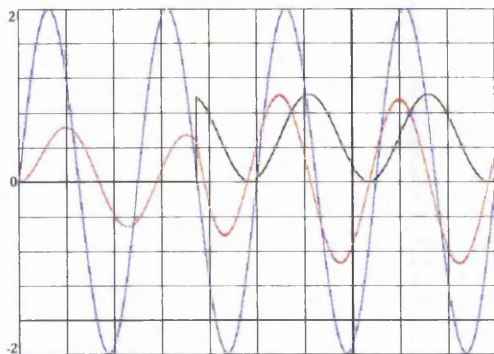


Fig. 4.8 - Circuit 1: $E = 18V$, $\varphi = -20$

$$i_m = 0.94, \varphi_m = -20.4$$

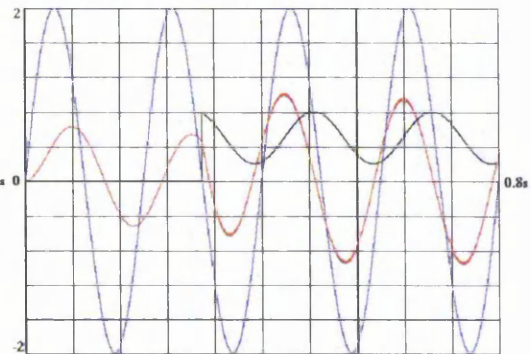
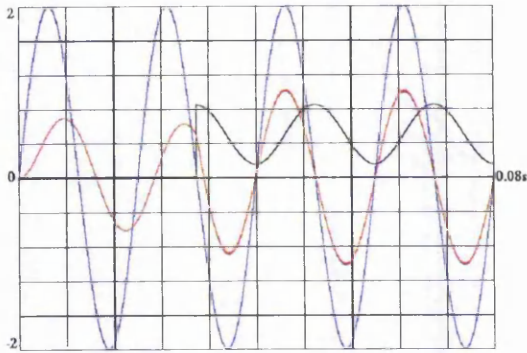
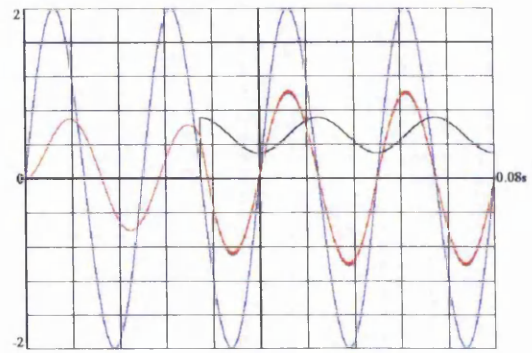


Fig. 4.9 - Circuit 1: $E = 30V$, $\varphi = -20$

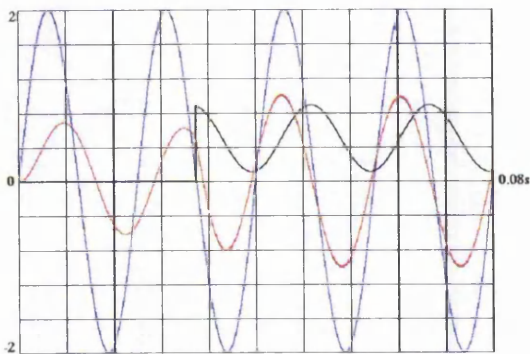
$$i_m = 0.94, \varphi_m = 19.2$$

Fig. 4.10 - Circuit 2: $E = 18V, \varphi = 0$

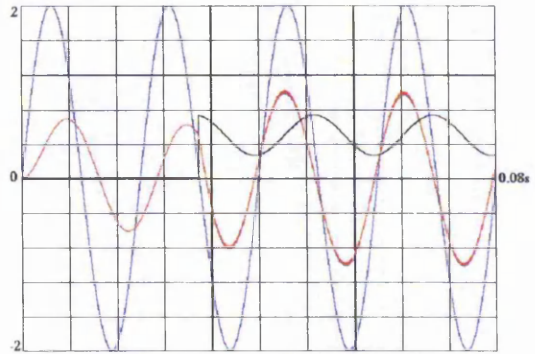
$$i_m = 2, \varphi_m = -0.6$$

Fig. 4.11 - Circuit 2: $E = 30V, \varphi = 0$

$$i_m = 2, \varphi_m = -0.6$$

Fig. 4.12 - Circuit 2: $E = 18V, \varphi = -10$

$$i_m = 1.9, \varphi_m = -9.3$$

Fig. 4.13 - Circuit 2: $E = 30V, \varphi = -10$

$$i_m = 1.9, \varphi_m = -9.4$$

Legend: Input voltage divided by 5, Current divided by 2, Duty ratio

φ represents the desired phase difference; i_m and φ_m are the resulting simulated values of the current and the phase difference respectively. They are calculated using Fourier series and sampled values of current and input voltage.

Among the conclusions that can be drawn from the simulation, the advantages of using this method are as follows :

- the current waveform is smooth;
- the amplitude and phase difference achieved are quite good;
- if E has the correct value, φ can take any value between -90° and 90° ;

There are also several drawbacks, listed as follows :

- the requirement of a supplementary DC source ;
- the variation of the duty ratio $d(t)$ – it is calculated almost continuously. The amplitude variation is influenced by the value of DC source – the higher the DC value, the smaller the variation - equation (4.11);

- the minimum value of the DC source has to be modified in accordance with the desired phase difference – equation (4.13);

4.5 Switched capacitor in RL circuits

If the DC source from figure 4.2 is replaced by a capacitor (figure 4.14), it will be a “middle case” between the switched capacitor from active filters and the switched DC source from RL circuits that were previously presented. The capacitor charging is not as fast as in active capacitor filters due to the presence of resistance and inductance. During interval t_1 , the capacitor is charged with a polarity (with respect to point a) that is applied in reverse to the RL circuit (with respect to the same point a) in interval t_2 . The functional mechanism is similar to the DC source case but, now, it can be considered with a variable source applied to the RL circuit.

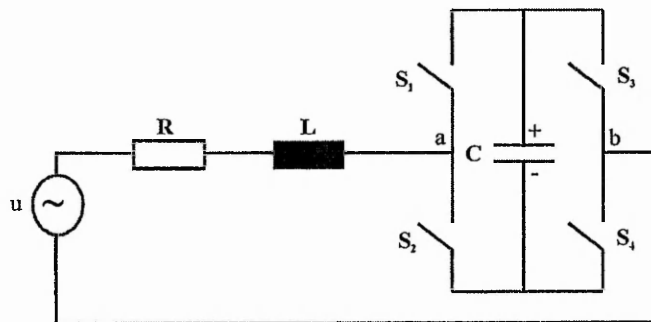


Fig. 4.14 - DC source replaced by a capacitor

Beside the variables (u, α, φ) defined for the switched DC source case, a new variable β is introduced, defined by the relation ,

$$\tan(\beta) = \frac{1}{\omega CR}$$

When the switch pair S_1, S_4 is ON (t_1 interval), the capacitor is charging – we have a RLC series circuit

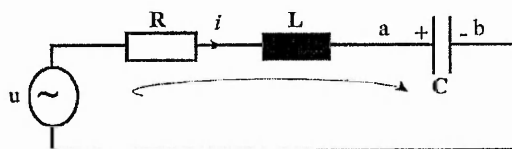
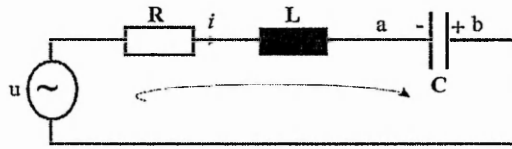


Fig. 4.15 - Circuit for interval t_1

For the interval t_2 the switches pair S_2, S_3 is ON .

Fig. 4.16 - Circuit for interval t_2

The AC capacitor does not have polarised terminals, but the beginning of the switching period is taken when the capacitor is charged as in figure 4.14. The current has the same sense as the arrows in figures 4.15 and 4.16. At the beginning and the end of the interval t_2 due to the high switching period and the inductance, the capacitor has the same polarity with respect to the terminals (except when the polarity of the input sine wave becomes negative). The current does not change polarity.

For the interval t_1 the following equations can be written :

$$u(t) = Ri(t) + L \frac{di(t)}{dt} + u_c(t) \quad (4.14)$$

$$u_c(t) = \frac{\int i(t) dt}{C}$$

And for t_2 :

$$u(t) = Ri(t) + L \frac{di(t)}{dt} - u_c(t) \quad (4.15)$$

$$u_c(t) = -\frac{\int i(t) dt}{C}$$

The state space averaging technique is applied to equations (4.14) and (4.15) for each switching period of a full supply cycle and, according to [24], results:

$$\tilde{u}(t) = R\tilde{i}(t) + L \frac{d\tilde{i}}{dt} + (2d(t) - 1)\tilde{u}_c \quad (4.16)$$

$$\tilde{u}_c(t) = (2d(t) - 1) \frac{\int \tilde{i}(t) dt}{C} \quad (4.17)$$

where

$$\tilde{u}(t) = u_{avn} \quad \text{for } t \in [nT_s, (n+1)T_s), n \in N \ \& \ n = 0, \text{ mod} \left(\frac{T}{T_s} - 1 \right), \text{ where } u_{avn} \text{ is the average value}$$

for the n^{th} interval

$\tilde{i}(t) = i_{avn}$ for $t \in [nT_s, (n+1)T_s), n \in N \& n = 0, \text{mod}\left(\frac{T}{T_s} - 1\right)$, where i_{avn} is the average value
for the n^{th} interval

$\tilde{u}_c(t) = u_{cavn}$ for $t \in [nT_s, (n+1)T_s), n \in N \& n = 0, \text{mod}\left(\frac{T}{T_s} - 1\right)$, where u_{cavn} is the average value
for the n^{th} interval

Introducing (4.17) into (4.16):

$$\tilde{u}(t) = R\tilde{i}(t) + L\frac{d\tilde{i}(t)}{dt} + (2d(t)-1)^2 \frac{\int \tilde{i}(t)dt}{C} \quad (4.18)$$

Using the same reasoning about the effective values as previously and taking the input voltage $u = U_m \sin(\omega t)$ and the resulting current $i_d = \frac{U_m}{R} \cos(\varphi) \sin(\omega t - \varphi)$ as in the previous case and introducing these terms into (4.18) give:

$$u = Ri_d + L\frac{di_d}{dt} + (2d(t)-1)^2 \frac{\int i_d dt}{C}$$

$$U_m \sin(\omega t) = U_m \cos(\varphi) \sin(\omega t - \varphi) + \frac{\omega L U_m}{R} \cos(\varphi) \cos(\omega t - \varphi) -$$

$$-(2d(t)-1)^2 \frac{U_m}{\omega RC} \cos(\varphi) \cos(\omega t - \varphi)$$

And :

$$-(2d(t)-1)^2 \tan(\beta) \cos(\varphi) \cos(\omega t - \varphi) = \sin(\omega t) - \cos(\varphi) (\sin(\omega t - \varphi) + \tan(\alpha) \cos(\omega t - \varphi))$$

Using the expression for X (4.10b) from the previous case :

$$-(2d(t)-1)^2 \tan(\beta) \cos(\varphi) \cos(\omega t - \varphi) = -\frac{\sin(\alpha - \varphi) \cos(\omega t - \varphi)}{\cos(\alpha)}$$

Resulting in :

$$d(t) = \frac{1}{2} \left(1 + \sqrt{\frac{\tan(\alpha) - \tan(\varphi)}{\tan(\beta)}} \right) \quad (4.19)$$

The duty ratio $d(t)$ has to obey two conditions:

- a. the expression under the square has to be positive, which means that :

$$\tan(\alpha) - \tan(\varphi) \geq 0$$

This implies that :

$$\varphi \leq \alpha \quad (4.20)$$

- b. the lower and upper limits of duty ratio are 0 respective 1:
- Equation (4.19) clearly shows that $d(t)$ is always real and positive if condition (4.20) is fulfilled ; more than this, duty ratio $d(t)$ is equal with or higher than 0.5;
 - $d(t) \leq 1$ means that :

$$\frac{1}{2} \left(1 + \sqrt{\frac{\tan(\alpha) - \tan(\varphi)}{\tan(\beta)}} \right) \leq 1$$

$$\tan(\varphi) \geq \tan(\alpha) - \tan(\beta) = \frac{\omega L - \frac{1}{\omega C}}{R}$$

$$\varphi \geq \arctan \left(\frac{\omega L - \frac{1}{\omega C}}{R} \right) \quad (4.21)$$

Conditions (4.20) and (4.21) show that the phase difference φ between input voltage and current can be varied over the range of the RL respective RLC circuits with passive components without switches.

When d varies between (0.5 and 1) the phase shift current-input voltage varies between

the minimum and maximum extremities $\left(\arctan \left(\frac{\omega L - \frac{1}{\omega C}}{R} \right), \alpha \right)$.

Some special cases have to be studied regarding the values of d needed to achieve the required phase differences :

1. if the condition $\varphi = \alpha$ is imposed, the duty ratio $d = \frac{1}{2}$;

2. if the condition $\varphi = \arctan \left(\frac{\omega L - \frac{1}{\omega C}}{R} \right)$ is required then $d = 1$;

3. if the current and the input voltage are to be in phase ($\varphi = 0$) the duty ratio has to be:

$$d = \frac{1}{2} \left(1 + \sqrt{\omega^2 LC} \right) \quad (4.22)$$

It is interesting to notice but not unexpected that for the in-phase condition, the duty ratio does not depend on resistance (4.22).

Applying Laplace transforms to the averaged model of the system (4.18) to achieve the s form of the system makes further analysis possible.

$$U(s) = RI(s) + sLI(s) + \frac{(2d-1)^2}{sC} I(s)$$

$$H(s) = \frac{I(s)}{U(s)} = \frac{sC}{LCs^2 + RCs + (2d-1)^2} \quad (4.23)$$

Considering the input voltage to be the excitation signal, the respective amplitude – frequency and phase-frequency characteristics may be derived and plotted as Bode diagrams from (4.23).

An estimation of the voltage across the inserted capacitor for the required phase difference between current and voltage can be made starting from the averaged equations (4.9) and (4.18). If it is assumed that the circuits from Fig. 4.2 and Fig. 4.6 have the same parameters R, L and u and the same phase difference then :

$$(2d_E - 1)E = (2d_C - 1)^2 \tilde{u}_c \quad (4.24)$$

The duty ratios d_E and d_C in these circuits have different values and expressions. Inserting equations (4.11) and (4.19) in (4.24),

$$\frac{U_m \sin(\alpha - \varphi) \cos(\omega t - \varphi)}{\cos(\alpha)} = \frac{\tan(\alpha) - \tan(\varphi)}{\tan(\beta)} \tilde{u}_c$$

$$\tilde{u}_c = U_m \frac{\cos(\varphi) \sin(\beta)}{\cos(\beta)} \cos(\omega t - \varphi)$$

The amplitude of the voltage across the capacitor can be calculated from:

$$U_{cm} = \frac{U_m \cos(\varphi)}{\omega RC} \quad (4.25)$$

As a final consideration, starting from (4.18) can be deduced the relation between the emulated capacitor on one hand and the used capacitor and duty ratio on the other.

$$C_e = \frac{C}{(2d-1)^2} \quad (4.26)$$

4.6 Some physical considerations

To try a physical explanation of what is happening in the presented phase control system, is taken into account the fact that the connection of a capacitor in an alternative RL circuit produces a transient regime. The current changes with frequency, reaching peak values higher than the value under steady state conditions.

In this analysis, it is assumed that the supply voltage is constant during intervals t_1 , when the switches S_1, S_4 are ON, and t_2 , when the switches S_2, S_3 are ON (taking into account the difference between the supply and the switching frequencies). Thus, it can be considered that there are two transient patterns in RLC circuits supplied by DC voltages (equal to the values of the supply at the beginning of intervals t_1 and t_2) occur during one switching period.

The mathematical analysis of the RLC circuit supplied by a DC source is presented in appendix 4.3 and, here, transient current is shown for the two different patterns: a RLC circuit with the initial positive voltage of the capacitor (*case 1*) and a RLC circuit with initial negative voltage of the capacitor (*case 2*). Also, it is represented the transient current of a RL circuit (*case 3*). The parameters R, L, C and the supply voltage are the same in all three cases.

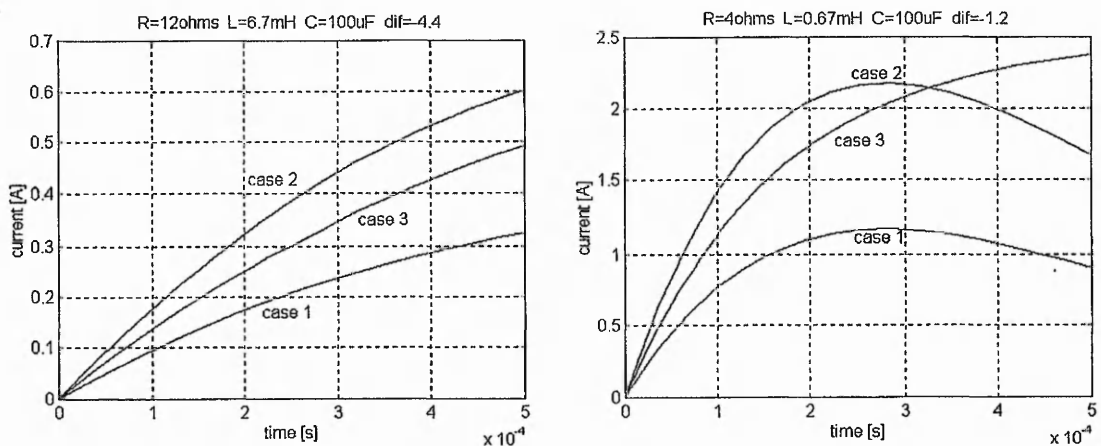


Fig. 4.17 – Transient currents for $R < 2\sqrt{L/C}$, $dif = R - 2\sqrt{L/C}$

The currents represented in figures 4.17 and 4.18 occurred when the supply voltage was switched in the circuits. It can be seen from the graphs that, in the early stages of the transient process, the currents in case 2 rise faster than the currents in cases 1 and 3, and this fact is used in controlling the phase between the voltage and current.

For the switched capacitor in series with an alternative RL circuit, the following sequence exists: At the time zero (the beginning of interval t_1) the initial capacitor voltage $u_{ci} = 0$; the capacitor then charges and at the end of this interval, it will have the voltage $+V_1$; At the start of interval t_2 , $u_{ci} = -V_1$; during this interval the capacitor

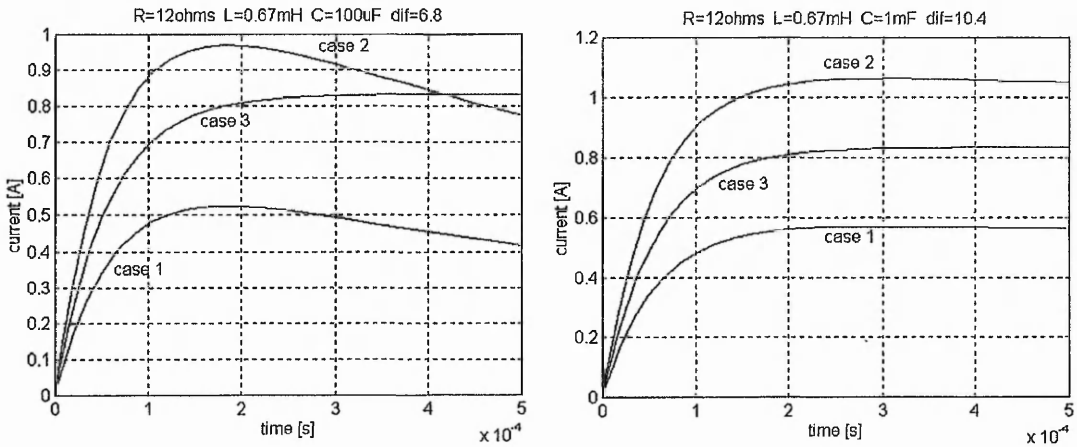


Fig. 4.18 – Transient currents for $R > 2\sqrt{L/C}$, $dif = R - 2\sqrt{L/C}$

voltage is decreasing and the switching frequency is chosen high enough to prevent the capacitor from discharging completely and charging again with reversed polarity ; Thus, at the end of switching cycle $u_c = -V_2$ ($|V_2| < |V_1|$); the current increases faster than the current of the simple RL circuit ; $u_{ci} = V_2$ at the start of the new interval t_1 (case 1); the increase of current is comparable raise of the current of a RL circuit(case 3) ; the capacitor voltage increases to V_3 at the end of the interval, ($|V_3| > |V_1|$) ; in this case, at the beginning of interval t_2 , $u_{ci} = -V_3$ (again case 2) ; the current again is increasing . The process will then be repeated in the same way.

4.7 Simulation results

The differential equations resulting from (4.14) are,

$$\frac{di}{dt} = \frac{u - Ri - u_c}{L}$$

$$\frac{du_c}{dt} = \frac{i}{C}$$

and from (4.15) are ;

$$\frac{di}{dt} = \frac{u - Ri + u_c}{L}$$

$$\frac{du_c}{dt} = -\frac{u}{C}$$

They are used to simulate the proposed application of the switched capacitor, using the Runge-Kutta algorithm.

Three circuit configurations are used in simulations. The second differs from the first by the supply frequency and the third differs from the first by the used capacitor. The Fourier series are involved to analyze the simulation results. Also, the phase angle variation function of duty ratio and the Bode characteristics for the resonance duty ratio are drawn for each circuit.

Circuit 1

$R = 5\Omega, L = 10mH, C = 10\mu F, u = 20 \sin(2\pi 50t)$, natural phase angle of 32°

$f_s = 5kHz, f_{sam} = 50kHz$

where f_s represents the switching frequency and f_{sam} is the sampling frequency for Fourier analysis.

Fig. 4.19a shows the variation of phase difference with duty ratio. Fig. 4.19b gives the Bode diagrams resulting from equation (4.23) for a duty ratio of 0.549 corresponding to resonance.

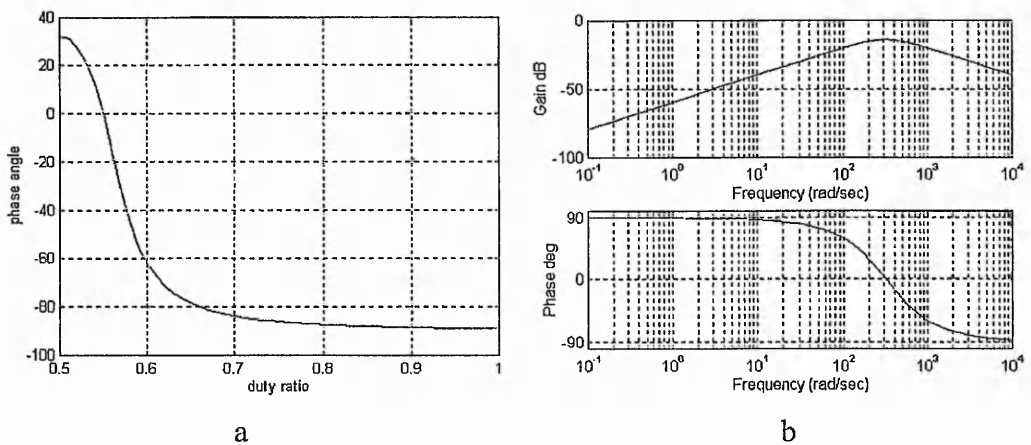


Fig. 4.19 - Phase and frequency response

Figure 4.20 shows a very significant result in that for a phase difference of 10° the emulated capacitance is of $1398\mu\text{F}$, being 139.8 times as big as that of the physical capacitor.

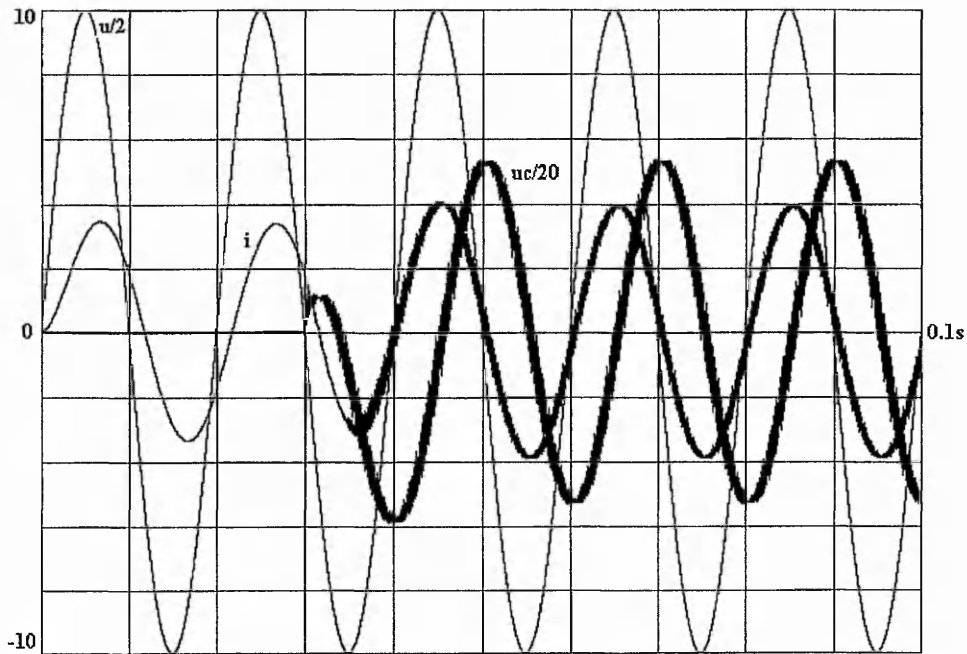


Fig. 4.20 – Circuit 1 response giving $\varphi = 10^\circ$ $\varphi_c = 9.87$ $i_c = 3.93$ $d = 0.542$

In figure 4.21, for a phase difference of 0° the emulated capacitor is of $1025\mu\text{F}$, being 102.5 times as big as the used capacitor.

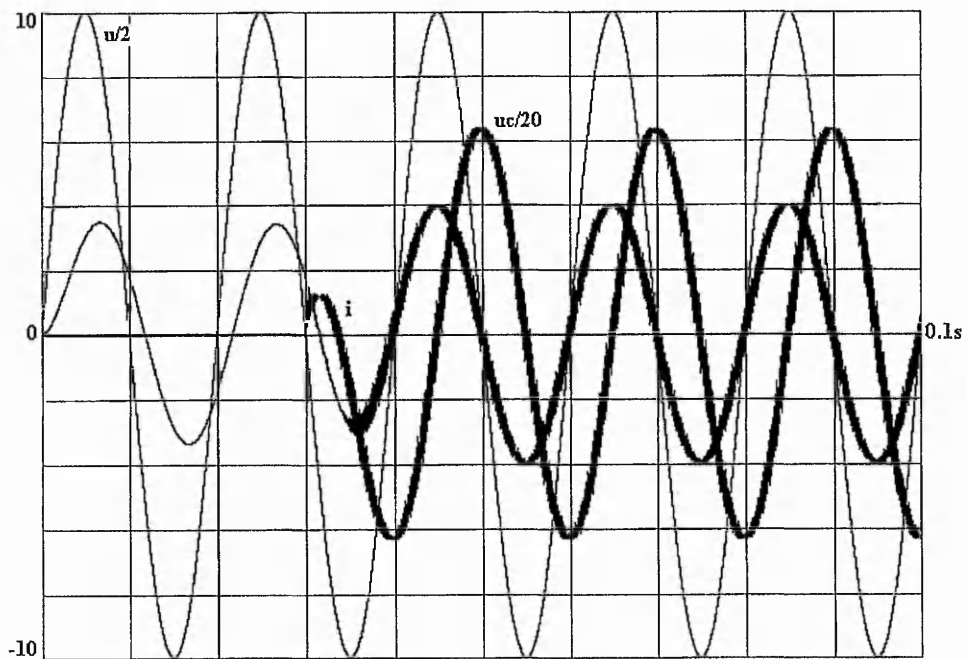


Fig. 4.21 – Circuit 1 response with zero phase-displacement

$$\varphi = 0 \quad \varphi_c = 0.41 \quad i_c = 3.96 \quad d = 0.549$$

Figure 4.22 shows a negative or leading phase-displacement, where for a phase difference of -20° the emulated capacitance is of $645\mu\text{F}$, being 64.5 times as large as that of the physical capacitor used.

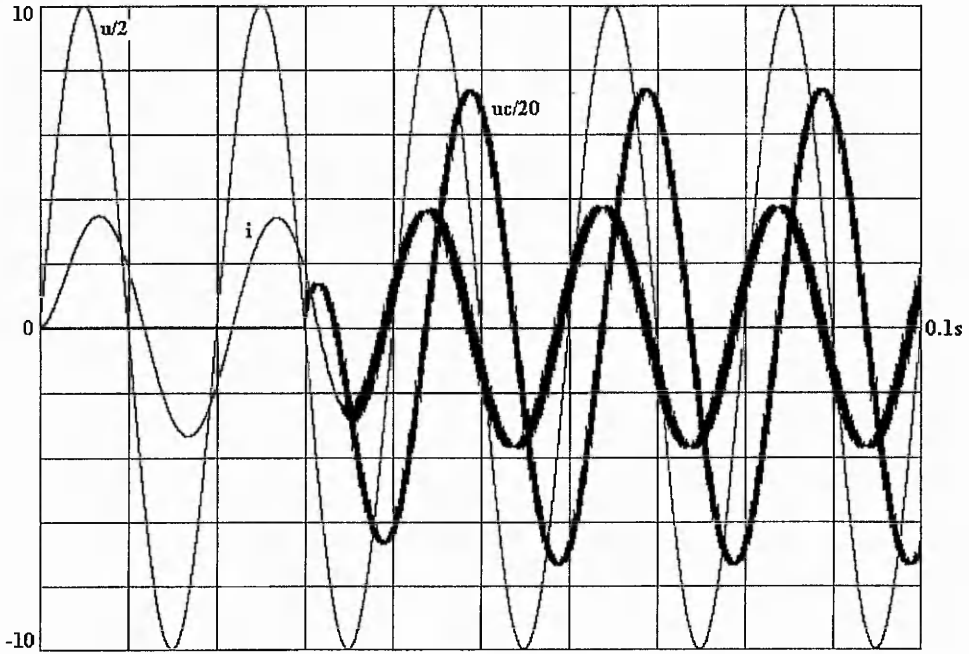


Fig. 4.22 – Circuit 1 response with leading current $\varphi = -20^\circ$ $\varphi_c = -19.69^\circ$ $i_c = 3.71$ $d = 0.562$

Circuit 2

$R = 5\Omega, L = 10\text{mH}, C = 10\mu\text{F}, u = 20 \sin(2\pi 25t)$, natural phase angle of 17°
 switching frequency $f_s = 5\text{kHz}, f_{sam} = 50\text{kHz}$ sampling frequency

Fig. 4.23a shows the variation of phase difference with duty ratio. Fig. 4.23b gives the Bode diagrams for a duty ratio of 0.524.

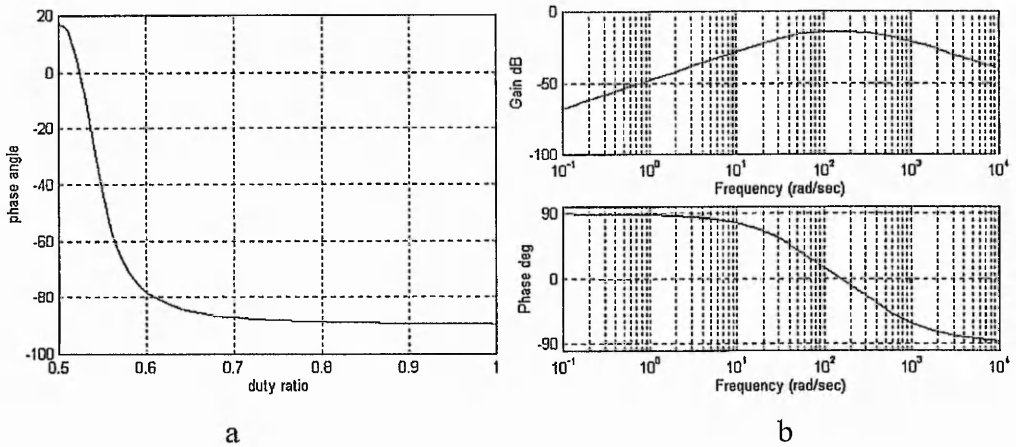


Fig. 4.23 - Phase and frequency response

Figure 4.24, shows that for a phase difference of 10° the emulated capacitance is of $9400\mu\text{F}$, being 940 times as big as that of the physical capacitor used, a very significant result.

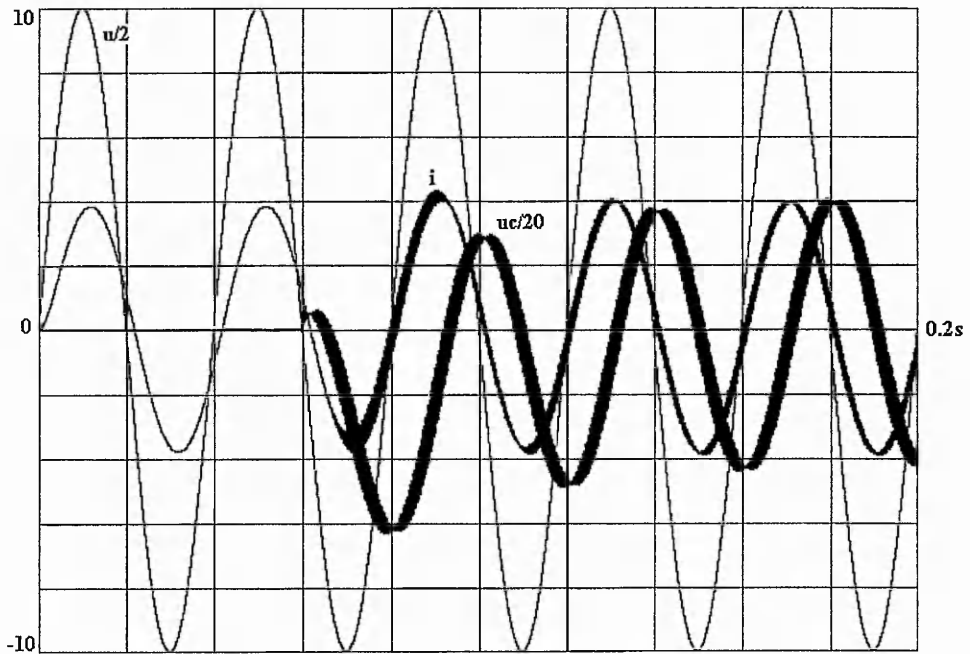


Fig. 4.24 - Circuit 2 response giving $\varphi = 10^\circ$ $\varphi_c = 10.14^\circ$ $i_c = 3.93$ $d = 0.516$

Figure 4.25 shows that for a phase difference of 0° the emulated capacitance is of $4090\mu\text{F}$, being 409 times as big as that of the physical capacitor used.

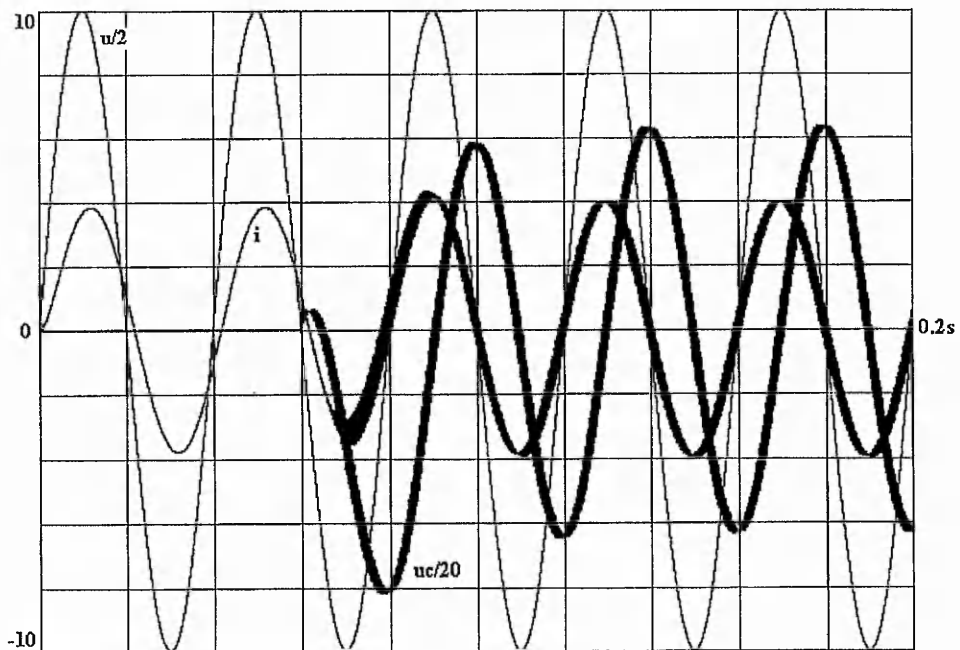


Fig. 4.25 - Circuit 2 response with zero phase-displacement

$$\varphi = 0^\circ \quad \varphi_c = -0.17^\circ \quad i_c = 3.96 \quad d = 0.524$$

Figure 4.26 shows that for a negative or leading phase-displacement of -20° the emulated capacitor is of $1890\mu\text{F}$, being 189 times as large as that of the physical capacitor used.

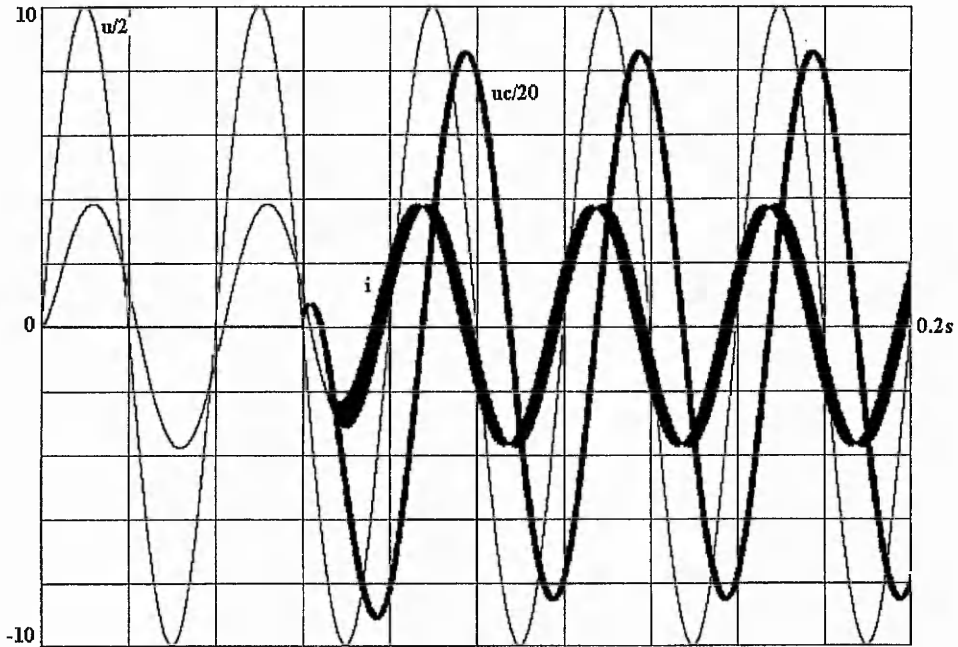


Fig. 4.26 - Circuit 2 response with leading current $\varphi = -20^\circ$ $\varphi_c = -19.66^\circ$ $i_c = 3.7$ $d = 0.536$
 Circuit 3

$R = 5\Omega, L = 10\text{mH}, C = 15\mu\text{F}, u = 20\sin(2\pi 50t)$ natural phase angle of 32°
 switching frequency $f_s = 5\text{kHz}, f_{sam} = 50\text{kHz}$ sampling frequency

Fig. 4.27a shows the variation of phase difference with duty ratio. Fig. 4.27b gives the Bode diagrams for a duty ratio of 0.56.

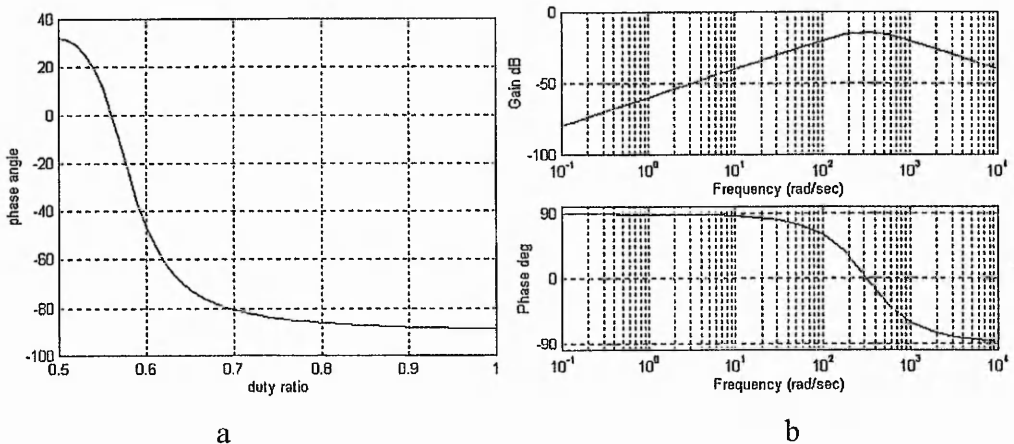


Fig. 4.27 - Phase and frequency response

Figure 4.28 shows that for a phase difference of 10° the emulated capacitance is of $1389\mu\text{F}$, being 92.6 times as big as that of the physical capacitor used.

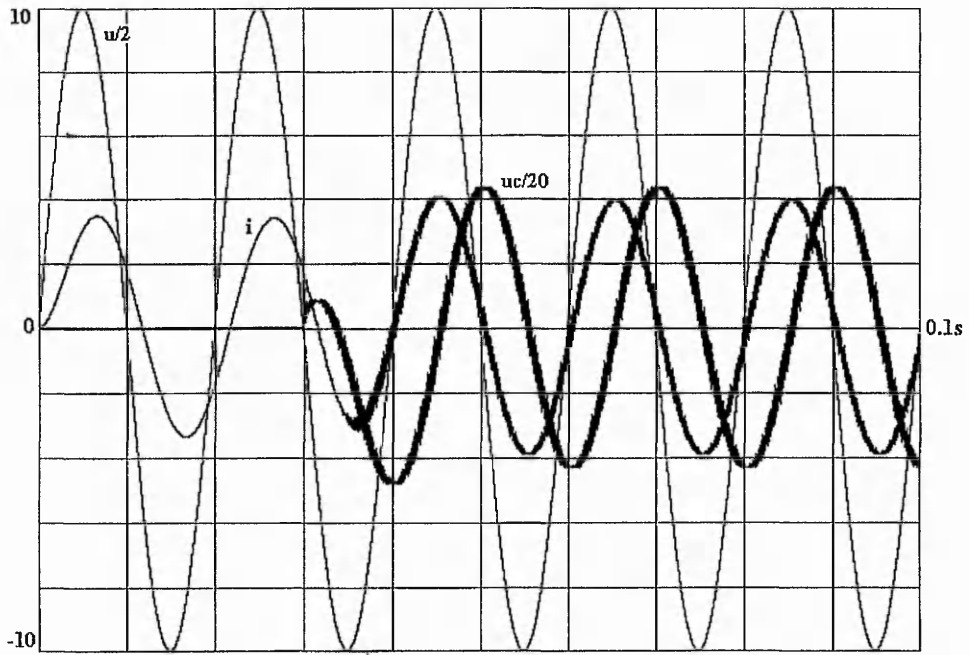


Fig. 4.28 - Circuit 3 response giving $\varphi = 10$ $\varphi_c = 9.65$ $i_c = 3.93$ $d = 0.551$

Figure 4.29 shows that for a phase difference of 0° the emulated capacitance is of $1010\mu\text{F}$, being 67.84 times as big as that of the physical capacitor used.

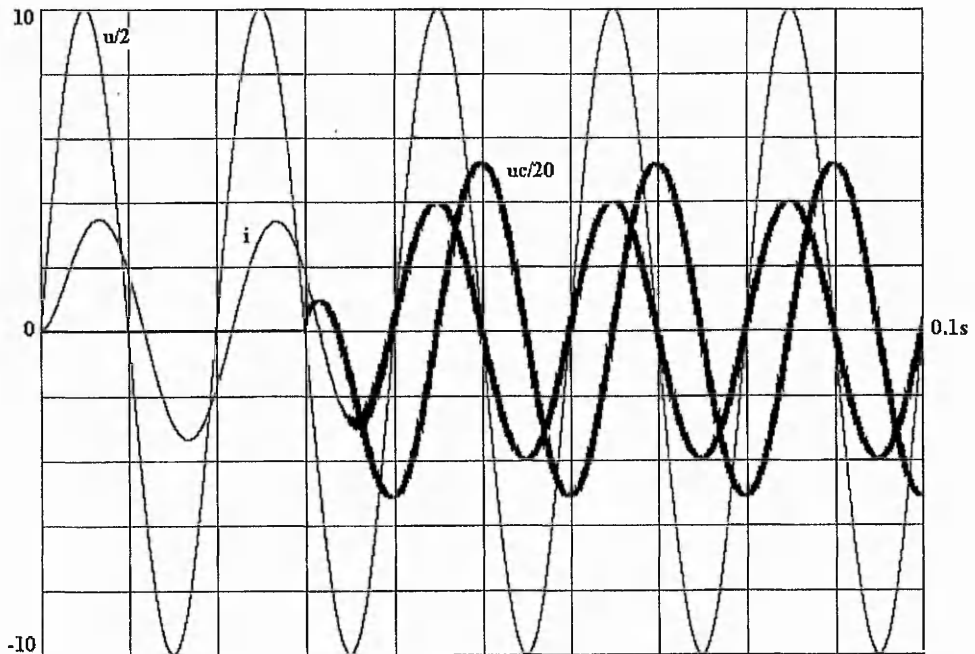


Fig. 4.29 - Circuit 3 response with zero phase-displacement

$$\varphi = 0 \quad \varphi_c = -0.15 \quad i_c = 3.98 \quad d = 0.56$$

Figure 4.30 shows that for a negative or leading phase displacement of -20° the emulated capacitance is of $645\mu\text{F}$, being 42.98 times as large as that of the physical capacitor used.

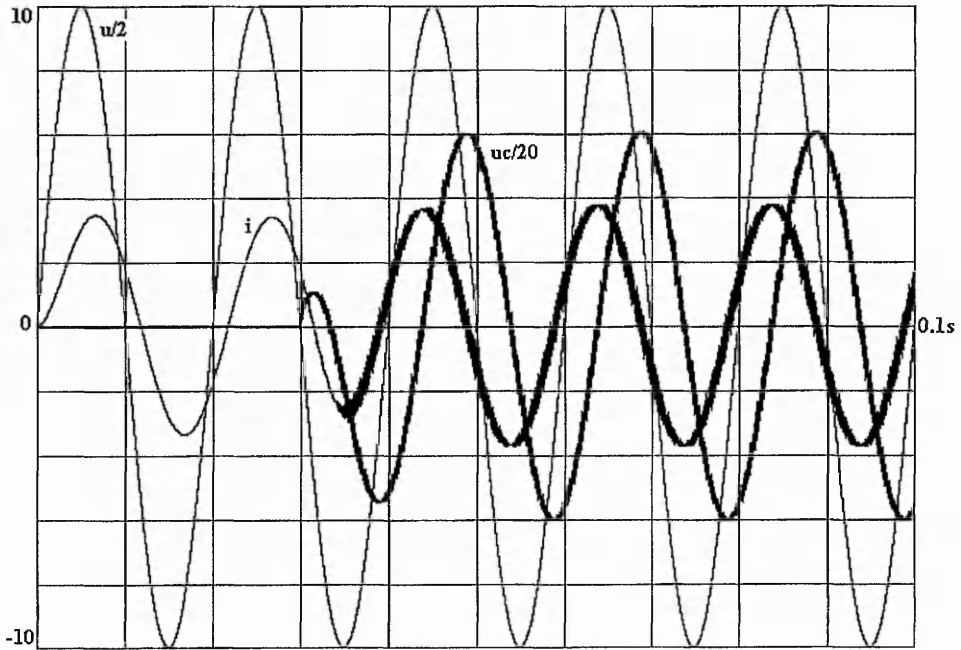


Fig. 4.30 - Circuit 3 response with leading current $\varphi = -20$ $\varphi_c = -19.75$ $i_c = 3.73$ $d = 0.576$

The graphics show that the phase angle control of a RL circuit is viable at simulation level using switched capacitor principle.

The simulations show that if the same duty ratio is applied to circuits that have different parameters, different phase angles occur. Circuits 1 and 2 differ just by the supply frequency but the 'in phase' condition is achieved for different duty ratios (figures 4.25 and 4.21). Also, if the same duty ratios are applied (figures 4.20, 4.22 and 4.24, 4.26 respectively), different phase angles occur. The same situation can be seen if the simulations for circuit 3 are compared with simulations for circuit 1. The same conclusions can be drawn from Bode characteristics. They were simulated for the duty ratios that produce the 'in-phase' conditions in these circuits. It can be seen that for different supply frequencies the in phase condition is not reached anymore.

4.8 Conclusions

The present chapter tackles two methods for current phase control in RL circuits. First method requires a DC supply whose polarities are periodically switched in the RL circuits. The simulation results show a good control of the phase and amplitude of the resulting current. The method presents a few drawbacks such as that the minimum value of the DC source has to be adjusted according to the desired phase angle and that a new value of the duty ratio has to be calculated at the beginning of each switching period.

The second method replaces the DC source with an AC capacitor and eliminates, at the simulation level, most of the disadvantages of the first method

Phase control of the H bridge is relatively simple, except that the accuracy of the phase control is dependent on the resolution of duty ratio. Smaller the used capacitor, higher the resolution of the duty ratio is required to achieve the desired phase angle (equation 4.11).

Simulation show capacitor values that are ten or even hundred times as big as the actual capacitor placed in the H bridge can be emulated.

Contrasting the switched capacitor methods described in Chapter 3 ([6-8]) and corresponding simulated results shown in Fig.3-16 and 3-17 with Figs.4-20 to 4-30 show that switching strategy presented in this chapter is simpler.

In the switched capacitor method, the harmonic distortion is lower compared to methods presented in chapter 3. This is a considerable advantage.

Chapter 5

EXPERIMENTAL RESULTS

Abstract: This chapter presents experimental verification of the novel application of switched capacitors in series with a sinusoidal supply and a RL load. The rotor impedance of a wound induction motor is externally modified by inserting an H bridge in each phase of the rotor circuit. Experimental results are presented for a small induction motor.

A novel method of implementing the effect of large capacitance with a smaller capacitor placed in the middle of an H bridge, was introduced in chapter 4. The simulation results showed that the emulated capacitor is a ten, or even a hundred, times bigger than the actual capacitor used.

The following basic structure is used to verify the principle of a switched capacitor in controlling the phase difference between current and voltage in a RL circuit. The setup is shown in Fig.5.1.

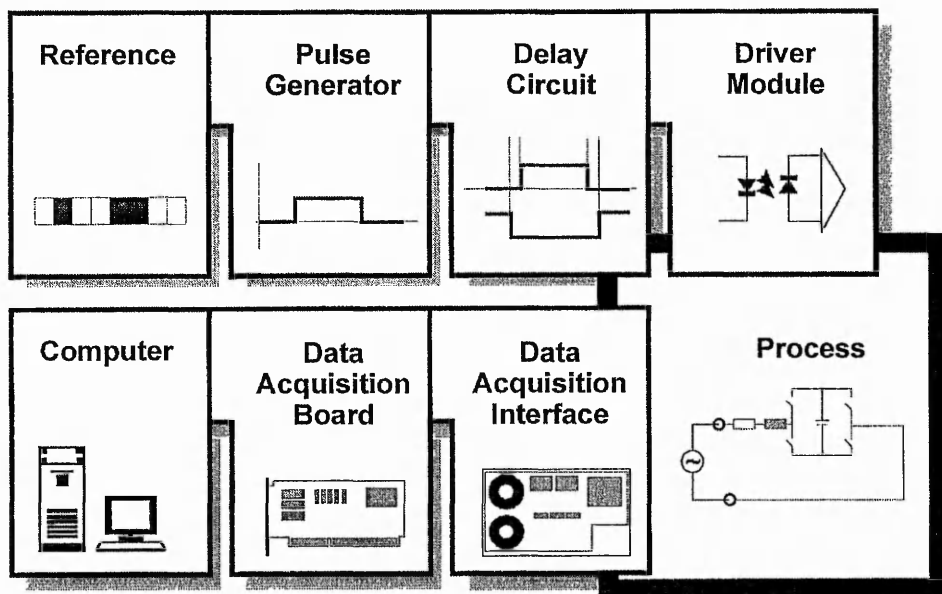


Fig. 5.1 – General system

The system has three main parts that are given below:

- a) the power circuit;
- b) the command system;
- c) the data acquisition system;

5.1 Power Circuit

The power circuit is made up of H-bridge, inductance and resistance connected in series. The circuit is supplied at 26V, 50Hz source. The switches used in H-bridge were bi-directional and are described in the next section.

5.1.1 Bi-directional switches

Bi-directional switch can be implemented using a triac, back to back thyristors or GTOs. Nielsen[28] investigated bi-directional switches using transistors, MOSFET or IGBT with diodes. Some configurations for bi-directional switches are shown in figures 5.2 and 5.3. The configuration of figure 5.3b was chosen, having lower on-state losses compared to those of figure 5.3a(at one instance there are in conduction 2 devices instead of 3) and considering the simplicity of gate drive requirements compared to 5.3c (5.3b requires just one common line per switch).

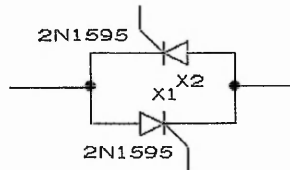


Fig. 5.2 – Bi-directional switch of reverse-pair thyristors

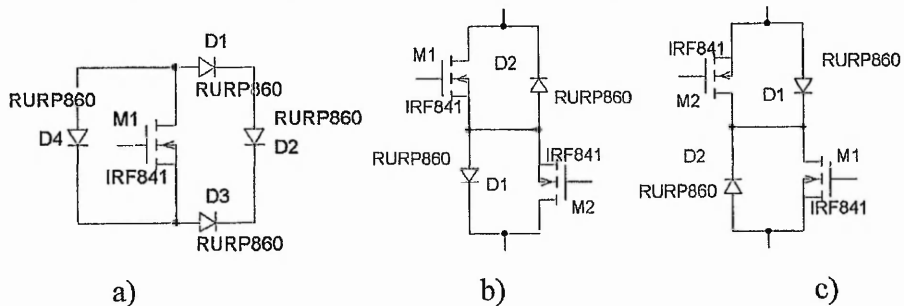


Fig. 5.3 – Bi-directional switches with transistors and diodes

5.2 Command system.

It is important that the control strategy prevents the simultaneous conduction of the switch pairs S_1, S_4 and S_2, S_3 (fig. 4.14). Simultaneous conduction creates a discharge path for the capacitor. Even though the discharging process is incomplete, it influences the system behaviour.

The command systems comprises of:

1. Pulse generator and reference circuit shown in figures 5.4a & 5.4b;
2. Delay circuit shown in figures 5.5a & 5.5b;
3. Driver system modules shown in figures 5.6a & 5.6 b;

5.2.1. Pulse generator & Reference circuit

As shown in equation (4.19), the command circuit has to generate pulses duty ratios of ≥ 0.5 . The resolution of the generator system must be of sufficient enough to permit fine adjustment of the duty ratio d .

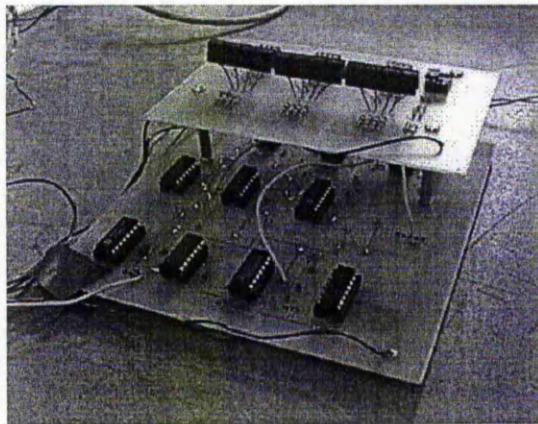


Fig. 5.4a – Pulse generator circuit practical implementation

The pulse generator circuit (figures 5.4a and 5.4b) consists of 2 counting groups of 11 bits each. The first group is responsible for generating the switching period. A 12 stage binary counter 74HCT4040 is used to produce the equivalent of a half period. The 12th output of the counter is connected to an OR gate which resets the group after every counted half period. The second group consists of 3 pre-settable synchronous 4-bit up/down counters 74HCT191. The most significant input bit of the most significant

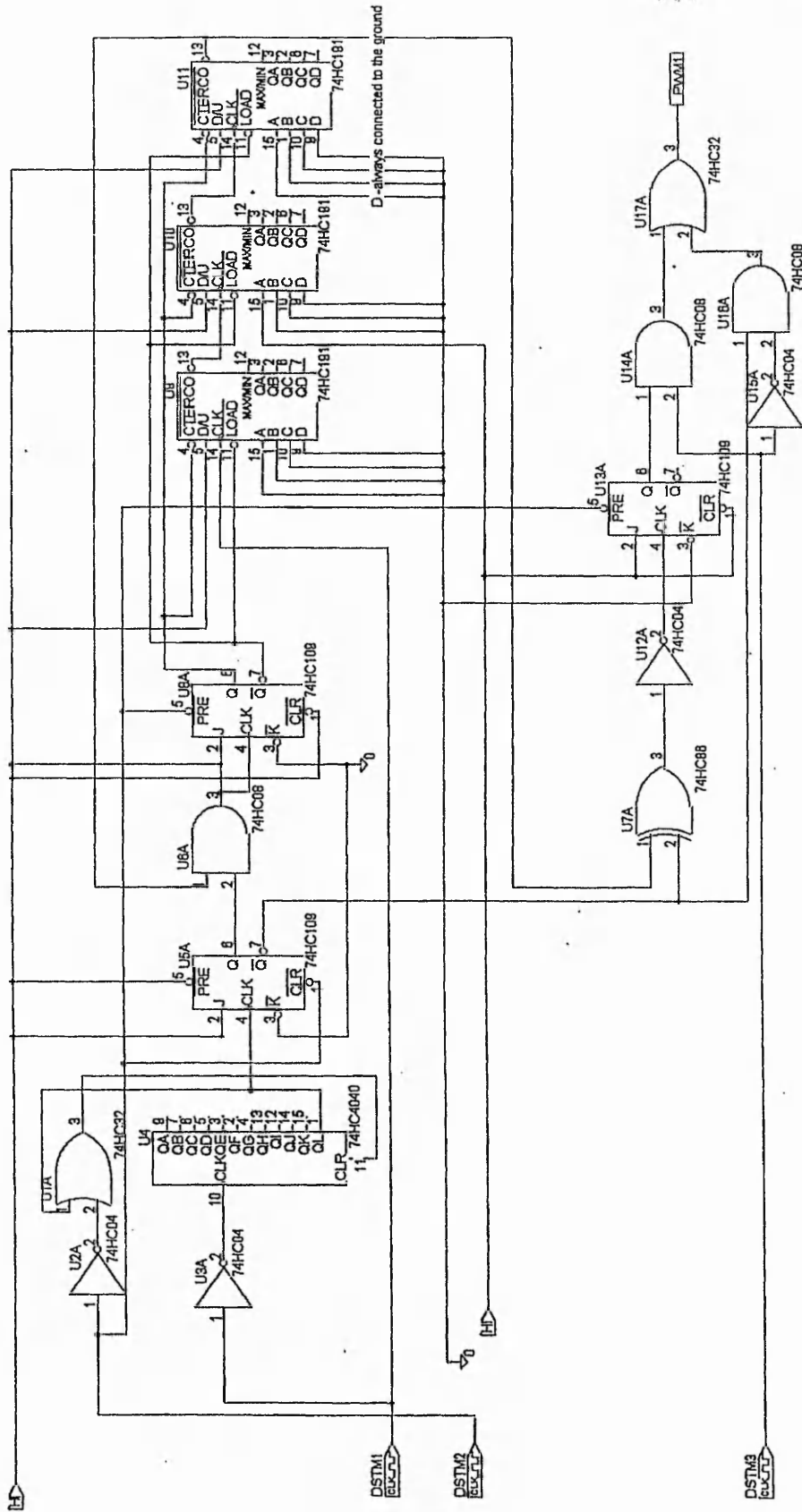


Fig. 5.4b – Pulse generator schematic

counter (U11) is always connected to the ground. The counters are enabled by the Q output of a J- \bar{K} flip-flop (U8A) and the pre-set value is loaded using the \bar{Q} output of the same device. The counter clock input DSTM1 is supplied from a 10MHz square signal generator and the system reset is achieved manually by pulling DSTM2 low.

At the beginning of the switching period the output Q of the flip-flop U5A is “0”, the output Q of U8A is “1” and the second group of counters is disabled. The pre-set value is loaded into the counters. Also, the output of U13A is “1” and the output PWM1 is “1”.

When 74HCT4040 finishes counting the first half period, the output QL switches U5A to “1” and thus the output Q of U8A becomes “0” and the second group of counters starts counting down the equivalent of $(d-0.5)T$. The output produced by U11 switches U8A from “0” to “1” and the 74HCT191 counters are disabled. Also, the Q output of U13A is reset and the output PWM1 of the system becomes “0” for the rest of the period. The counter 74HCT4040 sets the output of U5A to “0” at the end of the switching period. Then the whole process is repeated. The duty ratio is controlled by modifying the binary combination that is loaded into the inputs of the three 74HCT191 counters. This combination is set using 11 binary switches. The output PWM1 is connected to the input of the delay circuit.

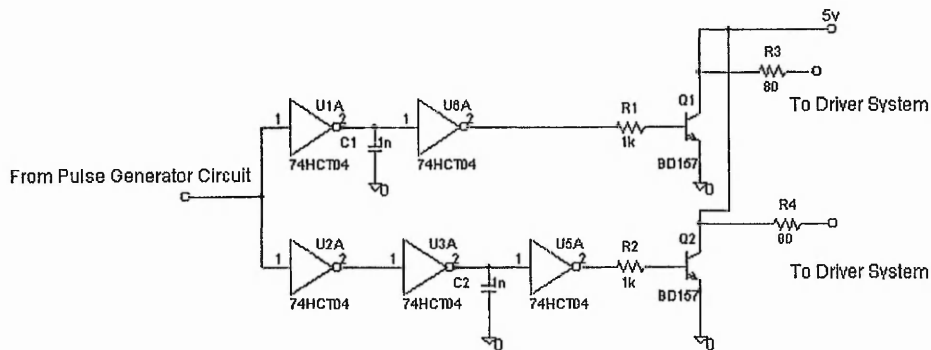


Fig. 5.5a – Delay circuit schematic

5.2.2 Delay circuit

The role of the delay circuit (fig. 5.5a&b) is to introduce a dead time between the falling edge and rising edge of the signals that control the state of the complementary switches. The functioning of this circuit is based on the rising and falling times of the voltage across the capacitors that are placed at the output of inverters. The rising time, that is

longer than falling time, is determined by the internal resistor placed in the collector of the output transistor of the inverter and by capacitor. The falling time is influenced by the capacitor and by the resistance of the collector-emitter junction. A role in creating the dead time is also played by the voltage levels at which the transition from HI to LO and from LO to HI is made. All these elements concur in producing a dead time of $\sim 2.5\mu\text{s}$. The command signals presented in figures 5.5c&d were acquired from the gates of two different transistors: one is part from the bi-directional switch S1 and the other one from the bi-directional switch S2. The switches S1 and S2 are complementary operated.

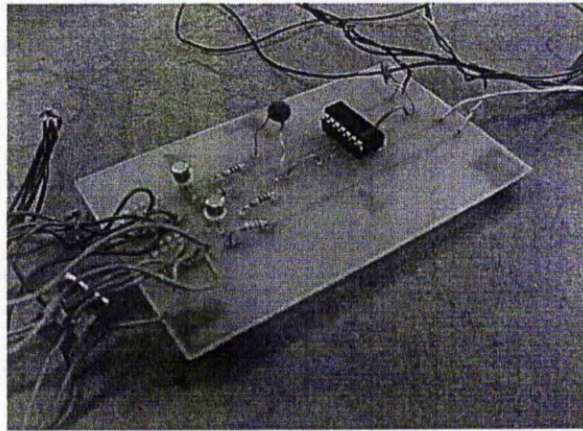


Fig. 5.5b – Delay circuit practical implementation

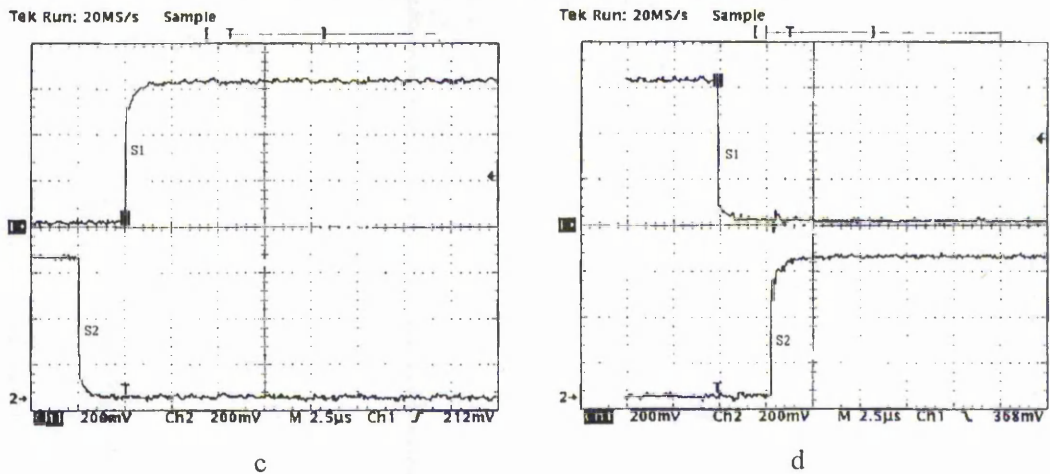


Fig. 5.5 – The command signals from complementary switches

5.2.3 Driver system modules

Each switch is controlled by a driver module shown in figure 5.6a. Each transistor is controlled through gate driver INT200. The command signal to the gate drive is received from the delay circuit through an opto-coupler (HP6N137).

The two winding transformer and the opto-coupler ensure isolation of the drive signals from power supply and between switches.

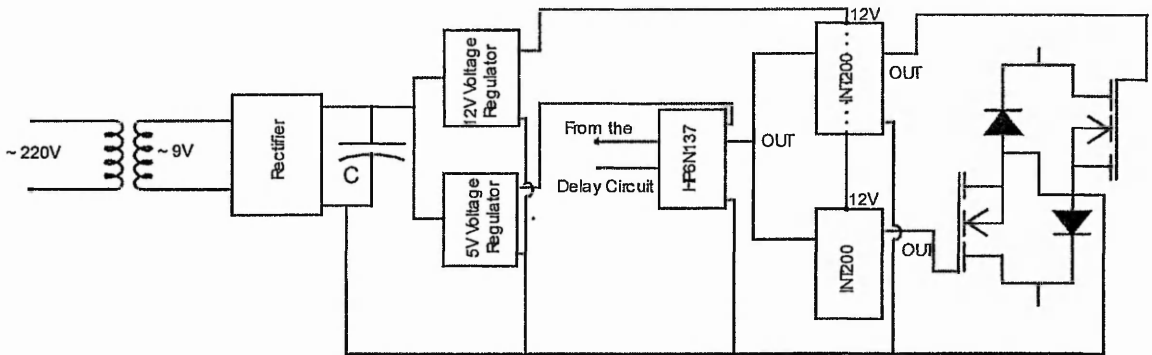


Fig. 5.6a – Driver system schematic

5.3 Data acquisition system

The data acquisition board is a National Instrument PCIO-MIO-16E-1 board that is a completely Plug and Play, multifunction analog, digital and timing I/O board for PCI bus computers. The board has 16 analog inputs and 8 digital I/O pins. The analog inputs can be programmed in three different modes: non-referenced single-ended, referenced single-ended and differential. The board has two input polarities: unipolar and bipolar. Unipolar means that the input signal voltage range is between 0 and 10V. Bipolar input means that the input signal voltage range is between -5V and 5V. The polarity and range settings can be programmed for each channel.

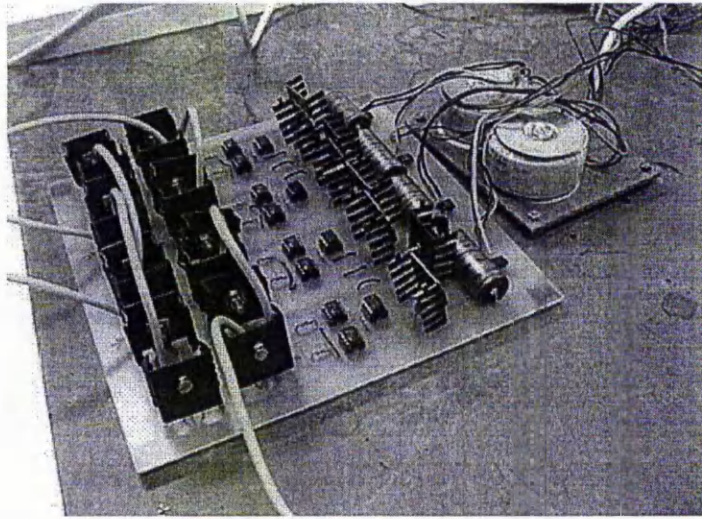


Fig. 5.6b – Driver system – practical implementation

The sampling rate ensured by the board is approximately 1.25 Msamples/sec for single-ended channel acquisition and 333 Ksamples/sec for multi-channel scanning (for the best accuracy of the A/D conversion). A 12 bit converter is used for A/D conversion.

The interface between the process signals and the acquisition board consists of LEM voltage and current transducers supplied at $\pm 15V$.

The acquisition process is controlled with a program based on the software supplied by the board manufacturer: LabWindows/CVI.(see appendix 5.1).

5.4 The experimental verification of switched capacitor principle

To verify the novel application of the switched capacitor in inductive systems, a RL circuit with the parameters $L = 53.6mH$, $R = 23.5\Omega$ is used. The circuit is supplied with a sinusoidal voltage of 26V peak.

Each bi-directional switch consists of two MOSFET transistors IRF841 and two diodes RURP860.

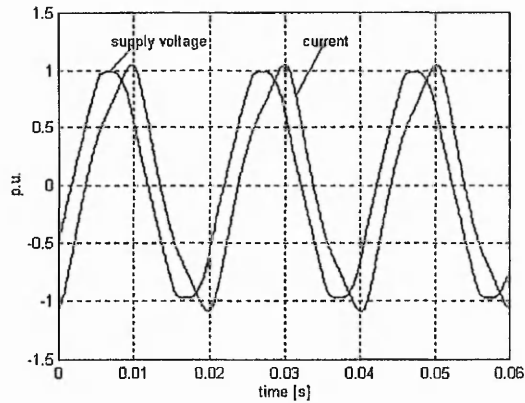


Fig. 5.7 – Voltage and current in the RL circuit without switching

Measurements were made for two different capacitors of $90\mu\text{F}$ and $30\mu\text{F}$ respectively, varying the duty ratio between 0.5 and 1. Also, similar sets of measurements were repeated for switching frequencies 0.7kHz, 1kHz, 1.5kHz and 2kHz.

The range of the used switching frequency was limited by the maximum frequency of the square signal 10MHz that was obtainable from the signal generator.

The waveforms (currents and voltages) are displayed in per unit [p.u.]. The currents were normalized relative to the fundamental of the current that occurs in the RL circuit without switching.

In figure 5.7, the supply voltage and the current are shown for the case of the simple RL circuit without the converter. The phase angle between the voltage and current is 35° and the fundamental of the current is 906mA, as obtained from Fourier series for the waveforms.

Figures 5.8 to 5.11 show current and supply voltage waveforms when a capacitor of $90\mu\text{F}$ is placed in the middle of the bi-directional H bridge at a switching frequency of 1.5 kHz. Due to the similarities of the acquired waveforms, the experimental results for the rest of switching frequencies are presented in a graphical form in figures 5.17 and 5.19. Figures 5.12 to 5.16 are for the capacitor value of $30\mu\text{F}$ replacing the $90\mu\text{F}$ capacitor at a switching frequency of 1.5KHz. Similarly, the experimental results for the other 3 switching frequency are presented in figures 5.18 – 5.20. The supply voltage frequency is constant in each case and the resultant phase displacement angle is shown

in degrees. Note that the phase angles are stated using the current phasor as reference. The curves from figures 5.19 and 5.20 represent magnitude of the current fundamental.

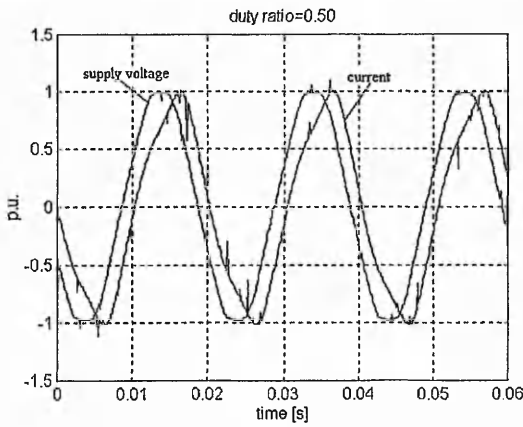


Fig. 5.8 - $f_s = 1.5\text{kHz}$, $\varphi_c = 32.75^\circ$

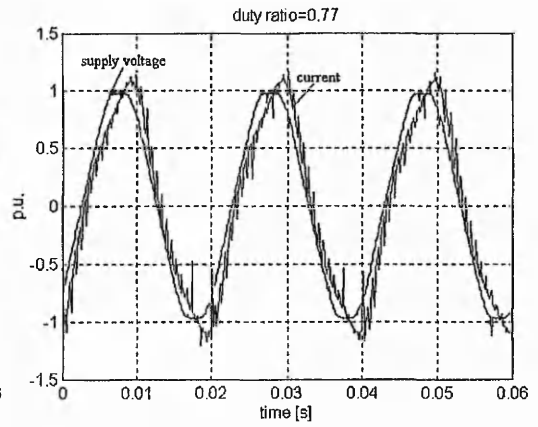


Fig. 5.9 - $f_s = 1.5\text{kHz}$, $\varphi_c = 13.81^\circ$

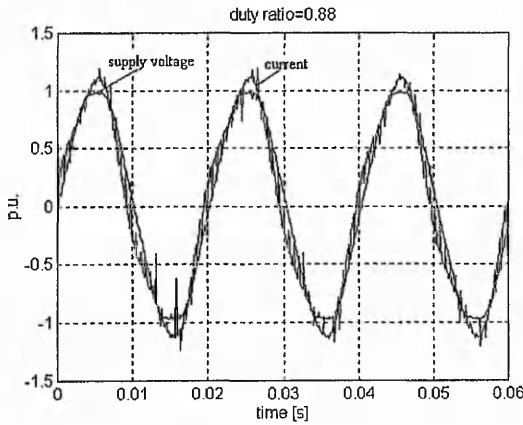


Fig. 5.10 - $f_s = 1.5\text{kHz}$, $\varphi_c = -7.65^\circ$

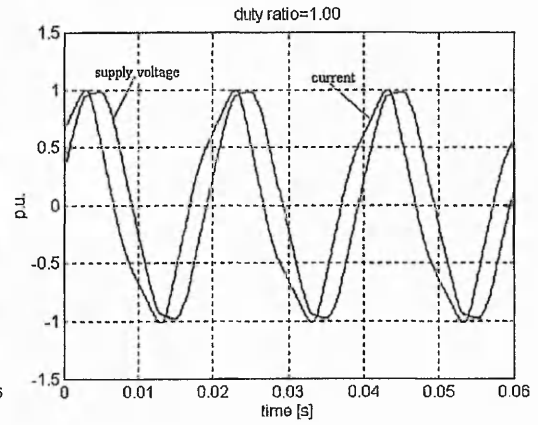


Fig. 5.11 - $f_s = 1.5\text{kHz}$, $\varphi_c = -38.11^\circ$

The waveforms for a capacitor of $30\mu\text{F}$ at a switching frequency of 1.5kHz

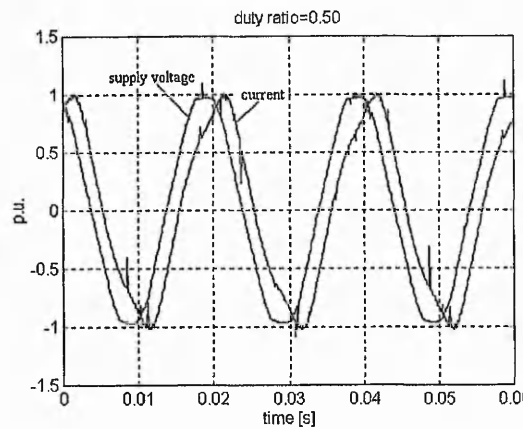


Fig. 5.12 - $f_s = 1.5\text{kHz}$, $\varphi_c = 33.14^\circ$

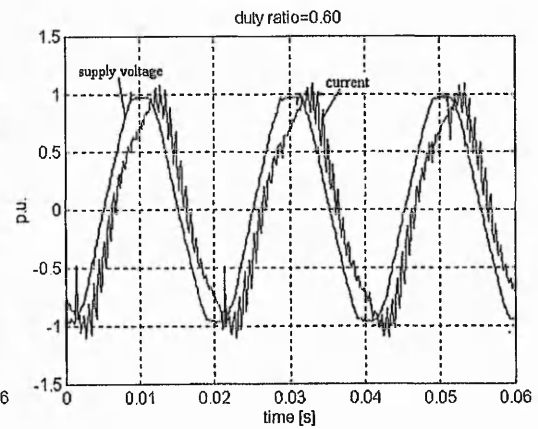


Fig. 5.13 - $f_s = 1.5\text{kHz}$, $\varphi_c = 25.74^\circ$

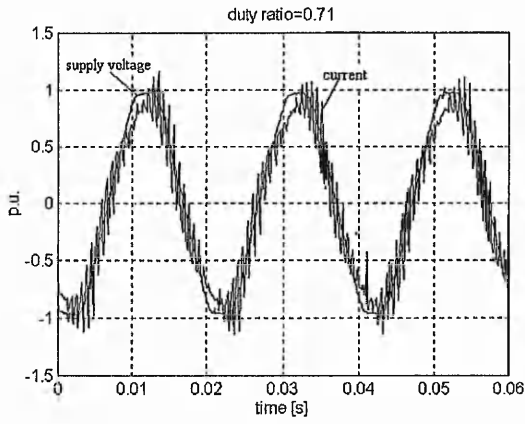


Fig. 5.14 - $f_s = 1.5\text{kHz}$, $\varphi_c = -0.39^\circ$

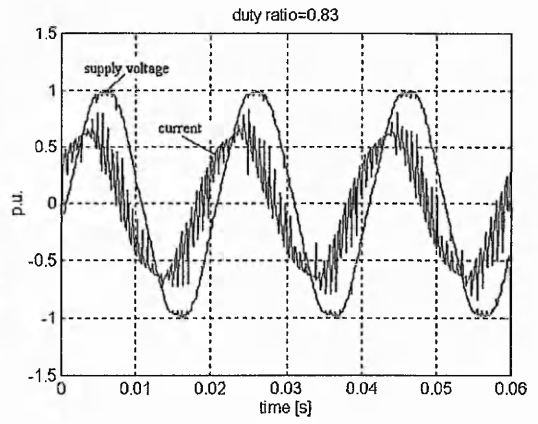


Fig. 5.15 - $f_s = 1.5\text{kHz}$, $\varphi_c = -42.49^\circ$

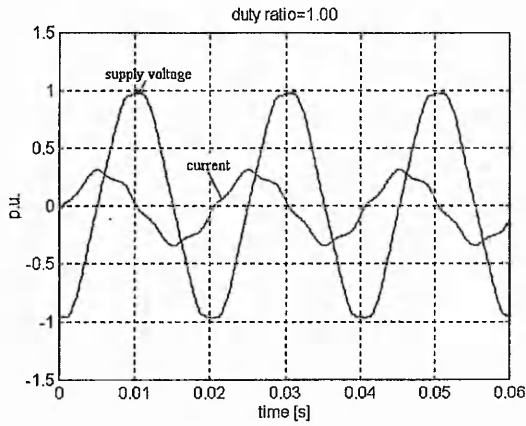


Fig. 5.16 - $f_s = 1.5\text{kHz}$, $\varphi_c = -79.75^\circ$

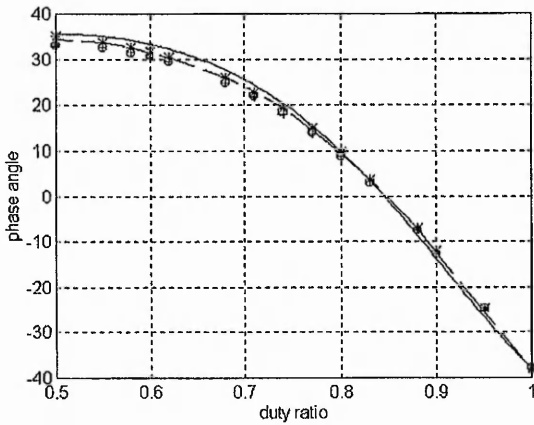


Fig. 5.17 - $C=90\mu\text{F}$

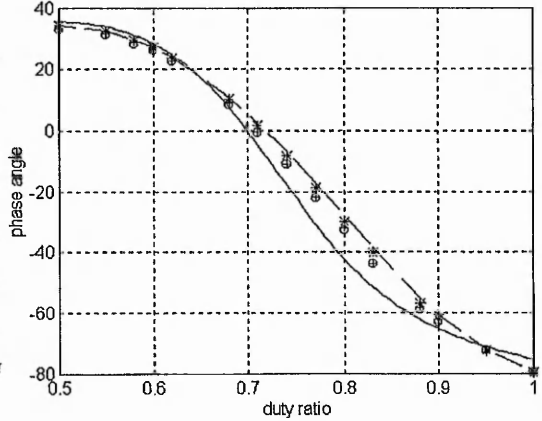


Fig. 5.18 - $C=30\mu\text{F}$

Phase angle as a function of duty ratio for a selected switching frequency of:

- - - theoretical, -- - 0.7kHz, * - 1kHz, + - 1.5kHz, o - 2kHz

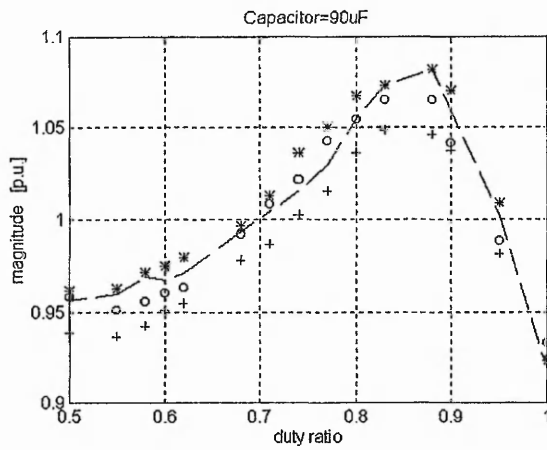


Fig. 5.19

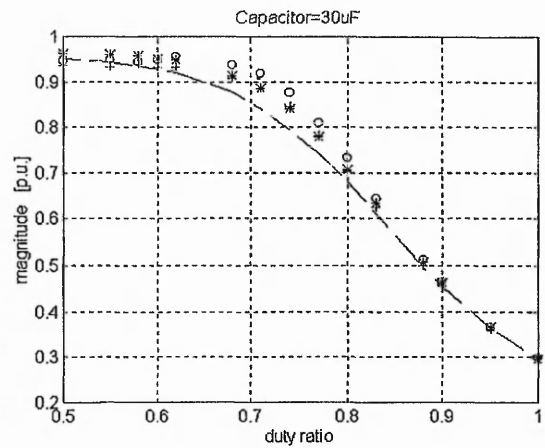


Fig. 5.20

Current magnitude as function of duty ratio for switching frequency of:

-- - 0.7kHz, * - 1kHz, + - 1.5kHz, o - 2kHz

The in-phase condition of the present circuit corresponds to that of a passive circuit with a normal capacitor of 0.19 mF , that is 2.1 times as big as 90 μ F and 6.3 times as big as 30 μ F. These figures, perhaps, are not as spectacular as expected, but in [29] it was proved that the in-phase condition is achieved with a switched capacitor of 10 μ F, that is 151 times smaller than the required value of 1.512mF for a circuit of 12.3 Ω resistance in series with 6.7 mH inductance; the supply frequency being 50Hz.

The experimental results verify the feasibility of the novel application of the principle of switched capacitors in controlling the phase angle. The phase angle (from the results shown in figures 5.17, 5.18) varies between the natural limits of the RL circuit and the RLC circuit, as it was expected from expressions (4.20) and (4.21).

The experimental results show close agreement to the computed theoretical values.

It can be noticed from graphics 5.17-5.20 that the insertion of the H bridge produces in the first instance, at a duty ratio of 0.5, a decrease of the phase angle between the voltage and current of 1.5-2⁰ and of the current magnitude (referred to RL circuit without switching) of 3-6%. These effects are determined by several factors such as: $r_{DS(ON)}$, equivalent series resistance of the capacitor and switching frequency.

The ON resistance of the used MOSFET transistors is around 1 Ω . The effect of neglecting this resistance in the simulations has given slightly overestimated phase angle

as seen in figures 5.17 and 5.18. The switching losses which are dependent on the circuit parameters, devices and switching frequency, will have a similar effect.

The used capacitor has a power factor around 0.001 at a supply frequency of 50Hz and the measured ESR for the frequency range up to 10kHz is of maximum 20m Ω . These values are negligible in relation to the circuit resistance.

Figures 5.19 and 5.20 show the effect of the capacitor value and switching frequency on the magnitude of current at duty ratios around the 'in phase' condition. This effect is related to the ratio that exists between R and $2\sqrt{L/C}$ and is discussed in section 4.6 of this thesis.

The limitations of the pulse generator system regarding the range of possible frequencies did not make possible the use of a wide range of switching frequencies to study the effects of enumerated factors over the system performances and these will be important issues of the further work.

The mathematical model of the switched capacitor system considers that the complementary switch pairs (S1, S4) and (S2, S3) are switched simultaneously and instantaneously. This means that the circuit current is not interrupted and, since the switching is instantaneous, the voltage across the capacitor does not change during the switching operation. In the experimental case, a small dead time, as shown in appendix 5.3, between the ON states of the complementary switch pairs practically prevents the capacitor to circulate a current through the outgoing and incoming devices and, thus, achieves a practical implementation close to simulation. The circuit current is negligible during the short dead time interval which is not the case in the mathematical model. The practical results deviate from simulations but the effect due to the minute dead time are expected to be insignificant.

The experimental results were achieved using a fix R/L ratio of 438.4, supply frequency of 50Hz and with capacitors values of 90 μ F and 30 μ F. It is noted from results in graphs of figures 5.17 and 5.18 that for a change in duty ratio from 0.5 to 1, the total change in

phase angle is 73° for $90\mu\text{F}$ and 114° for $30\mu\text{F}$. For both values of capacitors, the sensitivity of phase angle to duty ratio is low in the region of 0.5. The sensitivity is relatively high in the higher range of duty ratios. The substantial increase in the sensitivity occurs at duty ratio of 0.6 in the case of $30\mu\text{F}$ and 0.7 in the case of $90\mu\text{F}$. The sensitivities tend towards such high values that it requires a change in duty ratio of only 0.1 to achieve a change of 30° in phase angle. Thus, the duty ratio has to be generated to a high precision to achieve small changes in phase angle.

It has to be remarked that results from the graphs (5.17, 5.18) show that smaller the capacitor used with the H bridge, the smaller the duty ratio required to achieve the desired phase angle. This is a confirmation of equation (4.19) about the influence of the used capacitor value over the duty ratio in a given circuit and the need for a good resolution of the pulse generator circuit, especially when the emulated capacitor is required to be considerably bigger than the used capacitor.

A more in depth analysis of the experimental results implies harmonic analysis. The currents harmonic structure for $C=90\mu\text{F}$ and $C=30\mu\text{F}$ at the switching frequency of 1.5kHz is presented in figures 5.21-5.28. The harmonic content is shown for 4 different duty ratios that produce similar phase angles for both values of capacitor. The harmonic content is displayed in percents from the fundamental of the current at the respective duty ratio, starting with the second harmonic. A complete presentation of the harmonic content is given in tabular format for all experiments with capacitors of $30\mu\text{F}$ and $90\mu\text{F}$ in Appendix 5.2.

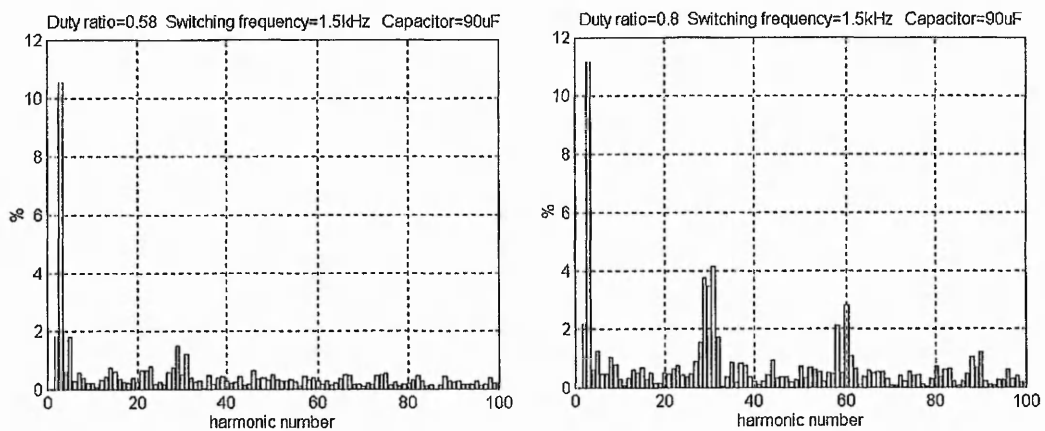


Fig. 5.21 – Harmonic content for duty ratios of 0.58 and 0.8 – Fig.5.22

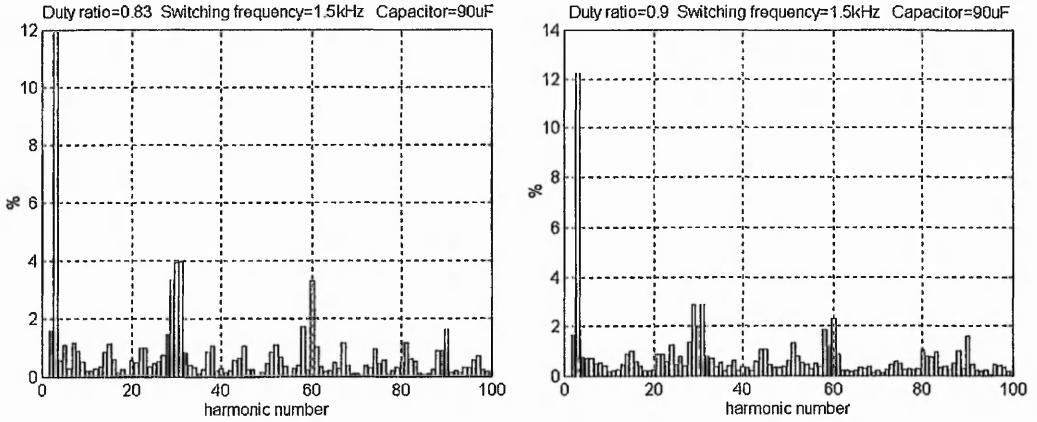


Fig. 5.23 – Harmonic content for duty ratios of 0.83 and 0.9 – Fig.5.24

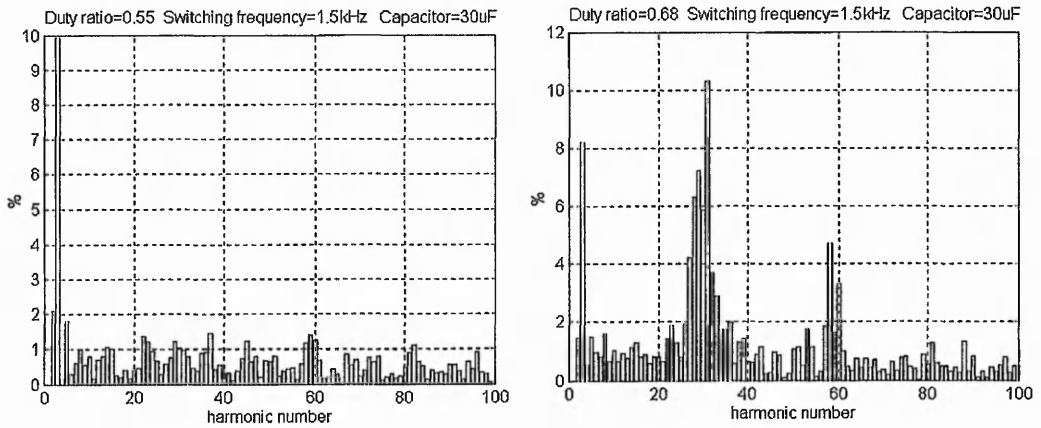


Fig. 5.25 – Harmonic content for duty ratios of 0.55 and 0.68 – Fig.5.26

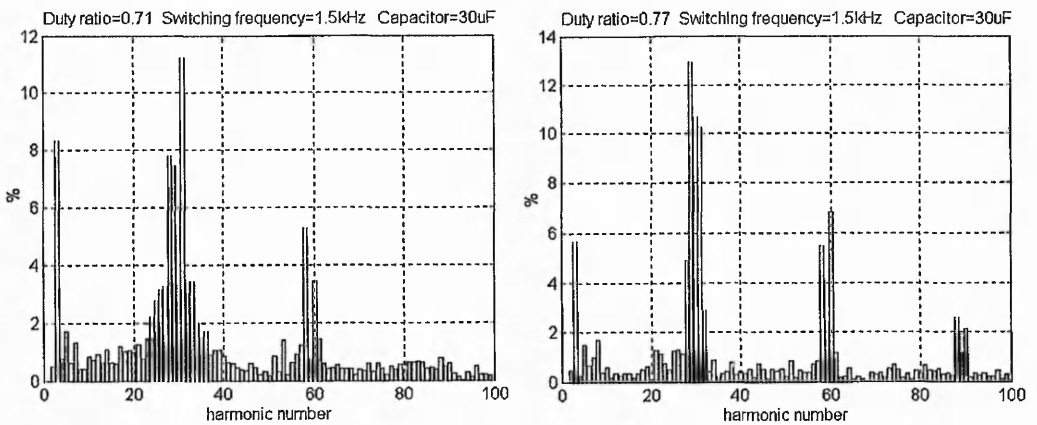


Fig. 5.27 – Harmonic content for duty ratios of 0.71 and 0.77 – Fig.5.28

The results show that, besides the fundamental, the 3rd harmonic is significant. The harmonics which are multiples of the ratio of switching frequency to supply frequency

are also significant. The amplitude of these harmonics increases for duty ratios that produce close to the in-phase condition.

Some conclusions can be drawn from the theoretical and experimental results to provide a guide for the choice of the central capacitor of the H- bridge:

- higher the capacitor value used, lower will be the demand on duty ratio resolution.
- the maximum voltage that could appear across the capacitor according to equation(4.25) should be considered.
- the switching frequency, though it does not affect the achieved phase angle, influences the amplitude of the resulting current; further study is required to establish a correlation between the used capacitor and switching frequency.

5.5 Induction machine experiment

As shown in previous chapters, the performance of an induction motor can be improved if the rotor impedance is externally modified by inserting equal capacitors in each phase of the rotor circuit. The values of these capacitors are large and so they are difficult to implement by connecting several capacitors in parallel and also the system will be slow to respond to changes. The solution proposed in this work is to place bi-directional H bridge with capacitor as the centre component in each phase of the rotor circuit.

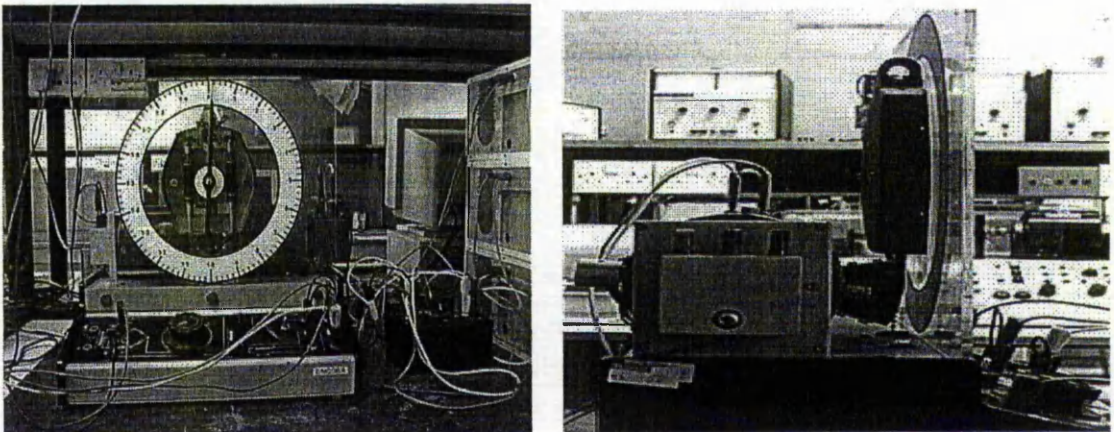


Fig. 5.29 – Induction motor experiment set-up

All three H-bridges are driven from a single Pulse Width Modulated signal. By varying the duty ratio between 0.5 and 1, the required high capacitive effects are produced in the rotor circuit.

The above scheme was tested in a low power wound induction motor with the estimated parameters $R_s = 85\Omega$, $R_r = 115\Omega$, $L_m = 3.16H$, $L_{st} + L_{rt} = 0.72H$. A set of two power analyzers was used to record the active and apparent power absorbed by the motor. An infrared speed transducer was used to measure the rotor speed. The motor set had a dynamometer with spring balance for monitoring the torque. The load torque on the motor was varied by current supplied to the dynamometer.

The first test was performed to obtain the variation of slip, efficiency and power factor as a function of load under the following two conditions:

- (i) rotor impedance externally modified using 60uF capacitor and a duty ratio of 0.68 for the H-bridges, emulated value for capacitor being 462uF.
- (ii) rotor impedance externally modified using 90uF capacitor and a duty ratio of 0.7 for the H-bridges, emulated value for capacitor being 562uF.

The following procedure was used for each condition: at a set load torque, the torque, speed, active and apparent power were recorded for the short circuited slip rings configuration; then, immediately, using a three phase switch, an H bridge was inserted on each phase of the rotor circuit. After the system settled down, the same measurements were recorded. The changes in the rotor configuration were introduced without stopping the motor and, thus, the measurements for the two configurations were performed in similar conditions.

The results for the test along with those obtained from simulation are presented in the figures 5.30-5.35. The following color code is used for all graphs presented in this chapter (* represents the experimental measurement points):

- induction machine without capacitor – simulated results
- induction machine with capacitor – simulated results
- induction machine without capacitor – experimental results
- induction machine with capacitor – experimental results

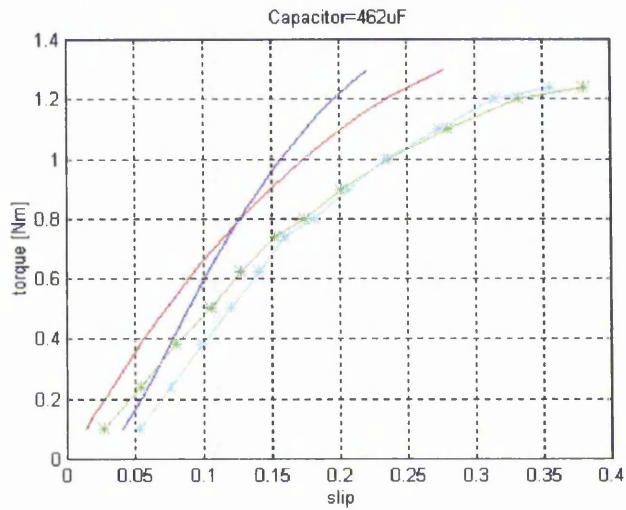


Fig. 5.30 - Torque / slip

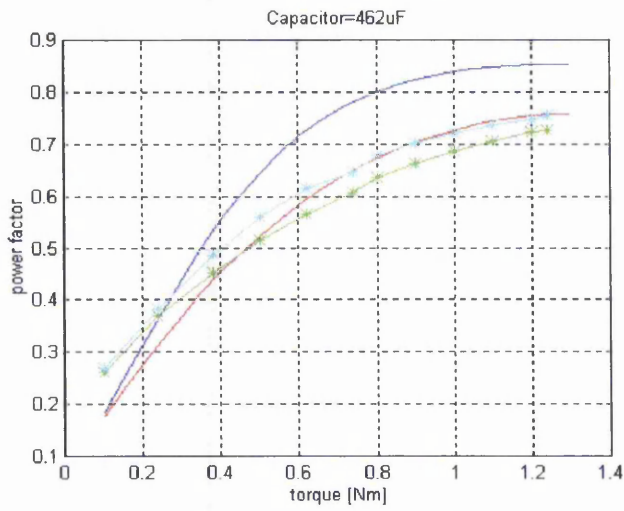


Fig. 5.31 - Power factor / torque

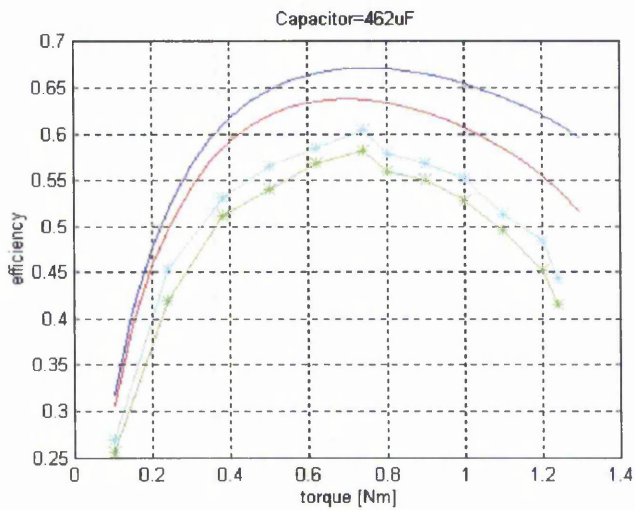


Fig. 5.32 - Efficiency / torque

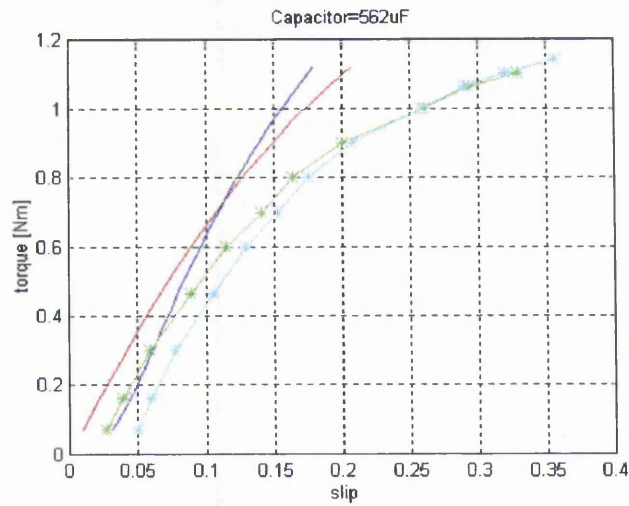


Fig. 5.33 - Torque / Slip

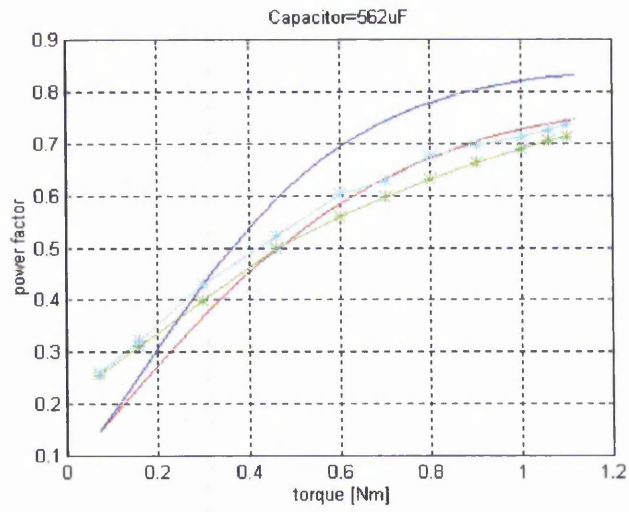


Fig. 5.34 - Power factor / torque

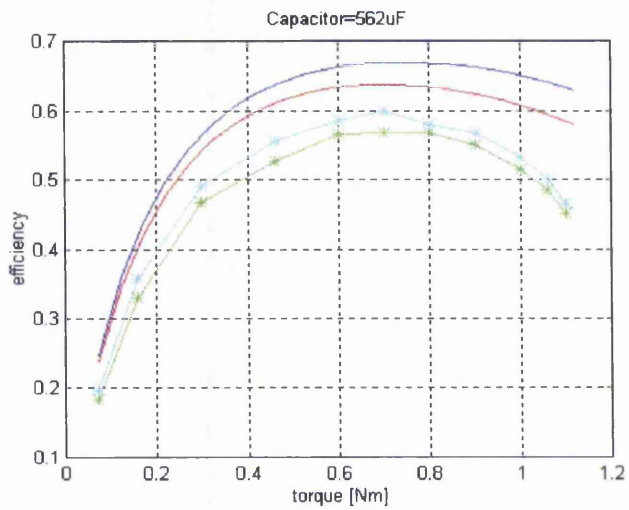


Fig. 5.35 - Efficiency / Torque

The experimental results bear a close resemblance to the theoretically predicted effects of a capacitor in the rotor circuit. For example, the existence of the cross-over for the torque-slip curves is seen in both figures 5.30 and 5.33. From the cross-over point onwards, the rotor speed is higher in the case of modified rotor than that of the short circuited rotor for the same torque.

Improvement in power factor and efficiency is obtained for the whole torque range; this gives an enhancement in the operation of the motor. It should be noted that the model used in simulations does not include iron and mechanical losses. The open rotor circuit test and the no load test were undertaken to estimate these losses. The iron losses were estimated to be 13.8W and the mechanical losses (at a speed of 1455rpm) were estimated to be 9.2W. These values were added to the simulated value of the input power, to present the theoretical efficiency curves.

The second set of tests was performed to study variation of slip, power factor and efficiency as a function of the duty ratio with torque constant at values of

(i) 0.5 Nm

and

(ii) 0.9 Nm

The central capacitor of the H-bridge was $90\mu\text{F}$ for throughout this test.

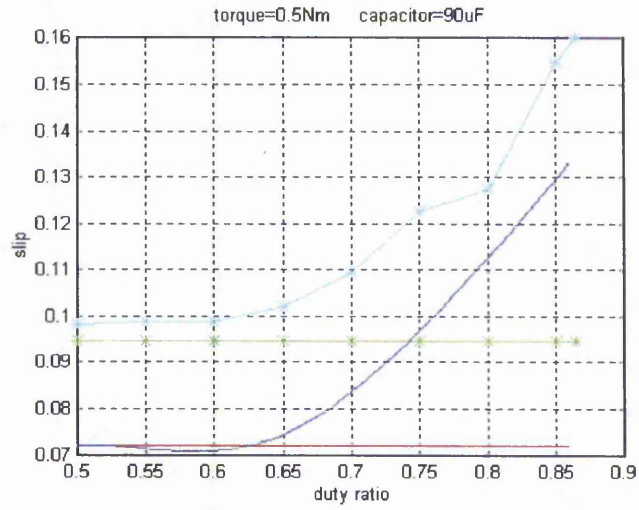


Fig. 5.36 - Slip / Duty Ratio

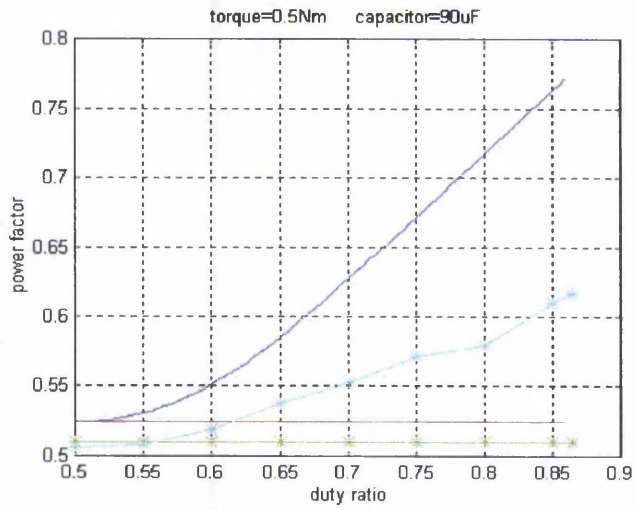


Fig. 5.37 - Power Factor / Duty Ratio

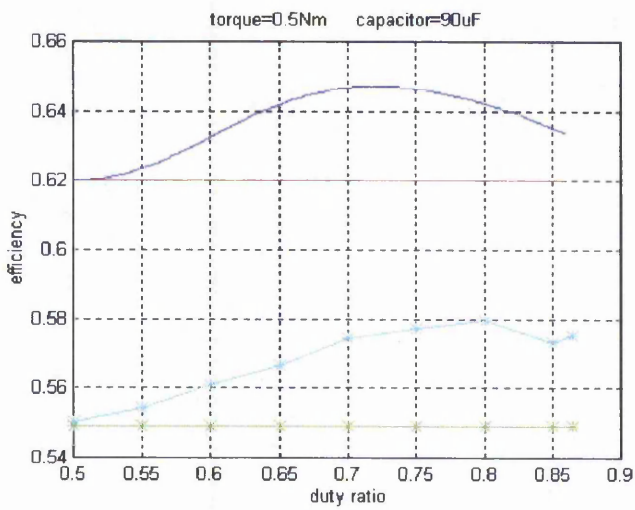


Fig. 5.38 - Efficiency / Duty Ratio

Chapter 5

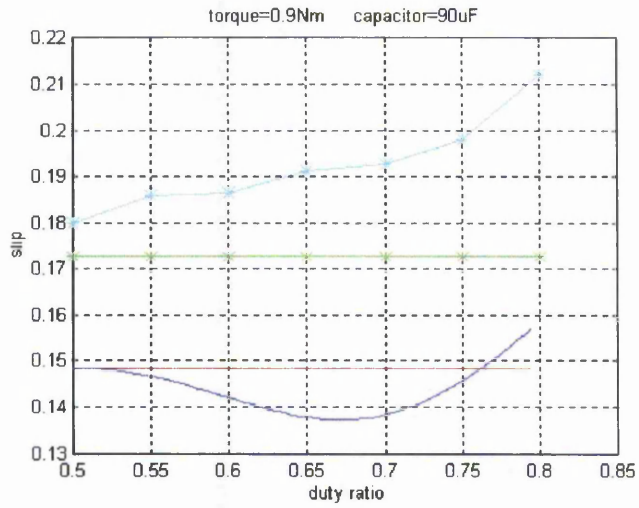


Fig. 5.39 - Slip / Duty Ratio

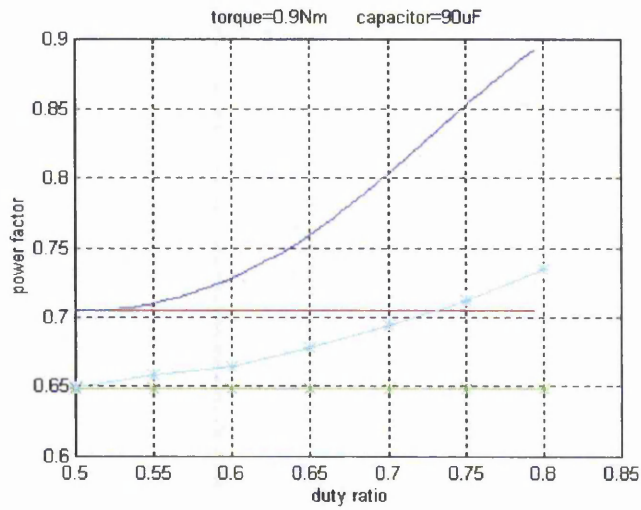


Fig. 5.40 - Power Factor / Duty Ratio

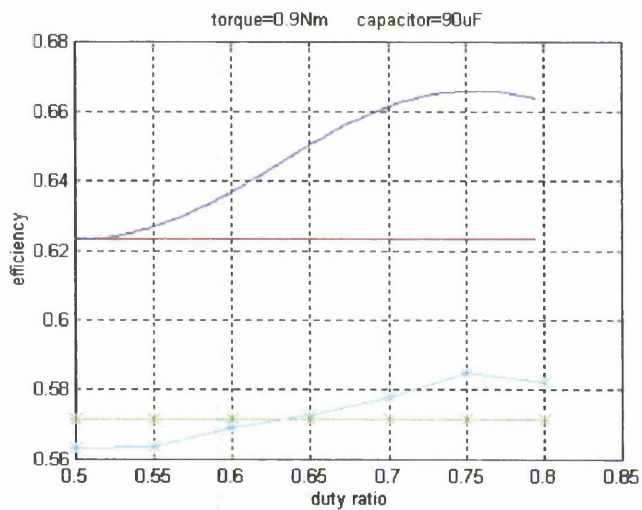


Fig. 5.41 - Efficiency / Duty Ratio

The experimental and simulation results show the speed variation as a result of the modification of the duty ratio. Usually the insertion of a resistance in the rotor circuit produces a decrease of the rotor speed, an improvement of the power factor but the efficiency decreases. In the presented application the power factor is improved while the efficiencies are at least equal to or better than that for the short-circuited rotor. This, also, gives the possibility of energy-efficient speed control schemes. Also, it has to be noted that the initial efficiency of motor with switched capacitor system in 0.9Nm case is lower than in the short circuited configuration. This is explained by the fact the increase of the load produces higher currents and the losses introduced by the switched capacitor system become more significant.

The tests on the low power motor having high rotor resistance show moderate improvements. But as per theoretical analysis, these improvements are expected to be significant in the case of high power motors. However slip-ring drives are used in very high power applications. At these powers, a 1% increase in efficiency is very significant.

5.6 Conclusions

Chapter 5 has discussed the hardware aspects and practical implementation of the novel principle of the switching system emulating large capacitors.

The novel principle was verified experimentally in two different circuits, using capacitors of different values and a range of switching frequencies.

Using the new mechanism for emulating large capacitive effects in each phase of the rotor circuit of a small power induction machine produces results similar to those determined by the insertion of a large fixed capacitor.

Tests on a low power motor have shown improvements in power factor and efficiency for the whole torque range. This gives an enhancement in the operation of the motor.

Chapter 6A FUZZY CONTROL STRATEGY FOR
THE SWITCHED CAPACITOR PRINCIPLE

Abstract: The chapter presents a brief introduction to fuzzy control. A fuzzy controller for the switched capacitors principle is implemented taking into account the general evolution of the phase angle as function of the duty ratio. Experimental results of the system with fuzzy control are presented.

A novel application of switched capacitors in power electronic systems giving output current phase control was presented theoretically and experimentally in chapters 4 and 5. This application is used to control the effective impedance of the load in a series RL circuit which controls the phase angle between the supply voltage and the current. To achieve a required phase angle a duty ratio derived from equation (4.19) must be applied to the bi-directional switches. The value of the duty ratio depends on the required phase angle, on the circuit parameters and the value of the capacitor in the H bridge.

In many applications, the circuit parameters are not known precisely or as in the case of an induction motor, may change their values due to saturation and temperature. In the rotor the frequency is a function of slip and may change with load. These additional variables make the calculation of the duty ratio difficult.

As an example, a circuit with the parameters $R=9.6\Omega$, $L=5.5\text{mH}$, $\omega=314\text{rad/s}$, $C=15\mu\text{F}$ is used. The duty ratio as function of the desired phase angle is shown for these parameters in figure 6.1(graph 1). If a modification of circuit resistance during the process to a value of $R=4.8\Omega$ is considered, then the new representation of the duty ratio (graph 2) is different from the previous one and for the same phase angles (except 0) different duty ratios are required. The same thing happens if the circuit frequency is modified to $\omega=157\text{rad/s}$, (graph 3).

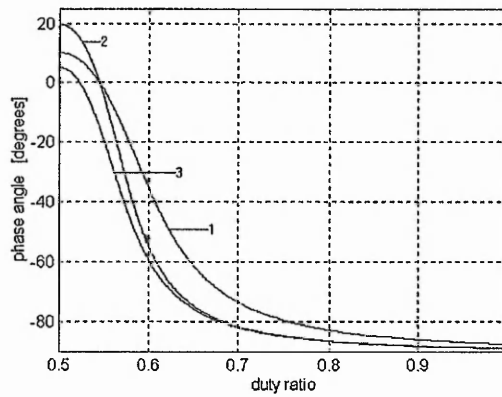


Fig. 6.1- Phase angle as a function of duty ratio
for the three circuit conditions

The pattern of evolution of the duty ratio can be seen in the three graphs of Fig.6.1. The phase angle of the circuit has its maximum value for a duty ratio of 0.5 and its minimum for a duty ratio of 1. If the duty ratio is increased from a given point, the phase angle decreases and vice versa.

These considerations impose a control strategy based on the knowledge of the general behaviour of the duty ratio as a function of a desired phase angle and not necessarily on the values of the circuit parameters.

6.1 Fuzzy Control

Intelligent systems have developed strongly in recent years [30]. The application of artificial intelligence has become more and more efficient and useful in high complexity processes but, also, in the case of simpler applications with high degrees of uncertainty.

There are two trends in the artificial intelligence field:

- *Logic-symbolic paradigm* that implies the symbolic representation of the knowledge and the use of different logic algorithms to deduce new knowledge from the recorded facts of the controlled system. Expert systems are an example of this model.
- *Connective paradigm* that introduces the concept of artificial neural networks.

Fuzzy controllers are a particular case of the knowledge based systems (expert systems). *Fuzzy control* strategy is based on *fuzzy logic*.

Fuzzy logic seems to imply an imprecise methodology that is useful only when accuracy is not necessary or important. In a world increasingly manipulated by computers with their absolute “1” or “0” and “on” or “off” concepts, a term like fuzzy logic suggests inaccuracy or imprecision. However, fuzzy logic can address complex control problems, such as robotic arm movement, chemical or manufacturing process control and automobile transmission control with more precision and accuracy.

6.1.1 Fuzzy sets

Fuzzy logic works with fuzzy sets.

A classic set may be finite, countable or uncountable. It may be described either:

- by listing up the individual elements of the set

For example: consider set B of cars with names starting with letter B:

$$B = \{\text{BMW, Buick, Bugati, Bentley}\}$$

- by stating a property for membership

example: $T = \{x \in Z \mid x \geq 0\}$

A method similar to the last one is the use of a predictor :

$$T = \{x \mid P(x)\} \text{ where } P(x) = x \in Z \ \& \ x \geq 0$$

where P is the predictor of the set T.

A third method that is interesting with respect to the extension from classic set theory to fuzzy set theory, is the use of the characteristic function μ_A . $\mu_A : X \rightarrow \{0,1\}$ is a characteristic function of the set A if for all values $x \in X$:

$$\mu_A(x) = \begin{cases} 1 & \text{when } x \in A \\ 0 & \text{when } x \notin A \end{cases} \quad (6.1)$$

In classical theory any element u of the universe U is either $u \in C$ (C being a classical set) or $u \notin C$. For any classical set C, a characteristic function is defined in (6.1). In

fuzzy set theory, the characteristic function is generalized to a membership function that assigns to every $u \in U$ a value from the unit interval $[0,1]$ instead of the two element set $\{0,1\}$.

For example, the fuzzy set S of the natural numbers close to 6 is defined, having the membership function

$$\mu_S(u) = \frac{1}{1 + (u - 6)^2}$$

Set S is expressed as :

$$S = \{0.1/3, 0.3/4, 0.6/5, 1/6, 0.6/7, 0.3/8, 0.1/9\}$$

This means that 4 is in proportion to 0.3 of S , 6 is in proportion to 1 of S or 2 in proportion to 0.05 of S . 'Close to 6' is the property of the fuzzy set.

More than one fuzzy set can be defined on the same universe for the same object or feature, for example a fuzzy set for cold, a fuzzy set for warm or a fuzzy set for comfortable can all be defined for temperature. For height a fuzzy set for short, and a fuzzy set for tall can be defined.

5 fuzzy sets related to the age bands of a person can be defined on the universe for a span of $[0,80]$ years are shown in figure 6.2 : child, teenager, young, mature and old. (the membership functions and the types of the membership functions are defined in appendix 6.1).

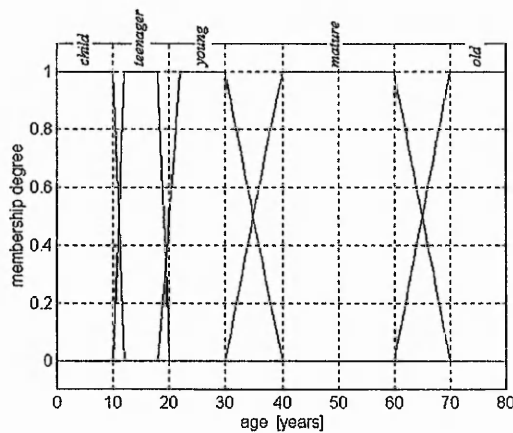


Fig. 6.2 – Membership functions for fuzzy age bands

A person of 25 years old is considered young because the value of young membership function for this age is 1 and all the other functions are 0.

6.1.2 Linguistic variables

Lofti Zadeh, considered to be the pioneer of fuzzy logic, defines linguistic variables in the following way :

“By a linguistic variable we mean a variable whose values are words or sentences in a natural or artificial language. For example, Age is a linguistic variable if its values are linguistic rather than numerical, i.e., young, not young, very young, quite young, old, not very old and not very young, etc., rather than 20,21,22,23, ...”

It is usual to have the following framework associated with the notion of a linguistic variable

$$\langle X, LX, \aleph, M_x \rangle$$

X denotes the symbolic name of the linguistic variable, e.g., age, height, temperature, error, change-of-error, etc.

LX is the set of linguistic values and is called the term set of X . A linguistic value denotes a symbol for a particular property of X . For height, it is possible to have the following term set $LH = \{\text{tiny, small, medium, not very tall, tall, huge}\}$.

\aleph is the actual physical domain over which the linguistic value takes its quantitative (classical) values . For example, for height $\aleph = [20,300]\text{cm}$ or for temperature $\aleph = [-10^0, 30^0] \text{C}$.

M_x is a semantic function which gives an interpretation of a linguistic value in terms of the quantitative elements.

$$M_x : LX \rightarrow \tilde{LX}$$

For the linguistic value young of the variable age, the following semantic function corresponds (fig. 6.2):

$$\tilde{young} = \Pi(u, 18, 22, 30, 40) = \mu_{young}(u)$$

(see appendix 6.1)

Usually in fuzzy control applications, the succeeding term set for the variables error or change-of-error is used:

$$\{\text{NB, NM, NS, ZO, PS, PM, PB}\}$$

with the meanings : NB – negative big, NM – negative medium, NS – negative small, ZO – zero, PS – positive small, PM – positive medium, PB – positive big.

The software programs used to implement expert systems are based on rules composed of propositions. The propositions in fuzzy logic have the structure:

$$E \text{ is NB} \tag{6.2}$$

This means that the variable E has the value negative big. The meaning of the symbolic expression (6.2) helps to decide the degree to which this symbolic expression is satisfied for a specific physical value for error.

For example, if for NB is defined the semantic function $\tilde{NB} = L(u, -6, -3)$ and if $e = -3.2$ then $\mu_{NB}(e) = -0.066$.

Based on the notion of fuzzy propositions and linguistic connectives such as ‘and’, ‘or’, ‘not’ and ‘if-then’ it is possible to form more complex fuzzy propositions called compound propositions.

Two of the mentioned conjunctions, ‘and’ and ‘if-then’, are defined in this section. Let p and q be the following two fuzzy propositions p : “ X is A ” and q : “ Y is B ” where A and B are fuzzy sets defined on the same universe. The conjunction relation between these:

$$r: p \text{ and } q$$

is represented by the fuzzy function:

$$\mu_r(x, y) = \min(\mu_A(x), \mu_B(y)) / (x, y)$$

A *fuzzy conditional* or a *fuzzy if-then* production rule is symbolically expressed as

$$\text{if } \langle \text{fuzzy proposition} \rangle \text{ then } \langle \text{fuzzy proposition} \rangle$$

where $\langle \text{fuzzy proposition} \rangle$ could also be a $\langle \text{compound fuzzy proposition} \rangle$.

For example, if e and \dot{e} are process state variables and \dot{u} is the control output variable then

$$\text{if } e \text{ is NB and } \dot{e} \text{ is PB then } \dot{u} \text{ is NS} \quad (6.3)$$

is a symbolic expression of the following relationship: *if* the current value of e is <negative big> and the current value of Δe is <positive big> *then* this causes a small decrease in the previous value of the control output.

The part that contains “if e is NB and Δe is PB” is called the antecedent rule and the last part “then Δu is NS” is called the consequent rule.

The value of decrease is deduced starting from the resulting value of the membership function of the relation that characterizes the first part of the statement (the premise). This value is used to deduce the structure of the membership function of the consequent rule and, thus, the change of the command signal is established. The resulting membership function can be deduced using several methods, called implications, but the most commonly used in fuzzy control is the Mamdani implication. The membership function that results from (6.3) according to this implication is:

$$\mu_{CNS}(\dot{u}) = \min\left(\min\left(\mu_{NB}(e), \mu_{PB}(\dot{e})\right) / (e, \dot{e}), \mu_{NS}(\dot{u})\right)$$

In fact, a trapezium is clipped from the fuzzy set NS (considering that it has a triangle shape) with $\min(\mu_{NB}(e), \mu_{PB}(\Delta e)) / (e, \Delta e)$ height. The C index, adjacent to NS, comes from clipping.

Let us consider the compound fuzzy proposition:

$$\text{if } e \text{ is NB then } u \text{ is PS}$$

If e takes the value e^* and it corresponds to $\mu_{NB}(e^*) = a$ then the membership function of the consequent rule is:

$$\mu_{CPS}(u) = \min(\alpha, \mu_{NB}(u))$$

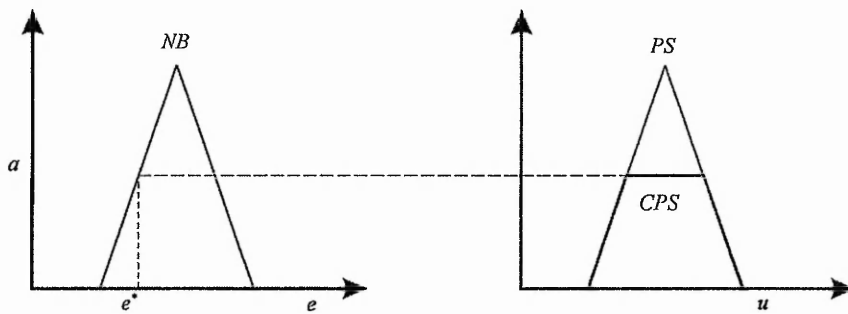


Fig. 6.3 – Example of the Mamdani implication

6.1.3 Fuzzy controller

The general structure of a fuzzy controller is presented in fig. 6.4.

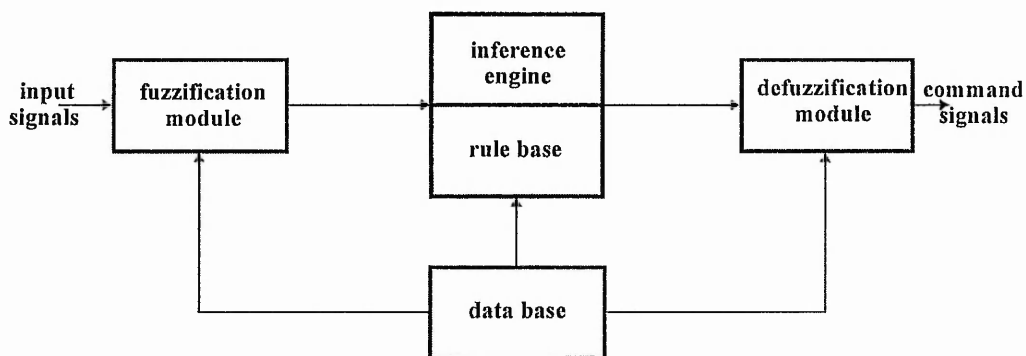


Fig. 6.4 – The basic structure of a fuzzy controller

The fuzzification module performs scale transformations which map the physical values of the current process state variables into a normalized universe on which the fuzzy sets are declared and converts the current value of a process state variable into fuzzy set.

The knowledge base is the core of the controller and consists of a data base and a rule base.

The basic function of the data base is to provide the necessary information for the correct functioning of the fuzzification module, of the rule base and of the defuzzification module. For example, if the values {NS, ZE, PS} are defined, then membership functions are expressed for each of them.

The basic function of the rule base is to represent in a structured way the control policy of an experienced process operator and/or control engineer in the form of a set of production rules such as:

if e is NB and Δe is PS then Δu is NS

which is translated as : if the error of y —that is the input signal- ($e = y - y_r$, where y_r is the reference signal) is NB and the change-of-error $\Delta e (e(k) - e(k-1))$ is PS then the command signal variation u is NS.

The inference machine is the module that decides for a pair of input variables which rules are activated. For example, the same pair $(e, \Delta e)$ could fire the proposition:

if e is NB and Δe is PS then Δu is NS

but also

if e is PB and Δe is PS then Δu is NB

Usually, the rules are defined in a table. An example is shown in table 6.1.

$e \rightarrow$	NS	ZE	PS
$\Delta e \downarrow$			
NS	PS	ZE	ZE
ZE	PS	ZE	NS
PS	ZE	NS	NS

Table 6.1 – example of a “firing” table

An example of the rules resulting from the table 6.1 is

if e is NS and Δe is PS then Δu is ZE

The defuzzification module performs the so called defuzzification which converts the set of modified control output values into a single point-wise value. There are several methods of defuzzification such as: center-of-area, center of sums, centers of largest area, first maxima, middle of maxima, height.

The Center-of -Area method is the most well-known defuzzification method [31]. In the discrete case of the universe $U (U = \{u_1, u_2, \dots, u_l\})$, the output signal is given by:

$$u^* = \frac{\sum_{i=1}^l u_i \mu_U(u_i)}{\sum_{i=1}^l \mu_U(u_i)} = \frac{\sum_{i=1}^l u_i \max_k \mu_{CLU^k}(u_i)}{\sum_{i=1}^l \max_k \mu_{CLU^k}(u_i)}$$

and in the continuous universe:

$$u^* = \frac{\int_U u \mu_U(u) du}{\int_U \mu_U(u) du} = \frac{\int_U u \max_k \mu_{CLU^k}(u) du}{\int_U \max_k \mu_{CLU^k}(u) du}$$

where \int is the classical integral. This method determines the center of area below the combined resultant membership functions (fig 6.5). If the areas of two clipped fuzzy sets overlap, then the overlapping area is not reflected in the above formula.

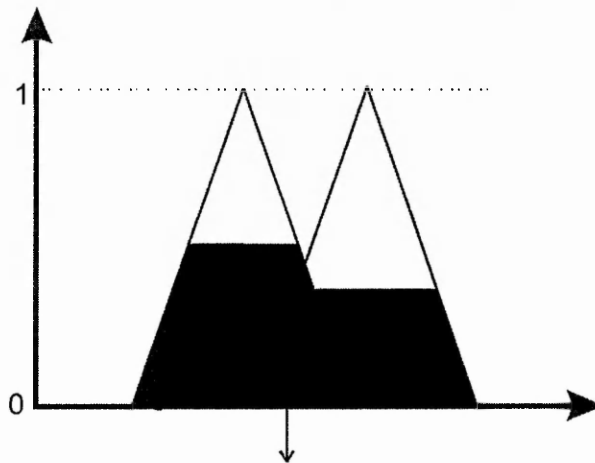


Fig. 6.5 – Center of Area method

6.2 Application controller

The hardware structure is presented in fig. 6.6. Most of the components are similar to those used in the structures presented in chapter 5. The exception is the fuzzy controller.

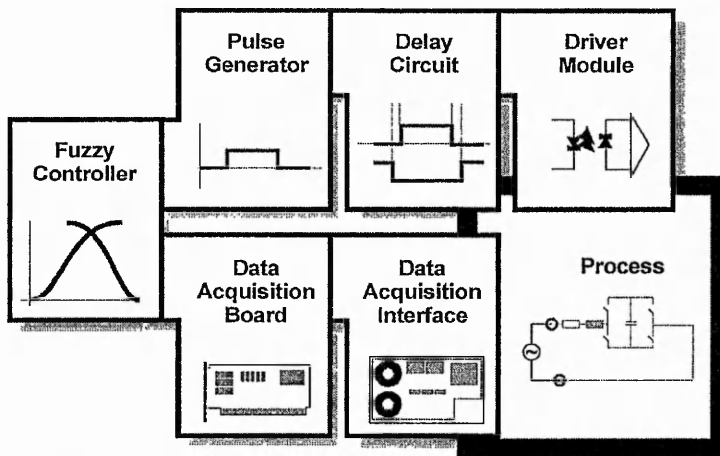
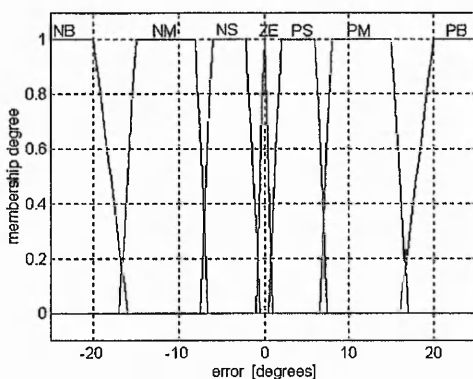


Fig. 6.6 – The basic structure of the experimental set

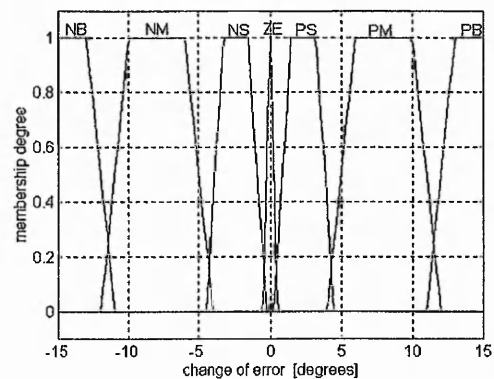
This may be implemented using specialized controllers such as Texas Instruments DSP TM320C25 but in this specific application, for a good monitoring of the results, a PC is used and the implementation of the controller is software using the C language.

One of the problems in application is the calculation of the phase angle between the supply voltage and the resulting current. Zero crossing detection or Fourier analysis are two possible methods.

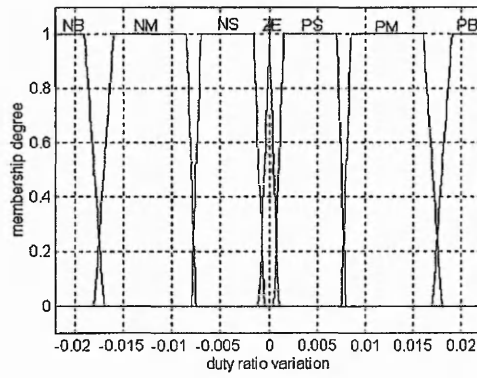
The first solution is often used in power electronic control. In this application the crossing point has to be detected on the fundamental component of the signal spectrum. This requires a current and voltage filter, to measure the time interval between the instants when these signals cross zero. The solution may be affected by further phase shift introduced by the filters affecting the phase angle calculation.



a



b



c

Fig. 6.7 – The membership functions of a) error; b) change-of-error
c) duty ratio variation

The second solution of Fourier analysis is chosen for this work in spite of its slow speed. The instantaneous current and voltage are sampled and memorized simultaneously at the same sampling rate during one period of the 50Hz supply. The resulting data strings are analyzed by Fourier series and, thus, the phase angle is calculated from the fundamental frequency. The drawback of the method comes from the delay (at least one period) between the moment when a new duty ratio is applied to the circuit and the phase angle calculation moment, but it has the advantage of relatively easy implementation in software.

$\Delta e \rightarrow$ $e \downarrow$	NB	NM	NS	ZE	PS	PM	PB
NB	PB	PB	PB	PB	PB	PM	PM
NM	PM	PM	PM	PM	PS	PS	PS
NS	PS						
ZE	ZE	ZE	ZE	ZE	ZE	ZE	ZE
PS	NS						
PM	NS	NS	NS	NM	NM	NM	NM
PB	NS	NS	NM	NM	NM	NM	NM

Table 6.2 – “Firing” table of application to the fuzzy controller

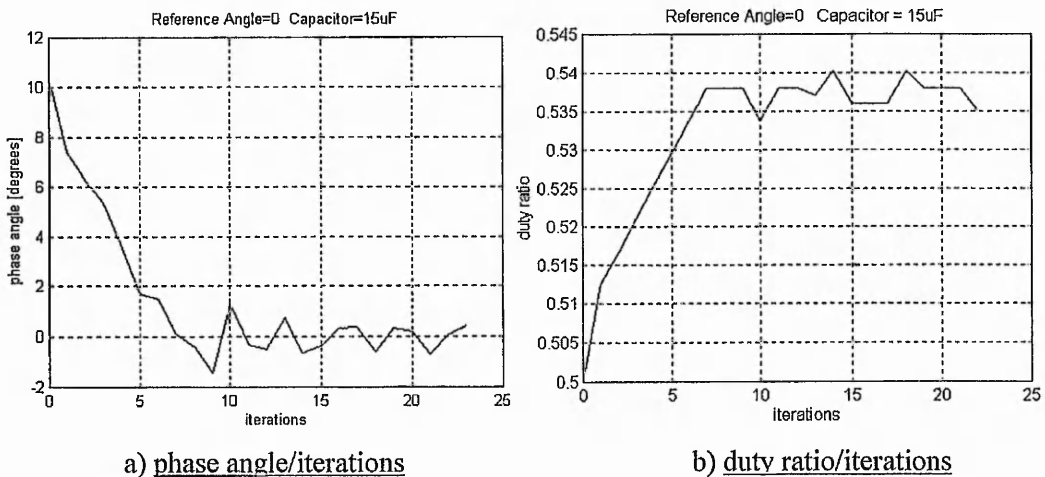
The program consists of a loop that in the first phase acquires the current and voltage, calculates the phase angle and, then deduces the phase angle error (difference between the reference phase angle and the calculated phase angle) and the change-of-error. The two values are the inputs to the fuzzy algorithm that calculates the membership degree of each for them to the corresponding 7 fuzzy sets (see fig 6.7) and deduces the rules for

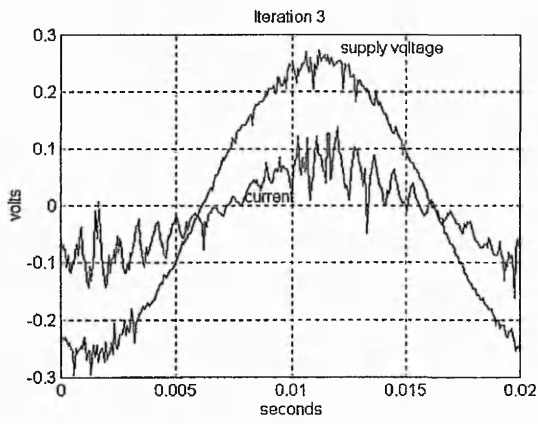
a pair of inputs from all 49 presented in table 6.2. The selected rules are activated and the duty ratio variation is calculated using the center of area method with respect to the new value of the duty ratio.

The experimental tests were carried out using a circuit with the parameters $L=5.5\text{mH}$ (resistance of the inductance is $5.1\ \Omega$) and $R=4.5\ \Omega$. The switching frequency of the bi-directional switches is 1kHz . The sampling rate of the acquisition board is set to 16kHz . The current is determined from a voltage transducer placed across the load resistance. A voltage transducer is also used for the supply voltage.

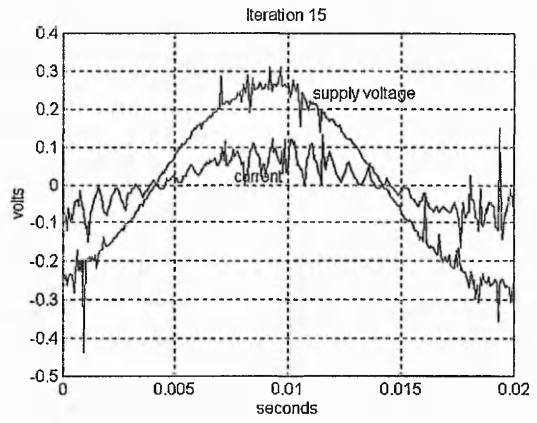
The test were made starting from an initial value of duty ratio of 0.5 that produce the phase angle of the plain RL circuit and, then, the phase angle is forced towards the reference phase angle modifying the duty ratio with the fuzzy algorithm.

The evolution of the phase angle and duty ratio as functions of the iterations (the numbers of the fuzzy algorithm called since the process was started) is represented in the graphs *a* and *b* of the figs. 6.8-6.11. The supply voltage and current waveforms for the various iterations are shown in graphs *c* and *d* of the same figures. The waveforms are calibrated in volts using the values given by the transducers.



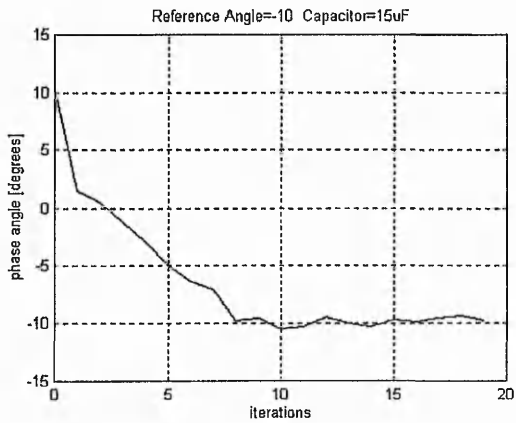


c) waveforms at 3rd iteration

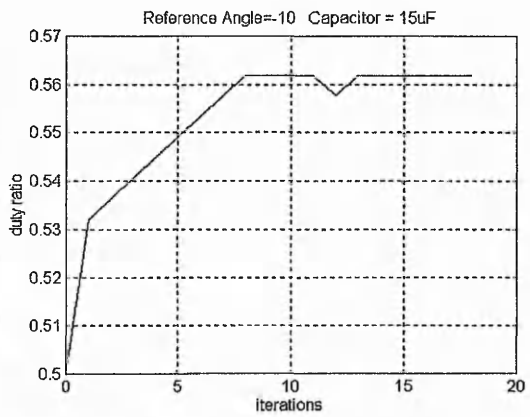


d) waveforms at 15th iteration

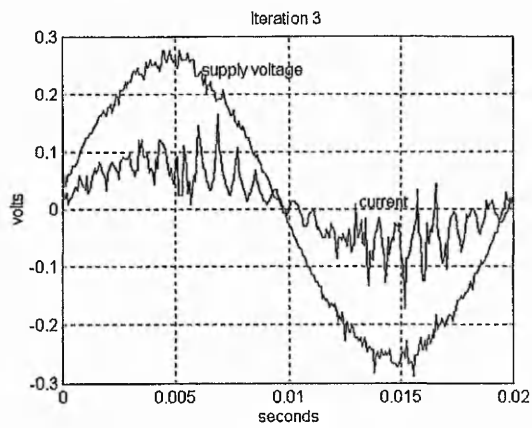
Fig. 6.8 – Reference angle = 0°, Capacitor = 15μF



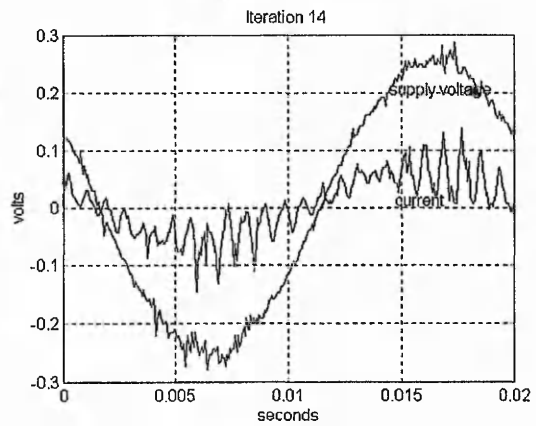
a) phase angle/iterations



b) duty ratio/iterations

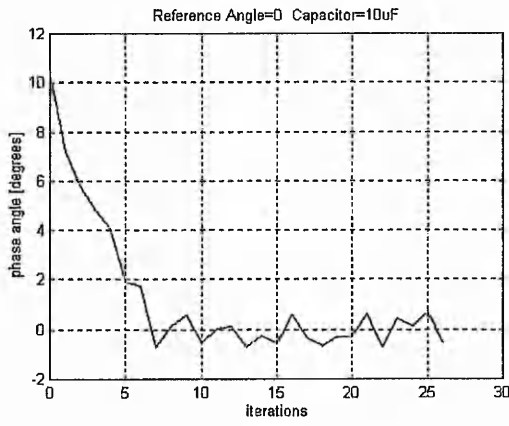


c) waveforms at 3rd iteration

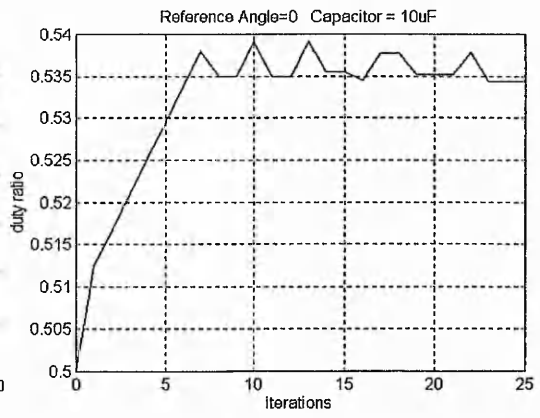


d) waveforms at 14th iteration

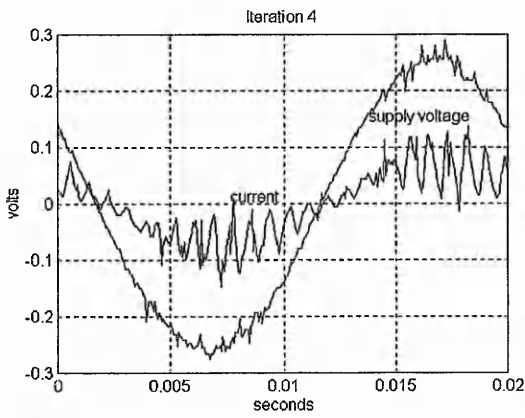
Fig. 6.9 – Reference angle = -10°, Capacitor = 15μF



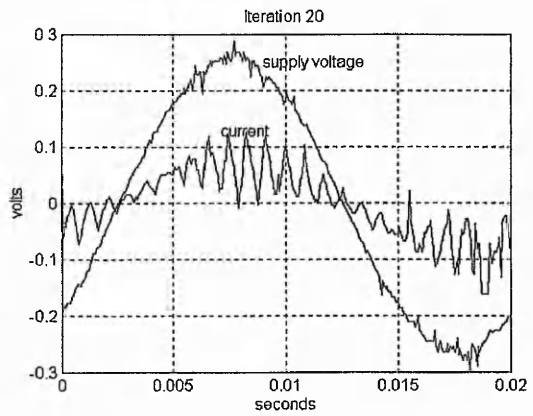
a) phase angle/iterations



b) duty ratio/iterations

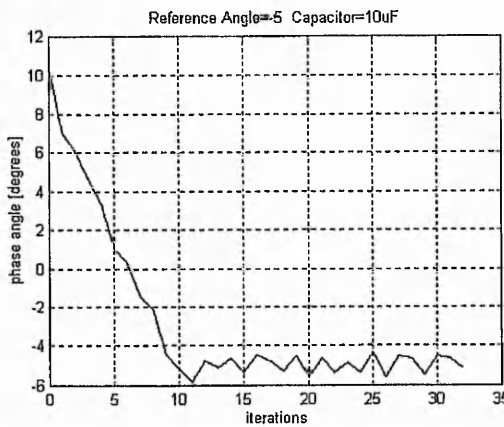


c) waveforms at 4th iteration

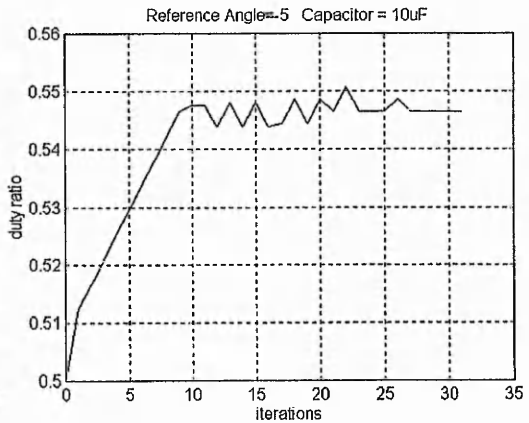


d) waveforms at 20th iteration

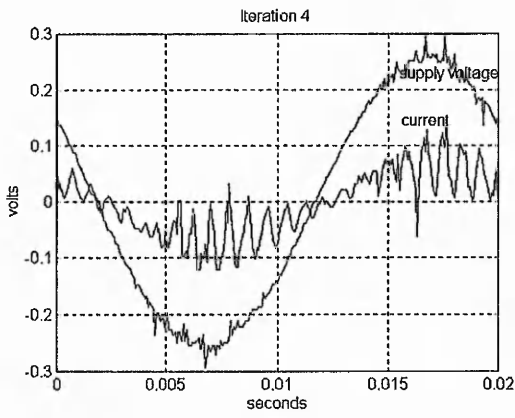
Fig. 6.10 – Reference angle = 0°. Capacitor = 10μF



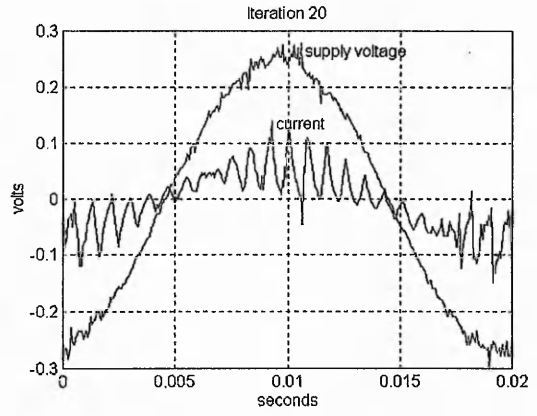
a) phase angle/iterations



b) duty ratio/iterations



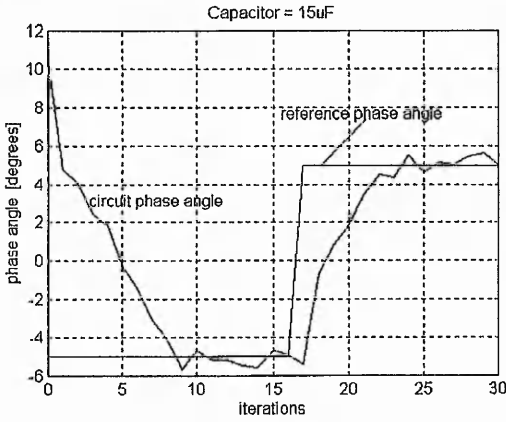
c) waveforms at 4th iteration



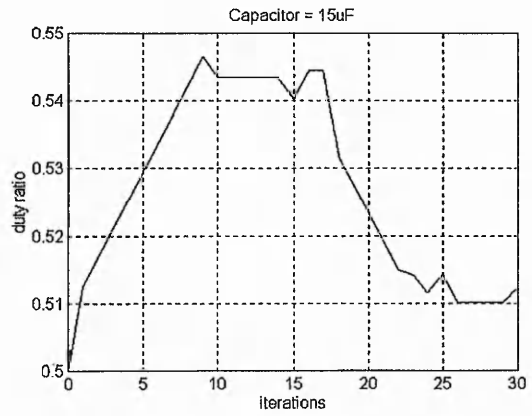
d) waveforms at 20th iteration

Fig. 6.11 – Reference angle = -5° , Capacitor = $10\mu\text{F}$

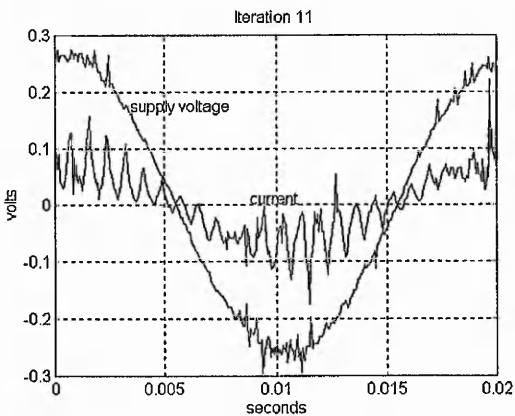
Fig. 6.12 presents the response of the system to a change of reference angle from -5° to 5° .



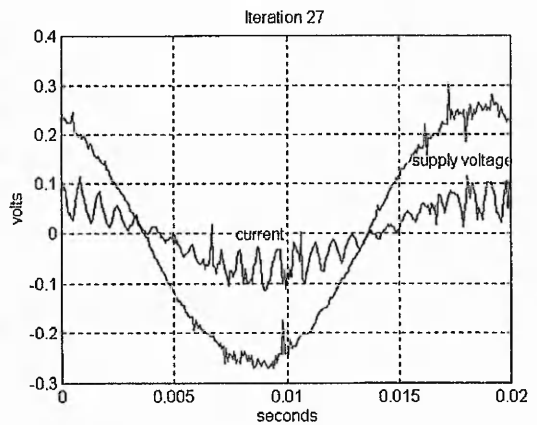
a) Phase angle



b) Duty ratio



c) waveforms at 11th iteration



d) waveforms at 27th iteration

Fig. 6.12 – Variable reference angle, Capacitor = $15\mu\text{F}$

The experimental results show good responses of the system even though 2 different capacitors of $15\mu\text{F}$ (figs. 6.8-6.9) respective of $10\mu\text{F}$ (figs. 6.10, 6.11) were used. In all figures, the phase angle changes within a maximum error of $\pm 0.7^\circ$. This deviation of the phase angle from the reference value is determined by the limits of the membership functions and by the accuracy of phase angle calculation.

If the limits of the membership functions are not the right ones, the controller will not be able to calculate the correct duty ratio value for forcing the phase angle towards the reference value. Also, an important role could be played by the defuzzification method but in this particular case the Center of Area has been used that is considered the most precise method.

The accuracy of the phase angle estimation is important. An incorrect appraisal determines a wrong calculation of applied duty ratio value that will remove the real phase angle from the required value. The accuracy is influenced, besides the algorithm, by the sampling rate: the higher the sampling rate, the better the accuracy achieved. On the other hand, the acquisition frequency is limited by the capabilities of the acquisition board and a higher sampling frequency requires longer times for the phase angle calculation.

The accuracy problem can be eliminated in a three phase system. It is possible to sample voltages and currents from two phases and to calculate the direct and quadrature axis components of voltage and current in phasor form and from this, the instantaneous phase angle between the voltage and current is calculated as described in chapter 2.

6.3 Conclusions

A control method of the phase angle in a RL circuit using fuzzy logic is presented in this chapter. The advantage of the method is that it is independent of the circuit parameters. The experimental results show good responses of the fuzzy controller.

The drawback of the method arises from the way phase angle is calculated; the length of the time required influences the system time response. This disadvantage may be eliminated in three phase circuits by the use of space vector theory allowing a quick calculation of the phase angle between the supply voltages and resulting currents (in balanced systems).

This control method is easy to adapt for performance control of the induction machine with externally modified rotor impedance. The adjustments to the fuzzy controller will be made depending on whether torque, speed, efficiency or power factor is being controlled.

Chapter 7

CONCLUSIONS AND FURTHER WORK

The aim of the work fulfilled in this thesis was to develop a system for rotor control of an induction machine by inserting a practical value of capacitor in the rotor circuit, thereby, eliminating the need for rotor resistance modification or the use of a rotor supply with all the inherent instability of the doubly-fed machine.

A theoretical analysis verifies the concept. This is shown by a set of equations derived for the evaluation of the most important criteria of induction machine performance - efficiency, power factor, peak and starting torque as functions of the machine parameters, load torque and the value of inserted capacitance. A novel fourth order equation for rotor angular velocity was deduced. This simplified the system simulation substantially compared to numerical methods used by previous researchers. Advantages of the system were demonstrated by comparison with the performance of the machine with short circuited rotor.

Simulation of the system shows that an optimisation of performances is achieved if the value of capacitance is varied as a function of the load torque. When the inserted capacitor is too small, the machine becomes unstable. In contrast, when the value of capacitance is too big, the machine behaviour is no different from its performance with short-circuited rotor.

The simulations showed that the value of capacitance needed for optimum performance is proportional to the power of the machine and its value is very large, in the range of hundred of millifarads or even Farads. These values of capacitance are too large to be practical, even with parallel banks of capacitors or with the use of a step-up transformer. Step-up transformation is impractical due to the large amount of iron required for the transformer to function at low slip-frequencies.

Electronic techniques for implementing high-capacitance effects thoroughly reviewed in literature showed the difficulties of using these techniques at the high powers and low

frequencies. Existing methods of electronically implementing high capacitance were aimed at power factor correction in power systems operating at 50 or 60Hz.

The work presented in this thesis showed the principal problem of using these methods in a rotor circuit. In the conventional power factor correction systems the converter is inserted between the source and the load. In the case of induction motor rotor circuit, this is not physical possible. In this work, the sequence of supply, load, converter is adopted.

The approach of controlling the rotor phase angle undertaken in this work moved away from the conventional methods of phase angle control in ac RL circuits by the use of gyrator techniques. The gyrator is successfully used in low power integrated circuits and recently it has aroused interest in power electronics. The realisation of the gyrator in practical power electronics has the drawback of using approximated gyrator concepts that produce pseudo-gyrators or involve a dc component of voltage.

The periodic short-circuiting of an ac capacitor by a bi-directional switch gives the effect of greatly enhanced capacitance in applications where current distortion is not a major factor. In short time duration applications such as the starting of single-phase induction motors, this technique is effective. Balanced two-phase operation from standstill to full-speed in a fully loaded machine can be achieved. In such applications of this method, since the circuit time constants are large, a high enough switching frequency cannot be used to minimise distortion of the current waveform.

The system introduced in this work to control the phase angle between the input voltage and resulting current in a RL circuit uses a H-bridge with bi-directional switches and a capacitor as the central component. From here onwards this is referred as a phase advance system. The control of the bi-directional switches is achieved using a Pulse Width Modulation strategy, with the duty ratio varying between 0.5 and unity. It has been shown that circuit phase angle can be varied by the duty ratio between the natural limits of the RL and the RLC circuit.

The quality of the resulting current is good. The third harmonic and harmonics which are multiples of the ratio of switching frequency to supply frequency are relatively significant. These, especially the harmonics related to the switching frequency, increase at the duty ratios which produce the in phase condition. In the induction motor applications, the rotor frequency is low under normal operation and as such the harmonics related to the switching frequency are expected to move towards the higher end of the frequency spectrum.

The tests carried out on a small induction motor with phase advance system in the rotor confirm the results of the simulation studies. The results show an increase in peak torque, improvement in power factor and efficiency over the whole torque range. The tests also demonstrate operation of the machine at optimum power factor while maintaining the efficiency slightly better than that of the motor with short circuited rotor.

In the work presented here, a fuzzy control system is developed and tested for controlling the phase angle between the input voltage and resulting current in a single phase circuit. The experimental results show good control of the phase angle; the error is $\pm 0.7^\circ$ while the response time corresponds to about 6 iterations.

Four main achievements have been made in this work :

- The development of a set of equations that simplifies simulation of an induction motor performance, in both the short circuited rotor mode and with externally modified rotor impedance.
- The development of a technique for controlling the phase angle in high power, low frequency RL circuits.
- Application of the technique to the rotor circuit of a small power induction machine to enhance its performance.
- The development of a fuzzy control system for switched capacitance in ac RL circuits.

The presented work can be further developed and applications extended as suggested:

- Further study of the influence of the switching frequency on the performance of the switched capacitor.
- Study of the voltage and current stresses in the system, to enable complete specification of components to be written.
- Study of EMC aspects.
- Extension of the experiments to medium and large industrial machines .
- Encapsulation of the whole system on the rotor shaft, thus eliminating the slip rings.
- Further development, starting from the presented fuzzy control stage, of the control and optimisation strategies for the induction machine from the rotor side. The system introduced in chapter 6 may be easily adapted to the induction machine using space vector theory.
- Study of the possibility of using the switched capacitor method presented in this thesis in the control of capacitor start/run single phase induction machines.
- Investigation of the application of the switched capacitor methodology used in this thesis to other fields such as power factor control or static var compensation.

References

1. W. Cheng, L. Xu – “Torque and reactive power Control of the Doubly-Fed Induction Machine by Position Sensorless Scheme”, IEEE Transactions, 1994, pp 496-502;
2. M.G. Ioannides, J.A. Tegopoulos – “Generalized Optimization Slip Power Recovery Drives”, IEEE Transactions on Energy Conversion, Vol. 5, No. 1, March 1990, pp. 91-97;
3. Y. Baghouz, O.T. Tan – “Optimal Efficiency Speed Control of Induction Motors by Variable Rotor Impedance”, IEEE Transactions on Energy Conversion, Vol. 4, No. 2, June 1989, pp. 216-223;
4. J. Reinert, M.J. Parsley – “Controlling the Speed of an Induction Motor by Resonating the Rotor Circuit”, IEEE Transactions on Industry Applications, Vol. 31, No. 4, July/August 1995, pp.887-891;
5. H. Salama, M. Kansara, P.G. Holmes, Y. Safar – “Optimal Steady - State Performance of Induction Motor Drives” - OPTIM'96 Conference, pp. 1347-1360, Brasov, 13-15 May 1996
6. T.A. Lettenmaier, D.W. Novotny, T.A. Lipo – “Single-Phase Induction Motor with an Electronically Controlled Capacitor”, IEEE Transactions on Industry Applications, Vol. 27, No. 1, January/February 1991, pp. 38-43;
7. E. Muljadi, Y. Zhao, T.H. Liu, T.A. Lipo – “ Adjustable ac Capacitor for a Single-Phase Induction Motor”, IEEE Transactions on Industry applications, Vol. 29, No. 3, May/June, 1993, pp.479-484;
8. T.H. Liu –“ A Maximum Torque Control with a Controlled Capacitor for a Single-Phase Induction Motor”, IEEE Transactions on Industrial Electronics, Vol. 42, No. 1, February 1995, pp. 17-24;
9. P. Vas – “Vector Control of AC Machines”, Clarendon Press, Oxford, 1990;
10. W. Leonhard – “Control of Electrical Drives”, Springer-Verlag, 1985;
11. J. Hindmarsh – “Electrical Machines and Their Applications”, Pergamon Press, Oxford, 1981;
12. M.J. Schutten, R.L. Steigerwald, M.H. Kheraluwala – “Characteristics of Load Resonant Converters Operated in High Power Factor Mode”, IEEE Transactions on Power Electronics, Vol. 7, No. 2, April 1992;
13. D.R. Veas, J.W. Dixon, B-T. Ooi – “A Novel Load Current Control Method for a Power Factor Voltage Source PWM Rectifier”, IEEE Transactions on Power Electronics, Vol. 9, No. 2, March 1994;
14. B.M.M. Mwinyiwiwa, P.M. Birks, B-O Ooi – “ Delta-Modulated Buck Type PWM Converter”, IEEE Transactions On Industry Applications, Vol. 28, No. 3, May/June 1992;
15. R. Liu, C.Q. Lee – “Power Factor Consideration in Resonant Converters”, IECON'90, 16th Annual Conference of IEEE Industrial Electronics Society, vol. 2, pp. 889-894, New York, 27-30 Nov. 1990
16. A.F. de Souza, I. Barbi – “A new ZVS-PWM unity power factor rectifier with reduced conduction losses”, PESC '94 Record, 25th Annual IEEE Power Electronics Specialists Conference, pp.342-8, vol.1., 1994, New York, NY, USA;
17. B.D.H. Tellegen – “The Gyrator, a New Electric Network Element”, Philips Research Reports, Vol. 3, No. 2, 1948, pp. 81-101;
18. L. T. Bruton – “RC-active circuits: theory and design, Englewood Cliffs, London, Prentice Hall, 1980;
19. S. Singer – “Gyrators Application in Power Processing Circuits”, IEEE Transactions on Industrial Electronics Vol.IE-34, No 3, August 1987, pp.313-318,;
20. S. Singer, R.W. Erickson – “Canonical Modeling of Power Processing Circuits Based on the POPI Concept”, IEEE Transactions on Power Electronics, Vol. 7, No. 1, Jan. 1992, 37-43;
21. D.M. Divan – “Nondissipative Switched Networks for High-Power Applications”, Electronics Letters 29th of March 1984, Vol. 20, No.7, pp.277-279;

22. M. Eshani, I. Husain, M.O. Bilgic – “Inverse Dual Converter (IDC) for High Power DC-DC Applications”, Record of 21st Power Electronics Specialists Conference, pp. 814-821, New York, USA, 1990;
23. M. Eshani, I. Husain, M.O. Bilgic – “Power Converters as Natural Gytrators”, IEEE Transactions On Circuits and Systems, Fundamental Theory and Applications, Vol. 40, No. 12, December, 1993;
24. S. Singer – “The Application of Loss Free Resistors in Power Processing Circuits”, IEEE Transactions on Power Electronics, Vol. 6, No. 4, October, 1991, pp. 595-600;
25. S. Srinivasan, G. Venkataramanan – “Versatile PWM Converters for Three Phase AC Power Conditioning”, Proceedings of Power Conversion and Intelligent Motion, PCIM '94, pp. 451-459, Ventura, USA, 17-22 September, 1994;
26. P.V. Ananda, V. Ramachandran, M.N.S. Swamy – “Switched Capacitors filters”, Prentice Hall, 1995;
27. J.G. Kassakian, M.F. Schlecht, G.C. Varghese – “Principles of Power electronics”, Addison-Wesley Publishing Company, Massachusetts, 1991;
28. P. Nielsen – “The Matrix Converter For An Induction Motor Drive”, Ph.D. thesis, Danfoss, 1993;
29. C. Suci, M. Kansara, P.G. Holmes, W. Szabo – “Phase Advancing for Current in R-L Circuits Using Switched Capacitors”, Electronics Letters, IEE Journal, vol. 35, no. 16, Aug. 1999, pp. 1296-7;
30. B. Kosko – “Neural networks and fuzzy systems : a dynamical systems approach to machine intelligence”, Prentice Hall, London, 1992;
31. D. Driankov, H. Hellendroon, M. Reinfrank – “An introduction to fuzzy control”, Springer Verlag, New York, 1996;
32. *** - “MATLAB-Reference Guide”, The MATH WORKS Inc., 1996;
33. D. A. Calahan, A.B. Macnee, E.L.McMahon – “Introduction to modern circuit analysis”, Holt, Rinehart and Winston, Inc., 1974;

Publications

Related to the thesis:

1. C. *Suciu*, L. Dafinca, M. Kansara, I. Margineanu – “Switched Capacitor Fuzzy Control for Power Factor Correction in Inductive Circuits”, IEEE Power Electronics Specialists Conference, pp. 773-777, vol. 2, Galway, Ireland, 18-23 June 2000;
2. C. *Suciu*, L. Dafinca, M. Kansara, A. Szabo: “Fuzzy Control of the Current Phase in Induction Circuits”, - Proc. of the 7th International Conference on Optimization of Electric and Electronic Equipment, pp. 631-636, vol. 3, Brasov, Romania, 11-12 May 2000;
3. C. *Suciu*, M. Kansara, P.G. Holmes, W. Szabo – “Phase Advancing for Current in R-L Circuits Using Switched Capacitors”, Electronics Letters, IEE Journal, vol. 35, no. 16, Aug. 1999, pp. 1296-7
4. C. *Suciu*, M. Kansara, W. Szabo, L. Dafinca – “Comparative Analysis of the Induction Machine with Variable Rotor Impedance”, Proc. of the International Conference on Engineering of Modern Electric Systems '99, Oradea, Romania 26-29 Mai 1999;
5. C. *Suciu*, M. Kansara, P.G. Holmes – “A Space Vector Model of a Static Leading VAR Secondary Controlled Induction Machine” –Proc. of OPTIM'98, Braşov, Romania, 13-15 Mai, 1998, pg. 375-378

Other papers:

1. L. Dafinca, C. *Suciu*, I. Margineanu – “Identification Method of Induction Motor Drives Using Artificial Neural Networks” - Proc. of the 7th International Conference on Optimization of Electric and Electronic Equipment, pp. 651-654, Brasov, Romania, 11-12 May 2000;
2. L. Dafinca, I. Margineanu, R. Craciun, C. *Suciu* – “Inertia Identification Method of Electrical Drive Systems”, Proc. of the International Conference of Electrical Engineering and Energetics EPE '99, Iasi, Romania, 4-6 Nov. 1999;
3. V. Comnac, M. Cernat, F. Moldoveanu, C. *Suciu*, R.M. Cernat, R. Ungar – “ The Control of Interior Permanent Magnet Synchronous Machines Using a Non-Linear Minimum Order Observer”, PCIM'99, Nüremberg, Germania, 22-24 Iunie 1999, pg. 345-350;
4. R. Craciun, L. Dafinca, I. Margineanu, C. *Suciu*, C. Pitis – “Control System of a Sewage Treatment Installation”, Proc. of the International Conference on Engineering of Modern Electric Systems '99, Oradea, Romania, 26-29 Mai 1999;
5. V. Comnac, M. Cernat, F. Moldoveanu, C. *Suciu*, R.M. Cernat – “The Control of an Interior Permanent Magnet Synchronous Machine Using Gopinath Observer”, ELEKTRO'99, Zilina, Slovacia, 25-26 Mai 1999, pg. 27-32;
6. V. Comnac, F. Moldoveanu, C. *Suciu*, I. Drăghici – “Mechanically Sensorless Control System for Servodrives with Synchronous Machines”, Bulletin of Transilvania University of Braşov, Vol. 5(40) – New Series, Series A, 1998, pg. 129-136;
7. V. Comnac, I. Ţopa, F. Moldoveanu, C. *Suciu* – “Real Time Observer based control of an Interior Permanent Magnet Synchronous Machine” – Proc. of OPTIM'98, Braşov, 13-15 Mai 1998, pg. 511-517;

Mathematical deduction of the differential equation system (2.11)

The system was deduced from system (2.8) which equations were split after their direct and quadrature components, resulting in:

$$u_{sx} = R_s i_{sx} + L_s \frac{di_{sx}}{dt} + L_m \frac{di_{rx}}{dt} - \omega_g L_s i_{sy} - \omega_g L_m i_{ry} \quad (1)$$

$$u_{sy} = R_s i_{sy} + L_s \frac{di_{sy}}{dt} + L_m \frac{di_{ry}}{dt} + \omega_g L_s i_{sx} + \omega_g L_m i_{rx} \quad (2)$$

$$u_{rx} = R_r i_{rx} + L_r \frac{di_{rx}}{dt} + L_m \frac{di_{sx}}{dt} - (\omega_g - \omega_r) L_m i_{sy} - (\omega_g - \omega_r) L_r i_{ry} \quad (3)$$

$$u_{ry} = R_r i_{ry} + L_r \frac{di_{ry}}{dt} + L_m \frac{di_{sy}}{dt} + (\omega_g - \omega_r) L_m i_{sx} + (\omega_g - \omega_r) L_r i_{rx} \quad (4)$$

Equation 1 is multiplied by L_r and equation 3 is multiplied by $-L_m$, then the resulting equations are added and gives in:

$$\begin{aligned} L_r u_{sx} - L_m u_{rx} &= R_s L_r i_{sx} + L_r L_s \frac{di_{sx}}{dt} + L_m L_r \frac{di_{rx}}{dt} - \omega_g L_r L_s i_{sy} - \omega_g L_m L_r i_{ry} - \\ &- R_r L_m i_{rx} - L_r L_m \frac{di_{rx}}{dt} - L_m^2 \frac{di_{sx}}{dt} + (\omega_g - \omega_r) L_m^2 i_{sy} + (\omega_g - \omega_r) L_r L_m i_{ry} \end{aligned}$$

$$\begin{aligned} (L_s L_r - L_m^2) \frac{di_{sx}}{dt} &= -R_s L_r i_{sx} + \omega_r L_m^2 i_{sy} + \omega_g (L_r L_s - L_m^2) i_{sy} + R_r L_m i_{rx} + \omega_r L_r L_m i_{ry} + \\ &+ L_r u_{sx} - L_m u_{rx} \end{aligned}$$

And, thus, results

$$\frac{di_{sx}}{dt} = \frac{-R_s L_r i_{sx} + \omega_r L_m^2 i_{sy} + R_r L_m i_{rx} + \omega_r L_m L_r i_{ry} + L_r u_{sx} - L_m u_{rx}}{L_s L_r - L_m^2} + \omega_g i_{sy}$$

Equation 1 is multiplied by $-L_m$ and equation 3 is multiplied by L_s , then the resulting equations are added and gives in:

$$\begin{aligned} -L_m u_{sx} + L_s u_{rx} &= -R_s L_m i_{sx} - L_m L_s \frac{di_{sx}}{dt} - L_m^2 \frac{di_{rx}}{dt} + \omega_g L_m L_s i_{sy} + \omega_g L_m^2 i_{ry} + \\ &+ R_r L_s i_{rx} + L_r L_s \frac{di_{rx}}{dt} + L_m L_s \frac{di_{sx}}{dt} - (\omega_g - \omega_r) L_m L_s i_{sy} - (\omega_g - \omega_r) L_r L_s i_{ry} \end{aligned}$$

$$\begin{aligned} (L_s L_r - L_m^2) \frac{di_{rx}}{dt} &= R_s L_m i_{sx} - \omega_r L_m L_s i_{sy} - R_r L_s i_{rx} - \omega_r L_r L_s i_{ry} + \omega_g (L_r L_s - L_m^2) i_{ry} - \\ &- L_m u_{sx} + L_s u_{rx} \end{aligned}$$

and results:

$$\frac{di_{rx}}{dt} = \frac{R_s L_m i_{sx} - \omega_r L_m L_s i_{sy} - R_r L_s i_{rx} - \omega_r L_r L_s i_{ry} - L_m u_{sx} + L_s u_{rx}}{L_r L_s - L_m^2} + \omega_g i_{ry}$$

Equation 2 is multiplied by L_r and equation 4 is multiplied by $-L_m$, then the resulting equations are added and gives in:

$$L_r u_{sy} - L_m u_{ry} = R_s L_r i_{sy} + L_r L_s \frac{di_{sy}}{dt} + L_m L_r \frac{di_{ry}}{dt} + \omega_g L_r L_s i_{sx} + \omega_g L_m L_r i_{rx} - \\ - R_r L_m i_{ry} - L_r L_m \frac{di_{ry}}{dt} - L_m^2 \frac{di_{sy}}{dt} - (\omega_g - \omega_r) L_m^2 i_{sx} - (\omega_g - \omega_r) L_r L_m i_{rx}$$

$$(L_s L_r - L_m^2) \frac{di_{sy}}{dt} = -R_s L_r i_{sy} - \omega_r L_m^2 i_{sx} - \omega_g (L_r L_s - L_m^2) i_{sx} + R_r L_m i_{ry} - \omega_r L_r L_m i_{rx} + \\ + L_r u_{sy} - L_m u_{ry}$$

And, thus, results

$$\frac{di_{sy}}{dt} = \frac{-\omega_r L_m^2 i_{sx} - L_r R_s i_{sy} - \omega_r L_r L_m i_{rx} + L_m R_r i_{ry} + L_r u_{sy} - L_m u_{ry}}{L_s L_r - L_m^2} - \omega_g i_{sx}$$

Equation 2 is multiplied by $-L_m$ and equation 4 is multiplied by L_s , then the resulting equations are added and gives in:

$$-L_m u_{sy} + L_s u_{ry} = -R_s L_m i_{sy} - L_m L_s \frac{di_{sy}}{dt} - L_m^2 \frac{di_{ry}}{dt} - \omega_g L_m L_s i_{sx} - \omega_g L_m^2 i_{rx} + \\ + R_r L_s i_{ry} + L_r L_s \frac{di_{ry}}{dt} + L_m L_s \frac{di_{sy}}{dt} + (\omega_g - \omega_r) L_m L_s i_{sx} + (\omega_g - \omega_r) L_r L_s i_{rx} \\ (L_s L_r - L_m^2) \frac{di_{ry}}{dt} = -R_s L_m i_{sy} + \omega_r L_m L_s i_{sx} - R_r L_s i_{ry} + \omega_r L_r L_s i_{rx} - \omega_g (L_r L_s - L_m^2) i_{rx} - \\ - L_m u_{sx} + L_s u_{rx}$$

and results:

$$\frac{di_{ry}}{dt} = \frac{\omega_r L_m L_s i_{sx} + L_m R_s i_{sy} + \omega_r L_r L_s i_{rx} - L_s R_s i_{ry} - L_m u_{sy} + L_s u_{ry}}{L_r L_s - L_m^2} - \omega_g i_{sx}$$

MATLAB programs used in simulations of the induction motor

Function `inter.m` was used to calculate the rotor pulsation ω_2 . The function is based on function `roots.m` that is implemented in MATLAB[32] and uses a matrix algorithm for solving high order equations.

inter.m

```
function ii=inter(x);
y=roots(x);
dim=size(y);
in=[];
for i=1:dim
    if imag(y(i))==0
        if y(i)>0
            in=[in y(i)];
        end;
    end;
end;
if (in==[])
    error('om2 does not exist');
end;
ii=min(in);
```

Program `tst.m` was used to draw graphics a,b,c from sets 2.13-2.15, , using equations 2.29-2.34

tst.m

```
% program for plotting torque-speed characteristic, efficiency and
% power factor for constant capacitor inserted on each phase of the
% rotor circuit

clear all;
um=240*sqrt(2);
f=50;
om=2*pi*f;
rs=85;      %stator resistance
rr=115;     %rotor resistance
lm=1.4;     %mutual inductance
tr=1;
lrs=0.36;   %rotor linkage inductance
lss=0.36;   %stator linkage inductance
lr=lrs+1/tr*lm;
ls=lss+tr*lm;
p=2;        %/pole pairs
cr=0.0035; %capacitor
scr=sprintf('C=%f F',cr);

s=0:0.01:1; %slip
om2=s*om;

%torque-speed characteristic for the machine in normal configuration
a=(om*(ls*lr-lm^2))^2+(lr*rs)^2;
b=2*om*lm^2*rr*rs;
```

```
c=(rr*rs)^2+(om*ls*rr)^2;
```

```
in1=3/2*p*rr*om2*lm^2*um^2;
```

```
in2=a*om2.^2+b*om2+c;
```

```
te=in1./in2;
```

```
% torque-speed characteristic for the machine with modified rotor
```

```
% impedance
```

```
a=(om*(ls*lr-lm^2))^2+(lr*rs)^2;
```

```
b=2*om*lm^2*rr*rs;
```

```
c=(rr*rs)^2-2*om^2*lr*ls^2/cr+2*(om*lm)^2*ls/cr+(om*ls*rr)^2-2*lr/cr*rs^2;
```

```
d=(om*ls/cr)^2+(rs/cr)^2;
```

```
in1=3/2*p*rr*om2.^3*lm^2*um^2;
```

```
in2=(a*om2.^4+b*om2.^3+c*om2.^2+d);
```

```
tec=in1./in2;
```

```
% power factor and efficiency for the machine in normal configuration
```

```
d=rr*rs+om*om2*(lm^2-lr*ls);
```

```
e=om*ls*rr+om2*lr*rs;
```

```
s1=rr*d+om2.*e*lr;
```

```
s2=rr*e-om2.*d*lr;
```

```
pf=s1./sqrt((s1.^2+s2.^2)); %power factor
```

```
pabs=3/2*um^2*s1./(d.^2+e.^2);
```

```
pdel=(om-om2).*te/p;
```

```
eff=pdel./pabs; %efficiency
```

```
% power factor and efficiency for the machine with modified rotor
```

```
% impedance
```

```
u=rs*rr+om*om2*lm^2-om*ls*om2*lr;
```

```
u1=1./om2/cr*om*ls;
```

```
u=u+u1;
```

```
v=om*ls*rr+om2*rs*lr;
```

```
v1=1./om2./cr*rs;
```

```
v=v-v1;
```

```
s1cr=rr*u+om2.*v*lr;
```

```
s1cr1=v./om2/cr;
```

```
s1cr=s1cr-s1cr1;
```

```
s2cr=om2.*u*lr-rr*v;
```

```
s2cr1=u./om2/cr;
```

```
s2cr=s2cr-s2cr1;
```

```
pfcrcr=s1cr./sqrt(s1cr.^2+s2cr.^2);
```

```
pabscrcr=3/2*um^2*s1cr./(u.^2+v.^2);
```

```
pdelcr=(om-om2).*tec/p;
```

```
effcr=pdelcr./pabscrcr;
```

```
plot(s,te,'g',s,tec,'r'),grid,
```

```
xlabel('slip'),ylabel('torque [Nm]');
```

```
title('scr');
```

```
gtext('without capacitor'),gtext('with capacitor');
```

```
zoom on;
```

```
pause;
```

```
zoom off;
```

```
plot(s,eff,'g',s,effcr,'r'),grid,
```

```
xlabel('slip'),ylabel('efficiency')
```

```
title('scr');
```

```
%gtext('without capacitor'),gtext('with capacitor');
```

```

zoom on;
pause;
zoom off;
plot(s,pf,'g',s,pfcr,'r'),grid,
xlabel('slip'),ylabel('power factor')
title(scr);
%gtext('without capacitor'),gtext('with capacitor');
zoom on;
pause;
close;

```

cur.m

```

% program for calculating the evolution of stator and rotor currents
% in both configuration for constant capacitor and whole load torque
% range that results from speed-torque characteristics

```

```

clear all;
um=220*sqrt(2);
f=50;
om=2*pi*f;
rs=10;
rr=6.5;
lm=0.42119;
tr=1;
lrs=0.040107;
lss=0.043067;
lr=lrs+1/tr*lm;
ls=lss+tr*lm;
p=2;
cr=0.07; %capacitor
scr=sprintf('C=%1.2f F',cr);

```

```

s=0.:0.01:1;
om2=s*om; %slip

```

```

a=(om*(ls*lr-lm^2))^2+(lr*rs)^2;
b=2*om*lm^2*rr*rs;
c=(rr*rs)^2+(om*ls*rr)^2;

```

```

% rotor and stator currents in standard configuration

```

```

in1=3/2*p*rr*om2*lm^2*um^2;
in2=a*om2.^2+b*om2+c;
te=in1./in2;
ir=lm*um*om2./sqrt(a*om2.^2+b*om2+c);
en1=sqrt(rr^2+lr^2*om2.^2);
en2=en1.*ir;
is=en2./om2/lm;

```

```

% rotor and stator currents in modified configuration

```

```

a=(om*(ls*lr-lm^2))^2+(lr*rs)^2;
b=2*om*lm^2*rr*rs;
c=(rr*rs)^2-2*om^2*lr*ls^2/cr+2*(om*lm)^2*ls/cr+(om*ls*rr)^2-2*lr/cr*rs^2;
d=(om*ls/cr)^2+(rs/cr)^2;
in1=3/2*p*rr*om2.^3*lm^2*um^2;
in2=(a*om2.^4+b*om2.^3+c*om2.^2+d);
tec=in1./in2;

```

```

irr=lm*um*om2.^2./sqrt(a*om2.^4+b*om2.^3+c*om2.^2+d);
en=(lr-1./(om2.^2)/cr).^2;
en1=sqrt(rr^2+en.*om2.^2);
en2=en1.*irr;
isr=en2./om2/lm;

zoom off;
plot(te,ir,'r',tec,irr,'y'),grid,
xlabel('torque [Nm]'),ylabel('rotor current [A]');
title(scr);
gtext('without capacitor'),gtext('with capacitor');
zoom on;
pause;

zoom off;
plot(te,is,'r',tec,isr,'y'),grid,
xlabel('torque [Nm]'),ylabel('stator current [A]');
title(scr);
gtext('without capacitor'),gtext('with capacitor');
zoom on;
pause;

zoom off;
plot(te,is.*ir,'r',tec,isr.*irr,'y'),grid,
xlabel('torque [Nm]'),ylabel('stator and rotor current multiplication [A]');
title(scr);
gtext('without capacitor'),gtext('with capacitor');
zoom on;
pause;
close;

```

Program tstb.m was used to draw graphics 2.16-2.18 using equation 2.26 and 2.46.

tstb.m

```

% calculation of the torque developed by the induction machine in both configuration for a set slip
% varying the inserted capacitor

```

```

clear all;
um=460*sqrt(2);
f=50;
om=2*pi*f;
rs=0.04;
rr=0.04;
lm=0.0073;
%tr=1.23/sqrt(3);
%tr=1/tr;
tr=1;
lrs=0.0001687;
lss=0.0001687;
lr=lrs+1/tr*lm;
ls=lss+tr*lm;
p=2;

s=0.05; %imposed slip
scr=sprintf('slip=%0.2f,s);
om2=s*om;
a=(om*(ls*lr-lm^2))^2+(lr*rs)^2;

```

```

b=2*om*lm^2*rr*rs;
c=(rr*rs)^2+(om*ls*rr)^2;
in1=3/2*p*rr*om2*lm^2*um^2;
in2=a*om2.^2+b*om2+c;

```

```

for i=1:1:299
cr(i)=(i-1)*0.1+0.04;
te(i)=in1/in2; %torque developed by the machine in standard configuration
ccr=(rr*rs)^2-2*om^2*lr*ls^2/cr(i)+2*(om*lm)^2*ls/cr(i)+(om*ls*rr)^2-2*lr/cr(i)*rs^2;
dcr=(om*ls/cr(i))^2+(rs/cr(i))^2;
in1r=3/2*p*rr*om2.^3*lm^2*um^2;
in2r=(a*om2.^4+b*om2.^3+ccr*om2.^2+dcr);
tec(i)=in1r/in2r; %torque developed by the machine in modified configuration
end;

```

```

plot(cr,te,'g',cr,tec,'r'),grid,
xlabel('capacitance [F]'),ylabel('torque [Nm]');
title('scr');
gtext('without capacitor'),gtext('with capacitor');
zoom on;
pause;
close;

```

Program pfef.m plotted the sets 2.4-2.12, using equations (2.21), (2.25), (2.26), (2.29), (2.30), (2.31), (2.43), (2.45), (2.46), (2.48), (2.49).

pfef.m

% program to calculate the evolution of rotor speed, power factor, efficiency and copper losses for
% constant load torque and variable capacitor

```

clear all;
um=380*sqrt(2);
f=50;
om=2*pi*f;
rs=1.64;// machine parameters
rr=1.45;
lm=0.1636;
tr=1;
lrs=0.003;
lss=0.003;
lr=lrs+1/tr*lm;
ls=lss+tr*lm;
p=2;
te=20;
scr=sprintf('torque=%1.2f Nm',te);
a=(om*(ls*lr-lm^2))^2+(lr*rs)^2; //parameters of equation (2.21)
b=2*om*lm^2*rr*rs;
c=(rr*rs)^2+(om*ls*rr)^2;
acr=(om*(ls*lr-lm^2))^2+(lr*rs)^2;
bcr=2*om*lm^2*rr*rs;
f=3/2*lm^2*um^2*p*rr/te;
q=[a b-f c];
om2=inter(q);
vii=(om-om2)/p;

d=rr*rs+om*om2*(lm^2-lr*ls);
e=om*ls*rr+om2*lr*rs;
s1=rr*d+om2*e*lr; //equations (2.29)and (2.28)

```

```

s2=rr*e-om2*d*lr;
pwf=s1/sqrt((s1^2+s2^2)); //power factor from (2.31)
pabs=3/2*um^2*s1/(d^2+e^2);
pdel=(om-om2).*te/p;
ef=pdel/pabs; //efficiency from (2.34)
pcu1=te/p*(om2+rs/rr*(rr^2+om2^2*lr^2)/om2/lm^2);

j=1;
for i=1:1:1194
    cr=0.005+(i-1)*0.001;
    ccr=(rr*rs)^2+(om*ls*rr)^2-2*om^2*ls^2*lr/cr+2*om^2*lm^2*ls/cr-2*lr*rs^2/cr; //parameters of
    dcr=(om*ls/cr)^2+(rs/cr)^2; // (2.43)
    qr=[acr bcr-f ccr 0 dcr];
    om2r=inter(qr);
    viri=(om-om2r)/p;

    u=rs*rr+om*om2r*lm^2-om*ls*om2r*lr+1/om2r/cr*om*ls;
    v=om*ls*rr+om2r*rs*lr-1/om2r/cr*rs;
    s1cr=rr*u+om2r*v*lr-v/om2r/cr; //(2.48) and (2.49)
    s2cr=om2r*u*lr-rr*v-u/om2r/cr;
    pwfcr=s1cr/sqrt(s1cr^2+s2cr^2);
    pabscr=3/2*um^2*s1cr/(u^2+v^2);
    pdelcr=(om-om2r)*te/p;
    efcrcr=pdelcr/pabscr;
    pcu1r=te/p*(om2r+rs/rr*(rr^2+om2r^2*(lr-1/om2r^2/cr)^2)/om2r/lm^2); //(2.45)

    if(viri>0)
        crr(j)=cr;
        vi(j)=vii;
        eff(j)=ef;
        pf(j)=pwf;
        pcu(j)=pcu1;
        vir(j)=viri;
        efcrcr(j)=efcrcr;
        pfcrcr(j)=pwfcr;
        pcu1r(j)=pcu1r;
        j=j+1;
    end;
end;

plot(crr,vi,'y',crr,vir,'b'),grid,
xlabel('capacitor [F]'),ylabel('rotor speed [rad/s]'),title(scr);
gtext('without capacitor'),gtext('with capacitor'),
zoom on;
pause;
zoom off;
plot(crr,eff,'y',crr,efcrcr,'b'),grid,
xlabel('capacitor [F]'),ylabel('efficiency'),title(scr);
gtext('without capacitor'),gtext('with capacitor'),
zoom on;
pause;
zoom off;
plot(crr,pf,'y',crr,pfcrcr,'b'),grid,
xlabel('capacitor [F]'),ylabel('power factor'),title(scr);
gtext('without capacitor'),gtext('with capacitor'),
zoom on;
pause;
zoom off;
plot(crr,pcu,'y',crr,pcu1r,'b'),grid,

```

```

xlabel('capacitor [F]'),ylabel('copper losses'),title(scr);
gtext('without capacitor'),gtext('with capacitor'),
zoom on;
pause;

close;

```

Program dinc.m was used to simulate the dynamic behavior of the induction machine with externally modified rotor impedance.

dinc.m

```

clear all;
t0=0;
tf=1.5;
global f;
f=50;
global om;
om=2*pi*f;
global Um;
Um=460;      %supply voltage

%the parameters of the machine
global rs;
rs=0.04;      %stator resistance
global rr;
rr=0.04;      %rotor resistance
global lm;
lm=0.0073;    %mutual inductance
global tr; %turn ratio
tr=1;%tr=1,67
global lrs;
lrs=0.0001687; %stator leakage inductance
global lss;
lss=0.0001687;
global lr;
lr=lrs+1/tr*lm; %rotor leakage inductance
global ls;
ls=lss+tr*lm;
global a;
a=lr*ls-lm^2;
global tl;
tl=9500;      %load torque
global tl1;
tl1=350;
global p;
p=2;          %pole pairs
global j;
j=0.01;      %inertia
global omg;
omg=0;       %general reference frame angular speed
global c;
c=0.5;       %capacitor
global c1;
c1=0.1;

scr=sprintf('C=%1.4f F',c);
scr1=sprintf('C=%1.3f F',c1);
scr2=sprintf('tl=%1.0f Nm',tl);
scr3=sprintf('tl=%1.0f Nm',tl1);

```

```

y0=[0 0 0 0 0 0];
%tic
[tc,y]=ode45('machingc',t0,tf,y0,0.00001,0); %runge-kutta function
%toc
isxc=y(:,1);
isyc=y(:,2);
irxc=y(:,3);
iryc=y(:,4);
omrc=y(:,5);
ucx=y(:,6);
ucy=y(:,7);
%save c:\coni\matl\simgc tc isxc isyc irxc iryc omrc

plot(tc,omrc/p),xlabel('time [s]'),ylabel('rotor speed [rad/s]'),title(scr2),grid,
%gtext(scr),gtext(scr1)%gtext(scr1);
zoom on;
pause;
close;
[q,f]=size(irxc);
v=omrc(q,1)/p
isc=sqrt(isxc(q,1).*isxc(q,1)+isyc(q,1).*isyc(q,1))
irc=sqrt(irxc(q,1).*irxc(q,1)+iryc(q,1).*iryc(q,1))
un=calun2(isxc(q,1),isyc(q,1),irxc(q,1),iryc(q,1));

pcu=3/2*(rr*irc^2+rs*isc^2);

```

File machiningc.m is used by ode45.m for solving the differential equations system: In this file are mentioned the differential equations that characterize the induction machine with modified rotor impedance - equations (2.38) and (2.13).

```

function yp=machingc(t,y)
%machine's parameters
global f;
global om;
global Um;
global rs;
global rr;
global lr;
global ls;
global lm;
global tl;
global tl1;
global p;
global j;
global a;
global c;
global c1;
global omrd;
global omg;
%omg=y(5);
global q;
global in;

%phase stator voltages
usa=Um*sqrt(2)*cos(om*t);
usb=Um*sqrt(2)*cos(om*t-2*pi/3);
usc=Um*sqrt(2)*cos(om*t+2*pi/3);

```

```
%in-phase and in quadrature stator voltage
usd=2/3*(usa-1/2*usb-1/2*usc);
usq=1/sqrt(3)*(usb-usc);
```

```
usx=cos(omg*t)*usd+sin(omg*t)*usq;
usy=-sin(omg*t)*usd+cos(omg*t)*usq;
```

```
urx=0;
ury=0;
```

```
if(t>.1)
% tl=tl1;
c=c1;
end;
```

```
yp=[lr/a*usx-lm*urx/a- lr*rs/a*y(1)+y(5)*lm*lm/a*y(2)+rr*lm/a*y(3)+y(5)*lr*lm/a*y(4)
+omg*y(2)+lm*y(6)/a
lr/a*usy-lm/a*ury-lr*rs/a*y(2)-y(5)*lm*lm/a*y(1)+rr*lm/a*y(4)-y(5)*lr*lm/a*y(3)
- omg*y(1)+lm*y(7)/a
-lm/a*usx+ls/a*urx+lm*rs/a*y(1)-y(5)*lm*ls/a*y(2)-rr*ls/a*y(3)-y(5)*lr*ls/a*y(4)
+omg*y(4)-ls*y(6)/a
-lm/a*usy+ls/a*ury+lm*rs/a*y(2)+y(5)*lm*ls/a*y(1)-rr*ls/a*y(4)+y(5)*lr*ls/a*y(3)
-omg*y(3)-ls*y(7)/a
p/j*(3/2*p*lm*(y(3)*y(2)-y(4)*y(1))-tl)
y(3)/c-y(5)*y(7)
y(4)/c+y(5)*y(6)
];
```

Considerations about the power factor of the induction motor

The power factor expression is given by:

$$\cos \varphi = \frac{P}{\sqrt{P^2 + Q^2}}$$

where P, Q are the active respective input power delivered by the supply.

In this appendix it will be considered the unity case for both machines: short circuited slip rings and with externally modified rotor impedance. This implies:

$$\frac{P}{\sqrt{P^2 + Q^2}} = 1 \rightarrow P^2 = P^2 + Q^2 \rightarrow Q = 0$$

The expressions of these powers are given for both situations in equations (2.29) and (2.30) respective (2.48) and (2.49).

Short circuited slip rings:

From (2.30) results:

$$\begin{aligned} R_r W - \omega_2 L_r V &= 0 \\ \omega_1 L_s R_r^2 + \omega_2 L_r R_s R_r - \omega_2 R_r R_s L_r - \omega_2^2 \omega_1 L_r L_m^2 - \omega_2^2 \omega_1 L_r^2 L_s &= 0 \\ \omega_2^2 \omega_1 L_r (L_m^2 - L_r L_s) - \omega_1 L_s R_r^2 &= 0 \end{aligned}$$

The resulting equation shows that the unity power factor is achieved just for a unique load torque.

Induction machine with modified rotor impedance

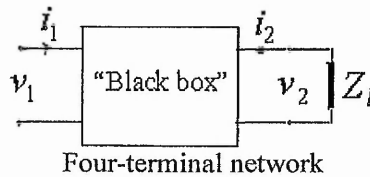
From (2.49) results:

$$\begin{aligned} R_r W_m - \omega_2 V_m \left(L_r - \frac{1}{\omega_2^2 C_r} \right) &= 0 \\ \omega_1 L_s R_r^2 + \omega_2 L_r R_s R_r - \frac{R_r R_s}{\omega_2^2 C_r} \omega_2 R_r R_s L_r - \omega_2^2 \omega_1 L_r L_m^2 - \omega_2^2 \omega_1 L_r^2 L_s - \frac{\omega_1 L_s L_r}{C_r} + \frac{R_r R_s}{\omega_2^2 C_r} + \\ &+ \frac{\omega_1 L_m^2}{C_r} - \frac{\omega_1 L_s L_r}{C_r} - \frac{\omega_1 L_s}{\omega_2^2 C_r^2} = 0 \\ \omega_1 L_r (L_m^2 - L_s L_r) \omega_2^4 - \left(\omega_1 L_s R_r^2 + \frac{\omega_1 L_m^2}{C_r} - \frac{\omega_1 L_s L_r}{C_r} \right) \omega_2 + \frac{\omega_1 L_s}{C_r^2} &= 0 \end{aligned}$$

The resulting equation shows that the unity power factor may be achieved for two different loads.

Impedance definitions in four pole networks

In Chapter 3, equation (3.1) is used to describe a four-terminal network. The parameters of the system have the following meanings:



Input impedance: $Z_{11} = \frac{v_1}{i_1}$, defined for output open-circuited

Reverse transfer impedance: $Z_{12} = \frac{v_1}{i_2}$, defined for input open-circuited

Forward transfer impedance: $Z_{21} = \frac{v_2}{i_1}$, defined for output open-circuited

Output impedance: $Z_{22} = \frac{v_2}{i_2}$, defined for input open-circuited

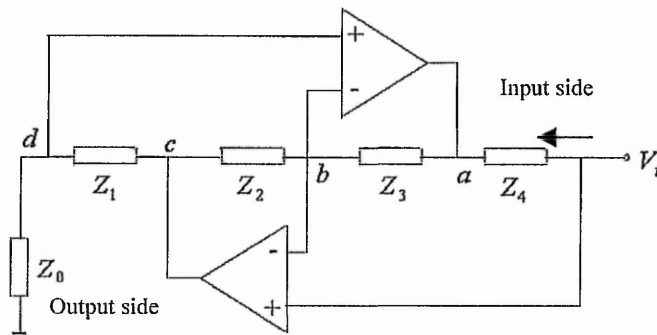
Using equations set (3.3) results:

$$Z_i = \frac{v_1}{i_1} = \frac{Z_{11}v_2 + (Z_{12}Z_{21} - Z_{22}Z_{11})i_2}{v_2 - Z_{22}i_2} = \frac{Z_{11}Z_l + (Z_{12}Z_{21} - Z_{22}Z_{11})}{Z_l - Z_{22}}$$

where $Z_l = \frac{v_2}{i_2}$ is the load(output) impedance

Gyrator implementation in integrated circuits

In the figure, it is presented the principle diagram of a gyrator implemented with operational amplifiers.



Node b:

$$\frac{V_b - V_a}{Z_3} + \frac{V_b - V_c}{Z_2} = 0$$

$$V_b = \frac{Z_2}{Z_2 + Z_3} V_a + \frac{Z_2}{Z_2 + Z_3} V_c$$

Node d:

$$\frac{V_d}{Z_0} = \frac{V_c - V_d}{Z_1}$$

$$V_d = \frac{Z_0}{Z_0 + Z_1} V_c$$

But:

$V_c = A(V_i - V_b)$, $V_a = A(V_d - V_b)$ and using in combination with the expressions of V_d, V_b will result (where A is op. amp. Amplification, and is considered very high):

$$V_c = AV_i - A \frac{Z_2}{Z_2 + Z_3} V_a - A \frac{Z_3}{Z_2 + Z_3} V_c$$

$$V_c = \frac{Z_2 + Z_3}{Z_3} V_i - \frac{Z_2}{Z_3} V_a$$

and

$$V_a = AV_d - A \frac{Z_2}{Z_2 + Z_3} V_a - A \frac{Z_2}{Z_2 + Z_3} V_c$$

$$V_a = \frac{Z_0(Z_2 + Z_3) V_c}{Z_0 + Z_1} \frac{1}{Z_2}$$

$$V_a = \frac{Z_0 Z_2 - Z_3 Z_1}{Z_0 Z_2} V_i$$

The input current:

$$I_i = \frac{V_i - V_a}{Z_4} = \frac{Z_1 Z_3}{Z_0 Z_2 Z_4} V_i$$

And the input impedance will be:

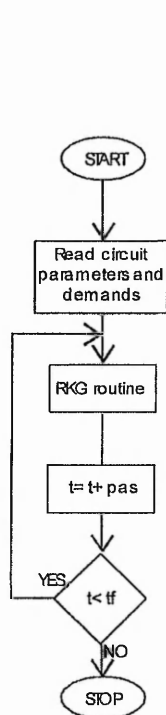
$$Z_i = \frac{V_i}{I_i} = \frac{Z_0 Z_2 Z_4}{Z_1 Z_3}$$

From the equation of the input impedance results that the input will have an inductive behavior if all the impedances from the circuit are resistive except Z_1 or Z_3 that is a capacitor.

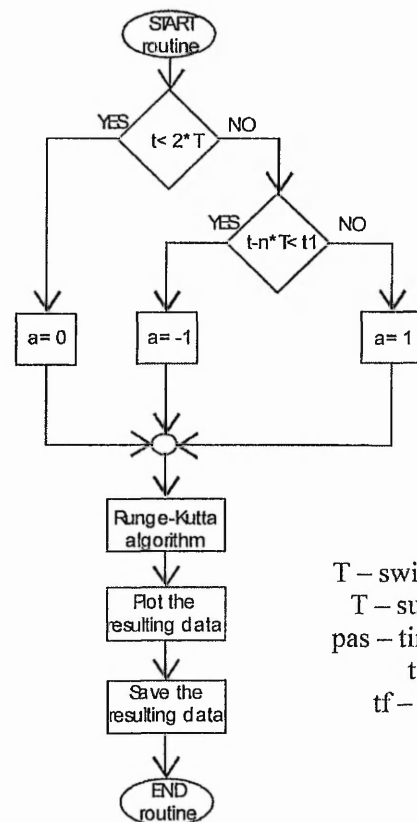
The gyrator effect is obtained due of the high input impedance and high amplification of the op. amp.

C program for the simulation of RL circuit with switched DC supply

The graphs presented beneath represent the flow chart of the program that simulates the R,L circuit with switched DC supply. The same chart is used in the case of R,L circuit with switched capacitor. The difference in the programs appears in the forms of the differential equations that are determined by coefficient a. This is 0 when no switching occurs in the circuit. The coefficient equals -1 the circuit is in the t_1 time interval and 1 when it is in the t_2 interval.



The main program



T – switching period
 T – supply period
 pas – time increment
 t – time
 tf – final time

RKG routine

```

#include <stdio.h>
#include <conio.h>
#include <dos.h>
#include <math.h>
#include <graphics.h>
#include <alloc.h>
#include <stdarg.h>
#define es 800
  
```

```

void rkg (double prmt[], double *y, double *dery, int ndim);
void fct (double x, double *y, double *dery);
void output (double x, double *y, double *dery,int ihlf);
const double k0=2., Tf=0.01 ;
  
```

```

int ndim=2 ;//number of differential equations
double y[3]={0.,0.,0.} ;/*y[ndim+1]={0. de ndim+1 ori} */
double dery[3]={0.,1./2,1./2} ;/*dery[ndim+1]={0.,1./ndim,...} */
const int nax=10, nay=10;
int auxx=0 ,auxy,jj=0 ;
double kx,ky;
int xg=0,yg1=0,yg2=0,yg3=0,yg4=0,xgi=0,ygi1=0,ygi2=0,ygi3=0,kc=0;
double x1=0,y1=0,y2=0,y3=0,y4=0,y5=0,xil=0,yil=0,yi2=0,yi3=0,usa,usb,usc;

double xmin=0.,xmax=0.1,pas=0.000001;//xmax–time interval,pas–integration
//step
double ymin=-10, ymax=10;
//Converter characteristics
double l=0.01,c=0.00001,r=5;
float fi=-10; //required phase angle
double *fu,*fuf,*ui,*fui,c1=0,s1=0,a1=0,c1u=0,s1u=0,a1u=0,fi1,fi,c,fiu,tf;
double per=0.0001,pere=0.000025;//per –switching time period, pere – sampling /
//time period

double d,d1=0.5;//duty ratio
double Um=20,f=50,pi=3.14,U1=10.7;
double q,fc1,a=0,inte,in2,in3,om;
int q1,qi=-1,iu=0,qe,qe1,qei=-1,i;

void main(void)
{
struct viewporttype vp;
double *nec, *necd, prmt[6];
int i, gdrv, gmod,maxx, maxy, xw, yw;
int dx, dy,xa, ya,xx,yy,sx,sy,ii;
om=2*pi*f;
fi=fi*pi/180;
fu = (double *) calloc(es, sizeof(double));
fuf = (double *) calloc(es, sizeof(double));
ui = (double *) calloc(es, sizeof(double));
fui = (double *) calloc(es, sizeof(double));
prmt[1]=xmin;
prmt[2]=xmax;
prmt[3]=pas;
prmt[4]=0.01 ;//0.0001;
nec=y;
necd=dery;
gdrv=DETECT;
initgraph( &gdrv, &gmod,"c:\\borlandc\\bgi");
/*getpalette paleta ; */
maxx=getmaxx();
maxy=getmaxy();
sx=64;
sy=48;
setviewport(0.,0.,maxx,maxy,1);
setbkcolor(BLACK);
setcolor(WHITE);
for(ii=0;ii<11;ii++)
{
xx=sx*ii;
if(ii!=10)
line(xx,0,xx,maxy);
else
line(xx-1,0,xx-1,maxy);
}
for(ii=0;ii<11;ii++)

```

```

{
yy=sy*ii;
if(ii!=10)
line(0,yy,maxx,yy);
else
line(0,yy-1,maxx,yy-1);
}
ky=maxy/(ymax-ymin);
kx=maxx/(xmax-xmin);
yg1=ymax/2*ky;
yg2=ymax/2*ky;
yg3=ymax/2*ky;
rkg(prmt,nec,necd,ndim);
getch();
printf("i=%f dfi=%f",a1,fiu-fic);
getch();
free(fu);
free(fuf);
free(ui);
free(fui);

return;
}
void fct(double x,double *y,double *dery)
{
usa=Um*sin(om*x);
q=x/per;
q1=floor(q);
if(q1!=qi)
{
d1=0.5*(1+sqrt((om*l/r-tan(fi))*om*c*r));
if(d1>1)
d1=1;
if(d1<0)
d1=0;
d=d1*per;
qi=q1;
}
fct1=x-q1*per;
if(fct1<d)
{
a=1;
}
else
{
a=-1;
}

dery[1]=(usa-y[1]+a*y[2])/l;
dery[2]=-a*y[1]/c;
}

void output(double x,double *y,double *dery,int ihlf)
{
qe=x/per;
qe1=floor(qe);
if(qe1!=qe)
{
if(iu<es)//Start Fourier Analysis
{

```

```

        fu[iu]=y[1];
        ui[iu]=usa;
        iu++;
    }
    else
    {
        for(i=0;i<es-1;i++)
        {
            fu[i]=fu[i+1];
            ui[i]=ui[i+1];
        }
        fu[es-1]=y[1];
        ui[es-1]=usa;
        c1=0;
        s1=0;
        a1=0;
        clu=0;
        slu=0;
        alu=0;
        for(i=0;i<es;i++)
        {
            c1=c1+fu[i]*cos(((2*(double)i+1)/f/es)/2*om);
            s1=s1+fu[i]*sin(((2*(double)i+1)/f/es)/2*om);
            clu=clu+ui[i]*cos(((2*(double)i+1)/f/es)/2*om);
            slu=slu+ui[i]*sin(((2*(double)i+1)/f/es)/2*om);
        }
        a1=2*sin(pi/es)/pi*sqrt(c1*c1+s1*s1);
        alu=2*sin(pi/es)/pi*sqrt(clu*clu+slu*slu);
        fic=-atan(c1/s1)*180/pi;
        fiu=-atan(clu/slu)*180/pi;
    } // End Fourier Analysis
    qei=qe1;
}
x1=x-xmin;
xg=kx*x1;
y1=ky*(ymax-y[1]);
y2=ky*(ymax-usa/2);
y3=ky*(ymax-y[2]/15);
putpixel(xg,y1,CYAN);
putpixel(xg,y2,YELLOW);
putpixel(xg,y3,GREEN);
}

void rkg( double prmt[], double *y, double *dery, int ndim) // Runge Kutta //Function
{
    int bog, ihlf, istep, iend, imod, itest, i, j ;
    double aj, bj, cj, r1, r2, s ;
    double x, xend, h, delt ;
    double *aux ;
    double a[ 5], b[ 5], c[ 5] ;

    aux = ( double *)calloc( ( 9 * ( ndim + 1)), sizeof( double)) ;
    if( aux == NULL)
    {
        printf("Insuficient memory for RKG !\n") ;
        return ;
    }
    bog = ndim + 1 ;
    for( i = 1; i <= ndim; ++i)
        *( aux + ( ndim + 1) * 8 + i) = 0.06666667 * ( *( dery + i)) ;

```

```

x = prmt[1];
xend = prmt[2];
h = prmt[3];
prmt[5] = 0.;
fct(x, y, dery);
s = h * (xend - x);
if(s < 0.)
{
ihlf = 13;
output(x, y, dery, ihlf);
return;
}
if(s == 0.)
{
ihlf = 12;
output(x, y, dery, ihlf);
return;
}

a[1] = .5;
a[2] = 0.2928932;
a[3] = 1.707107;
a[4] = 0.1666667;
b[1] = 2.;
b[2] = 1.;
b[3] = 1.;
b[4] = 2.;
c[1] = .5;
c[2] = .2928932;
c[3] = 1.707107;
c[4] = .5;

for(i = 1; i < ndim; i++)
{
*(aux + bog + i) = *(y + i);
*(aux + 2 * bog + i) = *(dery + i);
*(aux + 3 * bog + i) = 0.;
*(aux + 6 * bog + i) = 0.;
}
h += h;
ihlf = -1;
istep = 0;
iend = 0;
while(1)
{
s = h * (x + h - xend);
if(s >= 0.)
{
if(s != 0.)
h = xend - x;
iend = 1;
}
}

output(x, y, dery, ihlf);
if(prmt[5] != 0.)
return;
itest = 0;
while(1)
{
istep ++;
}

```

```

j = 1 ;

while( 1)
{
    aj = a[j] ;
    bj = b[j] ;
    cj = c[j] ;
    for( i = 1; i <= ndim; i ++ )
    {
        r1 = h * ( *( dery + i) ) ;
        r2 = aj * ( r1 - bj * ( *( aux + 6 * bog + i) ) ) ;
        *( y + i) = ( *( y + i) + r2) ;
        r2 = r2 + r2 + r2 ;
        *( aux + 6 * bog + i) = ( *( aux + 6 * bog + i) + r2 - cj * r1 ;
    }
    if( (j - 4) < 0)
    {
        j ++ ;
        if( (j - 3) != 0)
            x = x + .5 * h ;
        fct( x, y, dery) ;
    }
    else
        break ;
}

if( itest <= 0)
{
    for( i = 1; i <= ndim; i ++ )
        *( aux + 4 * bog + i) = ( *( y + i) ) ;
    itest = 1 ;
    istep = istep + istep - 2 ;
    ihlf ++ ;
    x -= h ;
    h *= .5 ;
    for( i = 1; i <= ndim; i ++ )
    {
        *( y + i) = *( aux + bog + i) ;
        *( dery + i) = *( aux + 2 * bog + i) ;
        *( aux + 6 * bog + i) = *( aux + 3 * bog + i) ;
    }
}
else
{
    imod = istep / 2 ;
    if( ( istep - imod - imod) != 0)
    {
        fct( x, y, dery) ;
        for( i = 1; i <= ndim; i ++ )
        {
            *( aux + 5 * bog + i) = *( y + i) ;
            *( aux + 7 * bog + i) = *( dery + i) ;
        }
    }
    else
    {
        deltax = 0. ;
        for( i = 1; i <= ndim; i ++ )
            deltax = deltax + ( *( aux + 8 * bog + i) ) * fabs( ( *( aux + 4 * bog + i) ) - ( *( y + i) ) ) ;
        if( ( deltax - prmt[ 4] ) <= 0.)

```

```

        break ;
    if( ( ihlf - 10) >= 0)
    {
        ihlf = 11 ;
        fct( x, y, dery) ;
        output( x, y, dery, ihlf) ;
        return ;
    }
    for( i = 1; i <= ndim; i++)
        ( *( aux + 4 + bog + i)) = ( *( aux + 5 * bog + i)) ;
    istep = istep + istep - 4 ;
    x -= h ;
    iend = 0 ;
    ihlf++ ;
    x -= h ;
    h = .5 * h ;
    for( i = 1; i <= ndim; i++)
    {
        ( *( y + i))          = ( *( aux + bog + i)) ;
        ( *( dery + i))       = ( *( aux + 2 * bog + i)) ;
        ( *( aux + 6 * bog + i)) = ( *( aux + 3 * bog + i)) ;
    }
}
}
}
fct( x, y, dery) ;
for( i = 1; i <= ndim; i++)
{
    ( *( aux + bog + i)) = ( *( y + i)) ;
    ( *( aux + 2 * bog + i)) = ( *( dery + i)) ;
    ( *( aux + 3 * bog + i)) = ( *( aux + 6 * bog + i)) ;
    ( *( y + i))          = ( *( aux + 5 * bog + i)) ;
    ( *( dery + i))       = ( *( aux + 7 * bog + i)) ;
}
output( x, y, dery, ihlf) ;
if( prmt[ 5] != 0)
    return ;
for( i = 1; i <= ndim; i++)
{
    ( *( y + i)) = ( *( aux + bog + i)) ;
    ( *( dery + i)) = ( *( aux + 2 * bog + i)) ;
}
if( iend > 0)
{
    output( ( x - h), y, dery, ihlf) ;
    return ;
}
ihlf-- ;
istep /= 2 ;
h += h ;
if( ihlf >= 0)
{
    imod = istep / 2 ;
    if( ( istep - imod - imod) == 0)
    {
        if( ( delt - 0.02 * prmt[ 4]) <= 0.)
            ihlf-- ;
        istep /= 2 ;
        h += h ;
    }
}

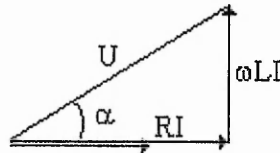
```

}
}
}

Considerations about phase angle calculation

The phase angle between the voltage and the current is measured considering the current phasor as reference. For exemplification are consider the following situations that occur during the thesis:

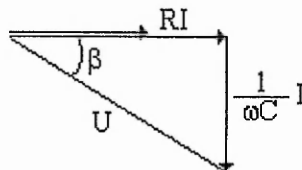
1. The circuit is ac RL.



The phase angle between the voltage and current is:

$$\alpha = a \tan\left(\frac{\omega L}{R}\right)$$

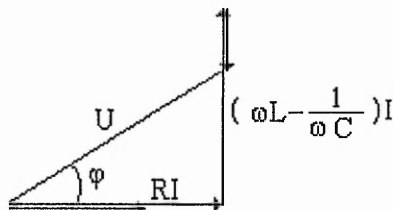
2. The circuit is ac RC



The phase angle between the voltage and current is:

$$\beta = a \tan\left(\frac{1}{\omega RC}\right)$$

3. The circuit is considered ac RLC

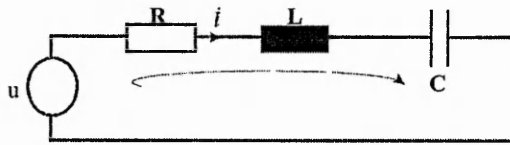


The phase angle between the voltage and current is:

$$\varphi = a \tan\left(\frac{\omega L - \frac{1}{\omega C}}{R}\right)$$

Phase angle between voltage and current is expressed relatively to the current phasor. In the case of capacitive reactance smaller than inductive reactance, φ is positive, other wise it is negative.

Analysis of the RLC circuit



The circuit from the figure is characterized by equation:

$$u(t) = Ri(t) + L \frac{di(t)}{dt} + \frac{1}{C} \int i(t) dt$$

where $L \frac{di(t)}{dt}$ is the voltage across the inductor (u_L) and $\frac{1}{C} \int i(t) dt$ is the voltage across the capacitor (u_C).

The current has the following expression:

$$i(t) = i_s(t) + i_t(t)$$

where $i_s(t)$ is the steady state component and $i_t(t)$ is the transient component of the current.

Following parameters are defined:

- damping ratio: $\delta = \frac{R}{2L}$;
- natural angular velocity: $\omega_0 = \frac{1}{\sqrt{LC}}$;
- damped angular velocity: $\omega_p = \sqrt{\delta^2 - \omega_0^2}$;

and

$$th(\alpha) = \frac{\omega_p}{\delta}$$

The transient regime can be classified in 3 situations [33]:

- a. overdamped case - $\omega_p^2 > 0$
- b. underdamped case - $\omega_p^2 < 0$
- c. critically damped case - $\omega_p^2 = 0$

a. overdamped

The transient component of the current is given by:

$$i_t(t) = e^{-\delta t} (k_1 e^{\omega_p t} + k_2 e^{-\omega_p t})$$

and the current has the expression:

$$i(t) = i_s(t) - \frac{\omega_0}{\omega_p} e^{-\delta t} \{ [i(0) - i_s(0)] sh(\omega_p t - \alpha) + C \omega_0 [u_C(0) - u_{Cs}(0)] sh(\omega_p t) \}$$

$$u_C(t) = u_{Cs}(t) + \frac{\omega_0}{\omega_p} e^{-\delta t} \left\{ [u_C(0) - u_{Cs}(0)] \operatorname{sh}(\omega_p t + \alpha) + [i(0) - i_s(0)] \sqrt{\frac{L}{C}} \operatorname{sh} \omega_p t \right\}$$

b. underdamped

The transient component of the current is given by:

$$i_t(t) = e^{-\delta t} (k_1' \cos \omega_p' t + k_2' \sin \omega_p' t)$$

where

$$\omega_p' = \sqrt{-\delta^2 + \omega_0^2}$$

and the current has the expression:

$$i(t) = i_s(t) - \frac{\omega_0}{\omega_p} e^{-\delta t} \left\{ [i(0) - i_s(0)] \sin(\omega_p' t - \alpha') + C \omega_0 [u_C(0) - u_{Cs}(0)] \sin(\omega_p' t) \right\}$$

and voltage across capacitor:

$$u_C(t) = u_{Cs}(t) + \frac{\omega_0}{\omega_p} e^{-\delta t} \left\{ [u_C(0) - u_{Cs}(0)] \sin(\omega_p' t + \alpha') + [i(0) - i_s(0)] \sqrt{\frac{L}{C}} \sin \omega_p' t \right\}$$

where

$$\operatorname{tg}(\alpha') = \frac{\omega_p'}{\delta}$$

c. critically damped

The current has the expression:

$$i(t) = i_s(t) - e^{-\delta t} \left\{ [i(0) - i_s(0)] + \left[\frac{i(0) - i_s(0)}{\sqrt{LC}} + \frac{u_C(0) - u_{Cs}(0)}{L} \right] t \right\}$$

and the voltage across capacitor:

$$u_C(t) = u_{Cs}(t) + e^{-\delta t} \left\{ \frac{[u_C(0) - u_{Cs}(0)]}{\sqrt{LC}} + \frac{[i(0) - i_s(0)]}{L} \right\}$$

If the voltage applied to the circuit is DC than

$$i_s(t) = i_s(0) = 0$$

$$u_{Cs}(t) = u_{Cs}(0) = U_a \text{ (the DC supply voltage)}$$

If the voltage supply voltage is:

$$u(t) = U_{\max} \sin(\omega t + \gamma)$$

then the steady state current is:

$$i_s(t) = \frac{U_{\max}}{Z} \sin(\omega t + \gamma - \varphi)$$

where

$$Z = \sqrt{R^2 + \left(\omega L - \frac{1}{\omega C} \right)^2}$$

$$\varphi = \alpha \tan \left(\frac{\omega L - \frac{1}{\omega C}}{R} \right)$$

The steady voltage:

$$u_{Cs}(t) = -\frac{I_{\max}}{Z} \cos(\omega t + \gamma - \varphi)$$

Appendix 5.1

LabWindows/CVI program used for experimental acquisition

```
#include <cvirte.h> /* Needed if linking in external compiler; harmless otherwise */
#include <ansi_c.h>
#include <userint.h>
#include <utility.h>
#include "ac.h"
#include "easyio.h"

static int      panelHandle;
static int      helpHandle;
static short    device=1;
static unsigned long numChannels;
static unsigned long numScans;
static char     channelString[100];
static double   upper=10;
static double   lower=-10;
static double   rate;
static double   * waveforms = 0;

static int ColorArray[8] = {VAL_GREEN, VAL_YELLOW, VAL_CYAN, VAL_WHITE, VAL_BLUE,
VAL_MAGENTA, VAL_GRAY, VAL_RED};

int main (int argc, char *argv[])
{
    if (InitCVIRTE (0, argv, 0) == 0) /* Needed if linking in external compiler; harmless otherwise */
        return -1; /* out of memory */

    panelHandle = LoadPanel (0, "ac.uir", PANEL);
    RateCallback (panelHandle, PANEL_RATE, EVENT_COMMIT, 0, 0, 0);
    SetBreakOnLibraryErrors (0);
    NumScansCallback (panelHandle, PANEL_NUMSCANS, EVENT_COMMIT, 0, 0, 0);
    ChannelCallback (panelHandle, PANEL_CHANNEL, EVENT_COMMIT, 0, 0, 0);
    SetBreakOnLibraryErrors (1);
    DisplayPanel (panelHandle);
    RunUserInterface ();

    return 0;
}

int CVICALLBACK ChannelCallback (int panel, int control, int event,
void *callbackData, int eventData1, int eventData2)
{
    switch (event) {
        case EVENT_RIGHT_CLICK:
            DisplayPanel(helpHandle);
            break;
        case EVENT_COMMIT:
            GetCtrlVal (panelHandle, PANEL_CHANNEL, channelString);
            GetNumChannels (device, channelString, ANALOG_INPUT, &numChannels);
            free (waveforms);
    }
}
```

```

        waveforms = (double *) malloc (numScans * numChannels sizeof(double));
        break;
    }
    return 0;
}

int CVICALLBACK ChannelRingCallback (int panel, int control, int event,
    void *callbackData, int eventData1, int eventData2)
{
    char * str;
    switch (event) {
        static int index;
        static int length;
        case EVENT_COMMIT:

            GetCtrlIndex (panelHandle, PANEL_CHANNELRING, &index);
            GetValueLengthFromIndex (panelHandle, PANEL_CHANNELRING, index,
                &length);
            str = (char *) malloc (length+1);
            GetCtrlVal (panelHandle, PANEL_CHANNELRING, str);
            SetCtrlVal (panelHandle, PANEL_CHANNEL, str);
            ChannelCallback (panelHandle, PANEL_CHANNEL, EVENT_COMMIT,
                0, 0, 0);
            free (str);
            break;
    }
    return 0;
}

int CVICALLBACK RateCallback (int panel, int control, int event,
    void *callbackData, int eventData1, int eventData2)
{
    switch (event) {
        case EVENT_COMMIT:
            GetCtrlVal (panelHandle, PANEL_RATE, &rate);
            break;
    }
    return 0;
}

int CVICALLBACK NumScansCallback (int panel, int control, int event,
    void *callbackData, int eventData1, int eventData2)
{
    switch (event) {
        case EVENT_COMMIT:
            GetCtrlVal (panelHandle, PANEL_NUMSCANS, &numScans);
            free (waveforms);
            waveforms = (double *) malloc (numScans * numChannels * sizeof(double));
            SetAxisRange (panelHandle, PANEL_GRAPH, VAL_MANUAL, 0.0, numScans - 1,
                VAL_NO_CHANGE, 0.0, 1.0);
            break;
    }
    return 0;
}

```

```

int CVICALLBACK AcquireCallback (int panel, int control, int event,
    void *callbackData, int eventData1, int eventData2)
{
    double actualRate;
    int i,j;
    FILE *date, *date1;

    switch (event) {
        case EVENT_COMMIT:
            AIAcquireWaveforms (device, channelString, numScans, rate,
                upper, lower, &actualRate, GROUP_BY_CHANNEL,
                waveforms);

            DeleteGraphPlot (panelHandle, PANEL_GRAPH, -1,
                VAL_DELAYED_DRAW);

            for (i=0; i<numChannels; i++)
            {
                /* The first 8 colors are defined by ColorArray[] */
                if (i<8)
                {
                    PlotY (panelHandle, PANEL_GRAPH, &waveforms[numScans*i],
                        numScans, VAL_DOUBLE, VAL_THIN_LINE,
                        VAL_EMPTY_SQUARE, VAL_SOLID, 1, ColorArray[i]);
                }
                else
                {
                    PlotY (panelHandle, PANEL_GRAPH, &waveforms[numScans*i],
                        numScans, VAL_DOUBLE, VAL_THIN_LINE,
                        VAL_EMPTY_SQUARE, VAL_SOLID, 1, VAL_RED);
                }
            }

            if (date1=fopen("\\date1.pt", "w+t"))
            {
                fprintf(date1, "%d\n", numScans);
                fprintf(date1, "%4f\n", rate);
                fprintf(date1, "%d\n", numChannels);
                fclose(date1);
            }
            else
                MessagePopup ("Error", "Could not open file date1");

            if (date=fopen("\\date.pt", "w+t"))
            {
                for (j=0; j<numScans; j++)
                {
                    for (i=0; i<numChannels-1; i++)
                        fprintf(date, "%f ", waveforms[j+i*numScans]);
                    fprintf(date, "%f\n", waveforms[j+i*numScans]);
                }
                fclose(date);
            }
            else
                MessagePopup ("Error", "Could not open file date");

            break;
    }
}

```

```
    }  
    return 0;  
}  
  
int CVICALLBACK QuitCallback (int panel, int control, int event,  
    void *callbackData, int eventData1, int eventData2)  
{  
    switch (event) {  
        case EVENT_COMMIT:  
            free (waveforms);  
            QuitUserInterface (0);  
            break;  
    }  
    return 0;  
}
```

Harmonic content

The harmonic content of the currents for all duty ratios and all switching frequencies are presented in this appendix in a table format. The harmonics are expressed in percents relative to the current fundamental for the respective duty ratio and switching frequency.

Harmonic number	Duty ratio														%
	0.50	0.55	0.58	0.60	0.62	0.68	0.71	0.74	0.77	0.80	0.83	0.88	0.90	0.95	
2	0.74	0.34	0.85	1.09	0.86	0.71	0.59	0.85	0.32	0.57	1.48	0.73	0.59	0.78	0.83
3	10.62	10.71	10.46	9.82	10.82	10.79	10.76	10.83	10.53	11.46	11.31	11.99	11.86	11.51	10.70
4	0.13	0.13	0.33	0.52	0.36	0.03	0.21	0.19	0.25	0.14	0.36	0.11	0.47	0.52	0.35
5	1.57	2.16	2.57	1.81	2.13	1.66	1.44	1.93	1.67	1.85	1.78	0.93	0.43	1.47	2.63
6	0.11	0.32	0.26	0.59	0.34	0.14	0.27	0.19	0.23	0.23	0.79	0.14	0.24	0.36	0.11
7	0.57	0.63	1.11	0.13	0.40	0.31	0.48	0.35	0.26	0.48	0.24	0.53	0.19	0.57	0.98
8	0.45	0.25	0.29	0.46	0.47	0.15	0.33	0.25	0.32	0.08	0.87	0.18	0.18	0.11	0.05
9	0.27	0.75	0.71	0.22	0.78	0.66	0.45	0.33	0.50	0.78	0.25	0.21	0.70	0.27	0.37
10	0.09	0.28	0.36	0.64	0.49	0.19	0.40	0.31	0.28	0.24	0.53	0.08	0.35	0.37	0.01
11	0.11	0.69	0.99	0.80	1.54	1.89	2.20	1.78	1.15	1.51	0.66	0.38	0.94	0.92	0.20
12	0.53	0.45	0.15	0.54	0.32	0.19	0.18	0.34	0.35	0.28	0.77	0.19	0.32	0.08	0.03
13	0.22	1.51	2.40	2.69	3.19	5.30	5.57	6.10	6.08	6.58	0.39	0.11	4.33	2.39	0.06
14	0.13	0.03	0.24	0.21	0.26	0.24	0.47	0.27	0.52	0.41	0.65	0.25	0.12	0.36	0.05
15	0.17	1.88	2.90	3.66	4.67	6.82	7.66	8.05	8.32	8.27	1.31	0.52	5.42	2.68	0.06
16	0.59	0.37	0.09	0.55	0.65	0.23	0.36	0.38	0.39	0.33	0.31	0.48	0.31	0.05	0.05
17	0.17	0.08	0.55	0.80	0.74	1.90	1.88	1.75	2.28	1.93	1.86	0.25	1.06	0.21	0.05
18	0.12	0.21	0.08	0.54	0.52	0.30	0.40	0.25	0.39	0.30	2.03	1.49	0.34	0.27	0.07
19	0.49	0.41	0.29	0.66	0.52	0.77	0.88	0.33	0.62	0.30	4.15	4.32	0.28	0.41	0.05
20	0.49	0.09	0.15	0.67	0.33	0.11	0.31	0.34	0.26	0.38	3.27	3.39	0.27	0.24	0.02
21	0.22	0.49	0.22	0.36	0.90	0.63	0.29	0.18	0.36	0.35	4.94	3.87	0.10	0.27	0.03
22	0.17	0.30	0.20	0.64	0.21	0.08	0.42	0.39	0.35	0.31	1.93	1.20	0.17	0.17	0.05
23	0.70	0.40	0.13	0.33	0.60	0.59	0.51	0.10	0.32	0.54	0.71	0.64	0.47	0.08	0.04
24	0.33	0.18	0.23	0.20	0.47	0.19	0.35	0.34	0.30	0.41	0.92	0.17	0.31	0.30	0.02
25	0.22	0.18	0.65	0.85	0.43	0.77	1.17	0.91	0.57	0.96	0.68	0.19	0.48	0.64	0.03
26	0.18	0.13	0.16	0.44	0.61	0.09	0.32	0.31	0.45	0.42	0.48	0.44	0.36	0.19	0.01
27	0.92	0.96	1.47	1.71	1.73	2.59	2.94	3.46	3.86	4.18	0.28	0.20	3.17	1.94	0.02
28	0.14	0.19	0.50	0.58	0.41	0.07	0.35	0.26	0.37	0.53	0.55	0.16	0.15	0.33	0.01
29	0.97	0.67	0.94	1.29	1.35	2.49	3.18	3.73	4.55	4.45	0.43	0.19	3.58	2.01	0.03
30	0.23	0.33	0.21	0.49	0.20	0.13	0.32	0.43	0.28	0.28	0.45	0.18	0.31	0.12	0.06

	0.50	0.55	0.58	0.60	0.62	0.68	0.71	0.74	0.77	0.80	0.83	0.88	0.90	0.95	1.00
31	0.39	0.26	0.76	0.78	0.35	0.60	1.03	0.76	0.70	0.77	0.75	0.20	0.50	0.09	0.08
32	0.21	0.04	0.48	0.60	0.31	0.21	0.27	0.35	0.33	0.32	0.47	0.21	0.37	0.26	0.04
33	0.69	0.16	0.31	0.44	0.48	0.31	0.10	0.17	0.57	0.27	0.38	0.14	0.06	0.36	0.01
34	0.17	0.35	0.34	0.33	0.58	0.20	0.32	0.39	0.40	0.36	0.46	0.31	0.36	0.30	0.03
35	0.35	0.20	0.60	0.46	0.13	0.21	0.35	0.11	0.46	0.10	0.75	0.15	0.08	0.31	0.02
36	0.41	0.21	0.38	0.29	0.53	0.13	0.29	0.21	0.31	0.38	0.53	0.42	0.22	0.09	0.02
37	0.44	0.29	0.24	0.47	0.30	0.18	0.38	0.16	0.51	0.30	1.29	0.16	0.39	0.03	0.03
38	0.10	0.20	0.36	0.61	0.28	0.08	0.37	0.22	0.44	0.35	3.01	2.36	0.26	0.32	0.03
39	0.19	0.26	0.51	0.54	0.60	0.31	0.20	0.31	0.67	0.60	1.53	1.52	0.30	0.56	0.02
40	0.51	0.39	0.22	0.52	0.21	0.05	0.34	0.29	0.39	0.42	3.01	3.53	0.31	0.24	0.05
41	0.23	0.10	0.22	0.53	0.55	0.57	1.08	1.54	2.23	2.18	1.11	0.93	2.38	1.64	0.01
42	0.11	0.01	0.36	0.43	0.41	0.22	0.26	0.13	0.34	0.41	1.32	0.63	0.17	0.25	0.01
43	0.10	0.68	0.37	0.76	0.72	0.05	0.55	1.05	1.99	2.01	0.40	0.07	2.47	1.53	0.04
44	0.47	0.28	0.12	0.49	0.60	0.09	0.30	0.43	0.19	0.19	0.79	0.09	0.29	0.04	0.03
45	0.15	0.26	0.32	0.50	0.20	0.53	0.45	0.27	0.40	0.26	0.74	0.33	0.16	0.19	0.03
46	0.10	0.16	0.23	0.27	0.40	0.02	0.39	0.11	0.33	0.30	0.29	0.28	0.24	0.28	0.02
47	0.36	0.39	0.10	0.35	0.33	0.27	0.28	0.34	0.43	0.39	0.42	0.07	0.12	0.43	0.04
48	0.46	0.06	0.03	0.60	0.20	0.22	0.19	0.26	0.32	0.23	0.51	0.26	0.27	0.35	0.04
49	0.30	0.50	0.11	0.35	0.52	0.13	0.44	0.28	0.37	0.09	0.35	0.23	0.14	0.31	0.01
50	0.07	0.17	0.04	0.53	0.38	0.18	0.29	0.14	0.25	0.30	0.36	0.30	0.24	0.16	0.02
51	0.53	0.35	0.00	0.51	0.39	0.25	0.14	0.18	0.36	0.16	0.78	0.07	0.33	0.09	0.03
52	0.26	0.24	0.07	0.41	0.47	0.12	0.36	0.11	0.37	0.15	0.22	0.12	0.18	0.30	0.07
53	0.30	0.31	0.26	0.36	0.29	0.31	0.46	0.12	0.53	0.24	0.54	0.11	0.15	0.51	0.01
54	0.21	0.15	0.08	0.52	0.44	0.12	0.24	0.30	0.27	0.25	0.59	0.20	0.21	0.31	0.02
55	0.64	0.46	0.53	0.52	0.33	0.59	0.45	0.51	1.05	0.76	0.18	0.17	1.65	1.37	0.02
56	0.11	0.13	0.28	0.28	0.24	0.21	0.38	0.20	0.41	0.16	0.86	0.23	0.26	0.29	0.03
57	0.59	0.32	0.56	0.82	0.81	0.86	0.77	0.42	0.61	0.53	0.39	0.22	1.61	1.11	0.00
58	0.21	0.36	0.18	0.47	0.37	0.17	0.32	0.34	0.24	0.14	2.35	2.05	0.23	0.06	0.05
59	0.44	0.22	0.46	0.54	0.39	0.31	0.20	0.28	0.66	0.07	0.27	0.52	0.17	0.31	0.05
60	0.22	0.09	0.35	0.53	0.40	0.17	0.30	0.09	0.33	0.11	1.49	2.04	0.13	0.25	0.01

Harmonic number

%

	0.50	0.55	0.58	0.60	0.62	0.68	0.71	0.74	0.77	0.80	0.83	0.88	0.90	0.95	1.00
61	0.02	0.22	0.33	0.18	0.18	0.21	0.14	0.21	0.41	0.37	0.43	0.63	0.13	0.18	0.03
62	0.18	0.29	0.20	0.33	0.47	0.07	0.28	0.21	0.18	0.05	0.52	0.26	0.29	0.32	0.03
63	0.31	0.03	0.51	0.46	0.37	0.31	0.25	0.26	0.30	0.01	0.35	0.26	0.10	0.30	0.02
64	0.34	0.27	0.34	0.40	0.30	0.09	0.33	0.25	0.29	0.10	0.36	0.15	0.23	0.19	0.07
65	0.41	0.26	0.25	0.35	0.23	0.22	0.19	0.12	0.08	0.21	0.58	0.25	0.20	0.10	0.03
66	0.11	0.10	0.39	0.36	0.29	0.19	0.26	0.31	0.29	0.07	0.23	0.16	0.09	0.29	0.03
67	0.20	0.30	0.52	0.54	0.38	0.24	0.49	0.18	0.29	0.01	0.57	0.12	0.07	0.47	0.02
68	0.46	0.30	0.21	0.32	0.37	0.14	0.25	0.29	0.24	0.11	0.33	0.26	0.13	0.27	0.03
69	0.24	0.23	0.37	0.59	0.55	0.57	0.39	0.47	0.24	0.37	0.38	0.17	1.10	1.07	0.02
70	0.08	0.04	0.44	0.54	0.37	0.03	0.33	0.25	0.33	0.08	0.34	0.19	0.27	0.25	0.00
71	0.09	0.45	0.46	0.57	0.53	0.72	0.91	0.77	0.66	0.20	0.49	0.16	1.15	0.80	0.06
72	0.47	0.15	0.22	0.39	0.36	0.10	0.27	0.30	0.26	0.16	0.40	0.14	0.22	0.05	0.04
73	0.08	0.27	0.54	0.61	0.43	0.21	0.48	0.39	0.48	0.06	0.35	0.12	0.35	0.33	0.02
74	0.04	0.18	0.33	0.26	0.22	0.17	0.23	0.21	0.38	0.09	0.63	0.06	0.11	0.22	0.02
75	0.31	0.32	0.29	0.30	0.17	0.23	0.17	0.28	0.37	0.09	0.23	0.16	0.16	0.56	0.01
76	0.39	0.18	0.15	0.39	0.37	0.11	0.28	0.26	0.22	0.21	0.71	0.07	0.17	0.31	0.04
77	0.24	0.43	0.31	0.32	0.24	0.22	0.21	0.17	0.38	0.04	0.86	0.51	0.13	0.34	0.01
78	0.08	0.05	0.15	0.32	0.40	0.10	0.29	0.27	0.29	0.02	1.16	1.11	0.18	0.19	0.03
79	0.38	0.19	0.11	0.45	0.35	0.13	0.31	0.02	0.20	0.30	0.30	1.18	0.16	0.12	0.04
80	0.31	0.23	0.15	0.53	0.29	0.09	0.30	0.28	0.19	0.20	0.29	0.60	0.10	0.20	0.04
81	0.32	0.18	0.13	0.27	0.45	0.26	0.10	0.17	0.23	0.08	0.56	0.26	0.06	0.37	0.06
82	0.13	0.19	0.04	0.49	0.20	0.11	0.30	0.16	0.23	0.13	0.24	0.30	0.05	0.26	0.04
83	0.52	0.27	0.13	0.31	0.20	0.26	0.40	0.45	0.39	0.58	0.47	0.50	0.71	0.85	0.00
84	0.13	0.16	0.05	0.22	0.26	0.19	0.23	0.11	0.23	0.21	0.27	0.12	0.24	0.21	0.06
85	0.43	0.12	0.20	0.45	0.36	0.11	0.43	0.52	0.77	0.43	0.30	0.08	0.80	0.61	0.01
86	0.20	0.36	0.08	0.43	0.44	0.12	0.24	0.27	0.18	0.17	0.35	0.10	0.21	0.06	0.04
87	0.41	0.12	0.08	0.31	0.22	0.42	0.44	0.21	0.51	0.25	0.49	0.14	0.46	0.39	0.03
88	0.11	0.12	0.16	0.33	0.34	0.03	0.32	0.13	0.28	0.19	0.37	0.20	0.14	0.21	0.01
89	0.46	0.21	0.08	0.34	0.36	0.21	0.12	0.26	0.55	0.25	0.28	0.22	0.27	0.58	0.03
90	0.12	0.20	0.13	0.39	0.21	0.11	0.19	0.27	0.24	0.27	0.39	0.06	0.10	0.26	0.05

Harmonic number

%

Harmonic number	0.50	0.55	0.58	0.60	0.62	0.68	0.71	0.74	0.77	0.80	0.83	0.88	0.90	0.95	1.00
91	0.32	0.09	0.31	0.34	0.44	0.13	0.43	0.15	0.42	0.07	0.20	0.18	0.12	0.34	0.02
92	0.03	0.14	0.14	0.22	0.07	0.17	0.07	0.07	0.17	0.20	0.50	0.10	0.30	0.21	0.03
93	0.36	0.20	0.15	0.27	0.24	0.21	0.11	0.08	0.31	0.22	0.26	0.15	0.14	0.13	0.04
94	0.08	0.06	0.24	0.16	0.33	0.07	0.25	0.14	0.23	0.24	0.48	0.06	0.12	0.19	0.03
95	0.17	0.35	0.39	0.39	0.08	0.24	0.27	0.20	0.35	0.09	0.27	0.07	0.10	0.32	0.01
96	0.34	0.19	0.21	0.24	0.38	0.07	0.19	0.14	0.25	0.22	0.22	0.11	0.07	0.23	0.05
97	0.21	0.27	0.34	0.42	0.31	0.26	0.32	0.31	0.54	0.46	0.75	0.54	0.41	0.65	0.03
98	0.06	0.06	0.35	0.35	0.23	0.12	0.25	0.05	0.20	0.25	0.36	0.19	0.15	0.17	0.02
99	0.08	0.30	0.44	0.55	0.47	0.35	0.17	0.20	0.61	0.37	0.26	0.84	0.55	0.41	0.00
100	0.33	0.11	0.17	0.35	0.21	0.12	0.26	0.27	0.11	0.21	0.25	0.05	0.16	0.02	0.04

%

	0.50	0.55	0.58	0.60	0.62	0.68	0.71	0.74	0.77	0.80	0.83	0.88	0.90	0.95	1.00
31	0.05	0.18	0.18	0.38	0.05	0.12	0.33	0.18	0.37	0.18	0.75	0.20	0.53	0.37	0.06
32	0.08	0.40	0.28	0.30	0.04	0.07	0.45	0.25	0.06	0.27	0.47	0.21	0.17	0.24	0.03
33	0.07	0.30	0.13	0.36	0.08	0.24	0.18	0.30	0.25	0.23	0.38	0.14	0.49	0.39	0.10
34	0.05	0.42	0.23	0.30	0.13	0.09	0.46	0.27	0.10	0.30	0.46	0.31	0.67	0.22	0.04
35	0.04	0.29	0.21	0.37	0.26	0.26	0.58	0.57	0.30	0.28	0.75	0.15	0.36	0.81	0.06
36	0.08	0.35	0.16	0.26	0.32	0.44	0.20	0.65	0.72	0.62	0.53	0.42	0.85	0.08	0.02
37	0.03	0.44	0.21	0.42	0.36	0.71	0.58	0.48	0.76	0.34	1.29	0.16	0.78	0.25	0.07
38	0.08	0.57	0.69	0.72	0.96	1.92	1.86	2.25	2.32	2.60	3.01	2.36	2.44	0.83	0.03
39	0.06	0.28	0.22	0.75	0.65	0.58	1.54	1.71	1.57	1.60	1.53	1.52	0.86	0.85	0.07
40	0.05	0.33	0.25	0.88	0.94	1.81	2.53	3.01	3.65	3.76	3.01	3.53	2.57	1.69	0.04
41	0.06	0.08	0.35	0.22	0.28	0.83	0.58	0.72	0.63	1.03	1.11	0.93	1.19	0.25	0.06
42	0.04	0.36	0.41	0.41	0.33	1.00	0.53	0.80	0.79	0.85	1.32	0.63	0.14	0.14	0.02
43	0.01	0.18	0.38	0.19	0.07	0.33	0.44	0.09	0.20	0.06	0.40	0.07	0.46	0.69	0.02
44	0.04	0.40	0.24	0.33	0.20	0.45	0.10	0.37	0.35	0.32	0.79	0.09	0.18	0.57	0.01
45	0.05	0.30	0.26	0.07	0.02	0.29	0.24	0.07	0.18	0.21	0.74	0.33	0.27	0.33	0.06
46	0.04	0.31	0.26	0.23	0.08	0.36	0.36	0.26	0.21	0.15	0.29	0.28	0.40	0.30	0.04
47	0.05	0.13	0.12	0.28	0.16	0.12	0.14	0.08	0.02	0.34	0.42	0.07	0.34	0.45	0.07
48	0.06	0.33	0.10	0.17	0.15	0.13	0.31	0.13	0.44	0.20	0.51	0.26	0.30	0.49	0.04
49	0.06	0.10	0.12	0.24	0.08	0.35	0.04	0.11	0.13	0.17	0.35	0.23	0.17	0.19	0.08
50	0.02	0.18	0.22	0.01	0.09	0.20	0.41	0.15	0.48	0.18	0.36	0.30	0.03	0.44	0.06
51	0.05	0.08	0.23	0.32	0.14	0.05	0.23	0.34	0.07	0.11	0.78	0.07	0.18	0.25	0.02
52	0.04	0.05	0.28	0.12	0.11	0.04	0.22	0.22	0.28	0.15	0.22	0.12	0.13	0.31	0.04
53	0.05	0.20	0.24	0.13	0.05	0.14	0.28	0.17	0.12	0.08	0.54	0.11	0.11	0.34	0.02
54	0.08	0.06	0.25	0.17	0.12	0.12	0.15	0.37	0.39	0.18	0.59	0.20	0.34	0.45	0.07
55	0.04	0.34	0.15	0.28	0.16	0.20	0.33	0.33	0.14	0.30	0.18	0.17	0.12	0.65	0.01
56	0.05	0.16	0.14	0.28	0.05	0.34	0.31	0.24	0.34	0.17	0.86	0.23	0.34	0.19	0.11
57	0.01	0.26	0.06	0.09	0.07	0.06	0.26	0.16	0.20	0.23	0.39	0.22	0.18	0.18	0.01
58	0.03	0.11	0.20	0.34	0.18	0.40	0.87	0.96	1.47	1.58	2.35	2.05	1.83	1.13	0.03
59	0.03	0.20	0.08	0.21	0.14	0.08	0.15	0.12	0.42	0.40	0.27	0.52	0.10	0.45	0.05
60	0.06	0.51	0.53	0.27	0.45	0.40	0.55	0.88	1.16	1.67	1.49	2.04	2.14	1.04	0.02

Harmonic number

%

	0.50	0.55	0.58	0.60	0.62	0.68	0.71	0.74	0.77	0.80	0.83	0.88	0.90	0.95	1.00
61	0.02	0.24	0.35	0.20	0.18	0.20	0.16	0.21	0.42	0.38	0.45	0.15	0.14	0.18	0.03
62	0.04	0.26	0.15	0.39	0.12	0.11	0.29	0.23	0.47	0.51	0.52	0.26	0.60	0.27	0.03
63	0.03	0.16	0.21	0.38	0.18	0.07	0.24	0.08	0.34	0.24	0.35	0.26	0.29	0.83	0.01
64	0.03	0.17	0.19	0.06	0.08	0.12	0.18	0.12	0.17	0.31	0.36	0.15	0.66	0.22	0.02
65	0.02	0.15	0.05	0.36	0.08	0.07	0.22	0.05	0.23	0.20	0.58	0.25	0.45	0.35	0.04
66	0.03	0.13	0.13	0.24	0.03	0.17	0.18	0.09	0.06	0.21	0.23	0.16	0.27	0.27	0.02
67	0.03	0.27	0.08	0.34	0.06	0.15	0.17	0.35	0.21	0.03	0.57	0.12	0.20	0.54	0.04
68	0.06	0.18	0.11	0.21	0.05	0.05	0.19	0.19	0.13	0.19	0.33	0.26	0.07	0.36	0.04
69	0.00	0.13	0.09	0.35	0.03	0.21	0.10	0.17	0.32	0.16	0.38	0.17	0.29	0.25	0.05
70	0.07	0.13	0.13	0.25	0.02	0.14	0.17	0.21	0.20	0.26	0.34	0.19	0.25	0.39	0.03
71	0.05	0.27	0.26	0.26	0.04	0.12	0.17	0.26	0.36	0.14	0.49	0.16	0.11	0.17	0.03
72	0.05	0.10	0.14	0.34	0.01	0.20	0.19	0.11	0.19	0.11	0.40	0.14	0.41	0.24	0.01
73	0.04	0.21	0.21	0.21	0.06	0.09	0.17	0.18	0.34	0.18	0.35	0.12	0.25	0.24	0.06
74	0.02	0.11	0.15	0.34	0.04	0.15	0.13	0.11	0.24	0.09	0.63	0.06	0.22	0.51	0.03
75	0.02	0.05	0.10	0.17	0.07	0.15	0.27	0.12	0.17	0.14	0.23	0.16	0.46	0.33	0.02
76	0.03	0.22	0.11	0.27	0.13	0.15	0.18	0.10	0.26	0.08	0.71	0.07	0.62	0.30	0.01
77	0.00	0.08	0.25	0.04	0.12	0.21	0.14	0.09	0.39	0.14	0.86	0.51	0.95	0.15	0.04
78	0.01	0.33	0.21	0.49	0.38	0.20	0.22	0.27	0.34	0.52	1.16	1.11	0.60	0.86	0.03
79	0.02	0.18	0.18	0.26	0.31	0.24	0.47	0.21	0.15	0.47	0.30	1.18	0.63	0.75	0.06
80	0.02	0.24	0.38	0.23	0.32	0.47	0.19	0.13	0.31	0.19	0.29	0.60	0.98	0.27	0.05
81	0.05	0.28	0.35	0.16	0.17	0.42	0.48	0.39	0.46	0.52	0.56	0.26	0.64	0.33	0.05
82	0.09	0.16	0.22	0.26	0.04	0.06	0.09	0.07	0.35	0.25	0.24	0.30	0.29	0.34	0.06
83	0.03	0.36	0.27	0.35	0.13	0.25	0.46	0.56	0.44	0.37	0.47	0.50	0.29	0.66	0.01
84	0.02	0.16	0.16	0.04	0.08	0.13	0.32	0.16	0.33	0.31	0.27	0.12	0.40	0.14	0.03
85	0.01	0.13	0.11	0.29	0.07	0.20	0.08	0.16	0.14	0.21	0.30	0.08	0.47	0.23	0.03
86	0.06	0.11	0.03	0.17	0.06	0.09	0.26	0.18	0.23	0.12	0.35	0.10	0.29	0.40	0.03
87	0.02	0.15	0.12	0.25	0.07	0.08	0.09	0.24	0.02	0.22	0.49	0.14	0.25	0.44	0.01
88	0.03	0.11	0.20	0.18	0.03	0.12	0.25	0.08	0.19	0.19	0.37	0.20	0.09	0.21	0.05
89	0.04	0.12	0.20	0.19	0.05	0.07	0.18	0.20	0.13	0.24	0.28	0.22	0.18	0.27	0.04
90	0.00	0.17	0.24	0.23	0.11	0.01	0.19	0.11	0.19	0.10	0.39	0.06	0.11	0.18	0.04

Harmonic number

%

Harmonic number	0.50	0.55	0.58	0.60	0.62	0.68	0.71	0.74	0.77	0.80	0.83	0.88	0.90	0.95	1.00
91	0.03	0.10	0.19	0.12	0.06	0.11	0.32	0.16	0.17	0.16	0.20	0.18	0.08	0.26	0.02
92	0.04	0.14	0.16	0.21	0.06	0.19	0.06	0.07	0.17	0.20	0.49	0.18	0.29	0.23	0.05
93	0.01	0.10	0.12	0.03	0.09	0.06	0.26	0.14	0.29	0.20	0.26	0.15	0.22	0.33	0.02
94	0.04	0.27	0.15	0.25	0.08	0.17	0.17	0.15	0.11	0.12	0.48	0.06	0.10	0.47	0.01
95	0.04	0.10	0.06	0.18	0.01	0.26	0.20	0.22	0.27	0.14	0.27	0.07	0.27	0.13	0.01
96	0.06	0.20	0.03	0.11	0.08	0.17	0.22	0.14	0.15	0.16	0.22	0.11	0.29	0.23	0.05
97	0.03	0.04	0.09	0.15	0.17	0.38	0.23	0.53	0.39	0.27	0.75	0.54	0.83	0.40	0.03
98	0.03	0.15	0.19	0.19	0.12	0.05	0.36	0.33	0.09	0.06	0.36	0.19	0.24	0.46	0.03
99	0.05	0.28	0.20	0.34	0.13	0.51	0.53	0.44	0.45	0.15	0.26	0.84	0.88	0.54	0.03
100	0.03	0.02	0.26	0.10	0.04	0.07	0.19	0.02	0.02	0.10	0.25	0.05	0.11	0.12	0.01

%

Harmonic number	Duty ratio																													
	0.50	0.55	0.58	0.60	0.62	0.68	0.71	0.74	0.77	0.80	0.83	0.88	0.90	0.95	1.00	0.50	0.55	0.58	0.60	0.62	0.68	0.71	0.74	0.77	0.80	0.83	0.88	0.90	0.95	1.00
2	0.79	1.66	1.84	0.56	0.62	1.54	1.06	1.65	2.23	2.17	1.59	1.59	1.66	1.01	1.60	0.79	1.66	1.84	0.56	0.62	1.54	1.06	1.65	2.23	2.17	1.59	1.59	1.66	1.01	1.60
3	10.04	10.55	10.51	10.62	10.83	9.88	10.85	10.34	10.46	11.14	11.92	12.00	12.23	10.64	11.38	10.04	10.55	10.51	10.62	10.83	9.88	10.85	10.34	10.46	11.14	11.92	12.00	12.23	10.64	11.38
4	0.42	0.92	0.62	0.53	0.49	0.44	0.34	0.26	0.17	0.59	0.57	0.69	0.74	0.38	0.71	0.42	0.92	0.62	0.53	0.49	0.44	0.34	0.26	0.17	0.59	0.57	0.69	0.74	0.38	0.71
5	1.88	1.52	1.78	2.71	2.45	2.08	2.26	2.28	1.73	1.22	1.10	0.43	0.68	1.24	2.70	1.88	1.52	1.78	2.71	2.45	2.08	2.26	2.28	1.73	1.22	1.10	0.43	0.68	1.24	2.70
6	0.17	0.76	0.27	0.52	0.20	0.30	0.77	0.61	1.22	0.46	0.27	1.18	0.68	0.59	0.31	0.17	0.76	0.27	0.52	0.20	0.30	0.77	0.61	1.22	0.46	0.27	1.18	0.68	0.59	0.31
7	0.30	0.61	0.56	0.90	1.22	0.09	0.31	0.47	1.36	0.46	1.16	0.65	0.49	0.65	0.89	0.30	0.61	0.56	0.90	1.22	0.09	0.31	0.47	1.36	0.46	1.16	0.65	0.49	0.65	0.89
8	0.11	0.51	0.39	0.60	0.54	0.29	0.56	0.36	1.13	1.04	0.89	1.07	0.55	0.54	0.22	0.11	0.51	0.39	0.60	0.54	0.29	0.56	0.36	1.13	1.04	0.89	1.07	0.55	0.54	0.22
9	0.51	0.20	0.20	0.45	0.70	0.36	0.36	0.62	0.80	0.77	0.54	0.41	0.40	0.46	0.15	0.51	0.20	0.20	0.45	0.70	0.36	0.36	0.62	0.80	0.77	0.54	0.41	0.40	0.46	0.15
10	0.71	0.14	0.21	0.30	0.51	0.17	0.24	0.39	0.35	0.29	0.21	0.72	0.17	0.19	0.25	0.71	0.14	0.21	0.30	0.51	0.17	0.24	0.39	0.35	0.29	0.21	0.72	0.17	0.19	0.25
11	0.32	0.19	0.08	0.30	0.38	0.15	0.18	0.18	0.22	0.07	0.21	0.23	0.22	0.16	0.09	0.32	0.19	0.08	0.30	0.38	0.15	0.18	0.18	0.22	0.07	0.21	0.23	0.22	0.16	0.09
12	0.64	0.31	0.30	0.30	0.44	0.16	0.15	0.22	0.29	0.30	0.27	0.40	0.23	0.08	0.12	0.64	0.31	0.30	0.30	0.44	0.16	0.15	0.22	0.29	0.30	0.27	0.40	0.23	0.08	0.12
13	0.79	0.54	0.42	0.34	0.10	0.29	0.29	0.30	0.39	0.61	0.36	1.01	0.46	0.18	0.12	0.79	0.54	0.42	0.34	0.10	0.29	0.29	0.30	0.39	0.61	0.36	1.01	0.46	0.18	0.12
14	0.13	0.66	0.73	0.16	0.69	0.26	0.98	0.31	0.66	0.49	0.83	0.92	0.87	0.52	0.10	0.13	0.66	0.73	0.16	0.69	0.26	0.98	0.31	0.66	0.49	0.83	0.92	0.87	0.52	0.10
15	0.53	0.74	0.62	0.14	0.52	0.16	0.16	0.20	0.89	0.66	1.13	1.55	0.99	0.31	0.11	0.53	0.74	0.62	0.14	0.52	0.16	0.16	0.20	0.89	0.66	1.13	1.55	0.99	0.31	0.11
16	0.42	0.43	0.33	0.57	0.33	0.29	0.92	0.54	0.87	0.29	0.59	0.79	0.58	0.29	0.08	0.42	0.43	0.33	0.57	0.33	0.29	0.92	0.54	0.87	0.29	0.59	0.79	0.58	0.29	0.08
17	0.71	0.21	0.23	0.32	0.41	0.33	0.66	0.34	0.19	0.49	0.13	0.82	0.43	0.43	0.13	0.71	0.21	0.23	0.32	0.41	0.33	0.66	0.34	0.19	0.49	0.13	0.82	0.43	0.43	0.13
18	0.30	0.16	0.22	0.29	0.27	0.24	0.47	0.20	0.38	0.14	0.23	0.06	0.21	0.13	0.09	0.30	0.16	0.22	0.29	0.27	0.24	0.47	0.20	0.38	0.14	0.23	0.06	0.21	0.13	0.09
19	0.29	0.22	0.39	0.33	0.33	0.15	0.37	0.10	0.42	0.13	0.06	0.20	0.22	0.09	0.11	0.29	0.22	0.39	0.33	0.33	0.15	0.37	0.10	0.42	0.13	0.06	0.20	0.22	0.09	0.11
20	0.74	0.41	0.24	0.35	0.25	0.21	0.13	0.23	0.31	0.49	0.55	0.71	0.24	0.21	0.12	0.74	0.41	0.24	0.35	0.25	0.21	0.13	0.23	0.31	0.49	0.55	0.71	0.24	0.21	0.12
21	0.53	0.72	0.64	0.62	0.53	0.22	1.09	0.70	0.80	0.45	0.48	0.58	0.85	0.86	0.14	0.53	0.72	0.64	0.62	0.53	0.22	1.09	0.70	0.80	0.45	0.48	0.58	0.85	0.86	0.14
22	0.60	0.70	0.62	0.25	0.79	0.30	0.43	0.29	1.19	0.62	0.98	0.95	0.87	0.32	0.08	0.60	0.70	0.62	0.25	0.79	0.30	0.43	0.29	1.19	0.62	0.98	0.95	0.87	0.32	0.08
23	0.59	0.55	0.78	0.13	0.42	0.38	0.86	0.53	1.60	0.74	0.98	1.19	0.57	0.55	0.06	0.59	0.55	0.78	0.13	0.42	0.38	0.86	0.53	1.60	0.74	0.98	1.19	0.57	0.55	0.06
24	0.94	0.41	0.16	0.42	0.31	0.41	0.29	0.51	0.35	0.44	0.36	0.90	1.21	0.59	0.08	0.94	0.41	0.16	0.42	0.31	0.41	0.29	0.51	0.35	0.44	0.36	0.90	1.21	0.59	0.08
25	0.36	0.17	0.25	0.25	0.41	0.36	0.20	0.50	0.33	0.34	0.47	0.50	0.44	0.16	0.05	0.36	0.17	0.25	0.25	0.41	0.36	0.20	0.50	0.33	0.34	0.47	0.50	0.44	0.16	0.05
26	0.17	0.34	0.18	0.59	0.64	0.38	0.41	0.53	0.28	0.47	0.53	0.18	0.79	0.16	0.07	0.17	0.34	0.18	0.59	0.64	0.38	0.41	0.53	0.28	0.47	0.53	0.18	0.79	0.16	0.07
27	0.51	0.31	0.56	0.05	0.21	1.32	0.74	1.48	1.77	0.89	0.75	0.87	0.42	0.63	0.07	0.51	0.31	0.56	0.05	0.21	1.32	0.74	1.48	1.77	0.89	0.75	0.87	0.42	0.63	0.07
28	0.42	0.99	0.76	0.89	0.81	1.94	0.47	2.17	2.07	1.56	1.44	0.91	1.36	1.14	0.04	0.42	0.99	0.76	0.89	0.81	1.94	0.47	2.17	2.07	1.56	1.44	0.91	1.36	1.14	0.04
29	0.37	0.15	1.50	1.41	1.50	3.00	3.73	3.23	3.70	3.76	3.35	3.92	2.86	1.08	0.08	0.37	0.15	1.50	1.41	1.50	3.00	3.73	3.23	3.70	3.76	3.35	3.92	2.86	1.08	0.08
30	0.12	0.74	0.51	1.20	1.80	1.99	3.47	2.49	2.05	3.47	3.94	2.56	1.98	0.51	0.06	0.12	0.74	0.51	1.20	1.80	1.99	3.47	2.49	2.05	3.47	3.94	2.56	1.98	0.51	0.06

Harmonic number

	0.50	0.55	0.58	0.60	0.62	0.68	0.71	0.74	0.77	0.80	0.83	0.88	0.90	0.95	1.00
31	0.53	1.44	1.21	1.93	2.54	3.11	3.22	4.01	3.28	4.15	3.96	2.85	2.86	1.65	0.05
32	0.49	0.70	0.38	0.39	0.46	1.26	1.01	1.48	1.66	1.74	0.82	0.89	0.80	0.48	0.04
33	0.15	0.53	0.26	0.57	0.69	0.31	0.66	0.29	0.79	0.04	0.40	0.70	0.72	0.16	0.09
34	0.37	0.39	0.29	0.19	0.17	0.22	0.38	0.19	0.52	0.37	0.31	0.50	0.39	0.19	0.05
35	0.69	0.37	0.03	0.30	0.44	0.33	0.38	0.38	0.12	0.84	0.12	0.62	0.52	0.33	0.05
36	0.42	0.47	0.46	0.34	0.71	0.73	0.57	0.72	1.51	0.17	0.26	0.71	0.21	0.61	0.05
37	0.47	0.52	0.16	0.22	0.13	0.14	0.28	0.08	1.26	0.80	0.86	0.42	0.39	0.26	0.07
38	0.58	0.66	0.38	0.11	0.46	0.09	0.51	0.47	0.62	0.73	1.04	0.91	0.60	0.54	0.03
39	0.84	0.55	0.44	0.12	0.29	0.10	0.63	0.15	0.51	0.36	0.21	0.33	0.21	0.20	0.07
40	0.23	0.41	0.29	0.12	0.09	0.05	0.20	0.02	0.51	0.21	0.28	0.40	0.36	0.05	0.03
41	0.20	0.27	0.22	0.08	0.17	0.05	0.12	0.04	0.41	0.11	0.15	0.21	0.31	0.08	0.04
42	0.47	0.40	0.25	0.19	0.17	0.13	0.06	0.09	0.36	0.23	0.20	0.43	0.19	0.23	0.07
43	0.51	0.43	0.43	0.22	0.49	0.30	0.74	0.27	0.69	0.43	0.55	0.84	0.59	0.12	0.03
44	0.63	0.53	0.14	0.21	0.39	0.08	0.41	0.22	1.19	0.92	0.64	0.79	1.05	0.42	0.07
45	0.33	0.52	0.17	0.15	0.39	0.10	0.43	0.42	1.34	0.31	1.04	1.38	1.07	0.36	0.05
46	0.84	0.54	0.65	0.19	0.33	0.10	0.59	0.33	0.89	0.36	0.26	0.59	0.47	0.03	0.05
47	0.45	0.35	0.35	0.04	0.19	0.07	0.11	0.17	0.08	0.34	0.23	0.68	0.33	0.20	0.05
48	0.12	0.34	0.39	0.09	0.12	0.13	0.07	0.09	0.23	0.17	0.04	0.14	0.34	0.10	0.07
49	0.44	0.33	0.30	0.03	0.08	0.16	0.18	0.07	0.45	0.26	0.14	0.45	0.37	0.08	0.04
50	0.30	0.49	0.51	0.13	0.21	0.22	0.65	0.05	0.58	0.71	0.47	0.64	0.61	0.28	0.02
51	0.40	0.43	0.32	0.27	0.53	0.27	0.73	0.33	0.50	0.32	0.84	0.28	1.31	0.66	0.05
52	0.25	0.57	0.27	0.15	0.20	0.14	0.29	0.26	0.87	0.68	1.08	1.39	0.80	0.17	0.04
53	0.57	0.33	0.27	0.35	0.76	0.59	0.17	0.61	0.81	0.58	0.68	1.35	0.52	0.87	0.03
54	0.53	0.44	0.32	0.07	0.28	0.09	0.41	0.07	0.26	0.52	0.34	0.63	0.43	0.27	0.07
55	0.21	0.29	0.24	0.09	0.22	0.14	0.22	0.16	0.10	0.21	0.06	0.31	0.27	0.23	0.04
56	0.05	0.39	0.11	0.28	0.34	0.24	0.47	0.23	0.08	0.49	0.27	0.38	0.48	0.15	0.08
57	0.57	0.42	0.44	0.18	0.30	0.37	0.68	0.47	0.96	0.47	0.38	0.58	0.37	0.27	0.04
58	0.79	0.86	0.32	0.75	0.90	1.46	1.36	1.99	2.84	2.11	1.73	1.98	1.84	1.44	0.03
59	0.66	0.59	0.38	0.19	0.47	0.56	0.94	0.87	1.68	0.50	0.26	1.90	1.16	0.23	0.08
60	0.57	0.70	0.27	0.68	0.92	1.37	2.21	2.09	1.15	2.81	3.30	2.22	2.30	0.95	0.04

Harmonic number

	0.50	0.55	0.58	0.60	0.62	0.68	0.71	0.74	0.77	0.80	0.83	0.88	0.90	0.95	1.00
61	1.00	0.53	0.18	0.26	0.34	0.58	0.85	0.68	0.14	1.04	1.00	0.76	0.83	0.51	0.07
62	0.42	0.36	0.29	0.06	0.21	0.42	0.45	0.51	0.42	0.64	0.34	0.45	0.19	0.25	0.07
63	0.18	0.30	0.14	0.19	0.16	0.17	0.09	0.15	0.15	0.11	0.16	0.28	0.19	0.08	0.05
64	0.44	0.36	0.21	0.07	0.18	0.12	0.06	0.13	0.32	0.34	0.21	0.43	0.18	0.07	0.03
65	0.31	0.37	0.34	0.10	0.08	0.02	0.37	0.21	0.48	0.57	0.48	0.57	0.20	0.26	0.02
66	0.61	0.47	0.50	0.05	0.43	0.07	0.59	0.48	0.42	0.48	0.29	0.68	0.34	0.37	0.02
67	0.13	0.40	0.45	0.19	0.44	0.07	0.33	0.11	0.57	0.54	1.15	0.32	0.30	0.31	0.04
68	0.64	0.35	0.16	0.30	0.36	0.20	0.84	0.15	0.65	0.51	0.37	0.74	0.38	0.44	0.01
69	0.38	0.28	0.18	0.09	0.25	0.05	0.04	0.11	0.08	0.27	0.10	0.24	0.12	0.26	0.02
70	0.10	0.29	0.09	0.04	0.01	0.05	0.18	0.06	0.15	0.07	0.11	0.18	0.20	0.12	0.08
71	0.31	0.25	0.22	0.05	0.08	0.09	0.28	0.09	0.26	0.07	0.06	0.11	0.12	0.06	0.05
72	0.41	0.38	0.16	0.07	0.15	0.08	0.51	0.03	0.35	0.37	0.39	0.58	0.24	0.31	0.00
73	0.42	0.46	0.46	0.23	0.43	0.06	0.53	0.45	1.10	0.22	0.33	0.48	0.47	0.42	0.01
74	0.25	0.51	0.51	0.06	0.29	0.14	0.17	0.09	0.95	0.54	0.97	0.64	0.59	0.15	0.03
75	0.56	0.31	0.51	0.19	0.39	0.33	0.61	0.36	1.18	0.39	0.44	0.94	0.48	0.41	0.03
76	0.54	0.34	0.13	0.02	0.10	0.11	0.28	0.04	0.45	0.44	0.56	0.39	0.24	0.33	0.03
77	0.16	0.23	0.23	0.06	0.13	0.08	0.19	0.03	0.29	0.10	0.10	0.39	0.28	0.10	0.05
78	0.10	0.29	0.11	0.08	0.10	0.07	0.20	0.05	0.20	0.05	0.22	0.16	0.25	0.14	0.02
79	0.32	0.29	0.19	0.11	0.15	0.15	0.33	0.16	0.13	0.28	0.32	0.54	0.30	0.23	0.01
80	0.72	0.57	0.21	0.31	0.45	0.20	0.29	0.30	0.59	0.70	0.50	0.45	1.02	0.66	0.04
81	0.48	0.51	0.32	0.28	0.63	0.22	0.53	0.29	0.48	0.35	1.17	0.08	0.80	0.27	0.06
82	0.58	0.50	0.46	0.02	0.20	0.42	0.17	0.40	0.71	0.60	0.61	1.66	0.75	0.29	0.05
83	0.64	0.43	0.27	0.18	0.10	0.37	0.59	0.40	0.63	0.65	0.54	0.98	0.95	0.72	0.02
84	0.29	0.31	0.10	0.11	0.24	0.17	0.07	0.21	0.13	0.20	0.11	0.55	0.34	0.18	0.02
85	0.06	0.21	0.15	0.12	0.12	0.09	0.19	0.05	0.12	0.08	0.06	0.20	0.38	0.11	0.05
86	0.26	0.17	0.01	0.12	0.26	0.10	0.25	0.17	0.41	0.22	0.12	0.57	0.23	0.23	0.01
87	0.25	0.33	0.16	0.06	0.11	0.11	0.20	0.15	0.49	0.45	0.25	0.48	0.50	0.35	0.03
88	0.44	0.23	0.43	0.28	0.61	0.32	1.24	0.87	1.62	1.02	0.88	1.91	0.99	0.81	0.02
89	0.11	0.51	0.28	0.06	0.32	0.05	0.19	0.16	0.72	0.66	0.89	0.51	0.27	0.12	0.03
90	0.47	0.46	0.24	0.32	0.43	0.20	0.98	0.72	0.29	1.21	1.61	0.97	1.59	0.85	0.02

Harmonic number

	0.50	0.55	0.58	0.60	0.62	0.68	0.71	0.74	0.77	0.80	0.83	0.88	0.90	0.95	1.00
91	0.26	0.30	0.26	0.07	0.16	0.09	0.13	0.08	0.33	0.21	0.13	0.61	0.46	0.05	0.05
92	0.11	0.15	0.18	0.02	0.11	0.03	0.29	0.03	0.28	0.10	0.21	0.13	0.17	0.07	0.08
93	0.12	0.18	0.17	0.05	0.10	0.09	0.29	0.04	0.25	0.06	0.13	0.19	0.16	0.11	0.06
94	0.27	0.24	0.18	0.06	0.19	0.09	0.28	0.06	0.26	0.26	0.32	0.27	0.22	0.23	0.02
95	0.51	0.42	0.27	0.19	0.32	0.19	0.65	0.12	0.56	0.25	0.32	0.55	0.04	0.18	0.04
96	0.33	0.43	0.15	0.12	0.26	0.11	0.11	0.11	0.81	0.61	0.57	0.59	0.45	0.15	0.00
97	0.54	0.44	0.18	0.14	0.34	0.19	0.54	0.32	0.61	0.27	0.70	0.21	0.42	0.33	0.03
98	0.55	0.31	0.38	0.08	0.13	0.11	0.24	0.06	0.50	0.40	0.24	0.57	0.31	0.21	0.02
99	0.11	0.21	0.22	0.03	0.17	0.02	0.06	0.08	0.11	0.19	0.19	0.12	0.17	0.08	0.01
100	0.08	0.18	0.20	0.07	0.08	0.01	0.02	0.01	0.02	0.03	0.03	0.21	0.21	0.03	0.04

Harmonic number

Harmonic number	Duty ratio															%
	0.50	0.55	0.58	0.60	0.62	0.68	0.71	0.74	0.77	0.80	0.83	0.88	0.90	0.95	1.00	
2	1.37	2.08	1.47	1.78	1.75	1.61	0.44	1.38	0.92	1.32	0.27	0.97	1.45	0.44	1.22	
3	10.19	9.72	10.29	10.46	9.91	11.41	11.39	11.78	11.48	11.92	12.82	11.78	10.59	11.58	11.10	
4	0.44	0.42	0.47	1.24	0.15	0.16	1.30	0.49	0.72	0.62	0.66	1.27	0.40	0.26	0.51	
5	2.52	2.47	2.29	2.16	2.38	2.54	2.52	2.13	2.28	1.13	1.37	0.31	0.86	1.90	3.04	
6	0.32	0.65	0.27	0.92	0.15	0.55	0.92	0.21	0.19	0.39	0.62	0.80	0.35	0.10	0.30	
7	0.51	0.40	0.43	0.48	0.49	0.49	0.32	0.44	0.32	0.41	0.61	0.34	0.14	0.46	0.97	
8	0.17	0.53	0.04	0.31	0.21	0.62	0.58	0.39	0.39	0.34	0.47	0.35	0.20	0.09	0.17	
9	0.34	0.22	0.25	1.03	0.30	0.37	0.16	0.83	0.10	0.44	0.15	0.63	0.90	0.59	0.28	
10	0.10	0.25	0.08	0.39	0.23	0.21	0.39	0.46	0.23	0.11	0.22	0.15	0.41	0.23	0.06	
11	0.58	0.69	0.05	1.30	0.25	0.56	0.56	0.52	0.14	0.28	0.74	1.06	0.57	0.80	0.22	
12	0.30	0.24	0.09	0.15	0.23	0.47	0.27	0.21	0.36	0.47	0.23	0.19	0.11	0.37	0.02	
13	0.28	0.32	0.04	0.80	0.04	0.46	0.50	0.26	0.16	0.09	0.16	0.52	0.21	0.38	0.13	
14	0.13	0.78	0.12	0.85	0.19	0.08	0.60	0.89	0.22	0.14	0.62	0.63	1.12	0.62	0.12	
15	0.10	0.21	0.09	0.16	0.40	0.22	0.24	0.58	0.37	0.46	0.34	0.07	0.61	0.21	0.01	
16	0.79	0.95	0.23	1.71	0.39	0.92	0.52	1.15	0.05	0.26	0.44	1.24	0.69	0.41	0.02	
17	0.29	0.40	0.24	0.36	0.07	0.55	0.35	0.45	0.36	0.04	0.35	0.12	0.27	0.23	0.03	
18	0.26	0.87	0.31	1.32	0.22	0.22	0.51	0.83	0.20	0.34	0.44	0.72	0.29	0.61	0.06	
19	0.13	0.79	0.37	0.62	0.63	0.39	0.88	0.73	0.21	0.43	0.52	0.67	1.32	0.80	0.07	
20	0.21	0.64	0.24	0.14	0.56	0.59	0.12	0.40	0.39	0.14	0.28	0.17	0.80	0.35	0.01	
21	0.89	0.76	0.39	1.58	0.28	0.98	0.84	0.14	0.11	0.16	0.43	1.18	0.58	1.10	0.01	
22	0.18	0.46	0.32	0.36	0.19	0.18	0.27	0.35	0.39	0.35	0.46	0.10	0.32	0.09	0.02	
23	0.09	0.69	0.48	1.37	0.64	0.28	0.74	0.86	0.13	0.25	0.69	0.79	0.32	0.31	0.03	
24	0.26	0.86	0.54	0.36	0.68	0.67	0.71	1.17	0.21	0.16	0.20	0.70	1.21	0.15	0.01	
25	0.31	0.21	0.40	0.25	0.49	0.46	0.14	1.00	0.32	0.30	0.22	0.07	0.88	0.07	0.01	
26	0.67	0.96	0.42	1.19	0.09	0.51	0.82	1.04	0.10	0.33	0.79	0.84	0.34	0.56	0.01	
27	0.05	0.20	0.35	0.32	0.27	0.23	0.06	0.32	0.30	0.22	0.29	0.08	0.23	0.21	0.03	
28	0.10	0.78	0.40	1.09	0.60	0.47	0.79	0.18	0.15	0.26	0.21	0.76	0.29	0.84	0.04	
29	0.21	0.40	0.43	0.28	0.51	0.50	0.15	0.31	0.11	0.33	0.30	0.54	0.89	0.23	0.01	
30	0.28	0.35	0.44	0.39	0.45	0.12	0.25	0.40	0.31	0.35	0.39	0.12	0.90	0.28	0.04	

	0.50	0.55	0.58	0.60	0.62	0.68	0.71	0.74	0.77	0.80	0.83	0.88	0.90	0.95	1.00
31	0.27	0.54	0.29	0.80	0.28	0.14	0.34	0.16	0.21	0.44	0.51	0.54	0.18	0.47	0.03
32	0.03	0.18	0.28	0.13	0.22	0.31	0.23	0.03	0.12	0.48	0.13	0.10	0.10	0.14	0.01
33	0.11	0.25	0.15	0.95	0.62	0.55	0.51	0.45	0.14	0.34	0.31	0.65	0.21	0.18	0.01
34	0.13	0.35	0.11	0.26	0.46	0.21	0.68	0.72	0.44	0.47	0.53	0.51	0.68	0.32	0.04
35	0.29	0.24	0.29	0.61	0.38	0.23	0.65	0.95	0.26	0.78	0.66	0.45	0.87	0.47	0.05
36	0.26	0.42	0.37	0.24	0.22	0.67	1.06	1.72	0.19	0.76	0.50	0.67	0.82	0.54	0.00
37	0.03	0.35	0.33	0.34	0.83	0.30	0.80	1.11	0.25	1.49	0.76	0.52	1.01	0.18	0.03
38	0.24	0.88	0.62	0.25	1.62	1.48	2.51	2.83	1.96	2.82	2.63	1.62	2.25	0.58	0.04
39	0.23	0.37	1.04	1.60	1.14	2.72	1.87	1.82	3.39	1.32	2.26	2.73	1.15	1.32	0.01
40	0.23	0.29	1.05	1.89	1.51	3.10	2.01	2.51	3.36	2.06	2.41	2.77	1.70	1.22	0.03
41	0.28	0.79	0.93	1.85	1.49	1.80	2.44	2.37	2.09	3.52	2.17	1.34	2.90	1.69	0.05
42	0.03	0.23	0.47	0.51	0.92	0.74	0.67	0.66	0.93	0.68	0.76	0.76	0.85	0.53	0.03
43	0.31	0.49	0.40	0.88	0.57	0.54	1.52	1.39	0.17	1.17	0.51	1.75	1.51	0.43	0.04
44	0.26	0.25	0.46	0.36	0.09	0.42	0.62	0.89	0.33	0.92	0.62	0.59	0.85	0.32	0.01
45	0.14	0.37	0.26	0.47	0.23	0.25	0.68	0.80	0.26	0.38	0.88	0.50	0.41	0.39	0.03
46	0.03	0.22	0.27	0.45	0.33	0.36	0.47	0.52	0.20	0.42	0.27	0.35	0.32	0.19	0.05
47	0.03	0.15	0.19	0.02	0.25	0.11	0.39	0.45	0.12	0.42	0.22	0.10	0.10	0.23	0.03
48	0.21	0.52	0.28	0.50	0.26	0.38	0.32	0.73	0.23	0.17	0.58	0.66	0.35	0.36	0.01
49	0.22	0.23	0.32	0.42	0.02	0.43	0.36	0.74	0.23	0.36	0.32	0.18	0.62	0.22	0.00
50	0.20	0.34	0.31	0.43	0.23	0.17	0.17	0.73	0.13	0.35	0.30	0.47	0.62	0.20	0.05
51	0.11	0.74	0.27	0.52	0.47	0.07	0.48	0.68	0.11	0.13	0.30	0.63	0.20	0.75	0.04
52	0.03	0.28	0.22	0.15	0.34	0.35	0.13	0.25	0.39	0.43	0.24	0.17	0.24	0.25	0.03
53	0.52	0.75	0.27	0.43	0.21	0.63	0.80	0.13	0.02	0.30	0.41	0.79	0.72	0.59	0.03
54	0.33	0.18	0.19	0.48	0.22	0.48	0.10	0.23	0.30	0.28	0.33	0.02	0.55	0.08	0.06
55	0.19	0.68	0.25	0.47	0.46	0.05	0.51	0.41	0.23	0.35	0.26	0.75	0.81	0.07	0.03
56	0.09	0.59	0.27	0.87	0.63	0.42	0.40	0.57	0.16	0.40	0.34	0.70	0.25	0.13	0.02
57	0.10	0.31	0.18	0.34	0.34	0.54	0.09	0.29	0.43	0.32	0.29	0.10	0.26	0.04	0.06
58	0.84	0.70	0.20	0.70	0.12	0.61	0.88	1.09	0.15	0.22	0.42	0.81	0.99	0.81	0.04
59	0.26	0.51	0.14	0.33	0.42	0.20	0.16	0.70	0.29	0.45	0.35	0.08	0.54	0.25	0.04
60	0.17	0.73	0.22	0.39	0.62	0.47	0.62	0.99	0.31	0.23	0.41	0.76	0.83	0.68	0.01

Harmonic number

%

	0.50	0.55	0.58	0.60	0.62	0.68	0.71	0.74	0.77	0.80	0.83	0.88	0.90	0.95	1.00
61	0.16	0.72	0.10	0.96	0.50	0.68	0.38	0.56	0.24	0.22	0.28	0.71	0.34	0.67	0.05
62	0.21	0.37	0.12	0.44	0.20	0.40	0.21	0.24	0.31	0.39	0.34	0.12	0.25	0.18	0.04
63	0.73	0.77	0.08	0.87	0.27	0.26	0.69	0.21	0.19	0.22	0.64	0.87	0.97	0.55	0.04
64	0.10	0.24	0.03	0.06	0.38	0.31	0.21	0.41	0.26	0.19	0.21	0.10	0.37	0.10	0.02
65	0.04	0.51	0.03	0.31	0.43	0.62	0.41	0.79	0.11	0.20	0.14	0.59	0.71	0.29	0.02
66	0.24	0.45	0.10	0.68	0.16	0.53	0.39	0.64	0.26	0.27	0.46	0.51	0.38	0.11	0.07
67	0.31	0.20	0.10	0.40	0.05	0.04	0.19	0.57	0.13	0.12	0.39	0.07	0.26	0.16	0.03
68	0.39	0.69	0.12	0.75	0.24	0.13	0.42	0.63	0.04	0.17	0.24	0.75	0.75	0.65	0.04
69	0.05	0.16	0.13	0.08	0.27	0.39	0.12	0.16	0.19	0.26	0.09	0.12	0.23	0.20	0.01
70	0.09	0.52	0.21	0.27	0.18	0.41	0.30	0.32	0.13	0.04	0.36	0.44	0.47	0.54	0.01
71	0.19	0.41	0.25	0.39	0.07	0.24	0.25	0.14	0.17	0.19	0.23	0.23	0.34	0.12	0.02
72	0.25	0.29	0.20	0.10	0.13	0.21	0.13	0.09	0.11	0.28	0.16	0.16	0.25	0.08	0.04
73	0.23	0.41	0.32	0.54	0.21	0.25	0.37	0.13	0.05	0.06	0.19	0.59	0.47	0.23	0.02
74	0.09	0.12	0.17	0.07	0.13	0.25	0.10	0.35	0.32	0.33	0.13	0.18	0.10	0.14	0.01
75	0.07	0.29	0.33	0.31	0.10	0.13	0.31	0.45	0.20	0.29	0.36	0.36	0.25	0.17	0.03
76	0.06	0.39	0.30	0.49	0.07	0.14	0.29	0.69	0.04	0.32	0.12	0.49	0.33	0.43	0.01
77	0.19	0.22	0.29	0.13	0.23	0.35	0.15	0.36	0.07	0.35	0.25	0.13	0.35	0.33	0.04
78	0.40	0.56	0.55	1.00	0.81	1.34	1.37	1.93	2.04	1.89	2.14	2.13	1.91	0.84	0.03
79	0.05	0.08	0.15	0.19	0.20	0.24	0.22	0.35	0.02	0.19	0.20	0.18	0.31	0.33	0.01
80	0.35	0.58	0.38	0.92	0.64	1.49	1.04	2.18	1.39	2.52	1.41	1.34	2.38	1.42	0.01
81	0.24	0.20	0.10	0.32	0.25	0.15	0.15	0.08	0.44	0.52	0.56	1.00	0.55	0.60	0.03
82	0.21	0.22	0.14	0.18	0.38	0.49	0.27	0.65	0.61	0.52	0.62	1.30	0.81	0.68	0.02
83	0.13	0.41	0.29	0.45	0.29	0.29	0.34	0.53	0.41	0.63	1.05	0.69	0.60	0.10	0.03
84	0.07	0.07	0.20	0.06	0.08	0.10	0.04	0.36	0.18	0.39	0.40	0.20	0.47	0.04	0.03
85	0.13	0.33	0.20	0.37	0.17	0.34	0.42	0.21	0.03	0.10	0.20	0.32	0.41	0.21	0.02
86	0.24	0.18	0.11	0.31	0.25	0.27	0.16	0.23	0.06	0.36	0.29	0.20	0.38	0.16	0.03
87	0.10	0.30	0.08	0.04	0.31	0.06	0.16	0.15	0.16	0.17	0.32	0.36	0.33	0.14	0.02
88	0.05	0.29	0.06	0.67	0.23	0.11	0.22	0.10	0.07	0.08	0.35	0.49	0.30	0.23	0.03
89	0.04	0.14	0.07	0.18	0.03	0.30	0.06	0.17	0.14	0.26	0.13	0.14	0.14	0.12	0.01
90	0.28	0.27	0.10	0.76	0.11	0.33	0.31	0.44	0.09	0.13	0.11	0.50	0.26	0.44	0.06

Harmonic number

%

	0.50	0.55	0.58	0.60	0.62	0.68	0.71	0.74	0.77	0.80	0.83	0.88	0.90	0.95	1.00
91	0.24	0.25	0.19	0.14	0.32	0.26	0.19	0.43	0.12	0.19	0.37	0.06	0.43	0.21	0.01
92	0.16	0.27	0.20	0.24	0.29	0.15	0.11	0.46	0.15	0.27	0.34	0.33	0.47	0.21	0.05
93	0.09	0.44	0.25	0.86	0.24	0.39	0.25	0.55	0.15	0.19	0.30	0.48	0.60	0.52	0.04
94	0.05	0.08	0.17	0.21	0.03	0.41	0.09	0.24	0.21	0.30	0.09	0.13	0.24	0.19	0.01
95	0.53	0.68	0.27	1.14	0.21	0.29	0.59	0.17	0.12	0.21	0.42	0.77	0.15	0.20	0.04
96	0.19	0.26	0.27	0.06	0.29	0.07	0.15	0.09	0.27	0.31	0.43	0.09	0.43	0.11	0.05
97	0.12	0.67	0.35	0.61	0.21	0.43	0.26	0.29	0.16	0.27	0.37	0.40	0.63	0.29	0.01
98	0.03	0.40	0.34	0.88	0.01	0.57	0.33	0.61	0.16	0.23	0.12	0.41	0.68	0.36	0.02
99	0.16	0.36	0.23	0.16	0.16	0.27	0.09	0.39	0.22	0.34	0.30	0.12	0.41	0.13	0.04
100	0.59	0.54	0.28	1.29	0.28	0.05	0.67	0.87	0.11	0.21	0.60	0.83	0.07	0.78	0.04

Harmonic number

%

Harmonic number	Duty ratio															%
	0.50	0.55	0.58	0.60	0.62	0.68	0.71	0.74	0.77	0.80	0.83	0.88	0.90	0.95	1.00	
2	0.77	0.90	0.91	0.71	1.11	0.66	0.67	0.86	0.75	0.48	0.68	0.59	0.74	0.38	0.19	
3	9.90	9.75	9.29	9.02	8.60	6.20	5.80	3.70	2.82	1.11	1.39	2.05	4.05	3.58	4.21	
4	0.14	0.52	0.34	0.41	0.21	0.53	0.20	0.66	0.08	0.05	0.61	0.78	0.74	0.49	0.18	
5	1.84	1.31	1.34	1.13	1.41	0.67	0.51	1.38	2.62	2.05	2.67	1.89	2.69	4.26	8.46	
6	0.20	0.23	0.33	0.17	0.32	0.54	0.28	0.48	0.11	0.15	0.14	0.89	0.52	0.31	0.40	
7	0.30	0.24	0.28	0.44	0.43	0.72	0.86	0.54	0.47	1.05	1.25	0.96	1.28	2.29	1.88	
8	0.12	0.21	0.30	0.31	0.50	0.35	0.22	0.74	0.06	0.14	0.29	1.01	0.57	0.30	0.12	
9	0.31	0.84	0.40	0.55	0.55	0.73	1.09	0.67	0.79	1.43	1.80	0.64	1.02	0.98	0.42	
10	0.08	0.15	0.31	0.34	0.38	0.25	0.29	0.78	0.07	0.05	0.56	0.52	0.73	0.18	0.09	
11	0.07	1.39	2.31	2.79	2.78	2.32	3.22	1.69	1.63	1.60	1.86	2.21	1.19	1.00	0.34	
12	0.03	0.14	0.21	0.41	0.29	0.52	0.62	0.14	0.19	0.20	0.27	0.77	0.34	0.27	0.23	
13	0.26	5.08	8.14	9.95	11.94	16.44	17.82	18.93	19.77	19.97	19.74	16.79	15.76	10.38	0.20	
14	0.07	0.15	0.20	0.21	0.25	0.75	0.19	0.53	0.08	0.43	0.90	0.54	0.60	0.31	0.10	
15	0.31	5.49	9.18	12.03	13.96	19.17	21.65	22.79	24.24	23.78	22.99	21.10	18.28	12.56	0.45	
16	0.10	0.28	0.09	0.16	0.76	0.41	0.67	0.28	0.27	0.52	0.45	1.14	0.76	0.23	0.16	
17	0.14	1.42	2.33	2.50	3.38	3.25	3.42	3.08	2.97	2.69	2.01	0.25	1.13	0.97	0.06	
18	0.16	0.07	0.11	0.31	0.36	0.44	0.42	0.63	0.35	0.15	0.26	1.11	0.61	0.14	0.16	
19	0.16	0.91	0.40	0.56	0.08	0.52	0.25	0.08	0.22	0.87	0.44	0.97	0.31	0.76	0.07	
20	0.05	0.32	0.12	0.35	0.50	0.28	0.35	0.37	0.15	0.16	0.09	0.56	0.15	0.36	0.13	
21	0.28	0.28	0.45	0.29	0.35	0.12	0.33	0.96	0.67	0.52	0.22	0.64	0.15	0.53	0.13	
22	0.19	0.31	0.17	0.35	0.25	0.22	0.25	0.57	0.20	0.29	0.42	1.06	0.73	0.18	0.11	
23	0.46	0.48	0.44	0.36	0.24	0.14	0.80	0.32	0.51	0.16	1.12	1.04	0.56	0.61	0.13	
24	0.10	0.36	0.29	0.22	0.19	0.50	0.33	0.74	0.12	0.04	0.49	0.50	0.81	0.30	0.05	
25	0.77	1.07	1.25	1.24	1.18	1.31	1.96	0.92	0.75	0.60	0.98	1.45	0.94	0.85	0.11	
26	0.28	0.37	0.11	0.09	0.61	0.48	0.46	0.50	0.19	0.38	0.30	0.61	0.19	0.32	0.12	
27	2.43	3.16	3.41	4.05	4.74	7.48	8.62	9.96	10.74	11.34	11.92	9.98	9.72	6.53	0.19	
28	0.11	0.22	0.44	0.39	0.11	0.53	0.39	0.75	0.27	0.19	0.99	0.90	0.74	0.36	0.07	
29	1.84	1.65	1.08	1.58	2.42	5.18	7.15	7.96	10.00	10.53	11.06	10.56	9.47	6.47	0.05	
30	0.22	0.33	0.27	0.34	0.36	0.34	0.30	0.29	0.46	0.28	0.37	0.94	0.84	0.23	0.08	

Harmonic number

	0.50	0.55	0.58	0.60	0.62	0.68	0.71	0.74	0.77	0.80	0.83	0.88	0.90	0.95	1.00
31	0.48	0.62	0.24	0.47	0.46	0.14	1.14	0.51	0.43	0.85	0.14	1.13	0.58	1.52	0.14
32	0.09	0.26	0.47	0.36	0.30	0.11	0.33	0.83	0.37	0.18	0.18	1.09	0.40	0.16	0.14
33	0.36	0.37	0.39	0.12	0.11	0.42	0.41	0.07	0.21	0.56	0.31	0.91	0.54	1.03	0.08
34	0.27	0.14	0.31	0.11	0.56	0.23	0.33	0.56	0.11	0.24	0.19	0.35	0.11	0.49	0.15
35	0.28	0.08	0.40	0.49	0.24	0.30	0.67	0.87	0.48	0.34	0.25	0.96	0.19	0.70	0.15
36	0.05	0.09	0.33	0.14	0.39	0.46	0.32	0.40	0.20	0.30	0.24	0.85	0.88	0.21	0.13
37	0.09	0.41	0.14	0.27	0.22	0.05	0.56	0.30	0.60	0.41	0.59	0.91	0.31	0.28	0.12
38	0.15	0.07	0.37	0.36	0.30	0.56	0.33	0.53	0.03	0.14	0.34	0.62	0.59	0.26	0.09
39	0.13	0.21	0.13	0.25	0.26	0.54	0.64	0.72	0.63	0.44	0.65	1.01	0.65	0.67	0.07
40	0.06	0.10	0.23	0.30	0.34	0.11	0.35	0.64	0.22	0.35	0.35	0.65	0.17	0.33	0.16
41	0.22	0.36	0.59	0.37	0.57	1.46	2.79	4.17	4.96	6.21	7.41	6.69	6.80	4.68	0.02
42	0.08	0.09	0.32	0.23	0.18	0.07	0.37	0.87	0.22	0.12	0.79	1.00	0.77	0.28	0.12
43	0.18	0.97	1.68	2.03	1.65	0.71	1.15	2.13	3.66	5.12	6.18	6.50	6.19	4.47	0.11
44	0.05	0.36	0.22	0.17	0.54	0.11	0.40	0.21	0.35	0.11	0.31	0.89	0.82	0.26	0.13
45	0.16	0.15	0.44	0.43	0.20	0.59	0.40	1.12	0.68	0.38	0.41	0.54	0.14	1.56	0.04
46	0.08	0.18	0.21	0.18	0.05	0.41	0.25	0.77	0.26	0.22	0.34	1.08	0.30	0.26	0.05
47	0.16	0.46	0.17	0.11	0.38	0.31	0.14	0.36	0.50	0.74	0.51	0.89	0.54	1.12	0.10
48	0.07	0.33	0.02	0.28	0.19	0.43	0.20	0.65	0.09	0.18	0.33	0.22	0.35	0.29	0.04
49	0.15	0.07	0.17	0.39	0.11	0.26	0.62	0.39	0.04	0.19	0.25	0.91	0.15	0.67	0.13
50	0.20	0.31	0.05	0.30	0.44	0.30	0.23	0.50	0.24	0.29	0.22	0.52	0.79	0.21	0.14
51	0.21	0.31	0.13	0.22	0.15	0.16	0.25	0.25	0.52	0.56	0.31	0.92	0.09	0.32	0.19
52	0.11	0.27	0.12	0.28	0.36	0.15	0.26	0.49	0.05	0.15	0.19	0.79	0.52	0.24	0.08
53	0.17	0.22	0.34	0.49	0.33	0.17	0.44	0.93	0.65	0.33	0.41	0.54	0.62	0.44	0.11
54	0.27	0.29	0.10	0.19	0.42	0.22	0.31	0.48	0.18	0.32	0.39	0.69	0.45	0.22	0.07
55	0.66	1.17	1.07	1.22	1.45	1.26	0.38	0.65	1.25	2.64	4.13	4.56	4.83	3.54	0.08
56	0.11	0.14	0.26	0.21	0.07	0.42	0.20	0.73	0.17	0.09	0.57	1.00	0.76	0.22	0.07
57	0.56	0.45	0.66	1.23	1.64	1.92	1.78	1.24	0.36	1.87	3.09	4.17	4.31	3.59	0.08
58	0.19	0.24	0.17	0.28	0.41	0.21	0.43	0.29	0.19	0.09	0.18	0.72	0.68	0.04	0.18
59	0.13	0.21	0.28	0.36	0.42	0.32	0.36	0.76	0.87	0.21	0.82	0.47	0.23	1.55	0.17
60	0.09	0.13	0.35	0.38	0.27	0.40	0.35	0.55	0.07	0.12	0.41	0.90	0.12	0.27	0.11

Harmonic number

%

	0.50	0.55	0.58	0.60	0.62	0.68	0.71	0.74	0.77	0.80	0.83	0.88	0.90	0.95	1.00
61	0.06	0.50	0.14	0.23	0.07	0.25	0.52	0.66	0.64	0.34	1.04	0.93	0.12	1.33	0.14
62	0.22	0.06	0.28	0.24	0.52	0.29	0.33	0.44	0.13	0.18	0.29	0.59	0.49	0.34	0.12
63	0.03	0.07	0.26	0.41	0.07	0.09	0.16	0.43	0.27	0.22	0.12	1.07	0.08	0.57	0.08
64	0.04	0.01	0.34	0.18	0.16	0.17	0.27	0.58	0.15	0.13	0.04	0.31	0.65	0.03	0.08
65	0.15	0.37	0.17	0.13	0.23	0.25	0.20	0.10	0.25	0.55	0.20	0.77	0.18	0.32	0.15
66	0.15	0.13	0.36	0.19	0.09	0.33	0.30	0.59	0.08	0.13	0.21	0.83	0.25	0.25	0.10
67	0.16	0.14	0.18	0.36	0.05	0.07	0.56	0.81	0.51	0.20	0.28	0.31	0.44	0.49	0.15
68	0.03	0.13	0.22	0.20	0.53	0.35	0.29	0.23	0.15	0.20	0.36	0.80	0.50	0.37	0.12
69	0.16	0.07	0.15	0.51	0.66	1.46	1.33	1.07	0.78	0.41	1.75	2.92	3.41	2.91	0.14
70	0.05	0.20	0.39	0.31	0.18	0.35	0.25	0.55	0.09	0.07	0.25	0.86	0.77	0.22	0.08
71	0.15	0.50	0.50	0.56	0.24	1.23	1.92	1.38	1.41	0.18	1.09	2.50	2.87	2.75	0.18
72	0.01	0.35	0.23	0.21	0.33	0.17	0.22	0.37	0.14	0.15	0.17	0.56	0.52	0.17	0.15
73	0.20	0.21	0.17	0.51	0.51	0.13	0.91	0.43	0.47	0.61	1.01	0.47	0.58	1.64	0.08
74	0.06	0.20	0.28	0.19	0.09	0.04	0.31	0.52	0.10	0.08	0.43	0.62	0.33	0.27	0.12
75	0.15	0.31	0.20	0.27	0.29	0.25	0.56	0.45	0.46	0.65	1.30	0.67	0.33	1.46	0.04
76	0.05	0.32	0.13	0.17	0.34	0.11	0.27	0.21	0.12	0.20	0.29	0.68	0.59	0.31	0.05
77	0.11	0.03	0.19	0.44	0.10	0.07	0.29	0.81	0.44	0.21	0.15	0.93	0.06	0.52	0.08
78	0.16	0.27	0.21	0.23	0.37	0.39	0.27	0.60	0.03	0.16	0.17	0.37	0.45	0.20	0.03
79	0.14	0.25	0.04	0.16	0.11	0.02	0.32	0.07	0.08	0.42	0.33	0.49	0.21	0.25	0.05
80	0.10	0.21	0.07	0.27	0.32	0.42	0.29	0.59	0.19	0.20	0.27	0.84	0.06	0.11	0.08
81	0.00	0.04	0.19	0.24	0.15	0.04	0.21	0.42	0.22	0.05	0.24	0.36	0.26	0.35	0.08
82	0.24	0.19	0.06	0.24	0.24	0.12	0.26	0.33	0.10	0.16	0.21	0.83	0.61	0.29	0.08
83	0.26	0.66	0.47	0.27	0.38	0.45	1.07	1.26	1.24	0.91	0.14	1.78	2.24	2.12	0.16
84	0.11	0.05	0.09	0.11	0.05	0.02	0.27	0.50	0.17	0.17	0.15	0.74	0.60	0.24	0.06
85	0.23	0.09	0.49	0.81	0.68	0.18	0.90	0.97	1.54	0.89	0.38	1.50	1.91	2.06	0.15
86	0.18	0.05	0.07	0.14	0.40	0.08	0.24	0.27	0.18	0.12	0.20	0.42	0.39	0.01	0.16
87	0.14	0.08	0.36	0.51	0.07	0.57	0.86	0.62	0.24	0.93	1.03	0.76	0.87	1.68	0.08
88	0.08	0.06	0.18	0.23	0.16	0.32	0.15	0.56	0.21	0.09	0.35	0.45	0.43	0.22	0.12
89	0.15	0.50	0.20	0.06	0.18	0.54	0.26	0.20	0.47	1.09	1.18	0.69	0.72	1.63	0.13
90	0.20	0.11	0.17	0.24	0.30	0.35	0.17	0.35	0.12	0.22	0.14	0.82	0.57	0.28	0.06

Harmonic number

%

	0.50	0.55	0.58	0.60	0.62	0.68	0.71	0.74	0.77	0.80	0.83	0.88	0.90	0.95	1.00
91	0.07	0.03	0.14	0.20	0.08	0.13	0.40	0.63	0.38	0.18	0.20	0.72	0.13	0.52	0.04
92	0.05	0.07	0.19	0.24	0.20	0.24	0.20	0.32	0.04	0.17	0.32	0.48	0.24	0.18	0.16
93	0.06	0.29	0.08	0.09	0.17	0.11	0.15	0.03	0.29	0.37	0.38	0.23	0.27	0.22	0.11
94	0.13	0.22	0.32	0.16	0.22	0.13	0.18	0.36	0.14	0.11	0.31	0.62	0.17	0.09	0.16
95	0.10	0.11	0.18	0.39	0.09	0.10	0.28	0.18	0.19	0.16	0.22	0.54	0.17	0.46	0.03
96	0.03	0.24	0.13	0.11	0.37	0.16	0.24	0.46	0.06	0.17	0.03	0.71	0.63	0.29	0.09
97	0.13	0.18	0.14	0.36	0.37	0.35	0.32	0.76	0.91	1.14	0.64	0.94	1.26	1.63	0.04
98	0.08	0.18	0.33	0.25	0.18	0.29	0.26	0.55	0.21	0.12	0.23	0.45	0.54	0.27	0.05
99	0.12	0.29	0.11	0.35	0.50	0.51	0.33	0.65	0.90	1.00	0.72	0.94	1.24	1.64	0.10
100	0.04	0.31	0.18	0.21	0.30	0.10	0.31	0.18	0.22	0.05	0.14	0.30	0.23	0.09	0.02

Harmonic number

%

Harmonic number	Duty ratio															%
	0.50	0.55	0.58	0.60	0.62	0.68	0.71	0.74	0.77	0.80	0.83	0.88	0.90	0.95	1.00	
2	0.76	0.57	1.11	1.76	1.01	1.40	1.57	1.76	1.35	1.15	0.58	1.71	1.01	1.08	1.65	
3	10.40	10.37	9.13	9.99	8.38	7.49	6.29	6.92	3.84	3.29	1.76	2.17	3.97	6.10	2.84	
4	0.21	0.97	0.57	1.51	0.28	0.41	0.25	0.41	0.69	0.52	0.41	0.46	0.42	0.70	0.79	
5	2.32	0.95	1.42	0.87	0.87	1.39	1.11	2.34	1.79	1.87	2.57	2.02	2.48	4.81	8.23	
6	0.18	0.37	0.55	0.90	0.55	0.33	0.42	0.59	0.91	0.31	0.64	0.92	0.55	0.44	0.66	
7	0.50	0.32	0.78	0.97	0.64	0.63	0.42	1.27	0.57	0.24	1.07	1.96	1.44	1.16	1.36	
8	0.23	0.44	0.59	0.59	1.11	0.36	0.28	1.28	0.53	0.21	0.46	1.10	0.30	0.11	0.15	
9	0.28	0.40	0.77	0.94	0.19	0.44	0.34	0.72	0.63	0.30	0.56	0.53	0.77	0.88	0.12	
10	0.22	0.37	0.80	0.69	1.06	0.43	0.40	0.81	0.81	0.50	0.42	1.49	0.08	0.64	0.23	
11	0.04	0.14	0.78	1.25	0.54	0.37	0.56	1.60	0.62	0.73	0.47	1.70	0.36	0.12	0.52	
12	0.33	0.21	0.84	0.98	1.21	0.49	0.58	0.77	0.36	1.21	0.44	1.48	0.36	0.31	0.12	
13	0.15	0.59	0.89	1.07	0.94	0.52	0.57	1.88	0.74	0.45	0.96	0.99	0.67	0.33	0.13	
14	0.18	0.13	1.22	1.28	1.40	0.90	0.62	2.03	1.07	0.87	0.19	2.17	0.58	0.61	0.25	
15	0.25	0.68	0.82	1.29	1.00	0.81	1.33	2.13	1.70	1.89	0.54	2.00	0.32	0.81	0.06	
16	0.22	0.92	1.94	2.12	2.31	0.71	1.24	3.89	1.77	2.54	0.95	2.98	1.18	0.85	0.10	
17	0.27	1.51	0.51	2.78	2.16	3.57	3.23	2.63	1.44	4.48	1.38	4.09	1.09	2.17	0.11	
18	0.04	2.22	3.51	4.81	5.06	6.07	6.49	8.59	6.62	9.09	5.41	8.47	4.71	3.29	0.07	
19	0.31	2.74	4.55	4.70	7.84	12.87	13.80	9.90	15.47	10.56	16.30	8.63	12.88	6.84	0.06	
20	0.14	1.61	3.55	3.76	5.24	9.73	10.34	5.57	11.51	6.25	12.51	6.77	9.29	4.45	0.17	
21	0.18	3.87	6.48	7.41	9.09	11.98	13.66	16.87	15.02	17.14	13.67	13.55	10.70	8.19	0.12	
22	0.15	1.61	1.47	1.71	3.20	4.07	4.50	5.69	4.73	5.62	4.10	4.01	2.92	3.97	0.13	
23	0.23	1.24	2.74	3.06	2.62	1.32	1.04	5.47	0.99	5.35	0.62	3.06	0.91	0.94	0.15	
24	0.10	0.66	0.80	1.15	1.08	0.72	0.40	3.20	1.34	3.76	0.63	2.04	1.24	1.98	0.08	
25	0.17	0.31	1.37	1.44	1.32	0.72	1.47	2.84	0.89	1.94	0.58	1.04	0.83	0.73	0.02	
26	0.31	0.60	0.58	0.53	0.68	0.71	0.72	2.54	0.71	2.19	0.15	1.20	1.02	1.15	0.09	
27	0.21	0.28	0.87	0.87	1.00	0.38	0.97	1.31	0.88	2.38	0.47	0.92	0.55	0.57	0.03	
28	0.24	0.35	0.27	0.53	0.41	0.20	0.81	2.09	0.53	2.36	0.80	0.92	0.36	0.66	0.07	
29	0.05	0.10	0.74	0.58	0.71	0.47	0.54	1.58	0.61	1.32	0.47	0.43	0.61	0.44	0.13	
30	0.45	0.29	0.45	0.78	0.22	0.53	0.31	1.38	0.50	1.46	0.52	1.24	0.56	0.99	0.19	

	0.50	0.55	0.58	0.60	0.62	0.68	0.71	0.74	0.77	0.80	0.83	0.88	0.90	0.95	1.00
31	0.03	0.45	0.62	0.07	0.76	0.18	0.74	1.91	0.60	1.54	0.53	0.66	0.99	0.40	0.08
32	0.37	0.26	0.47	0.71	0.38	0.27	0.80	0.91	0.76	2.27	0.56	0.79	0.27	0.67	0.04
33	0.13	0.07	0.52	0.35	0.43	0.30	0.37	1.80	0.36	1.48	0.85	0.13	0.85	0.59	0.09
34	0.51	0.62	0.69	0.33	0.79	0.28	0.97	1.79	0.73	1.86	0.33	1.30	0.75	1.00	0.15
35	0.10	0.06	0.50	0.26	0.57	0.30	0.42	1.56	0.75	1.07	0.57	0.69	0.60	0.41	0.03
36	0.60	0.44	1.06	1.17	1.56	0.71	0.68	2.99	1.47	2.12	1.24	1.51	0.99	1.19	0.09
37	0.23	0.60	0.44	0.29	0.22	0.85	1.22	2.08	0.80	2.86	0.90	1.44	1.39	1.72	0.08
38	1.19	1.43	2.31	2.54	3.67	5.01	6.25	8.20	7.13	9.32	7.25	7.99	6.64	4.70	0.05
39	0.36	0.95	0.95	1.18	1.26	2.39	2.53	1.88	4.05	1.94	4.65	1.67	3.84	1.64	0.22
40	0.84	1.11	0.65	1.35	1.19	4.63	5.68	5.77	8.12	7.33	9.60	6.84	7.55	4.43	0.10
41	0.22	0.10	0.72	0.49	0.76	1.21	1.98	1.96	2.53	2.72	1.74	3.19	1.84	1.72	0.14
42	0.08	0.35	0.18	0.27	1.07	1.17	1.31	1.69	1.15	2.00	1.62	2.20	1.56	2.45	0.11
43	0.14	0.16	0.57	0.22	0.22	0.40	0.45	0.64	0.64	1.30	0.38	1.29	0.32	0.46	0.07
44	0.09	0.24	0.11	0.53	0.63	0.56	0.40	0.51	1.54	1.35	1.08	0.96	0.85	2.11	0.09
45	0.14	0.33	0.32	0.37	0.21	0.42	0.73	0.67	0.78	0.14	0.42	0.40	0.08	0.37	0.18
46	0.06	0.25	0.41	0.19	0.72	0.39	0.30	0.30	0.75	0.31	0.34	0.60	0.49	0.73	0.11
47	0.20	0.23	0.38	0.71	0.17	0.33	0.45	0.75	0.43	0.66	0.23	0.52	0.53	0.21	0.02
48	0.14	0.25	0.20	0.36	0.72	0.19	0.52	0.55	0.43	0.85	0.54	0.68	0.21	0.67	0.10
49	0.24	0.28	0.21	0.20	0.22	0.26	0.28	0.34	0.71	0.23	0.58	0.43	0.45	0.26	0.24
50	0.06	0.11	0.39	0.51	0.64	0.46	0.15	0.76	0.45	0.22	0.37	0.39	0.21	0.57	0.03
51	0.23	0.09	0.23	0.20	0.55	0.31	0.33	0.13	0.38	0.37	0.20	0.20	0.35	0.30	0.15
52	0.20	0.12	0.38	0.50	0.31	0.32	0.53	0.85	0.55	0.73	0.25	0.40	0.15	0.55	0.06
53	0.22	0.32	0.16	0.16	0.29	0.28	0.21	0.44	0.63	0.57	0.40	0.76	0.31	0.22	0.03
54	0.15	0.25	0.35	0.58	0.44	0.48	0.68	0.67	0.54	0.64	0.51	0.25	0.75	0.95	0.02
55	0.18	0.12	0.23	0.50	0.29	0.32	0.28	0.64	0.02	0.35	0.16	0.40	0.43	0.19	0.15
56	0.21	0.03	0.47	0.04	0.38	0.31	0.22	0.33	0.66	0.20	0.99	0.60	0.47	1.58	0.12
57	0.09	0.40	0.16	0.26	0.14	0.32	0.18	0.51	0.35	0.64	0.37	1.36	0.43	0.11	0.20
58	0.24	0.28	0.41	0.08	0.15	0.67	2.10	3.26	4.34	4.91	5.67	4.85	5.72	3.62	0.11
59	0.13	0.04	0.38	0.24	0.08	0.22	0.51	0.03	0.76	0.02	1.47	0.70	0.82	0.59	0.22
60	0.19	0.64	1.34	1.12	1.24	0.14	0.66	1.97	3.15	4.57	4.41	5.73	4.93	3.89	0.03

Harmonic number

%

	0.50	0.55	0.58	0.60	0.62	0.68	0.71	0.74	0.77	0.80	0.83	0.88	0.90	0.95	1.00
61	0.15	0.26	0.11	0.22	0.23	0.31	0.08	0.68	0.79	1.32	0.80	1.34	0.78	1.67	0.08
62	0.19	0.05	0.60	0.84	0.54	0.59	0.46	0.33	1.13	0.89	0.98	0.39	1.54	1.10	0.07
63	0.13	0.19	0.14	0.31	0.42	0.38	0.19	0.92	0.99	0.69	0.66	0.28	1.08	1.01	0.11
64	0.20	0.18	0.52	0.58	1.02	0.54	0.28	1.02	0.50	0.91	0.91	0.91	1.40	1.33	0.14
65	0.23	0.22	0.08	0.28	0.06	0.14	0.35	0.29	0.24	0.64	0.41	0.15	0.95	0.79	0.12
66	0.16	0.13	0.38	0.47	0.70	0.36	0.14	0.52	0.40	0.80	0.05	0.34	0.39	0.19	0.02
67	0.23	0.15	0.13	0.34	0.32	0.30	0.12	0.41	0.26	0.62	0.36	0.14	0.07	0.18	0.15
68	0.05	0.26	0.33	0.29	0.39	0.18	0.20	0.55	0.28	0.28	0.15	0.42	0.48	0.26	0.04
69	0.21	0.17	0.15	0.46	0.18	0.24	0.20	0.44	0.05	0.43	0.47	0.41	0.62	0.51	0.15
70	0.14	0.14	0.37	0.49	0.22	0.08	0.30	0.32	0.22	0.67	0.51	0.23	0.74	0.08	0.10
71	0.17	0.25	0.19	0.25	0.32	0.20	0.24	0.58	0.30	0.73	0.43	0.20	0.43	0.31	0.06
72	0.05	0.24	0.32	0.52	0.12	0.12	0.29	0.34	0.30	0.27	0.42	0.15	0.55	0.12	0.02
73	0.21	0.20	0.33	0.44	0.34	0.43	0.12	0.26	0.18	0.58	0.47	0.74	0.38	0.47	0.14
74	0.06	0.15	0.32	0.29	0.18	0.20	0.28	0.75	0.22	0.41	0.66	0.17	0.51	0.24	0.00
75	0.17	0.27	0.36	0.39	0.59	0.18	0.38	0.20	0.33	0.71	0.66	0.29	0.53	0.36	0.16
76	0.13	0.38	0.29	0.28	0.18	0.27	0.16	0.30	0.48	0.67	0.75	0.54	1.20	1.26	0.07
77	0.26	0.28	0.67	0.73	1.04	0.93	0.56	0.53	0.38	1.61	1.27	2.53	2.31	1.56	0.12
78	0.19	0.41	0.54	0.38	0.82	0.91	0.36	0.34	1.11	0.88	2.27	1.77	2.94	1.64	0.05
79	0.18	0.21	0.53	0.70	0.20	1.14	0.73	0.61	0.79	0.59	2.16	1.56	2.59	1.40	0.17
80	0.06	0.24	0.49	0.29	0.49	0.73	0.84	0.90	0.49	1.27	1.01	2.99	2.04	2.01	0.04
81	0.08	0.26	0.36	0.13	0.54	0.26	0.89	1.02	1.48	0.99	0.72	2.50	1.97	2.29	0.05
82	0.12	0.04	0.45	0.25	0.15	0.12	0.31	0.29	0.45	0.24	0.12	0.53	0.68	0.62	0.07
83	0.07	0.36	0.27	0.10	0.35	0.28	0.78	1.08	1.16	0.69	0.36	1.16	1.93	1.76	0.06
84	0.15	0.10	0.31	0.49	0.34	0.05	0.34	0.61	0.13	0.08	0.34	0.90	0.60	0.28	0.05
85	0.07	0.13	0.28	0.24	0.35	0.10	0.41	0.25	0.62	0.17	0.36	0.60	0.79	0.77	0.04
86	0.15	0.24	0.28	0.35	0.23	0.13	0.15	0.40	0.40	0.35	0.21	0.46	0.61	0.11	0.10
87	0.07	0.08	0.20	0.43	0.19	0.30	0.24	0.55	0.28	0.06	0.31	0.40	0.44	0.29	0.01
88	0.17	0.20	0.23	0.17	0.20	0.13	0.19	0.16	0.15	0.13	0.37	0.38	0.27	0.24	0.07
89	0.05	0.17	0.28	0.33	0.20	0.16	0.26	0.30	0.45	0.14	0.41	0.44	0.19	0.36	0.06
90	0.14	0.12	0.18	0.12	0.42	0.10	0.15	0.43	0.24	0.26	0.29	0.24	0.43	0.10	0.08

Harmonic number

%

	0.50	0.55	0.58	0.60	0.62	0.68	0.71	0.74	0.77	0.80	0.83	0.88	0.90	0.95	1.00
91	0.14	0.18	0.31	0.48	0.35	0.30	0.37	0.14	0.19	0.19	0.50	0.44	0.42	0.31	0.10
92	0.17	0.13	0.14	0.20	0.26	0.04	0.17	0.21	0.26	0.16	0.15	0.23	0.55	0.15	0.02
93	0.09	0.11	0.24	0.13	0.47	0.12	0.22	0.39	0.19	0.25	0.40	0.52	0.64	0.51	0.05
94	0.15	0.21	0.11	0.36	0.34	0.08	0.12	0.25	0.33	0.14	0.37	0.43	0.20	0.05	0.17
95	0.13	0.11	0.33	0.26	0.46	0.08	0.48	0.56	0.24	0.29	0.53	0.41	0.02	0.62	0.01
96	0.11	0.17	0.06	0.15	0.05	0.04	0.08	0.17	0.31	0.32	0.49	0.35	0.56	0.54	0.12
97	0.14	0.19	0.29	0.32	0.79	1.09	1.13	1.02	0.26	0.18	1.05	1.93	2.36	1.87	0.15
98	0.13	0.21	0.10	0.41	0.10	0.11	0.20	0.34	0.22	0.11	0.04	0.53	0.76	0.32	0.13
99	0.15	0.20	0.42	0.49	0.39	0.86	1.28	0.97	0.76	0.26	0.64	2.10	2.37	1.85	0.06
100	0.04	0.12	0.09	0.06	0.02	0.15	0.23	0.23	0.25	0.35	0.06	0.91	0.33	0.23	0.17

Harmonic number

%

Harmonic number	Duty ratio															%
	0.50	0.55	0.58	0.60	0.62	0.68	0.71	0.74	0.77	0.80	0.83	0.88	0.90	0.95	1.00	
2	1.02	2.07	0.67	0.31	0.58	1.44	0.50	1.20	0.43	1.14	1.55	1.59	2.30	1.47	0.14	
3	10.23	9.94	9.56	9.66	9.40	8.20	8.31	6.87	5.67	4.68	2.91	4.19	2.94	5.71	3.84	
4	0.56	0.14	0.11	0.67	0.79	0.58	0.77	0.54	0.25	1.14	0.32	0.90	0.36	0.44	0.11	
5	1.96	1.80	1.87	1.99	0.86	1.48	1.74	1.22	1.49	1.68	1.89	2.61	2.34	3.98	9.34	
6	0.70	0.28	0.35	0.68	0.18	0.97	0.64	0.16	0.67	1.07	0.55	0.71	1.87	1.34	0.59	
7	0.98	0.61	0.85	0.38	0.51	0.82	1.32	0.66	0.98	0.63	0.80	1.09	1.72	0.95	1.42	
8	0.01	1.00	0.22	0.54	1.07	1.60	0.42	0.46	1.67	1.49	1.56	0.75	0.63	1.69	0.28	
9	1.04	0.55	0.11	0.16	0.63	0.66	0.41	0.35	0.37	0.84	0.10	1.30	0.57	0.73	0.41	
10	0.71	0.79	0.08	0.63	0.67	1.02	0.85	0.46	0.57	0.61	0.91	0.66	0.74	0.86	0.28	
11	0.24	0.19	0.12	0.60	0.33	0.65	0.75	0.43	0.16	0.67	0.43	1.12	0.92	0.78	0.37	
12	0.54	0.70	0.02	0.62	0.31	0.92	0.90	0.49	0.35	0.24	0.75	0.86	0.76	0.71	0.20	
13	0.17	0.80	0.31	0.40	0.54	0.76	0.62	0.36	0.23	0.22	0.24	0.84	0.71	0.51	0.08	
14	0.74	1.07	0.52	0.32	0.53	1.12	1.09	0.90	0.32	1.14	1.27	1.62	0.96	1.25	0.12	
15	0.89	1.00	0.67	0.46	0.75	1.27	0.62	0.15	0.35	0.48	0.72	0.94	0.67	0.34	0.25	
16	0.29	0.27	0.19	0.67	0.63	0.79	0.60	0.73	0.15	0.93	0.54	0.56	0.84	0.90	0.16	
17	0.52	0.19	0.21	0.95	0.78	0.88	1.20	0.33	0.34	0.85	0.62	0.77	0.50	0.43	0.09	
18	0.20	0.42	0.32	0.79	0.92	0.59	1.04	0.33	0.49	0.98	0.39	0.45	0.15	0.60	0.02	
19	0.28	0.19	0.30	0.45	0.85	0.82	1.04	0.46	0.60	0.40	0.35	0.98	0.53	0.73	0.08	
20	0.79	0.42	0.33	0.37	1.07	0.79	1.00	0.10	0.12	0.56	1.04	0.33	0.79	0.93	0.09	
21	0.19	0.47	0.14	0.50	1.35	0.67	1.25	0.95	1.25	1.60	1.03	1.71	0.84	1.29	0.06	
22	0.78	1.34	1.22	1.11	0.48	1.42	0.78	0.49	1.13	2.04	0.91	0.94	1.43	1.20	0.19	
23	0.92	1.20	0.35	1.39	0.52	1.86	1.49	1.38	0.72	1.64	1.04	1.60	0.55	2.08	0.11	
24	0.21	0.93	0.86	1.58	0.35	1.28	2.21	0.19	0.49	1.31	0.88	1.59	3.02	0.64	0.15	
25	0.55	0.69	0.77	1.22	0.98	0.80	2.78	1.19	1.22	2.03	1.33	2.03	2.41	1.07	0.08	
26	0.21	0.30	1.48	1.45	1.07	1.89	3.16	1.38	1.26	2.47	1.57	1.63	1.88	0.45	0.29	
27	0.47	0.58	1.13	1.04	2.84	4.24	3.27	1.31	1.12	1.86	1.67	2.39	3.41	1.03	0.17	
28	0.77	0.75	2.66	4.58	5.28	6.31	7.78	4.64	4.89	7.09	5.42	5.12	6.97	1.47	0.11	
29	0.25	1.19	3.76	2.95	4.84	7.22	7.42	12.75	12.95	9.40	11.43	9.02	6.51	6.46	0.05	
30	0.34	1.02	3.33	2.73	4.33	5.86	5.42	9.73	10.68	8.37	9.36	6.85	4.96	5.13	0.08	

	0.50	0.55	0.58	0.60	0.62	0.68	0.71	0.74	0.77	0.80	0.83	0.88	0.90	0.95	1.00
31	0.81	0.96	4.82	6.66	7.40	10.33	11.23	9.81	10.25	12.01	10.93	9.87	8.85	4.99	0.08
32	0.26	0.78	1.89	2.00	2.03	3.69	3.05	2.96	2.89	3.96	3.58	3.67	1.96	1.66	0.09
33	0.06	0.46	1.46	2.46	2.39	2.89	3.45	0.51	0.42	2.79	1.55	1.00	1.17	0.17	0.11
34	0.18	0.37	0.82	0.87	1.47	1.72	2.02	0.66	0.85	2.01	1.48	1.37	1.09	0.83	0.09
35	0.48	0.89	0.81	1.14	1.10	1.73	1.52	0.07	0.20	1.60	0.99	0.51	1.29	0.27	0.11
36	0.82	0.90	0.53	0.80	0.88	1.98	1.72	0.41	0.31	1.19	1.76	0.94	1.37	1.60	0.09
37	0.44	1.42	0.41	1.34	0.76	0.59	0.87	0.36	0.40	0.66	1.06	1.34	0.30	0.08	0.16
38	0.57	0.44	0.67	0.86	0.58	1.30	1.06	0.47	0.80	1.50	1.09	1.56	0.81	1.35	0.17
39	0.84	0.56	0.66	0.71	0.56	1.40	1.06	0.34	0.27	0.68	1.26	0.11	1.09	0.44	0.02
40	0.18	0.18	0.29	0.29	0.18	0.68	0.86	0.49	0.42	0.70	0.39	1.21	0.90	0.53	0.02
41	0.18	0.32	0.24	0.47	0.23	0.64	0.63	0.61	0.32	1.01	0.61	0.26	0.57	0.74	0.08
42	0.37	0.13	0.44	0.89	0.38	0.86	0.61	0.55	0.51	0.63	0.11	1.22	0.49	0.43	0.10
43	0.58	0.38	0.36	0.74	0.18	1.12	0.46	0.18	0.18	0.76	0.77	0.42	1.02	0.47	0.11
44	0.91	0.74	0.15	0.71	0.54	0.26	0.38	0.72	0.71	1.23	0.50	0.98	0.08	0.96	0.12
45	0.46	1.20	0.47	0.28	0.45	0.29	0.35	0.21	0.50	0.26	0.27	0.71	0.19	0.96	0.11
46	0.32	0.66	0.43	0.02	0.35	0.96	0.60	0.12	0.14	0.39	0.73	1.00	0.60	0.75	0.14
47	0.54	0.80	0.12	0.25	0.43	0.85	0.47	0.40	0.47	0.40	0.33	0.49	0.66	0.69	0.18
48	0.18	0.21	0.05	0.40	0.22	0.11	0.22	0.39	0.40	0.81	0.33	0.83	0.50	0.57	0.07
49	0.41	0.67	0.16	0.41	0.30	0.24	0.31	0.49	0.51	0.54	0.42	0.50	0.72	0.84	0.03
50	0.31	0.63	0.12	0.27	0.27	1.06	0.16	0.41	0.22	0.33	0.53	0.73	0.09	0.54	0.04
51	0.44	0.80	0.48	0.31	0.32	1.12	0.85	1.19	0.81	0.59	1.18	2.32	2.00	1.96	0.19
52	0.56	0.22	0.46	0.02	0.53	0.53	0.31	0.37	0.17	0.84	0.36	0.60	0.32	0.32	0.11
53	0.38	0.39	0.38	0.58	0.45	1.73	1.40	1.21	0.43	0.81	1.55	1.79	2.72	2.03	0.08
54	0.37	0.44	0.27	0.33	0.16	1.13	0.21	0.49	0.38	0.60	0.70	0.36	0.76	1.05	0.14
55	0.21	0.46	0.16	0.40	0.26	0.13	0.62	0.15	0.36	0.96	0.51	1.01	0.91	0.63	0.22
56	0.08	0.14	0.39	0.20	0.51	0.31	0.93	0.53	0.70	1.59	1.03	0.35	0.43	0.80	0.08
57	0.86	0.58	0.29	0.26	0.19	1.83	1.25	0.93	0.83	1.08	0.73	1.25	1.01	1.07	0.03
58	1.01	1.15	1.31	2.08	2.28	4.73	5.29	4.77	5.48	6.28	6.24	5.26	5.95	2.83	0.09
59	0.65	1.37	0.91	0.30	0.60	1.63	0.73	2.56	2.41	1.44	2.47	2.28	1.30	1.72	0.08
60	1.40	1.24	0.87	1.35	1.99	3.30	3.44	5.47	6.79	6.42	6.77	5.91	4.54	4.15	0.02

Harmonic number

%

	0.50	0.55	0.58	0.60	0.62	0.68	0.71	0.74	0.77	0.80	0.83	0.88	0.90	0.95	1.00
61	0.45	0.68	0.25	0.84	0.50	0.97	1.46	0.94	1.15	1.63	1.40	1.33	1.70	0.89	0.07
62	0.43	0.16	0.17	0.84	0.32	0.48	0.58	0.22	0.15	0.81	0.98	1.33	0.51	0.86	0.06
63	0.10	0.21	0.06	0.38	0.09	0.35	0.44	0.34	0.22	0.26	0.60	0.41	0.07	0.37	0.03
64	0.16	0.43	0.18	0.07	0.08	0.73	0.46	0.49	0.55	0.51	1.07	1.16	0.55	0.73	0.09
65	0.74	0.29	0.22	0.64	0.38	0.44	0.57	0.29	0.11	0.36	0.25	0.52	0.49	0.56	0.10
66	0.34	0.07	0.43	0.56	0.22	0.73	0.41	0.71	0.20	0.99	1.23	0.36	0.60	1.38	0.08
67	0.18	0.84	0.61	0.88	0.60	0.44	0.42	0.52	0.14	0.62	1.00	0.57	0.18	1.12	0.12
68	0.57	0.57	0.04	0.37	0.14	0.71	0.41	0.60	0.04	0.85	0.38	0.89	0.37	0.49	0.01
69	0.39	0.70	0.11	0.53	0.39	0.32	0.21	0.35	0.37	0.77	1.02	0.51	0.55	0.49	0.09
70	0.04	0.24	0.18	0.26	0.32	0.40	0.38	0.47	0.28	0.43	0.44	0.73	0.54	0.68	0.12
71	0.21	0.40	0.18	0.48	0.29	0.22	0.34	0.41	0.38	0.26	0.67	0.22	0.48	0.51	0.12
72	0.24	0.77	0.17	0.72	0.50	0.62	0.60	0.20	0.19	0.16	0.67	0.83	0.71	0.37	0.08
73	0.63	0.63	0.09	0.58	0.33	0.34	0.32	0.24	0.54	0.60	0.79	0.68	0.48	0.76	0.07
74	0.42	0.80	0.74	0.62	0.16	0.76	0.58	0.38	0.70	1.30	0.53	0.65	0.15	0.32	0.12
75	0.14	0.13	0.08	0.33	0.24	0.81	0.42	0.45	0.47	0.74	0.57	0.73	0.37	1.23	0.05
76	0.68	0.20	0.23	0.49	0.42	0.50	0.21	0.28	0.16	0.32	0.56	0.62	0.48	0.24	0.06
77	0.31	0.31	0.28	0.48	0.18	0.43	0.51	0.40	0.31	0.46	0.61	0.89	0.33	0.58	0.04
78	0.23	0.18	0.24	0.46	0.14	0.04	0.38	0.41	0.12	0.10	0.60	0.81	0.22	0.49	0.10
79	0.54	0.23	0.22	0.68	0.38	0.87	0.58	0.51	0.44	0.68	1.19	1.10	0.20	0.76	0.03
80	0.12	0.51	0.01	0.57	0.39	0.57	0.36	0.14	0.33	0.97	1.14	1.68	1.01	0.81	0.13
81	0.89	0.88	0.86	0.84	1.08	1.26	0.63	0.33	0.66	0.82	1.49	1.81	1.80	1.95	0.14
82	0.70	1.09	0.21	0.34	0.34	0.59	0.64	0.30	0.46	0.85	1.55	1.74	1.15	1.66	0.11
83	0.23	0.64	0.54	0.97	0.75	0.48	0.68	0.22	0.39	1.23	1.89	1.78	3.13	0.83	0.13
84	0.53	0.53	0.34	0.39	0.14	0.50	0.64	0.37	0.51	0.87	0.04	0.92	1.09	0.99	0.14
85	0.15	0.14	0.33	0.05	0.10	0.31	0.41	0.43	0.30	0.88	0.30	0.11	0.55	0.38	0.18
86	0.24	0.42	0.24	0.34	0.07	0.46	0.44	0.35	0.32	0.22	0.19	0.85	1.04	0.71	0.12
87	0.41	0.33	0.27	0.62	0.30	0.27	0.38	0.04	0.25	0.68	0.94	0.67	1.74	0.48	0.08
88	0.09	0.35	0.40	0.35	0.20	1.29	0.76	1.76	2.58	2.94	3.91	3.18	3.10	2.49	0.07
89	0.44	0.30	0.35	0.46	0.13	0.31	0.51	0.69	1.14	1.24	1.05	0.51	0.64	0.71	0.03
90	0.48	0.56	0.74	0.76	0.88	0.80	0.61	1.20	2.14	2.65	3.22	3.51	2.75	2.05	0.03

Harmonic number

%

	0.50	0.55	0.58	0.60	0.62	0.68	0.71	0.74	0.77	0.80	0.83	0.88	0.90	0.95	1.00
91	0.15	0.55	0.25	0.22	0.28	0.11	0.25	0.15	0.17	0.59	0.99	1.06	0.13	0.69	0.10
92	0.17	0.39	0.10	0.09	0.32	0.32	0.13	0.36	0.34	0.02	0.26	0.28	0.39	0.48	0.02
93	0.06	0.15	0.02	0.22	0.23	0.11	0.03	0.25	0.23	0.34	0.34	0.57	0.42	0.37	0.07
94	0.49	0.64	0.13	0.43	0.06	0.45	0.27	0.24	0.32	0.58	0.17	0.25	0.62	0.55	0.07
95	0.50	0.45	0.19	0.29	0.32	0.33	0.15	0.44	0.21	0.67	0.80	0.64	0.30	0.83	0.13
96	0.08	0.91	0.36	0.21	0.51	0.55	0.49	0.49	0.21	0.25	0.28	0.37	0.04	0.59	0.06
97	0.58	0.35	0.35	0.16	0.17	0.77	0.21	0.52	0.46	0.61	0.49	0.44	0.14	0.87	0.16
98	0.55	0.28	0.17	0.10	0.06	0.27	0.21	0.25	0.12	0.55	0.40	0.20	0.72	0.23	0.06
99	0.12	0.05	0.14	0.18	0.17	0.48	0.18	0.26	0.30	0.37	0.24	0.61	0.28	0.41	0.08
100	0.01	0.21	0.15	0.17	0.03	0.20	0.04	0.23	0.17	0.12	0.05	0.11	0.38	0.19	0.00

Harmonic number

%

Harmonic number	Duty ratio															%
	0.50	0.55	0.58	0.60	0.62	0.68	0.71	0.74	0.77	0.80	0.83	0.88	0.90	0.95	1.00	
2	0.39	0.62	0.84	1.66	0.99	2.48	1.12	0.34	1.41	0.95	1.28	0.95	2.27	1.98	0.52	
3	10.43	10.88	10.19	9.20	9.35	7.64	8.82	7.78	6.24	4.60	4.49	4.69	6.71	6.41	3.49	
4	0.24	0.86	0.37	0.45	0.60	0.70	1.16	1.74	0.86	0.80	1.79	1.78	0.95	0.83	0.47	
5	2.38	2.17	2.31	2.02	2.00	0.96	1.65	0.65	1.33	1.44	2.70	3.18	3.44	4.83	9.15	
6	0.30	0.70	0.62	0.78	0.71	0.73	0.39	0.93	0.62	0.06	2.17	1.05	1.18	0.97	0.61	
7	0.57	0.26	0.66	0.28	0.83	0.31	0.72	0.59	0.44	0.47	1.30	1.53	1.40	1.20	1.58	
8	0.61	0.96	0.33	0.22	0.49	0.62	0.88	0.62	0.44	0.56	1.37	0.45	0.45	0.47	0.43	
9	0.38	0.12	0.33	0.66	0.60	0.26	0.40	0.50	0.55	0.61	0.17	0.60	0.75	1.19	0.26	
10	0.45	0.40	0.10	0.45	0.16	0.28	0.76	0.31	0.44	0.06	0.69	0.54	0.31	0.35	0.18	
11	0.21	0.65	0.12	0.58	0.33	1.13	0.48	1.02	0.60	0.35	0.42	1.30	1.54	0.66	0.74	
12	0.14	0.22	0.11	0.32	0.60	0.45	0.49	0.44	0.08	0.42	0.42	0.80	0.14	0.29	0.13	
13	0.80	0.29	0.27	1.06	0.20	0.77	1.14	0.98	0.74	0.72	0.23	0.28	0.29	0.13	0.06	
14	0.15	0.22	0.19	0.38	0.58	0.81	0.40	0.90	0.25	0.12	0.56	0.86	1.03	0.95	0.32	
15	0.81	0.93	0.19	0.50	0.08	0.64	0.58	0.30	0.38	0.26	0.43	0.20	0.23	0.20	0.06	
16	0.36	0.18	0.79	1.10	0.51	0.73	0.80	0.39	0.23	0.86	1.53	1.14	1.63	0.25	0.09	
17	0.66	1.10	0.79	0.42	0.22	0.57	0.24	0.68	0.57	0.67	0.91	0.99	0.33	0.25	0.19	
18	0.59	0.96	1.45	0.89	0.79	0.90	1.14	1.05	0.09	0.58	1.75	0.87	0.54	0.73	0.12	
19	0.32	0.17	1.14	0.59	0.15	1.06	0.76	0.69	0.40	0.17	0.95	0.94	0.95	0.39	0.03	
20	0.88	1.01	0.90	1.01	0.49	1.08	0.40	0.26	0.52	0.75	0.60	0.54	0.13	0.20	0.03	
21	0.40	0.40	0.06	0.61	0.73	0.78	1.07	1.95	0.36	0.73	1.18	0.98	1.71	0.94	0.16	
22	0.93	0.31	0.69	0.42	0.58	0.42	0.16	0.40	0.42	0.81	1.10	0.35	0.68	0.25	0.11	
23	0.19	0.13	1.38	0.99	1.29	0.46	0.78	0.86	0.56	0.19	1.47	1.25	1.04	0.22	0.13	
24	0.69	1.02	1.67	0.06	1.26	0.80	1.09	0.38	0.31	0.23	0.99	0.77	0.68	0.64	0.09	
25	0.43	0.47	1.42	0.58	1.04	1.09	0.58	0.38	0.33	0.88	0.86	1.02	0.33	0.35	0.13	
26	0.30	0.52	1.01	0.67	0.94	1.24	0.97	0.75	0.36	0.48	1.06	0.48	1.22	0.36	0.16	
27	0.69	0.99	0.31	0.43	0.26	0.23	0.53	0.59	0.49	0.58	0.69	0.74	0.49	0.34	0.11	
28	0.14	0.26	0.34	0.42	0.28	0.35	0.45	0.76	0.14	0.57	0.95	0.95	0.92	0.75	0.09	
29	0.71	0.62	0.82	0.44	0.60	0.10	1.16	1.10	0.38	0.56	0.53	0.30	0.27	0.39	0.16	
30	0.17	0.24	0.90	0.69	0.31	0.67	0.89	0.55	0.46	0.87	0.40	0.90	0.48	0.25	0.03	

	0.50	0.55	0.58	0.60	0.62	0.68	0.71	0.74	0.77	0.80	0.83	0.88	0.90	0.95	1.00
31	0.30	0.45	0.88	0.18	0.59	1.56	0.95	1.72	0.64	0.60	1.48	0.37	1.01	1.02	0.11
32	0.32	0.21	0.49	0.29	0.43	0.58	1.09	0.88	0.39	0.65	0.86	1.12	0.20	0.28	0.11
33	0.12	0.70	0.33	0.72	0.46	0.53	0.80	1.36	0.06	0.97	1.97	1.17	0.50	0.12	0.21
34	0.50	0.24	0.33	0.68	0.63	0.61	1.65	1.22	0.98	0.91	1.55	0.64	0.24	1.23	0.10
35	0.23	0.59	0.44	0.29	0.47	0.88	1.45	2.03	1.30	1.17	1.75	1.24	0.26	0.88	0.13
36	0.63	1.21	1.09	0.29	1.23	1.74	1.75	1.94	0.72	1.66	1.31	0.25	2.33	1.62	0.09
37	0.08	1.02	0.98	2.10	0.89	2.77	2.04	2.44	2.49	2.69	3.72	3.29	0.55	0.33	0.08
38	0.45	1.89	2.38	3.65	3.67	5.16	6.07	7.88	7.09	6.87	8.05	6.40	2.11	1.24	0.17
39	0.15	1.41	3.90	3.70	5.36	6.68	6.52	6.23	8.84	7.86	4.86	4.72	7.99	4.78	0.10
40	0.11	1.57	4.04	4.38	5.83	7.40	7.47	6.94	9.09	8.51	6.12	5.35	8.30	4.64	0.04
41	0.59	2.67	3.72	5.32	6.07	8.19	8.89	8.54	8.22	9.50	8.57	5.83	6.93	4.53	0.18
42	0.07	0.40	1.22	1.78	2.19	2.68	2.93	3.31	3.26	2.83	3.23	2.60	1.56	1.22	0.06
43	0.67	1.83	1.39	1.60	1.27	1.70	1.39	2.82	1.32	1.00	5.01	4.04	2.29	1.17	0.10
44	0.21	0.45	0.41	0.95	0.42	1.27	1.43	1.36	0.84	1.41	2.11	1.29	0.47	0.71	0.16
45	0.37	0.75	0.28	0.51	0.19	1.06	1.24	1.12	1.14	1.52	1.83	0.92	0.20	0.70	0.14
46	0.20	0.52	0.34	0.36	0.45	0.61	0.92	1.88	0.73	0.49	0.36	0.54	1.37	0.24	0.19
47	0.12	0.56	0.76	0.51	0.32	0.50	0.55	0.89	0.58	0.27	0.85	0.83	0.23	0.19	0.04
48	0.29	0.37	0.89	0.43	0.17	0.23	0.58	1.33	0.95	0.92	0.08	0.93	0.26	0.91	0.13
49	0.19	0.27	0.97	0.24	0.26	0.69	0.62	0.81	0.51	0.66	0.40	0.91	0.29	0.34	0.12
50	0.62	0.65	0.65	0.45	0.19	1.01	0.51	0.93	0.14	0.58	0.19	0.68	0.23	0.33	0.10
51	0.11	0.25	0.30	0.55	0.48	0.31	0.48	0.53	0.75	0.39	0.06	0.37	1.23	0.69	0.09
52	0.60	1.02	0.34	0.14	0.17	0.44	0.32	0.70	0.79	0.59	0.24	0.21	0.51	0.36	0.08
53	0.20	0.38	0.83	0.42	1.08	0.18	0.25	0.70	0.18	1.03	0.82	0.73	0.64	0.62	0.09
54	0.27	0.31	1.20	0.62	0.62	0.28	0.54	0.76	0.20	0.38	0.92	0.65	0.27	0.34	0.09
55	0.72	0.74	1.14	0.31	1.24	1.09	0.62	0.69	0.91	0.56	1.33	0.78	0.66	0.44	0.16
56	0.09	0.37	0.99	0.52	0.71	0.67	0.43	1.25	0.32	0.74	1.10	0.62	1.34	0.49	0.13
57	0.83	0.27	0.36	0.57	0.53	0.69	0.31	0.31	0.22	0.76	0.57	0.24	0.62	0.28	0.13
58	0.35	0.09	0.16	0.68	0.61	0.68	0.09	0.76	0.48	0.92	0.98	0.46	0.87	0.63	0.16
59	0.74	1.14	0.47	0.63	0.86	0.38	0.60	0.60	0.82	0.27	0.60	0.29	0.41	0.25	0.02
60	0.36	0.43	0.24	0.38	1.00	0.64	0.74	1.34	0.12	0.80	0.90	0.70	1.15	0.61	0.03

Harmonic number

%

	0.50	0.55	0.58	0.60	0.62	0.68	0.71	0.74	0.77	0.80	0.83	0.88	0.90	0.95	1.00
61	0.40	0.70	0.53	0.85	1.39	0.59	0.23	0.34	0.26	0.66	0.56	0.69	0.94	0.60	0.10
62	0.62	0.94	0.08	0.26	0.65	0.70	0.13	0.49	0.53	0.77	0.29	0.47	0.41	0.23	0.14
63	0.33	0.13	0.32	0.63	0.94	0.99	0.44	1.30	0.64	0.67	0.25	0.53	0.98	0.51	0.10
64	0.78	0.61	0.10	0.61	0.11	0.65	0.47	0.51	0.35	0.29	0.21	0.19	0.35	0.43	0.11
65	0.08	0.27	0.55	0.49	0.26	0.26	0.51	0.41	0.24	0.77	0.49	0.30	1.23	0.61	0.07
66	0.66	0.48	0.37	0.62	0.44	0.20	0.24	0.51	0.42	0.44	0.83	0.28	0.45	0.29	0.10
67	0.19	0.04	0.71	0.19	0.03	0.38	0.15	0.08	0.46	0.53	0.52	0.55	0.04	0.21	0.03
68	0.21	0.56	0.36	0.69	0.26	0.80	0.30	0.80	0.27	0.54	0.91	0.60	0.77	0.77	0.08
69	0.48	0.51	0.30	0.24	0.09	0.50	0.32	0.25	0.22	0.41	0.07	0.17	0.38	0.33	0.10
70	0.07	0.02	0.25	0.35	0.35	0.47	0.35	0.87	0.31	0.70	0.64	0.32	1.15	0.50	0.02
71	0.56	0.64	0.35	0.42	0.11	0.13	0.27	0.47	0.43	0.21	0.68	0.12	0.34	0.42	0.15
72	0.22	0.28	0.75	0.15	0.47	0.17	0.20	0.34	0.25	0.28	0.54	0.38	0.18	0.34	0.06
73	0.35	0.13	0.60	0.37	0.17	0.57	0.13	0.87	0.14	0.59	0.58	0.75	0.18	0.77	0.09
74	0.07	0.26	0.56	0.23	0.28	0.17	0.24	0.51	0.32	0.27	0.26	0.55	0.36	0.17	0.15
75	0.20	0.33	0.21	0.36	0.38	0.50	0.50	0.37	0.61	0.58	0.07	0.58	1.11	0.25	0.07
76	0.28	0.20	0.31	0.54	0.78	0.21	0.37	0.18	0.99	0.92	0.37	0.58	1.11	1.06	0.12
77	0.16	0.20	0.46	0.24	0.58	0.33	0.36	0.45	0.57	0.78	0.52	0.26	0.72	0.65	0.02
78	0.79	1.19	1.66	1.79	2.26	3.36	3.85	4.03	5.20	4.77	5.92	4.87	3.70	2.08	0.07
79	0.08	0.14	0.57	0.25	0.09	0.34	0.10	0.63	0.53	0.61	1.09	1.06	0.67	0.63	0.04
80	0.66	0.91	1.23	1.62	1.93	3.02	3.37	3.21	5.70	6.48	5.45	3.47	5.53	3.45	0.06
81	0.07	0.40	0.46	0.50	0.51	0.63	0.44	0.36	1.65	2.02	1.28	1.35	2.65	1.55	0.03
82	0.08	0.32	0.54	0.17	0.33	0.76	0.70	0.92	1.94	2.06	1.68	1.84	2.69	1.71	0.09
83	0.30	0.14	0.09	0.09	0.09	0.91	1.04	0.87	1.28	1.75	2.81	2.21	0.88	0.14	0.12
84	0.06	0.42	0.17	0.23	0.04	0.30	0.32	0.38	0.44	0.74	1.13	1.09	0.41	0.22	0.13
85	0.42	0.34	0.07	0.21	0.31	0.30	0.35	0.74	0.17	0.77	1.27	0.24	1.19	0.79	0.04
86	0.23	0.16	0.22	0.22	0.35	0.31	0.38	0.21	0.11	0.23	0.47	0.46	0.40	0.62	0.13
87	0.43	0.33	0.14	0.12	0.33	0.38	0.20	0.42	0.05	0.50	0.60	0.13	0.37	0.61	0.03
88	0.13	0.29	0.21	0.35	0.38	0.44	0.39	0.43	0.14	0.65	0.60	0.47	0.30	0.13	0.14
89	0.28	0.19	0.17	0.21	0.08	0.33	0.31	0.16	0.11	0.34	0.30	0.42	0.28	0.15	0.03
90	0.20	0.23	0.41	0.34	0.53	0.28	0.12	0.35	0.23	0.52	0.55	0.44	1.00	0.65	0.10

Harmonic number

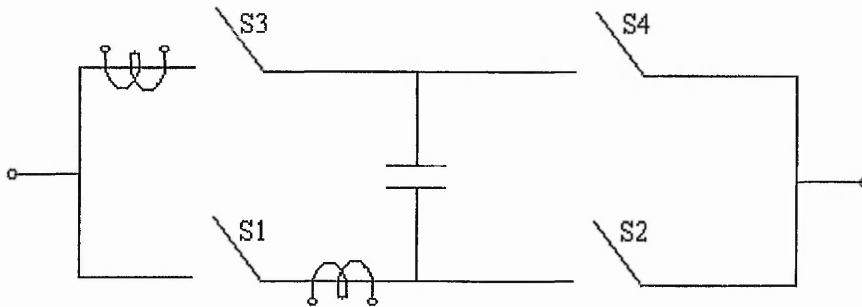
%

	0.50	0.55	0.58	0.60	0.62	0.68	0.71	0.74	0.77	0.80	0.83	0.88	0.90	0.95	1.00
91	0.11	0.28	0.30	0.34	0.49	0.22	0.19	0.37	0.20	0.46	0.21	0.44	0.24	0.05	0.09
92	0.56	0.19	0.45	0.42	0.48	0.50	0.24	0.29	0.26	0.57	0.40	0.14	0.14	0.01	0.11
93	0.06	0.27	0.06	0.41	0.46	0.48	0.28	0.25	0.34	0.56	0.66	0.55	0.46	0.55	0.11
94	0.55	0.61	0.18	0.34	0.09	0.59	0.40	0.05	0.30	0.25	0.13	0.11	0.28	0.25	0.08
95	0.25	0.37	0.69	0.53	0.27	0.62	0.21	1.09	0.33	0.71	1.09	0.55	1.20	0.21	0.07
96	0.37	0.65	0.87	0.39	0.48	0.33	0.19	0.10	0.27	0.49	0.43	0.47	0.14	0.25	0.08
97	0.43	0.68	1.18	0.51	0.29	0.23	0.33	0.63	0.36	0.65	0.92	0.37	0.21	0.57	0.05
98	0.13	0.22	0.95	0.55	0.58	0.25	0.40	0.74	0.08	0.63	0.20	0.70	0.29	0.29	0.11
99	0.61	0.33	0.65	0.44	0.24	0.59	0.35	0.19	0.37	0.36	0.29	0.27	0.23	0.12	0.04
100	0.26	0.42	0.01	0.52	0.39	0.82	0.17	0.29	0.01	0.77	0.25	0.55	1.38	0.64	0.02

Harmonic number

%

Current commutation

Fig. A5.3-1 – The H bridge and current transducer positions

The waveforms of the currents through switches S1 and S3 are displayed in figures A5.3-2 and A5.3-3. The current transducers were placed as shown in figure A5.3-1. The switches S1 and S3 are complementary operated. The current waveforms shown are for positive half cycle in the peak values.

Initially, the switch S3 is ON and the switch S1 is OFF. The switch S3 is turn off and the current through the switch goes towards 0. Both switches are OFF for $\sim 1.5\mu\text{s}$. Then, the switch S1 is turn ON and the current rises towards the current value that passed through switch S3 before commutation.

It has to be noted that the dead time at the command signal level is $\sim 2.5\mu\text{s}$. This is reduced to $1.5\mu\text{s}$ at the switch level due to the turn on and turn off times of the MOSFET transistors.

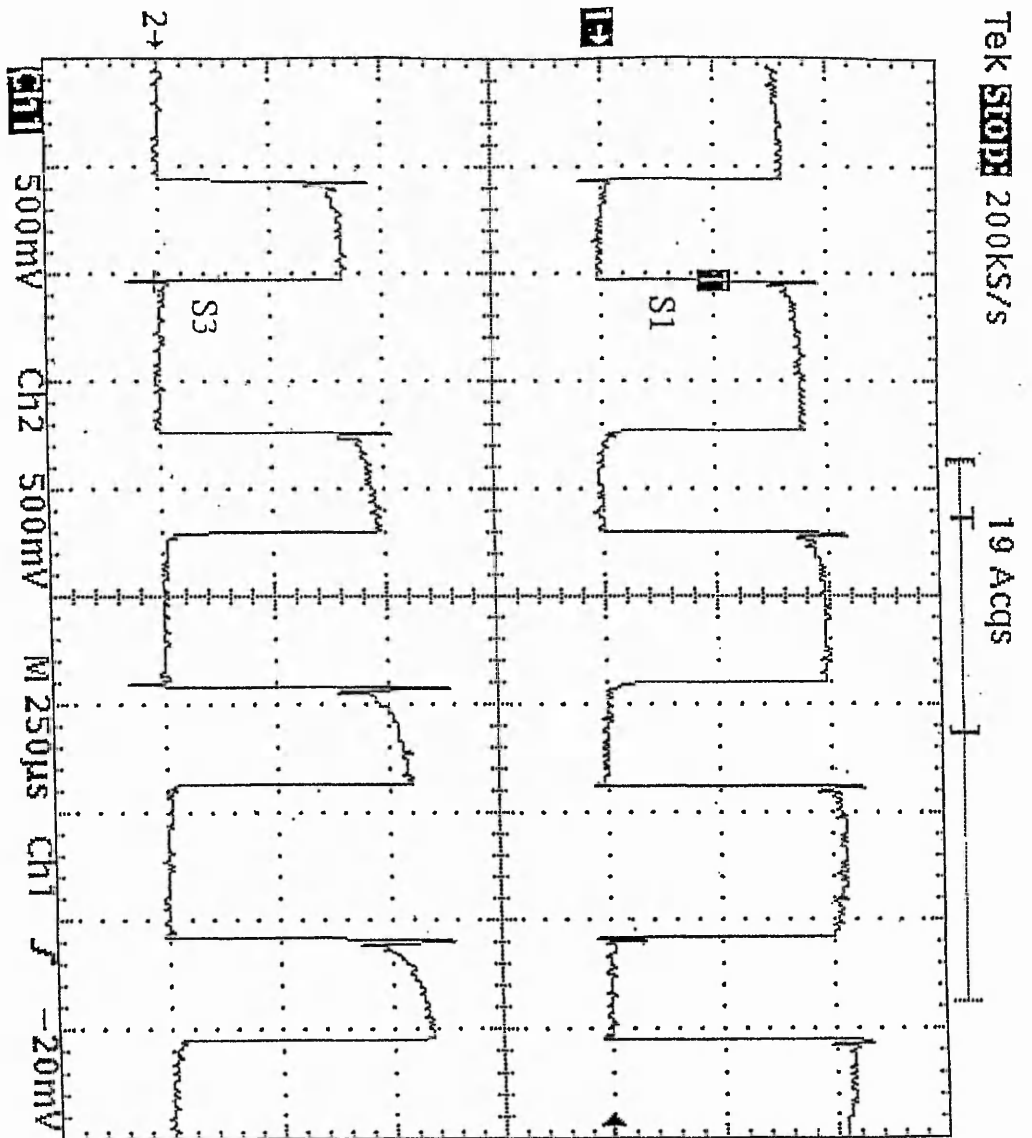


Fig. A5.3-2 – The currents through switches S1 and S3

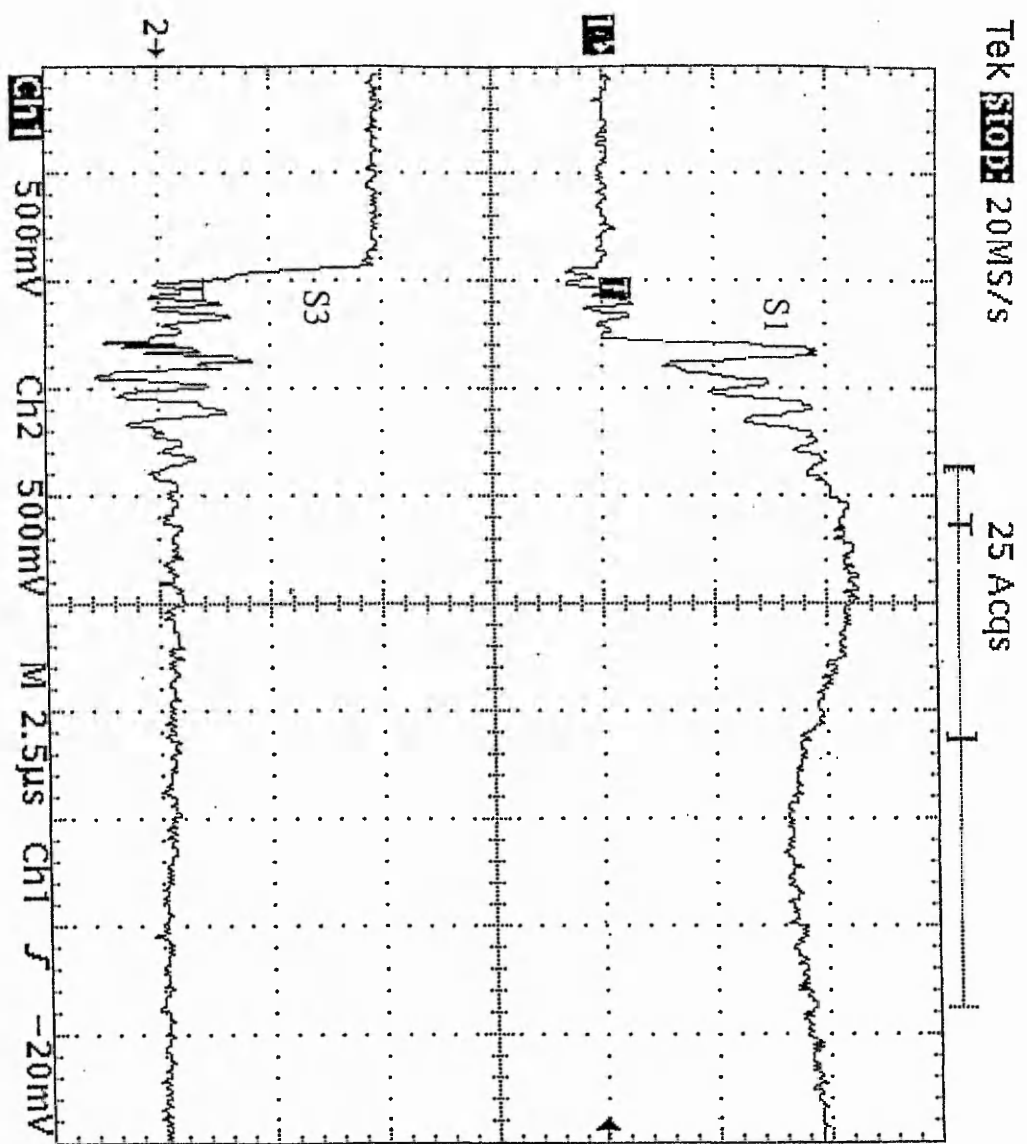
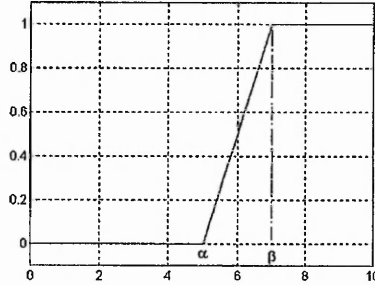


Fig. A5.3-3 – Currents through S1 and S3 during switching

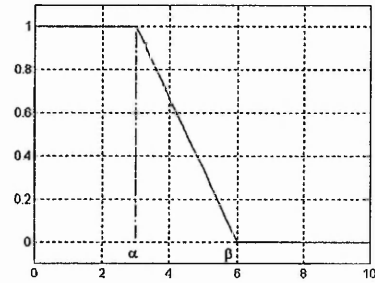
Fuzzy membership functions

Four types of membership are the most used in fuzzy control:

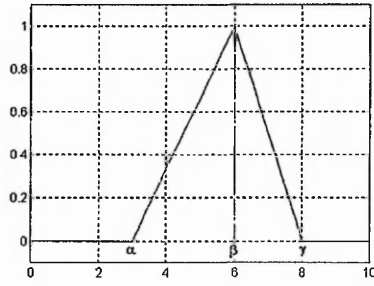
$$\Gamma(u; \alpha, \beta) = \begin{cases} 0 & u < \alpha \\ \frac{u - \alpha}{\beta - \alpha} & \alpha \leq u \leq \beta \\ 1 & u > \beta \end{cases}$$



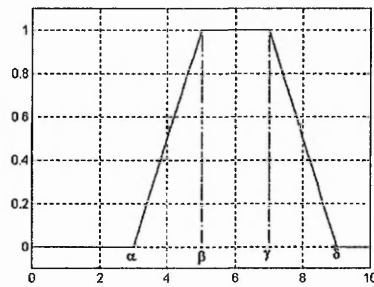
$$L(u; \alpha, \beta) = \begin{cases} 1 & u < \alpha \\ \frac{\beta - u}{\beta - \alpha} & \alpha \leq u \leq \beta \\ 0 & u > \beta \end{cases}$$



$$\Lambda(u; \alpha, \beta, \gamma) = \begin{cases} 0 & u < \alpha \\ \frac{u - \alpha}{\beta - \alpha} & \alpha \leq u \leq \beta \\ \frac{\gamma - u}{\gamma - \beta} & \beta \leq u \leq \gamma \\ 0 & u > \gamma \end{cases}$$



$$\Pi(u; \alpha, \beta, \gamma, \delta) = \begin{cases} 0 & u < \alpha \\ \frac{u - \alpha}{\beta - \alpha} & \alpha \leq u \leq \beta \\ 1 & \beta \leq u \leq \gamma \\ \frac{\delta - u}{\delta - \gamma} & \gamma \leq u \leq \delta \\ 0 & u > \delta \end{cases}$$



For fig. 6.2 following membership functions are defined:

- $\mu_{child} = L(u, 10, 12)$
- $\mu_{teenager} = \Pi(u, 10, 12, 18, 20)$
- $\mu_{young} = \Pi(u, 18, 20, 30, 40)$
- $\mu_{mature} = \Pi(u, 30, 40, 60, 70)$
- $\mu_{old} = \Gamma(u, 60, 70)$